AD-764 322

FUSION WELDING OF ALUMINUM TO STEEL

V. R. Ryabov

Foreign Technology Division
Wright-Patterson Air Force Base, Ohio

9 July 1973

FTD-MT-24-111-73

FOREIGN TECHNOLOGY DIVISION

FUSION WELDING OF ALUMINUM TO STEEL

by

V. R. Ryabov

UNCLASSIFIED

Security Classification

DOCUMENT CONTROL DATA - R & D

(Security classification of title, body of abstract and indexing annotation must be entered when the overall report is classified)

1. ORIGINATING ACTIVITY *(Corporate author)*
Foreign Technology Division
Air Force Systems Command
U. S. Air Force

2a. REPORT SECURITY CLASSIFICATION
UNCLASSIFIED

2b. GROUP

3. REPORT TITLE
FUSION WELDING OF ALUMINUM TO STEEL

4. DESCRIPTIVE NOTES *(Type of report and inclusive dates)*
Translation

5. AUTHOR(S) *(First name, middle initial, last name)*
V. R. Ryabov

6. REPORT DATE
1969

7a. TOTAL NO. OF PAGES
~~220~~ 234

7b. NO. OF REFS
249

8a. CONTRACT OR GRANT NO.

b. PROJECT NO.
735102

c.

d.

9a. ORIGINATOR'S REPORT NUMBER(S)
FTD-MT-24-111-73

9b. OTHER REPORT NO(S) *(Any other numbers that may be assigned this report)*

10. DISTRIBUTION STATEMENT
Approved for public release; distribution unlimited.

11. SUPPLEMENTARY NOTES

12. SPONSORING MILITARY ACTIVITY
Foreign Technology Division
Wright-Patterson AFB, Ohio

13. ABSTRACT

13

DD FORM 1 NOV 65 1473

UNCLASSIFIED

Security Classification

EDITED MACHINE TRANSLATION

FTD-MT-24-111-73

FUSION WELDING OF ALUMINUM TO STEEL

By: V. R. Ryabov

English pages: 220

Source: Svarka Plavleniyem Alyuminiya so Stal'yu, 1969, pp. 1-232.

Country of origin: USSR

Requester: AFML/LLM

This document is a SYSTRAN machine aided translation, post-edited for technical accuracy by: Dean F. W. Koolbeck.

Approved for public release; distribution unlimited.

PREPARED BY:

TRANSLATION DIVISION
FOREIGN TECHNOLOGY DIVISION
WP-AFB, OHIO.

TABLE OF CONTENTS

U. S. BOARD ON GEOGRAPHIC NAMES TRANSLITERATION SYSTEM

Block	Italic	Transliteration	Block	Italic	Transliteration
А а	*А а*	A, a	Р р	*Р р*	R, r
Б б	*Б б*	B, b	С с	*С с*	S, s
В в	*В в*	V, v	Т т	*Т т*	T, t
Г г	*Г г*	G, g	У у	*У у*	U, u
Д д	*Д д*	D, d	Ф ф	*Ф ф*	F, f
Е е	*Е е*	Ye, ye; E, e*	Х х	*Х х*	Kh, kh
Ж ж	*Ж ж*	Zh, zh	Ц ц	*Ц ц*	Ts, ts
З з	*З з*	Z, z	Ч ч	*Ч ч*	Ch, ch
И и	*И и*	I, i	Ш ш	*Ш ш*	Sh, sh
Й й	*Й й*	Y, y	Щ щ	*Щ щ*	Shch, shch
К к	*К к*	K, k	Ъ ъ	*Ъ ъ*	"
Л л	*Л л*	L, l	Ы ы	*Ы ы*	Y, y
М м	*М м*	M, m	Ь ь	*Ь ь*	'
Н н	*Н н*	N, n	Э э	*Э э*	E, e
О о	*О о*	O, o	Ю ю	*Ю ю*	Yu, yu
П п	*П п*	P, p	Я я	*Я я*	Ya, ya

* ye initially, after vowels, and after ъ, ь; e elsewhere. When written as ё in Russian, transliterate as yё or ё. The use of diacritical marks is preferred, but such marks may be omitted when expediency dictates

FOLLOWING ARE THE CORRESPONDING RUSSIAN AND ENGLISH

DESIGNATIONS OF THE TRIGONOMETRIC FUNCTIONS

Russian	English
sin	sin
cos	cos
tg	tan
ctg	cot
sec	sec
cosec	csc
sh	sinh
ch	cosh
th	tanh
cth	coth
sch	sech
csch	csch
arc sin	$\sin^{-1}$
arc cos	$\cos^{-1}$
arc tg	$\tan^{-1}$
arc ctg	$\cot^{-1}$
arc sec	$\sec^{-1}$
arc cosec	$\csc^{-1}$
arc sh	$\sinh^{-1}$
arc ch	$\cosh^{-1}$
arc th	$\tanh^{-1}$
arc cth	$\coth^{-1}$
arc sch	sech^{-1}
arc csch	csch^{-1}
rot	curl
lg	log

Designations

см	cm
г	g (grams)
атом	atom
кг	kg
град	deg
дж	J
вт	W
дан	daN
мдж	mJ
дм	dm
Мдж	MJ
вес.%	wt.%
ат.%	at.%
сек	s
мин	min
ч	h
мкм	μm
ккэл/моль	kcal/mole
л	l
св	weld(ing) [as subscript]
пл	melting/melt [as subscript]
г-моль	g-mole
моль	mole

имп - pulse

ом - ohm, Ω

кв - kV

ма - mA

The monograph discusses questions of the theory and practice of making welded joints of aluminum and its alloys with steel of various classes.

Thermodynamic calculations are used as a basis for substantiating the selection of elements for alloying the molten pool during welding of aluminum to steel. Thermal cycles, welding procedures, and methods of testing the steel/aluminum joints are described. Examples of production application of such joints are given.

The book is intended for specialists in scientific research and design institutes and also for engineering and technical workers occupied with welding problems.

Responsible Editor:
Dr. of Technical Sciences
D. M. Rabkin

FOREWORD

In the aeronautical and chemical industries, machine building, rocket engineering, shipbuilding, and other fields light alloys - especially aluminum-based alloys such as AMts, AMg5V, AMg6, ATsM, etc. - are finding ever wider application. The broad utilization of these alloys in all branches of the national economy is facilitated by the fact that in addition to low specific weight they possess good thermal and electrical conductivity in combination with relatively high specific strength. In terms of specific strength aluminum alloys surpass copper-based alloys and approach the best types of steels.

However, owing to the fact that as compared with structural steels aluminum alloys have lower strength, lower melting temperature, low hardness, and comparatively poor wear resistance their application is connected with an increase in the thickness of a number of structural units. Along with this it is a well-known fact that during operation any structure experiences stresses which are different in magnitude at different points: at certain places the maximum permissible value of stresses is achieved, while in other points stresses are virtually absent. Therefore a combination of greatest effectiveness in the operation of structures with a simultaneous reduction in weight can be achieved by using unlike metals in different sections of the structure

in accordance with the stresses which arise during operation. In this respect the production of welded steel/aluminum combined structures is especially suitable. In this case the greatest possible use is made of the properties inherent to each metal.

The use of combined welded units made from steel and aluminum would also make it possible to create types of structures which are fundamentally new and have never before been utilized. For example, in building oxygen equipment it is necessary to provide fixed and portable vessels for liquified gases consisting of two vessels - an outer one of steel Kh18N10T and an inner vessel of the aluminum-manganese alloy AMts. The use of such vessels would sharply reduce the volatility of the liquified gases and consequently would reduce losses both during storage and during transportation. In this connection the need arises to obtain strong, tight joints which will ensure retention of a vacuum in the interwall space.

However, the production of welded steel/aluminum joints is connected with major difficulties. As yet we have no industrially substantiated method of welding aluminum and aluminum alloys to steels of different types. Existing methods of welding aluminum to steel provide strength of the combination joint which is no higher than the strength of pure aluminum. At the same time a number of steel/aluminum structures can be sensibly utilized only if the strength indices are at the level of strength of aluminum alloys of the AMts, AMg6, etc. type.

The goal of this work is as follows:

1. Study of the special features of the interaction of aluminum with steel under variable temperature and time factors, as well as the composition of the interacting metal; investigation of the nature of the phases arising during welding of aluminum to steel and a search for a method of alloying and for other conditions under which these phases will not be formed.

2. Using results of research to develop a technology for welding aluminum alloys of the AMts, AMg6, etc. types to the steels St. 3 and 1Kh18N9T to ensure production of effective welded units; investigation of the properties of steel/aluminum joints under static loads, at low temperatures, under conditions of hard vacuum, etc.

3. Investigation of the corrosion resistance of welded joints and methods of increasing it.

The production of steel/aluminum welded joints is a relatively new technological process and is accompanied by complex and varied phenomena along the transition line. Therefore in selecting research methods we attempted to carry out complex evaluation of the nature of the occurring processes and to clarify the properties of the combined joints which are obtained. The following were selected as the principal methods: metallographic, electron-microscope, and measurement of microhardness. X-ray studies and mechanical tests were also carried out; the distribution of elements in the fusion zone was studied by means of a microprobe, the nature of destruction was investigated on the MKU-1 microcinema projector, etc.

The author considers it his pleasant duty to express his gratitude to Doctor of Technical Sciences D. M. Rabkin, Candidate of Technical Sciences I. Ya. Dzykovich, and Engineers A. V. Lozovskiy, V. I. Yumatova, and L. M. Onopriyenko for assistance in the work and for preparing the materials for this monograph.

CHAPTER I

PRESENT STATE OF THE ART IN WELDING ALUMINUM AND ITS ALLOYS TO STEEL

1. Aluminum, Iron, and Their Properties

Fusion welding of aluminum to steel is accompanied by substantial difficulties caused primarily by the difference in the physicochemical properties of the welded metals. Table 1 [94, 201] presents the most characteristic physical properties of aluminum and iron.

Table 1. Physical properties of aluminum and iron.

Parameter	Aluminum	Iron
Atomic weight	26.97	55.85
Atomic volume at 293°K, cm^3/g-atom	10.00	7.19
Crystal lattice at 293°K	fcc	bcc
Atomic radius, Å	1.43	1.26
Density, kg/m^3	2.699	7.876
Coefficient of linear expansion $\alpha \cdot 10^{-6}$, 1/deg	23.5	11.9
Melting temperature, °C	660.2	1539
Specific heat, J/(kg·deg)	894.52	451.44
Thermal conductivity, W/(m·deg)	238.64	71.17
Tensile strength, daN/mm^2	7.0-10.0	25

Table 1 (Cont'd).

Yield point, daN/mm^2	3.0	20
Relative elongation, %	50	30
Modulus of normal elasticity, daN/mm^2	6960-7220	20000-21550
Shear modulus, daN/mm^2	2600-2730	7800-8000
Brinell hardness, daN/mm^2	18	60

As is evident from the data in the table, aluminum has a lower density, comparatively low melting temperature, and satisfactory thermal and electrical conductivity. An outstanding feature of aluminum is its ability to react intensively with oxygen. The reducing capacity of aluminum is extremely high [156]. Aluminum is easily oxidized in air even at room temperature. Despite its great density as compared with aluminum (2.85-3.95 kg/m^3) the oxide film on aluminum is easily maintained on the surface of the liquid metal by the force of surface tension; this is one of the major obstacles during welding of aluminum to steel and to other metals [119]. Aluminum is a typical electronegative element: in ordinary conditions it does not form continuous solid solutions with any other element (Fig. 1).

Limited solid solutions based on aluminum (with lithium, magnesium, copper, zinc, etc.) consist, as a rule, of small or moderate concentrations. In high concentrations aluminum is dissolved in other metals, especially in the transition metals [72].

As the most electronegative metal, aluminum can form compounds with many electropositive metals; these are called aluminides. Aluminum will form with a given element a number of compounds of different stoichiometric composition; the latter is frequently complex - e.g., V_4Al_{23}, $MoAl_{12}$, $ReAl_{12}$, etc.

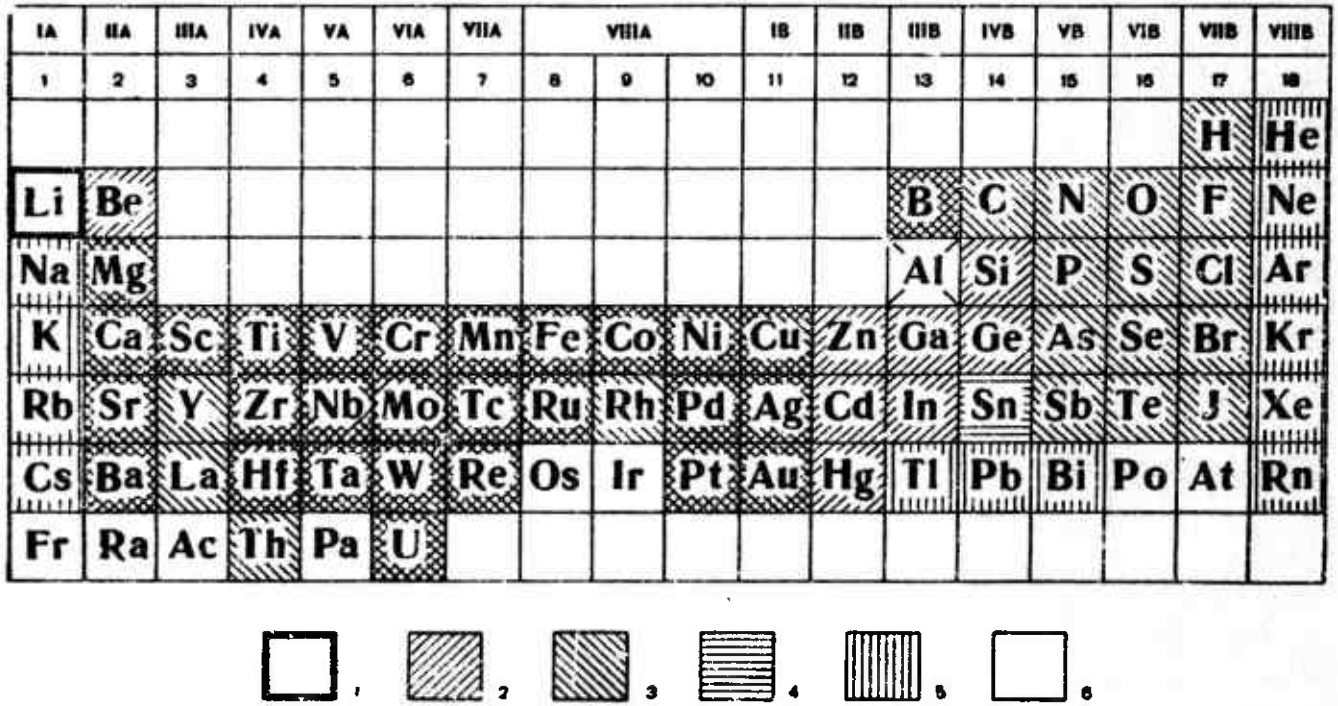

Fig. 1. Interaction of aluminum with elements of the periodic system: 1, 2, 3, 4 - elements which form continuous solid solutions, limited solid solutions, compounds, and eutectic mixtures, respectively; 5 - elements which do not react with Al; 6 - elements which have not been studied.

Aluminum is used in industry both in pure form (in chemical machine building, electrical engineering, the food industry) and in the form of alloys. Aluminum-based alloys are finding ever wider application. This is explained by the fact that aluminum alloys, like aluminum, are low in weight and possess satisfactory thermal conductivity and strength [34].

The chemical composition and mechanical properties of aluminum alloys which are typical of a number of the most widely used Al alloys in the manufacture of a wide variety of welded structures are given in Table 2.

Iron is an element of group VIIIA of the periodic system; it is a transition metal with an incomplete d-shell and it has several crystal modifications. The latter fact determines particular features of its interaction with other elements.

α-Iron with a body-centered cubic lattice and γ-iron with a face-centered cubic lattice are considered to be the basic modifications of iron. The high-temperature modification δ-iron has a structure which is similar to that of α-iron. α-Iron forms continuous solid solutions with only two isomorphic elements (V and Cr). α-Iron forms limited solid solutions of various concentrations and also compounds with many elements (Fig. 2). The γ-modification will form continuous solid solutions with a family of elements (Mn, Co, Rh, Ir, Ni, Pd, Pt) located close to it in the periodic system and which are isomorphic in structure. A large number of elements form limited solid solutions with γ-iron. These include elements which are somewhat removed from iron in the periodic system and which have different crystal structure and differences in atomic radii as compared with iron. Gamma-iron forms compounds with the majority of elements. There are many elements with which iron does not interact. These include elements of group IA (Li, Na, K, Cs, Rb, Fr), group IIA (Mg, Ca, Sr, Ba) and certain elements in groups IB, IIB, IIIB, IVB and VB (Ag, Hg, Tl, Pb, Bi).

Table 2. Chemical composition and mechanical properties of certain aluminum-base alloys.

Alloy designation	Chemical composition, %							
	Cu	Mg	Mn	Ni	Fe	Si	Zn	Other admixtures
AD1	≤0.05	-	-	-	≤0.3	≤0.35	-	Total 0.4-0.7
AMts (annealed)	≤0.2	≤0.05	1.0-1.6	-	≤0.7	≤0.6	≤0.1	≤0.1
AMg (annealed)	≤0.1	2.0-2.8	0.15-0.4	-	≤0.4	≤0.4	-	≤0.1
AMg3	≤0.05	3.2-3.8	0.3-0.6	-	≤0.5	≤0.5-0.8	≤0.2	≤0.1
AMg5V	≤0.05	4.8-5.5	0.3-0.5	V = 0.02-0.2	≤0.5	≤0.5	≤0.2	≤0.1
AMg6	≤0.1	5.8-6.8	0.5-0.8	Ti = 0.02-0.1	≤0.4	≤0.4	≤0.2	≤0.1

Alloy designation	Mechanical properties							
	σ_B, daN/mm^2	$\sigma_{0.2}$, daN/mm^2	δ_{10}, %	ψ, %	E, daN/mm^2	a_K, mJ/m^2	HB, daN/mm^2	Specific strength σ/γ, dm/10^{-5}
AD1	7-10	-	-	-	7000	-	-	3.7
AMts (annealed)	11-15	-	18-20	70	7100	-	30	5.5
AMg (annealed)	20	10	16	35-64	7000	10	45	7.4
AMg3	20	10	15	36	7000	3.5	50	7.5
AMg5V	25-28	15	18	24	7000	5.0	65	10.5
AMg6	32-38	16-18	15-20	22-23	7200	3-4	70	14

Remark. Density of aluminum alloys, g/cm^3: AMts - 2.73; AMg - 2.7; AMg3 - 2.67; AMg5V - 2.65; AMg6 - 2.64.

a)

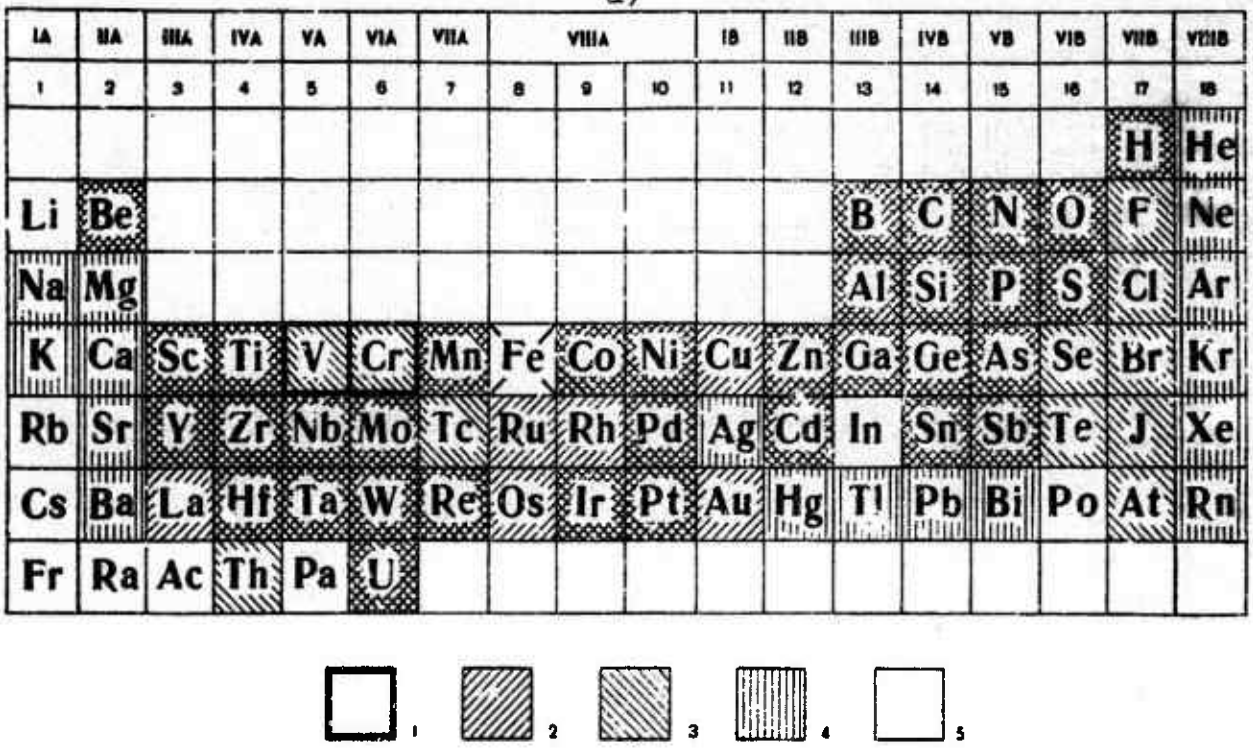

b)

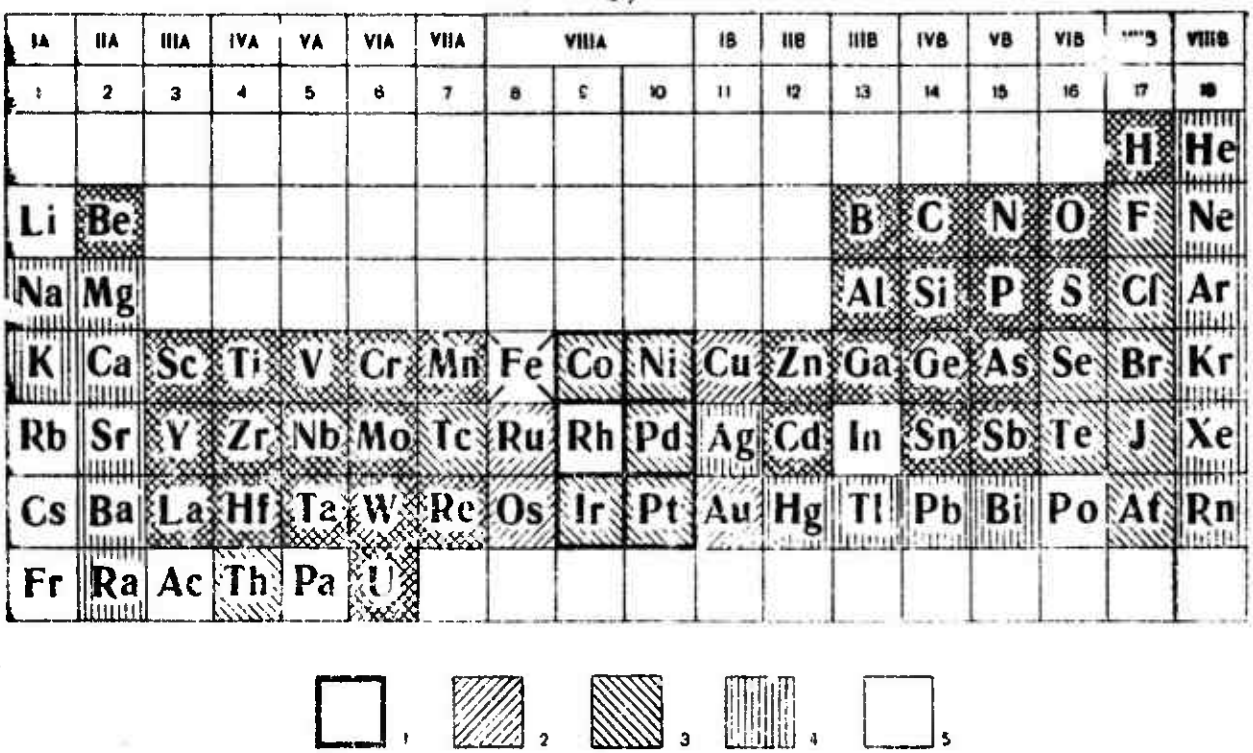

Fig. 2. Interaction of γ-iron (a) and α(δ)-iron (b) with elements of the periodic system: 1-5 - the same as in Fig. 1.

While iron is used in technically pure form, it is applied especially broadly in various alloys with other elements. It is easily oxidized, forming a number of oxides with different valences. The intensity of iron oxidation in air increases sharply when it is heated above 140-150°C. In the presence of moisture iron becomes covered with corrosion products consisting of iron oxides and water. Numerous types of steel with different properties are formed on the basis of iron. The chemical composition and mechanical properties of certain of these steels are given in Table 3.

Steels of two types - St. 3 and 1Kh18N9T - were selected from the great number of contemporary steels; these are felt to be typical representatives of two classes of steels. Armco iron (0.03% C), steel 08 kp (up to 0.1% C) and certain other steels were used in the experiments to clarify the role of carbon.

In comparison with low-carbon and austenitic steels, aluminum has higher thermal conductivity (5-8 times) and about half the volume heat capacity. Therefore the effectiveness of heating and melting by local heat sources depends essentially on the regime parameters.

As is known, the coefficient of thermal conductivity of a metal depends on its chemical composition, structure, and temperature. The value of this coefficient for iron and for carbon and low-alloy steels is reduced with an increase in temperature, while for stainless steels of the austenite class it is increased. At room temperature the coefficients of thermal conductivity for steels of various types will differ significantly, but as temperature increases the differences between them are smoothed.

Values of coefficients of thermal conductivity for aluminum AD1, the aluminum-manganese alloy AMts, and the aluminum-magnesium alloys AMg3, AMg5V, and AMg6 differ more sharply from one another. Alloying

Table 3. Chemical composition and mechanical properties of armco iron and certain types of steel.

Material	Chemical composition, %								Mechanical composition							Specific strength $\frac{\sigma}{\gamma}$, $\partial M \cdot 10^{-5}$
	C	Mn	Si	Ni	Cr	Ti	Cu	others	σ_B, dan/mm²	$\sigma_{0,2}$, dan/mm²	ψ, %	δ, %	E, dan/mm²	α_K, Mdж/m²	HB, dan/mm²	
Armco iron (hot-rolled rods)	0,03	0,035	0,03	—	—	—	0,15	0,04	27	—	—	60	—	—	—	3,4
08kp	0,09–0,1	0,03	0,03	0,3	0,15	—	—	0,08	28—37	—	—	—	19500	6	125	4,7
St.3	0,16	0,58	0,1	Traces	Traces	—	—	—	35—40	30	16	45	20000	—	—	5,1
1Kh18N9T	0,06	—	—	10,18	17,73	0,57	—	Ost.	55—60	50	45	55	20500	27,6	—	7,5
Kh21N5T	0,09	—	0,011	4,10	21,27	0,46	—	Ost.	70	40	20	—	—	6	—	7,5

Remark. Density of materials, g/cm^3: armco iron = 7.3; 08kp - 7.83; St. 3 - 7.82: 1Kh18N9T and Kh21N5T - 8.0.

of aluminum with manganese, magnesium, copper, and other elements causes a reduction in values of coefficients of thermal conductivity. The thermal conductivity of aluminum and its alloys is increased with an increase in temperature, in contrast to other metals. The substantial differences in coefficients of thermal conductivity [128, 149-151] and in heat capacity for aluminum alloys and steels are illustrated on Figs. 3 and 4, respectively.

Fig. 3. Coefficient of thermal conductivity for aluminum alloys and steels as a function of temperature.

The difference in the values of coefficients of linear expansion between joined metals causes the appearance of large thermal stresses along the line of transition from steel to aluminum.

Figure 5 shows a graph of the coefficient of linear expansion for AD1 aluminum, alloy AMts, and steels of types 08kp and 1Kh18N9T as functions of temperature; this difference is clear from the figure [150, 201]. If we trace the changes in the magnitudes of the coefficient of linear expansion in the low-temperature region - e.g., 0-196°C - it is possible to note a greater "shortening" of aluminum as compared with steel 1Kh18N9T; in the case of certain types of welded joints, for example tubular telescoping joints, this can be a favorable factor.

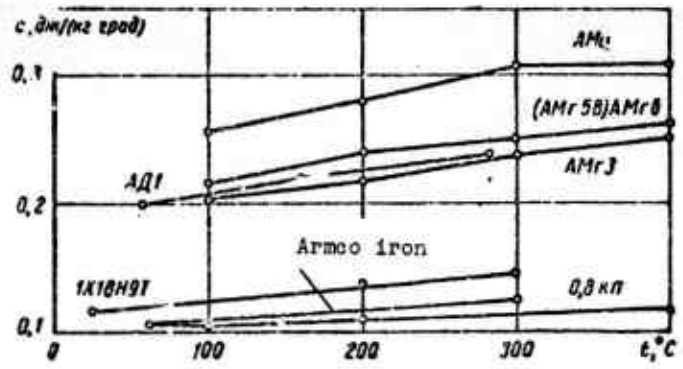

Fig. 4.

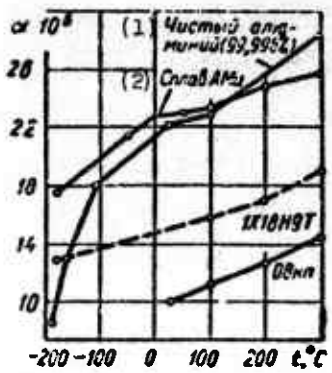

Fig. 5.

Fig. 4. Heat capacity of aluminum alloys and steels as a function of temperature.

Fig. 5. Coefficient of linear expansion for aluminum, the alloy AMts, and steels as a function of temperature.
KEY: (1) Pure aluminum (99.996%); 2 - Alloy AMts.

2. Some Data on the Fusion Welding of Unlike Metals

When metals with different physicochemical properties are welded the properties of the welded metal will, as a rule, be lower than the properties of the metals being joined. Therefore the principal goal in welding unlike metals is directional control of diffusion, thermal and other physicochemical processes which ensure the required properties of the weld and of the welded joints.

At present no generally accepted positions have been developed concerning the conditions which determine the possibility of welding unlike metals.

A number of studies have been concerned with the processes of the formation of strong bonds between unlike metals [116, 174]. These processes can tentatively be divided into two stages:

1) preparatory, when the substances to be joined are brought together at the distance required for interatomic interaction and the surfaces are prepared for the interaction. The surfaces can be brought together in various ways: in the wetting process, when there is a liquid phase which wets the surface of the solid material; in the process of combined plastic deformation of two solid substances or of one of them, and also as a result of surface diffusion transfer of atoms between these solids;

2) the final stage, leading to the formation of a strong joint. In the case of joining pure metals or solid solutions the processes of forming strong bonds reduces to collectivization (collecting) of valence electrons by positive ions, which results in the appearance of a strong metallic bond between systems of atoms forming the crystal lattice.

The types of bonds between unlike materials vary widely. Considering the special features of joining aluminum to steel which will be described below, one should assume the possibility of the formation of a strong metallic bond and also partial formation of a bond of the covalent type, since in a number of cases the metals react with intermetallides (with chemically bonded metals).

The occurrence of processes of electron interaction in the region of contact of the metals to be joined requires determination of the magnitude of the energy required to activate the state of the surfaces [95, 127]. This may be energy imparted in the form of

heat, mechanical energy of elastoplastic deformation, etc. Its selection is determined by the technological parameters.

It is noted in the literature [105, 130, 173] that the possibility of the formation of a metallic bond between particles of metals to be joined - i.e., the ability of the metals to be welded to one another - is determined by the structure of their atoms, the types and parameters of their crystal lattices, and also by other factors which determine the chemical affinity between the metals being joined. Welded joints are formed most easily between metals and alloys whose composition includes elements which possess unlimited mutual solubility in both the liquid and solid states - i.e., which form continuous series of solid solutions [160].

Unlimited mutual solubility of the metals requires the following basic conditions [46, 111]: the metals should have identical crystal lattices; if the metals are polymorphous unlimited solubility will be observed only between their isomorphic modifications - e.g., γ-Fe and β-Co with a face-centered cubic lattice. It follows that one should strive toward the maximum possible similarity in the type and parameters of the crystal lattices, and toward the appropriate reflection of angles of lattice disorientation of the phases relative to the interface [98].

Experiments have shown that during direct welding of metals which have the same crystal structure with similar lattice parameters and similar electrochemical properties it is possible to obtain welded joints with mechanical properties which are similar to those of the metals being welded. As a characteristic example we can cite the welding of metals based on copper (copper M2, chrome bronze BrKh05) and nickel, which form a series of solid solutions.

In works by N. V. Ageyev [1], I. I. Kornilov [72], and other investigators [42] it is noted that one of the most important conditions for the formation of solid solutions by elements is a difference in their atomic diameters of no more than 15-16%. In this case the crystal lattice of iron has maximum deformation. During diffusion into iron of elements for which the difference in atomic diameters exceeds 15-16% the distortions in the crystal lattice of the solvent metal are excessively great and lead to strains which cause rupture of its atomic bonds and, consequently, destruction of a solid body.

Analyzing results from research on the pairs of metals which we selected, one can note that the difference in parameters of the crystal lattice for aluminum and α-iron comprises about 22%, while that between aluminum and γ-iron is about 12%. Besides this, during interaction of aluminum with γ-iron under conditions of elevated temperatures the crystal lattice is of identical type in the two metals. One should therefore expect that welding of aluminum to stainless steel will occur under more favorable conditions than welding of aluminum to low-carbon steel.

Nickel, manganese, molybdenum, chromium, tantalum, niobium, vanadium, germanium, and gallium show differences in atomic diameters of less than 15%; copper, zinc, titanium, silicon, germanium, tin, tantalum, chromium, and nickel moreover possess a certain solubility in both aluminum and iron.

From analysis of Figs. 1 and 2 it follows that only a limited quantity of elements (23-25) can be regarded as "plasticizers" for the iron-aluminum system and for iron/aluminum compounds (this number does not include the lanthanide group).[1]

---

[1]The introduction of other elements is either inadvisable (gases, salts, artificially prepared elements), difficult due to their toxicity (Po, Hg, etc.), or economically unsound (Au, Pt, Ge, etc.). Certain elements (W, Ge, etc.) represent analogs of those studied (Mo, Si, etc.).

The particular features noted above serve as the basis for selecting the alloying systems for the welding pool and the types of coatings on the steel.

Attention should be directed toward the fact that the relative dimensions of atomic diameters and the solubility of different elements in iron will vary as a function of temperature [42].

We will list the basic factors which determine the temperature dependence of the solubility of elements in iron.

1. Relative change in the dimensions of the atomic diameters.

2. Change in coefficients of linear expansion. If the difference between atomic diameters and the difference between the coefficients of linear expansion grows, solubility remains virtually unchanged. The aluminum-iron (steel) pair is extremely indicative in this respect: the coefficient of linear expansion for aluminum amounts to $23.5 \cdot 10^{-6}$ and that for iron is $11.9 \cdot 10^{-6}$ at room temperature; the values at 500°C are $31.1 \cdot 10^{-6}$ and $14.3 \cdot 10^{-6}$. There is a corresponding growth in the difference of atomic diameters [at higher temperature], and as a result there is no essential change in the solubility of aluminum in iron. Thus, for example, at room temperature the solubility of aluminum in iron comprises 32%, while at 1232°C the value is 35%. This can apparently explain the absence of any positive effect from preheating of the steel when aluminum and steel are welded.

The electrochemical properties (electron affinity) must not differ strongly, since if they do the formation of intermetallic compounds is possible; as a rule these embrittle the metal in the weld zone. This condition is usually observed with metals which fall in the same group or in contiguous related groups in the periodic system of elements.

Correct selection of the means, conditions, and technology of welding in combination with metallurgical operating means will in the majority of cases make it possible to either eliminate completely or reduce to a minimum the harmful consequences of limited solubility [79, 80, 108].

Thus, complex processes occur on the fusion boundary between unlike metals and the study of these processes both experimentally and theoretically [98, 109, 122, 174] is fraught with difficulty.

At present two basic directions have been marked in the solution of the problem of joining metals with differing properties: 1) welding with predominant melting of one metal; 2) the application of intermediate metals.

Joining of aluminum to steel is a characteristic example of the first direction. Here the basic problem consists in reducing to a minimum or completely eliminating the formation of brittle compounds in the weld metal. Welding without melting of the refractory metal is the most promising from this point of view; this involves melting only the metal with the lower melting temperature when two metals with different melting points are fused. Sometimes such melting is called braze-welding [58]. During braze-welding liquid metal interacts with solid metal. The major physicochemical processes occurring during the interaction of the materials to be welded are as follows: wetting of the solid surface of unfused metal by the liquid metal (adhesion); flow of the liquid metal over the surface of the solid, during which surface diffusion occurs (establishment of physical contact) [174]; dissolution of the refractory metal in the liquid metal. The first two processes are necessary for the formation of a weld, while the last one determines the quality of the welded joint and its properties.

While the possibility of separate regulation of temperature and time parameters exists during calorizing, zinc coating, and immersion brazing, during welding these parameters are mutually connected and are determined primarily by the welding conditions.

The second method is used, for example, in joining titanium to steels: welding is accomplished through an intermediate metal (vanadium) or through two layers in the form of tantalum (on the titanium side) and nickel (on the steel side) [51]; copper alloys can be joined with titanium through tantalum [153].

Generalized data on the weldability of a number of unlike metals have been published by M. V. Poplavko [113], A. S. Mikhaylov, L. G. Strizhevskaya, D. Young and A. Smith [247] and by other investigators [190]. Of particular interest is one of the new methods of joining unlike metals, proposed by F. Zimmer [248].

Considering the available data on welding of aluminum to steel, one can draw a preliminary conclusion regarding the difficulties of joining these metals due to the following factors:

a) the great difference in melting temperatures of aluminum and steels;

b) the great difference in the coefficients of linear expansion of the metals to be joined, which leads to the appearance of substantial thermal stresses along the line of transition from steel to aluminum;

c) the significant difference between the thermal conductivity and heat capacity of the joined metals, which also gives rise to the appearance of thermal stresses;

d) the presence of the refractory oxide film of Al_2O_3, creating inclusions in the weld itself. Special fluxes are used

to dissolve them. The fluxes used during welding of aluminum are low-melting, highly fluid, and do a poor job of wetting the weld surface on the steel; because of this they are unsuitable for welding the given metal. Correspondingly, the standard fluxes used to weld steel will react with liquid aluminum, sharply disturbing its composition. Therefore these too cannot be used directly during the welding of steel to aluminum. However, the major obstacle is the chemical interaction of these metals, leading to irreversible formation of intermetallic compounds along the transition line. We will pause to consider this matter in more detail.

Aluminum-iron phase diagrams and certain other diagrams can be used as the basis for a preliminary judgement concerning the structures formed during fusion welding in steel/aluminum joints, the properties of steels containing aluminum, and the properties of aluminum alloys containing iron.

As is evident from the Fe-Al phase diagram [33] (Fig. 6a), aluminum forms solid solutions, intermetallic compounds, and a eutectic with iron. The solubility of iron in solid aluminum is extremely insignificant; the boundary of the solid solution of iron in aluminum at 225-600°C is found at an iron content of 0.01-0.022%. The solubility of iron in aluminum at the eutectic temperature (654°C) amounts to 0.053% [231], and according to data in work [46] at 450°C it is about 0.002%. Iron does not dissolve at all in aluminum at room temperature [68].

Even with insignificant quantities of introduced iron, crystals of the compound $FeAl_3$ (59.18% Al) will appear in the structure of alloys of aluminum with iron in the case of hardening. With an iron content up to 1.8% and temperature of 654°C the eutectic $Al+FeAl_3$ is formed. With a further increase in the iron content in the alloys chemical compounds will appear: Fe_2Al_7 (62.93% Al), Fe_2Al_5 (54.71% Al), $FeAl_2$ (49.13% Al), FeAl (32.57% Al), etc. Of these compounds, only Fe_2Al_5 melts at a definite temperature.

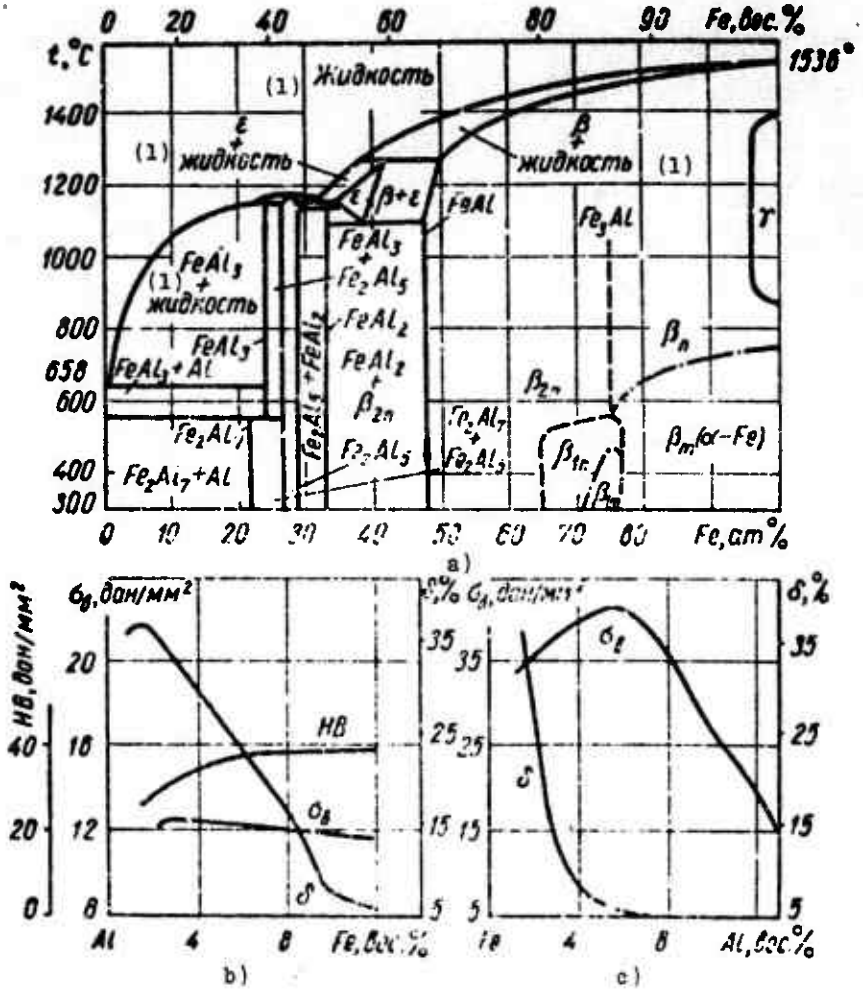

Fig. 6. Phase diagram of aluminum-iron alloys (a); change in mechanical properties of aluminum-iron alloys as a function of iron content (b) (per A. Ye. Vol); and the change in mechanical properties of iron-aluminum alloys as a function of aluminum content (c) (per S. Keys and K. Van Horn).
KEY: (1) Liquid.

Iron in aluminum alloys is always present in the form of chemical compounds; this determines the mechanical properties and workability of the alloys. The introduction of iron causes an increase in ultimate strength and hardness and a sharp drop in ductility of aluminum (Fig. 6b). Iron-aluminum alloys containing 8-10% Fe possess insignificant ductility and those even richer in iron are very brittle; because of this they have not found practical application at present [70, 71, 141, 152, 186].

In connection with the contradictory literature data on the compounds forming in the system Fe-Al [13, 185], we carried out a preliminary investigation of this system in order to obtain standard Debye powder diagrams of the system phases, data on the lattice constants of the α-phase as a function of the quantitative content of aluminum in it, and to refine the degree of solubility of aluminum and iron in welds. For this purpose we used the classical method of physicochemical analysis connected with the construction of diagrams of phases vs. properties in the section corresponding to a high concentration of iron in aluminum. The method of X-ray phase analysis (powder method) was used [172]. The X-ray patterns were photographed on the URS-55 apparatus in a Debye chamber (diameter 57.3 mm) in chromium radiation (CrK). This chamber was used to carry out phase analysis and determination of crystal structures and to perform precision measurements of the lattice constant.

The lattice constants were calculated according to X-ray diagrams with asymmetric backing of the film (per Straumanis [22, 50]. For this purpose a number of alloys were prepared in an arc furnace from pressed briquettes of high-purity carbonyl iron (99.98% Fe, remainder C, Ni) with small pieces of AV000 aluminum (aluminum content no less than 99.990%) in an atmosphere of technical helium. For better mixing of the liquid components, smelting in the arc furnace was carried out at temperatures close to the boiling point of aluminum. Total miscibility of the components was achieved by double remelting. During cooling the alloys underwent cracking [splitting] in the interval of concentrations corresponding to the presence of Fe_2Al_5 and $FeAl_3$ (especially Fe_2Al_5). The remaining alloys were not destroyed. Both cast and annealed specimens of iron-aluminum alloys were subjected to X-ray analysis. In order to achieve phase and also concentration equilibrium it was necessary to use heat treatment: specimens of alloys with a polished surface were placed in evacuated quartz ampules and annealed at 500 and 800°C for 1500 and

700 h, respectively. The quantitative composition of the specimens was monitored by chemical analysis [5].

X-ray phase analysis of alloys of the Fe-Al system (Table 4) confirms the existence in this system of the intermetallic compounds $FeAl_3$, Fe_2Al_5, $FeAl_2$, FeAl and also the presence of a wide region of solid solution based on α-Fe (α-phase) [168]. X-ray patterns of these phases are shown on Fig. 7.

Table 4. Data from X-ray and chemical analysis of iron-aluminum alloys.

Content of Fe in the alloy per charge, wt.%	Annealing temperature, °C	Content of Fe in the alloy, chemical analysis wt.%	Phase composition of the specimens	Lattice constant, A	
				α-phase	FeAl type CsCl
94.91	Cast	95.10	α	2.880	-
	500	94.23	α	-	-
	800	95.02	α	-	-
91.19	Cast	90.87	α	2.893	-
	"	86.18	α	2.904	-
86.14	500	85.94	α	-	-
	800	86.28	α	-	-
	Cast	82.98	α	2.911	-
82.85	500	82.94	α	-	-
	800	82.67	α	-	-
75.64	Cast	75.59	α + FeAl	2.923	2.905
	"	67.33	FeAl + α + $FeAl_2$ (traces)	2.925	2.906
67.44	500	67.20	FeAl + $FeAl_2$ (traces)	-	-
	800	67.18	FeAl + $FeAl_2$ (traces)	-	-
57.99	Cast	57.90	FeAl + $FeAl_2$	-	-
	500	58.41	FeAl + $FeAl_2$	-	-
	800	58.02	FeAl + $FeAl_2$	-	-
50.86	Cast	50.93	$FeAl_2$	-	-
	500	51.07	$FeAl_2$	-	-
	800	50.67	$FeAl_2$	-	-

Table 4 (Cont'd).

47.91	Cast	47.60	Fe_2Al_5 + $FeAl_2$	-	-
	500	48.23	Fe_2Al_5 + $FeAl_2$	-	-
	800	48.11	Fe_2Al_5 + $FeAl_2$	-	-
45.29	Cast	45.28	Fe_2Al_5	-	-
	500	45.20	Fe_2Al_5	-	-
	800	45.16	Fe_2Al_5	-	-
45.95	Cast	42.79	Fe_2Al_5 + $FeAl_3$	-	-
	500	43.03	Fe_2Al_5 + $FeAl_3$	-	-
	800	42.65	Fe_2Al_5 + $FeAl_3$	-	-
	Cast	41.07	$FeAl_3$ + Fe_2Al_5	-	-
	5 0	40.50	$FeAl_3$ + Fe_2Al_5 (traces)	-	-
40.83	800	40.68	$FeAl_3$	-	-
	Cast	29.64	$FeAl_3$ + Al	-	-
29.27	500	30.14	$FeAl_3$ + Al	-	-

Information on ternary phase diagrams Fe-Al-x is extremely scarce [195, 247]. K. Leberg and V. Shmidt carried out a study of the ternary system iron-aluminum-carbon using procedures of thermal, microscopic, and X-ray analysis [228]. They studied systems containing up to 20% aluminum and up to 3% carbon. The authors demonstrated that the nature of equilibrium in the iron corner of the ternary system iron-aluminum-carbon is determined by separation of the ternary carbide K, whose composition was not definitively clarified. The phase diagram for aluminum-iron-silicon is complex and has not been adequately studied [87]. The region of the ternary solid solution α of the aluminum corner is extremely insignificant.

During diffusion of iron in aluminum containing silicon the formation of the following phases in a diffusion layer is possible, depending on the concentration of the indicated component: a solid

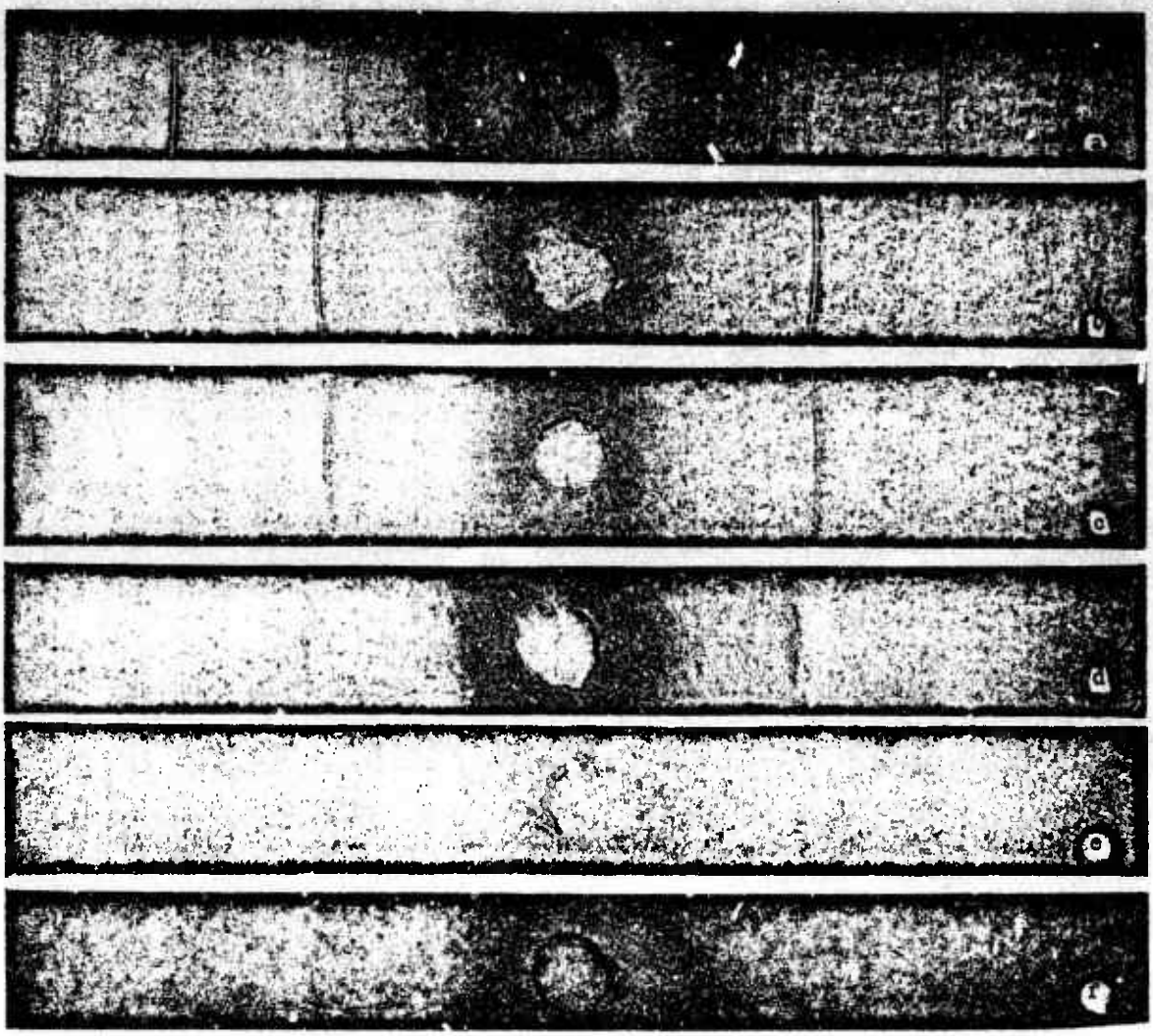

Fig. 7. X-ray patterns of aluminum and binary iron-aluminum alloys: a) Al on Cr; b) Fe_3Al; c) FeAl; d) $FeAl_2$; e) Fe_2Al_5; f) $FeAl_3$.

solution of α-(AlFeSi) on an aluminum base, α + $FeAl_3$, α + Fe_2Al_7, α + $FeSiAl_5$ and α + $FeSiAl_5$ + Si.

Study of a system of three components, aluminum-iron-zinc, was carried out by E. Gebhardt [195]. Initial materials for preparing the alloy were zinc (99.99%), aluminum (99.99%), and armco iron (99.95%).

Alloys containing less than 10% iron can be obtained by smelting pure metals under a layer of flux in unglazed porcelain crucibles. It was substantially more difficult to prepare alloys

containing more than 10% iron, since the higher temperatures of the liquidus for these alloys lead to the beginning of evaporation of the zinc. Preparation of alloys in closed crucibles led to explosion.

3. Properties of Intermetallic Compounds of the Aluminum-Iron System and Certain Laws Governing Their Formation

As has been noted, the major obstacle in joining aluminum to steel (besides the substantial differences in the physicochemical properties of the joined metals) is the formation of intermediate compounds - intermetallic phases of the Fe_nAl_m type - during contact heating above certain temperatures [229, 245]. Depending upon composition, these intermediate compounds possess ordered or unordered crystal structures; certain of them have definite chemical compositions and others dissolve a substantial quantity of their own components, as a result of which they form homogeneous regions (in a certain interval of concentrations).

Intermetallic compounds possess the following physical properties: brittleness and high hardness with respect to the hardness of their constituent components. Although many intermetallic phases are known in aluminum, there are few data on their properties. In certain cases the crystal structure is known, but information on it is frequently contradictory. Study of mechanical properties is, as a rule, limited to measurement of microhardness of these compounds in the aluminum matrix.

The strength properties of intermetallic iron-aluminum phases in pure form have not been studied, owing to the difficulty of obtaining these substances. Only limited information is available [27, 29] on the properties of the transition layers obtained during casting of bimetallic compounds; rupture strength on the order of 3-4 daN/mm^2; shear strength up to 7 daN/mm^2; impact toughness of 0.008-0.01 MJ/m^2, and other characteristics, given in Table 5.

Table 5. Certain properties of intermediate compounds Fe_nAl_m.

Alloy	Al content, %	Microhardness		Density		Linear coefficient of thermal expansion, $\alpha \cdot 10^{-6}$, 1/deg
		measured	literature data	measured	literature data	
Fe_3Al	13.9	250-350	340	6.67	-	14.6
FeAl	32.6	400-520	650	5.37	-	18.9
$FeAl_2$	49.1	1000-1050	1090	4.36	-	17.9
Fe_2Al_5	55.0	1000-1100	1050	4.11	4.04-4.05	15
$FeAl_3$	59.0	820-980	770	3.95	3.77-3.81	-
Fe_2Al_7	63.0	650-680	-	-	-	19.35

Despite the brittleness of intermetallic compounds at low temperatures, at high temperatures they become ductile to a certain degree [229]. The intermetallic compounds rarely possess perfected or close to ideal crystal structure [62].

Alloying of solid solutions based on intermetallic compounds would permit substantial alterations in their properties, especially mechanical properties. The mechanism for such alloying is not altogether clear; in work [245] it is indicated that in this case the creation of substitution solid solutions is possible. In the multiphase alloy formed during such alloying the determining influence of the second phase is reduced to an increase in mechanical properties at the expense of its inherent strength, especially at high temperatures. Here the dependence of strength (hardness) of the intermetallic phase on temperature is expressed by a straight line with a deflection (Fig. 8a). The point of inflection for these compounds does not equal half the value of the melting temperature, as holds true for pure metals, but is normally located in the 0.5-0.75 t_{melt} region; for the compounds $FeAl_3$ and Fe_2Al_5 this comprises about 460 and 450°C, respectively. On the basis of this fact the hypothesis was put forward [229] that different mechanisms exist for the deformation of intermetallic

phases, acting on both sides of the temperature point of inflection $t_к$: below point $t_к$ a slipping process predominates, while above it determined diffusion processes of dislocation displacement and shifting of grain boundaries occur.

At low temperatures the complexity of the crystal lattice structure of intermetallic compounds hampers slipping processes and it is possible to assume that their atoms are joined by strong localized bonds. Slipping or displacement of atoms relative to one another occurs extremely easily at elevated temperatures, owing to weakening of the interatomic bonds in the region above the temperature point $t_к$.

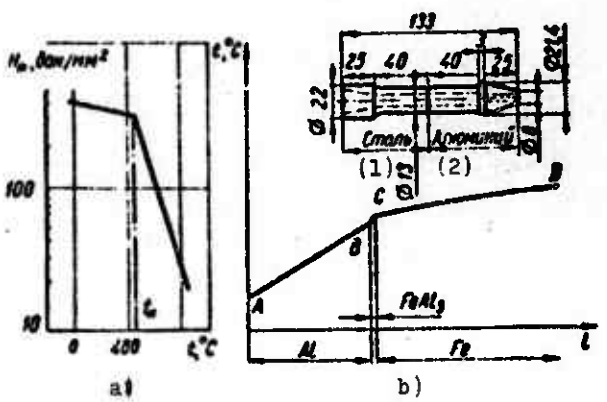

Fig. 8. Temperature dependence of hardness and heat conductivity of intermetallic phases: a) for Fe_nAl_m; b) for $FeAl_3$ (AB corresponds to the steel portion of the specimen and BC, to the compound $FeAl_3$, and CD to the aluminum portion of the specimen [191]). The average thickness of the FeAl layer is ∿0.12 mm. KEY: (1) Steel; (2) Aluminum.

In work [191] by I. Garcia the coefficient of thermal conductivity is determined for the intermetallic compound $FeAl_3$. Thermal conductivity was measured on an installation whose basic elements were a small resistance furnace, a wattmeter, and two thermocouples. One thermocouple was fastened rigidly inside the furnace and the other, moving inside a hollow bimetallic specimen, was used to measure the thermal conductivity of the latter and for automatic recording of thermal conductivity in the form of a curve on a graph.

Comparison of the microstructure on different segments of this specimen in the zone of contact between aluminum and steel with

the curve of the change in thermal conductivity made it possible to detect a small segment with a low value of the coefficient of thermal conductivity - 7.94 W/(m·deg) (Fig. 8b).

For a correct understanding of the processes occurring during calorization of iron and also during welding of iron to aluminum, it is necessary to have available sufficiently reliable data concerning the mobility of atoms in the diffusion interlayers which arise in the zone of contact of the two metals and especially in the intermediate intermetallic phases. Intermetallic compounds are usually obtained by smelting in an arc furnace on a copper water-cooled bottom, by the method of replacement of the eutectic, or by ordinary smelting under a layer of flux. In this case the intermetallic compounds are obtained in the form of ingots weighing 20-30 g or in the form of a crucible. As a rule, after such smelting it is necessary to carry out mechanical treatment of the extremely hard intermetallic alloy; however, this is not always possible. Alloys obtained by these methods are porous and are broken up during the cooling process; this is due to contamination of the boundaries of the intermetallic compounds and by the presence of oxide films, oxygen, etc. In order to determine the characteristics of the individual phases, a method was proposed and realized in practice for obtaining intermetallic compounds of the iron-aluminum system in the form of rods 3-10 mm in diameter and up to 200-250 mm in length [132].

Smelting of an intermetallic compound of definite stoichiometric composition was accomplished in a vacuum furnace by the firm "Gereus" [exact spelling not determined - Translator]. A magnesite crucible was used to avoid enriching the intermetallic compound with carbon during smelting. After the melting chamber was vacuum-treated, it was filled with argon or helium. In order to ensure that the intermetallic specimen would have a cylindrical shape of the required diameter a special device was used to pump the molten metal into a quartz tube up to 10 mm in diameter; one

end of the tube was dipped in the melt and the other was connected with the evacuation (vacuum) device.

To avoid contamination of grain boundaries of the intermetallic specimen with oxide films and inclusions, the pulling (suction) of the sample into the quartz tube was carried out from the middle portion of the molten metal in the crucible; the high rate of cooling of the metal in the quartz tube helped to ensure that the obtained intermetallic compounds would have pure boundaries, without inclusions, porosity, or any type of defect.

Mark AV000 Al and iron (Fe 99.97%) were used as the initial materials during smelting. The composition of the charge corresponded to the phase composition on the phase diagram. Chemical (Table 6) and X-ray analyses were carried out to establish correspondence of the composition of the obtained alloys to the composition of the chemical compounds on the phase diagram.

Table 6. Data from chemical analysis of alloys.

Alloy	Composition per the diagram, wt.%		Al content according to chemical analysis, wt.%	Structural type of lattice
	Fe	Al		
Fe_2Al_7	37.07	62.93	63.32	Monoclinic
$FeAl_3$	40.82	59.18	59.40	"
Fe_2Al_5	45.29	54.71	54.92	Rhombic
$FeAl_2$	50.87	49.13	49.??	Rhombohedral
FeAl	67.43	32.57	33.64	Isostructural;
Fe_3Al	86.13	13.87	14.04	structure of Cu$^{??}$ type

As an example, Fig. 9 gives the external appearance (a) and nature of fracture (b) of the intermetallic compound $FeAl_2$. As is clear from the figure, specimens of intermetallic compounds have a clean smooth surface (making it possible to avoid subjecting them

to mechanical working) and a fine-crystal fracture in which there are no visible defects. Analysis of the microstructure indicates the presence of adequately clean grain boundaries. Data from X-ray structural analysis confirmed the fact that the given phase is inherent to $FeAl_2$ in strict correspondence to the stoichiometric composition.

Fig. 9. External appearance (a) and nature of fracture (b) for the intermetallic compound $FeAl_2$.

Analogous data were obtained for all phases in accordance with the iron-aluminum phase diagram. The suitable quality of the intermetallic compounds enabled us to use them as standards in determining microhardness, electrical resistivity, diffusion coefficients, and mechanical characteristics.

From the microstructures shown on Fig. 10 it is clear that the obtained alloys are sufficiently uniform, with the exception of the alloy corresponding to the phase Fe_2Al_7. Photographs of the microstructure of the latter show segments of a second phase, insignificant in size, between the grains of the intermetallic compound.

Figure 11 gives data on the properties of intermetallic compounds in cast (unmarked columns) and annealed (shaded columns) states.

The microhardness of the phases Fe_2Al_5, Fe_2Al_7, $FeAl_3$, and $FeAl_2$ varies within the interval 960-1150 daN/mm^2; with an increase in iron content the microhardness is reduced to 660 daN/mm^2 (phase FeAl) and 270 daN/mm^2 (Fe_3Al). To determine electrical conductivity of the intermetallic phases specimens 8-10 mm in diameter and 120 mm in length were manufactured. The specimens were clamped in

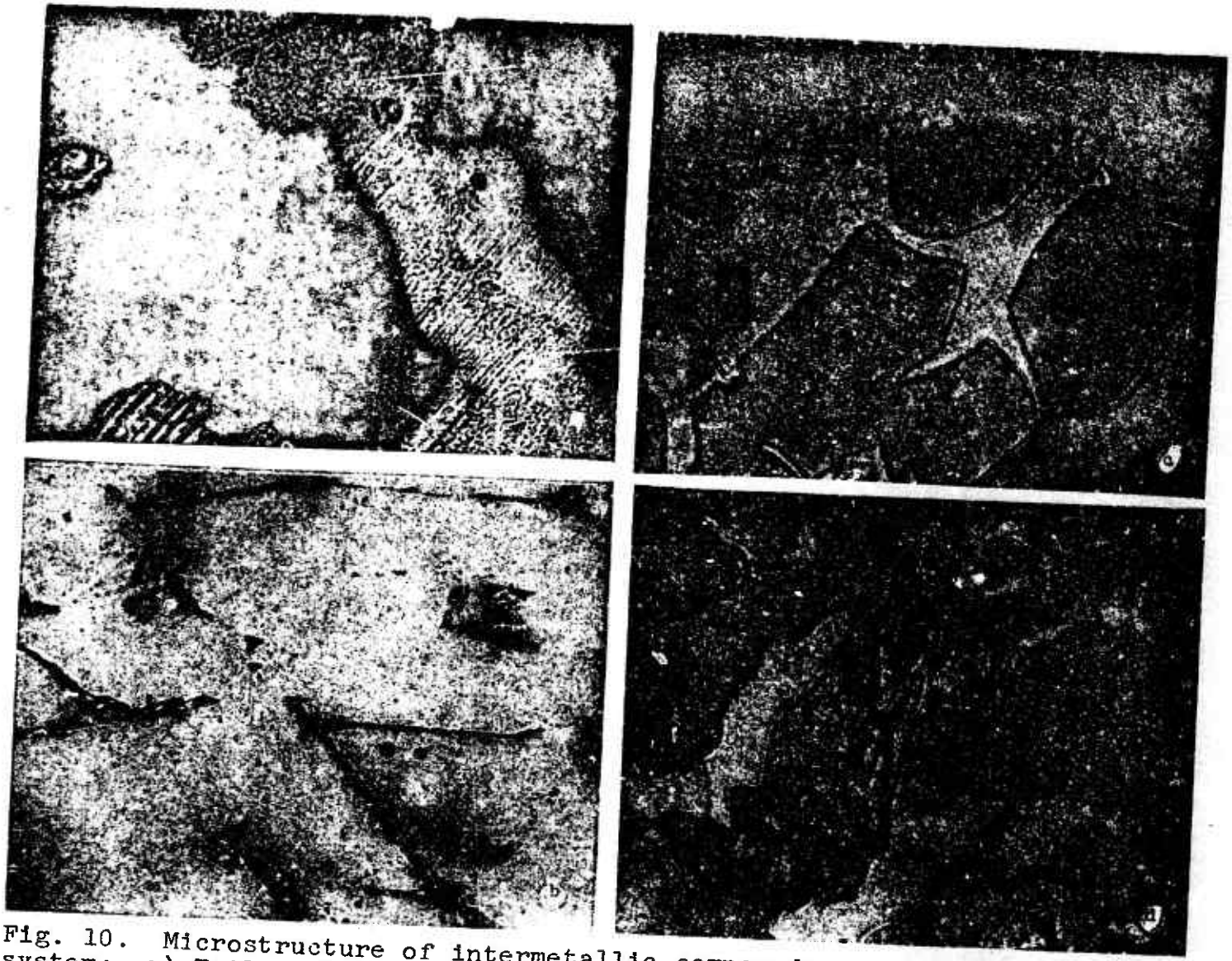

Fig. 10. Microstructure of intermetallic compounds of the iron-aluminum system: a) $FeAl_3$; b) Fe_2Al_7; c) Fe_2Al_5; d) $FeAl_2$ (×500); e) FeAl; f) Fe_3Al (×500).

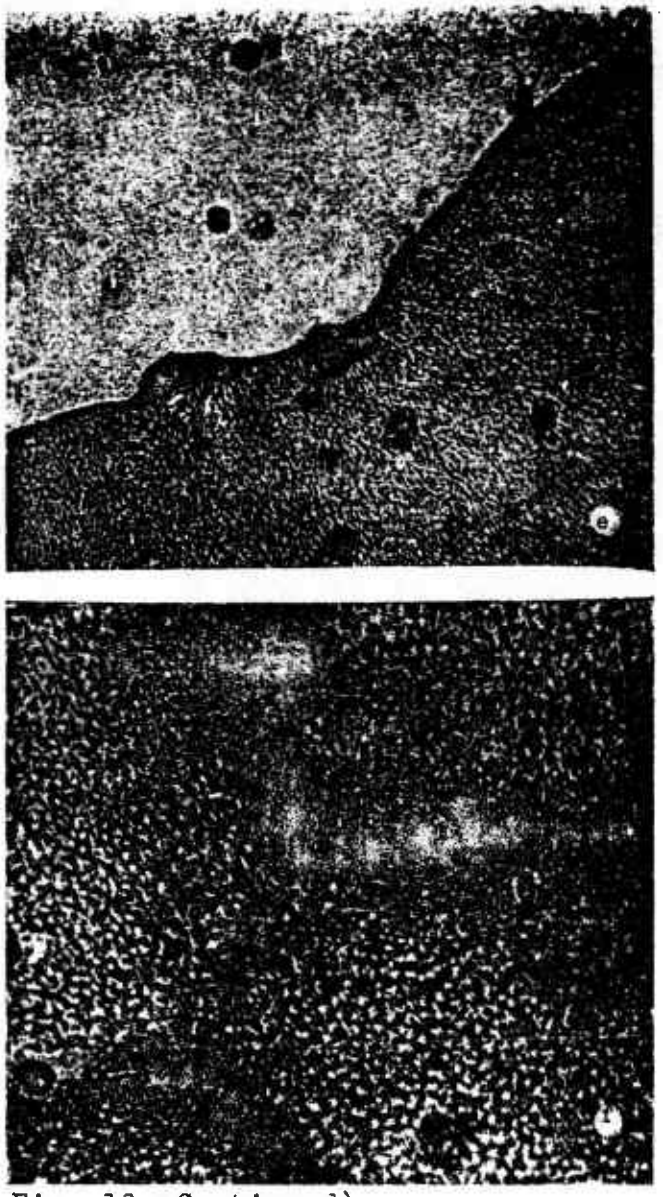

Fig. 10 (Continued).

a special attachment with movable contacts, from which the voltage drop was taken. The measurement base comprised 60 mm. Resistance was measured over a double-bridge d-c circuit with internal and external standard resistors (a type R-329 bridge was used). The magnitude of electrical resistance in each case was determined as the average of three to five measurements. Electrical resistivity of intermetallic phases of the iron-aluminum system differs little in the cast and annealed states. The phase Fe_2Al_5 is distinguished by anomolously high electrical resistance (3.3 $\Omega \cdot mm^2/m$).

The diffusion mobility of iron in the phases indicated above was investigated [88] by means of radioactive tracers in the temperature interval 900-1150°C. Before the diffusion research, the intermetallic phases of the iron-aluminum system were subjected to prolonged homogenizing annealing at 1100°C in a medium of argon for several days; this led to the formation of a coarse-grained structure, which remains stable through the duration of all diffusion annealings.

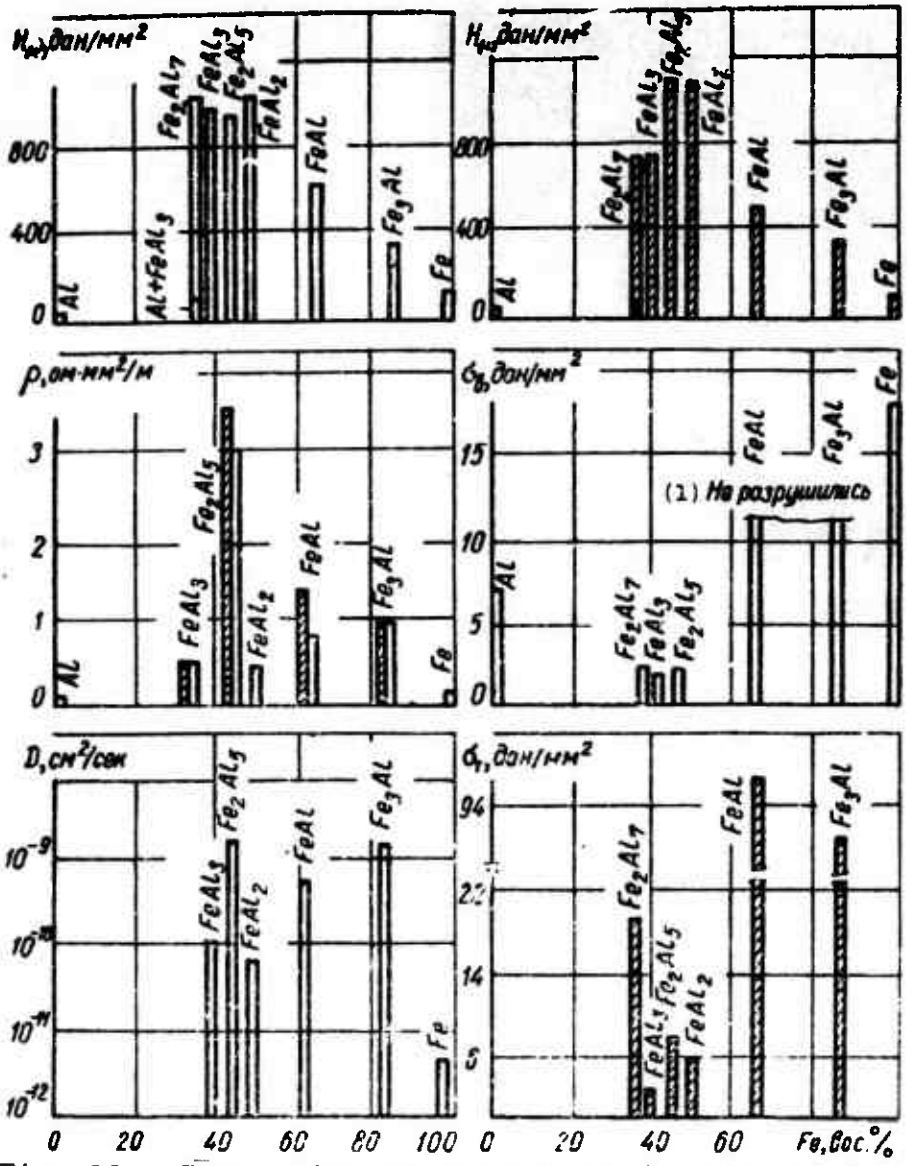

Fig. 11. Properties of intermetallic phases of the iron-aluminum system.
KEY: (1) Not destroyed.

Parallel shape of the faces was ensured by grinding. A thin layer (about 1 μm) of iron containing Fe^{55} was applied to one of the faces by means of an electrolyte consisting of a mixture of six parts of ammonium oxalate (saturated solution) and one part saturated ferric chloride (solution with a pale-green color). The specimens had an activity on the order of (5-6) 10^3 pulse/min. Diffusion annealing was carried out in the 600-1100°C interval, with the temperature maintained to an accuracy of ±10 degrees. Diffusion coefficients were determined by removing layers according

to the known formula $D = -0.1086/\tau \text{ tg } \alpha$, where τ is annealing time and tg α is determined from the graph of the experimentally determined relationship lg c (c is the concentration of radioactive atoms) from the square of the depth of the diffusion layer. Values of the coefficients of self-diffusion for iron and its alloys with aluminum in the investigated temperature interval are given in Table 7 and on a diagram (Fig. 11).

The obtained values for coefficients of self-diffusion for iron and its alloys with aluminum, corresponding in composition to certain intermetallic phases, in the investigated temperature interval attest to the fact that an increase in the concentration of the low-melting metal does not lead to a monotonic change in the values of the diffusion coefficient. This is apparently connected with particular features of the structure of the corresponding intermetallic phases. The Fe_2Al_5 has the highest value of diffusion coefficient. Tensile testing established the fact that the phases Fe_2Al_7, $FeAl_3$ and Fe_2Al_5 possess lowest strength (1.8, 1.5, and 1.7 daN/mm^2, respectively). These data attest to the fact that there is a measurable reserve of strength in the investigated compounds. Strength of the compound $FeAl_3$ turned out to be least (1.5 daN/mm^2) under compression. As is evident from the diagram, a deviation in compressive strength is observed in the Fe_2Al_7 phase (19 daN/mm^2).

The presence of intermetallic compounds in the form of individual inclusions and, especially, as continuous interlayers also has an essential influence on the corrosion resistance of welded joints.

Studies were made of the chemical properties of the metals to be joined and of the intermetallic phases in certain solutions, and evaluations were made of diffusion processes between unlike metals on the basis of layer-by-layer phase analysis; this made it possible to study diffusion layers which are nonuniform in composition and structure.

Table 7. Diffusion coefficients of intermetallic phases.

Alloys	Diffusion coefficients, cm^2/s, at T, °K									
	1373	1323	1273	1173	1073	973	873			
γ-Fe	$1,83 \cdot 10^{-10}$	$1,11 \cdot 10^{-10}$	$2,23 \cdot 10^{-11}$	$7,0 \cdot 10^{-12}$*	—	—	—			
$FeAl_3$	$2,14 \cdot 10^{-8}$	$1,18 \cdot 10^{-8}$	$4,0 \cdot 10^{-9}$	$2,3 \cdot 10^{-9}$	$3,25 \cdot 10^{-10}$	$4,65 \cdot 10^{-11}$	$2,06 \cdot 10^{-11}$			
FeAl	$3,0 \cdot 10^{-8}$	$1,57 \cdot 10^{-8}$	$1,41 \cdot 10^{-9}$	$7,9 \cdot 10^{-10}$	$4,42 \cdot 10^{-11}$	$9,67 \cdot 10^{-11}$	$1,31 \cdot 10^{-12}$			
$FeAl_2$	$6,3 \cdot 10^{-9}$	$1,62 \cdot 10^{-9}$	$4,48 \cdot 10^{-10}$	$2,3 \cdot 10^{-10}$	$5,11 \cdot 10^{-11}$	—	—			
Fe_2Al_5	$1,98 \cdot 10^{-8}$	$1,23 \cdot 10^{-8}$	$6,15 \cdot 10^{-9}$	$2,24 \cdot 10^{-9}$	—	—	$1,67 \cdot 10^{-11}$			
$FeAl_3$	$1,31 \cdot 10^{-9}$	$5,0 \cdot 10^{-10}$	$2,08 \cdot 10^{-10}$	$1,09 \cdot 10^{-10}$	—	—	—			

*Coefficient of self-diffusion of Fe^{55} in γ-Fe was determined at 920°C.

Studies were made of specimens of the aluminum-steel bimetal preliminarily annealed at temperatures of 200, 300, 400, 500°C for 10 hours and at temperatures of 300, 400, 500, and 600°C for 20 min. Also studied were the intermetallic phases $FeAl_3$, Fe_2Al_5, $FeAl_2$, and FeAl of the iron-aluminum system, obtained artificially in the form of cylindrical rods 8-10 mm in diameter. Intermetallic compounds in the transition layer of the aluminum-steel bimetal were revealed by the method of anode dissolution of the specimen from the aluminum side.

In the course of electrochemical dissolution of the specimen-anode the emf was measured and the potential vs. time relationship was constructed.

Bimetallic specimens of AD1 aluminum and steel Kh18N10T 25 × 25 × 10 mm in size with holders attached to them were placed in a bath to measure potential. The bath contained dilute hydrochloric acid (1:3). Then the specimens were removed and placed in another bath, containing a 1:1 solution of hydrochloric acid; there they were subjected to etching for 1-3 min to remove a layer of metal. After a quick wash in water the specimens were once again placed in the bath designed to determine the solution potential. As layer after layer was removed by

etching the solution potential was determined in each of them; measurements were carried out more frequently close to the transition line.

Figure 12 shows results from measurement of solution potential for the aluminum-steel Kh18N10T bimetal and also for intermetallic phases of the Fe-Al system. Measurements were made in the solution indicated above.

4. Present Methods of Joining Aluminum and Its Alloys to Steels

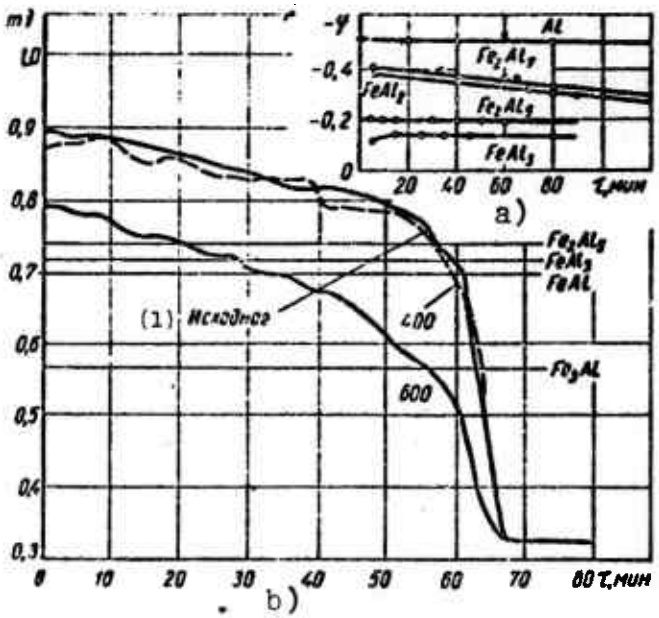

Fig. 12. Change in the solution potential mV as a function of dissolution time τ for intermetallic phases of the Fe-Al system and for pure aluminum (a) and for the bimetal aluminum-steel Kh18N10T (b). KEY: (1) Initial.

Few data are available on joining aluminum alloys to steels [91, 112, 148, 159, 215, 225, 241, 249]. There is interest in the method of joining aluminum and aluminum alloys to steel by welding with the use of one or several intermediate metals, analogous to the method of welding titanium to steel [51, 153]. However, analysis of the binary phase diagram of aluminum with various elements indicates that there is no one such metal or pair of metals. Elements which permit alloying of aluminum (Mg, Si, Cu, etc.) either have negligible solubility in iron or they form one or several intermetallic (intermediate) phases with it.

The formation of phases of intermediate composition in steel/aluminum joints is extremely undesirable, and their elimination

(or reduction) can, as will be shown below, substantially improve the mechanical properties of combined joints.

The periodical technical literature contains a few journal articles and short reports on experimental work. The most essential of these data are given below.

Existing methods of joining aluminum to steel can be tentatively broken down into the following basic types: 1) joining with the application of external pressure; 2) brazing of aluminum to steel; 3) the process connected with melting one of the metals (aluminum) - the so-called braze welding. The first two joining methods were studied in survey articles [133, 134, 187, 200, 202-206, 216, 217, 245].

The first information on practical methods of joining aluminum to steel by fusion was published as early as 1935 [208]. These materials indicated that direct joining of aluminum and its alloys with steel by fusion welding was difficult.

All methods of fusion welding are based on the creation of a reliable transition layer between aluminum and steel. H. Holler and A. Maier studied the process of gas welding of aluminum in the form of wire and sheet iron, precoated with tin solder. Pure aluminum was used as the filler material. The ultimate strength of the obtained joints reached 6-7 daN/mm^2.

With application of a zinc coating on the steel A. Muller [218] obtained a joint with a strength reaching 7.4 daN/mm^2. He also attempted to coat steel with aluminum for subsequent welding.

A number of works indicate the possibility of satisfactory welding of aluminum to steel with the application of a zinc coating on one metal or the other [176, 177, 223].

Numerous methods which have found development from the process "al'-fin" [alpha-deposition] are used to create a transition layer; the "al'-fin" is one method of joining aluminum and aluminum alloys to steel by teeming. For example, steel articles are calorized by immersing them in molten aluminum. After calorizing and before teeming the surface of the article may be covered with tin or copper [44]. In other cases [59, 82] the surface of the iron or steel is coated with a solution of ammonium chloride and dried at 150°C before immersion in the molten aluminum.

Grenell [45] presents information on the possibility of welding pipelines from unlike metals. A layer of aluminum is applied on steel tubes at the points to be welded, after which they are lap-welded with aluminum tubes.

The American investigators M. Miller and E. Mason [224] developed a method of welding aluminum to steel by means of tungsten and consumable electrodes in a medium of inert gases. Satisfactory results were obtained during welding of thin-walled tubes. Telescoping joints were destroyed at the weld under loads of 4-4.2 daN/mm^2. The average shearing force amounted to 7 daN/mm^2. Similar data (7-8 daN/mm^2) in shear tests were obtained by Van Sommeren [238] with welding by an analogous method. He also conducted experiments on the application of a high-quality film of aluminum on steel by metal spraying [238]. A film thickness of 0.0002 mm is sufficient to obtain a joint. However, the obtained layer of metal is joined weakly to the steel, since during application on steel the drops of metal are oxidized and the bond obtained between the coating layer and the steel is basically purely mechanical.

The literature also contains data on methods of joining aluminum and steel using tin and nickel coatings on the steel [9]. The positive influence of silver as a metal to be used for a transition layer is especially emphasized. Examples are given

of joining tubes of stainless steel with aluminum with an intermediate silver layer [7-11] and welding the cylinder of a piston engine, made of steel of the martensite class, to aluminum cooling fins [207]. It is indicated in the last work that the optimum magnitude of the galvanically applied layer of silver is 0.25 mm. The welds possess adequate strength and ductility.

As data from the various investigations indicate [12, 114], an intermetallic layer almost always arises along the steel/aluminum boundary during calorizing of steel by immersion and by the chemicothermal method. In particular, its appearance is unavoidable under the calorizing conditions recommended by M. Miller and E. Mason in their experiments (calorizing at temperatures of 700-800°C).

Interesting studies concerned with welding aluminum alloys to steels and with investigation of the properties of the obtained joints were carried out by G. A. Bel'chuk and co-workers [14-17]. They developed two types of technology for argon-arc welding of aluminum to steel.

According to the first variant, a layer of aluminum 0.1 mm thick is first applied to shipbuilding steel SKhL-4 and St. 4S by calorizing (at 700-740°C with a hold of 10 min). Argon-arc welding is used to lay pure aluminum in three layers on the surface of the initial layer under the following conditions: welding current 110-130 A, welding speed 0.12-0.24 m/min. A tungsten electrode 2 mm in diameter and an aluminum filler (AD1) 2 mm in diameter were used. Joining of the obtained aluminum facing to the steel occurs in the presence of an intermetallic layer up to 0.1-0.12 mm thick. Elements of aluminum or its alloys were then welded to the facing. The ultimate strength of the obtained butt joint reaches the value of the ultimate strength of pure aluminum - i.e., on the order of 8-10 daN/mm^2; strength values are somewhat lower for T-specimens.

In the second variant, the steel (after cleaning) is subjected to hot or galvanic zinc coating (zinc layer thickness 0.02-0.04 mm), after which three layers of pure aluminum are also built up on it by argon-arc welding under the same conditions.

A distinguishing feature of the technology developed by G. A. Bel'chuk for argon-arc welding of aluminum and its alloys to steel is the application of pure aluminum of brand AD1 (Si $\leq$ 0.2%) for a facing on calorized or zinc-coated steel. The use of wire with an increased magnesium content - e.g., brand AMg6 - did not give satisfactory results in terms of strength [18]. For this procedure for arc-welding of the indicated materials joints of limited strength were obtained. However, in the particular case when the joint must have a strength which is not equal to the strength of the aluminum alloy but only adequate, the developed technology can be recommended.

In the work by D. R. Andrews [183], concerned mainly with technological questions, a study was made of the welding of low-carbon steel to aluminum and its alloys. Sheet steel with a content of 0.08% C, steel tubes (0.15% C), pure aluminum, and three aluminum alloys (Al-Mn, Al-Mg, and Al-Mn-Mg) were used in the experiments. The steel was covered completely with a layer of aluminum, tin, or zinc, aluminum with 0.75% cadmium, and aluminum with 5% silicon by hot immersion, electrodeposition, and metal spraying. The ultrasonic method was used for local coating with tin and tin-zinc. During subsequent welding an intermetallic transition layer was formed over the coatings in all cases. During coating with a layer of tin by hot immersion a solid and brittle $FeSn_2$ phase is also formed; however, its quantity is insignificant and consequently the plastic properties of the welded joints are higher than, for example, joints of aluminum with zinc-coated or calorized steel. The average value of ultimate strength did not exceed 12 daN/mm^2 for all types of tested coatings. With a zinc coating the ultimate strength amounted to 10 daN/mm^2;

with tin it was 7.8 daN/mm^2. Owing to the poor quality of the coatings a large scatter in test data was observed. While he carried out a limited number of experiments, the author nonetheless draws a conclusion concerning preferred application of tin and zinc coatings obtained by electrodeposition before coating with aluminum. On the basis of this work refinements were made in the welding technology: for protection of the back side of the weld it is necessary to blast it with argon; the most suitable filler material is aluminum with 5% silicon. In one of the last studies Andrews [184] considers the formation of intermetallic layers during hot immersion. The author notes that during welding the thickness of these layers is increased and the plastic properties of the joints are impaired. He also studied the effect of heat treatment on the properties of welded joints; heat treatment was carried out with prolonged holds and at temperatures of 350-560°C. The rupture strength of steels coated with tin joined by the method of hot immersion to technically pure aluminum comprised the following values after holding for 15 days at 350, 400, and 450°C: 1.18, 1.18, and 1.26 daN/mm^2. Weld strength prior to heat treatment was 7.5-7.8 daN/mm^2.

According to data from Y. Sugiyama [237], prolonged temperature treatment of welds does not give the desired results (Fig. 13).

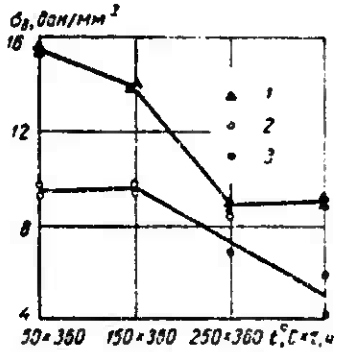

Fig. 13. Graph characterizing the effect of heat treatment on ultimate tensile strength for a weld between pure aluminum and steel with a zinc coating (filler material 4043). 1 - base metal; 2 - destruction of weld on base metal; 3 - destruction of weld on the interface.

Thus, analysis of different methods of joining aluminum to steel shows that the selection of the welding method must be guided by specific requirements imposed on the unit or the article as a whole. For a number of parts of limited shape it is possible to weld steel to aluminum by the application of pressure [175, 194].

Welding of all possible types of fittings (brackets, lugs, etc.) to, for example, the walls of vessels can be accomplished by means of an industrially produced insert of bimetal [125]. Vacuum-tube parts can be soldered [99, 100, 131]. Finally, to join large-dimension units of aluminum alloys to steel items it is necessary to develop methods of direct automatic welding of aluminum to steel.

Results obtained from tests differ and, owing to the different conditions under which the tests were carried out, they cannot be compared directly. At the same time analysis of literature data shows that, as a rule, the strength of combined steel/aluminum units does not exceed the strength of the pure aluminum - i.e., it reaches 8-12 daN/mm^2. Past research is of a tentative, laboratory nature. No description of industrially developed technology or testing of unit properties is given. At the same time the advisability of using a number of steel/aluminum structures can be validated only if the strength indices will be on a level with the strength of the aluminum alloys of the type AMts, AMg6, etc. Here it should be noted that in addition to joining aluminum-manganese, aluminum-magnesium, and other alloys with low-carbon steel for equipment of the most advanced technology operating under specific conditions, a primary problem is that of obtaining high-quality welds between stainless steel and these aluminum alloys.

Thanks to the rational use of aluminum units in combination with steel it is possible to lower substantially the weight of flight vehicles - i.e., to increase their range, create new types of structures and units for portable and stationary vessels, etc. Thus, we see it as necessary in our work to carry out a set of studies which will, on the one hand, make it possible to refine the nature of the interaction of molten aluminum with solid steel and to clarify the laws governing the formation and composition of intermetallic phases forming under various conditions and to plan for their regulation and, on the other hand, to use these studies

as the basis for the development and testing on specific industrial objects of the technology of joining aluminum alloys to steel so as to obtain strength indices of the steel/aluminum joints which are comparable to the strength of the aluminum alloys.

5. Search for Methods of Joining Aluminum to Steel by Fusion

Realization of the welding of aluminum to steel requires first of all correct selection of the type and indices of the heat source.

During the preliminary search for and selection of the welding method we tested methods which differ in the nature of the action on the base metal: welding with heat sources dependent upon and independent of the article and also welding with an independent double arc [74, 75].

A number of methods (welding with an aluminum strip electrode over the surface of the steel, welding with a steel wire over the aluminum surface, welding over liquid zinc, welding through an intermediate insert of copper and brass, etc.) were eliminated during subsequent examination; however, the application of certain methods creates definite possibilities for joining the metal pair which we selected, in particular during automatic welding under flux. Nevertheless, as will be shown below, this method has more limited application.

During manual argon-arc welding with a nonconsumable tungsten electrode over a plate of steel St. 3 using a filler wire of aluminum or its alloys, flowing of the molten aluminum is observed ahead of the pool on the steel; as a result the arc burns between the tungsten electrode and a thin layer of aluminum. The filler material, upon arriving in the pool on the steel, is spattered intensively and spreads over the surface of the heated steel. Therefore it would be more correct to call this process

soldering of steel with aluminum. If, however, continuous formation of a pool on the steel is achieved (for example by tilting the plate), as a result of interaction of the molten metals a bead is formed; immediately after termination of welding this bead begins to crack up intensively. During subsequent cooling the bead flakes off spontaneously.

The microstructure of the deposited metal is shown on Fig. 14. Large needles of the intermetallic phase predominate against a background of a solid solution of aluminum; the quantity of these needles grows with approach to the fusion line, with a solid layer of intermetallic compounds being formed on the fusion line itself. In connection with this, "cleavage" of the bead occurs, as a rule, close to the brittle intermetallic layer. Clearly, its elimination or reduction to the minimum possible thickness will facilitate an increase in strength of the bond between the two metals.

Fig. 14. Microstructure of weld metal during facing with a filler of aluminum AD1 on steel St. 3 (×300).

Strength can be increased by depositing zinc on the surface of the steel [15]. During subsequent facing the aluminum, pushing aside the zinc, interacts with the steel and forms a compound.

Owing to the fact that the reactivity of zinc with respect to the surface of the steel is higher than that of aluminum, during interaction the aluminum enters into contact with a purified steel surface, facilitating the production of an adequately strong bond. However, the formation of an intermetallic layer is inevitable in this case. Therefore the basic problem in developing a technology for welding aluminum to steel should include the elimination or reduction to the minimum possible thickness of this intermetallic layer.

The most widely varied methods were used to obtain minimum depth of fusion of the steel surface: argon-arc welding with a nonconsumable electrode at minimum possible currents, facing with aluminum strip 25-40 mm wide and 1 mm thick. The major drawbacks of the indicated methods reduce to impermissibly great degree of depth of fusion of the surface layers of the steel - the appearance of brittle phases.

During both automatic and manual welding with an independent arc it was not possible to achieve total removal of the oxide film from the aluminum surface; as a result, as a rule, there was no joining. The use of fluxes to deoxidize the aluminum surface complicated the process and did not lead to the desired results.

We tried preliminary metal spraying with zinc and aluminum on a surface of etched steel in a medium of argon with subsequent welding of the aluminum part to the steel. However, due to the fact that joining of the coating to the steel occurs as the result of mechanical adhesion the coating peels off during welding. Virtually no joint is formed.

In the course of the work we tested different designs of the welding head for welding with a double independent arc, electrical circuits, and also a wide variety of technological methods in order to ensure reliable quality of the joint. However, it is

clear that even those methods which ensure a minimum degree of depth of fusion and small duration of contact between the liquid and solid phases for aluminum-steel pairs do not completely eliminate the formation of brittle intermetallic compounds along the transition line.

Thus, not a single one of the tested methods of welding with the introduction of heat by direct, indirect, or combined methods makes it possible to avoid the formation of intermetallic compounds along the line of transition from steel to aluminum.

It was established that by preliminary coating of the surface of the steel part with a layer of aluminum (calorizing in a bath with molten aluminum or by means of hf currents) or with a layer of zinc (hot or galvanic zinc coating) with subsequent deposition on such surfaces of beads of aluminum alloys make it possible to join steel to aluminum alloys by welding.

However, when any of the described methods for joining steel to aluminum are used, when the liquid molten aluminum interacts with the surface of steel an interlayer with a greater or lesser quantity of solid and brittle chemical compounds of the type Fe_nAl_m is inevitably formed in the joint. It should be noted that the thickness of the intermediate layer is small, in contrast with that obtained when steel is joined to aluminum by the fusion of both metals. Therefore in this work during the study of the properties of the layer and of steel/aluminum joints major attention was paid to the process of the preparation of the surface of the steel for welding, and for welding to aluminum we applied the most widespread in industry method of argon-arc welding with a nonconsumable tungsten electrode with certain characteristic features in the technology of producing composite joints. There is another possible method - welding under flux; however, its application is extremely limited.

CHAPTER II

STUDY OF THE INTERACTION OF ALUMINUM WITH IRON AND STEEL DURING HEATING

In order to study the kinetics of the interaction of aluminum with iron and steel in a solid state two bimetal compositions were obtained by rolling: 1) aluminum/armco iron; 2) steel Kh18N10T/alloy AMg6 with a sublayer of mark AD1 aluminum.

The bimetals of aluminum and armco iron were obtained by single-component cold rolling. Here diffusion processes, which occur in the bimetal in hot rolling, were eliminated. The degree of compression during rolling was 54%. The thickness of the obtained bimetal was 5-6 mm. The bimetal of steel Kh18N10T and alloy AMg6 with an intermediate layer of aluminum was obtained by a multipass rolling method. Thus, the study of such a material is essentially reduced to studying the reation between aluminum and steel [3, 84].

Specimens measuring 20 × 20 × 5 mm were cut from bimetal sheets of aluminum AD1 and armco iron. The specimens were placed in vacuum quartz ampoules and annealed in muffle furnaces with the temperature regulated at ±5 deg. The annealing temperature (300, 400, 500, 540, 570, 600 630, 650°C) was selected such that it was possible to follow and study the change in structure in the contact zone of the studied metals in a solid state and in a state close to the melting temperature of aluminum. Annealing time varied from 15 min to 8-10 h. The specimens were air cooled together with the quartz ampoules. After cooling a layer of metal 1.5-2 mm thick

was removed from the surface of the specimens in order to eliminate the effect of surface hardening on the diffusion process. On one of the specimen surfaces a microscopic section was prepared, which was treated according to the method described thoroughly in [104, 120]. By means of the microscopic section the structure and nature of the forming intermetallic layer were studied, its thickness and microhardness measured, its phase composition and distribution of elements examined, and the nature and law of its growth determined.

1. Structure of Transition Zone

The microstructure was studied by means of a microscope set at different magnifications.

Table 8 presents data on the change in thickness of the intermetallic layer as a function of heating temperature and time. (The layer thickness is given in the tables and growth diagrams are mean arithmetic values of 20-40 measurings.) As follows from both the table and the data on metallographic analysis of the structure of the bimetal, which was heated according to the indicated regimes, the holding time required for the development of intermetallides in the welding zone depends basically on temperature. Thus, for example, at a temperature of 540°C the formation of the intermetallic layer occurred over 2 h, at 570°C this time was 0.5 h, and at a temperature of 600°C - 5 min.

At first the intermetallic layer consists of individual, seemingly disconnected pieces of intermetallides. In the individual sections it cannot be seen at all under a microscope with a magnification of 1000×.

Table 8. Thickness of intermetallic layer as a function of temperature and time of heating.

Annealing temperature, °C	Thickness of intermetallic layer, μm, during holding, h						
	0.25	0.5	1	2	4	6	8
540	Not found	Not found	Not found	6	8	9	10
570	The same	The same	5.1	8.5	10.2	12	14
600	5.7	-	8.5	14	-	15.8	16
	10.7	14	30.7	51	56.6	85.8	-
	(on the part of aluminum)						
650	Not found	Not found	148	199	310	420	-
	(on the part of iron)						
	10.7	14	168	246	384	477	-
	(overall thickness)						

In examining the structure of the aluminum/armco iron bimetal by means of electrolytic and chemical etching in the state after rolling, it was possible to detect on the contact border oxide inclusions of an oblong shape on the iron base as well as segments of the accumulating aluminum oxide film. The oxide inclusions were encountered relatively infrequently along the contact border, so that henceforth their influence on the growth kinetics of the layer will not be considered. However, they serve as a kind of indicator by which it is possible to determine the current direction of diffusion processes in the bimetal.

With an increase in holding time at each of the studied temperatures the thickness of the intermetallic layer increases.

In Fig. 15 we see that thickness of the layer along the contact line is not uniform, and that in certain sections thick and thin areas in the layer appear. However, despite such nonuniformity in the thickness of the layer, it does grow under diffusion conditions and depends on the temperature and time conditions of heating.

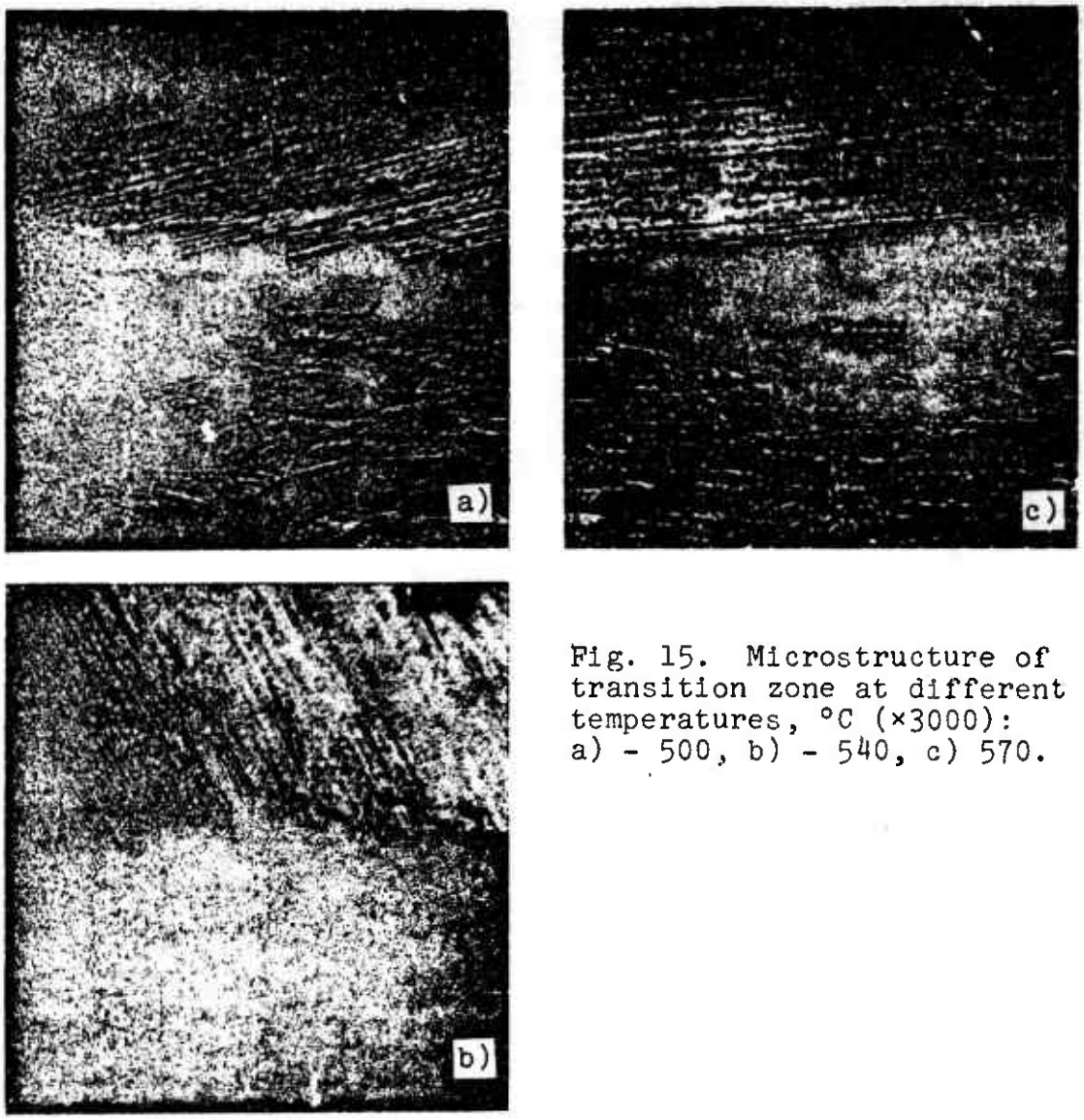

Fig. 15. Microstructure of transition zone at different temperatures, °C (×3000): a) - 500, b) - 540, c) 570.

All of the above is also true of a temperature range right up to 600°C. As the heating temperature of the armco iron/aluminum bimetal increases up to 630 and 650°C sharp changes occur in the transition zone of the studied compounds.

In the case of heating up to a temperature of 650°C for 15 and 30 min an intermetallic layer of nonuniform thickness forms in the contact zone. The structure of this layer is similar to that of the layer formed at a temperature of 600°C. Layer thicknesses at these holding times are 10 and 14 μm, respectively. As holding

time is increased up to 1 h and beyond the intermetallic layer acquires a characteristic shape: the interface boundary between the intermetallic layer and the iron has the shape of "tongues" or "teeth," deeply penetrating into the iron (Fig. 16). As we see in the microstructure, the individual tongues of the layer cut deeply into the iron, whereas the others fall behind in their growth. With an increase in holding time up to 1 h and above the thickness of the layer increases by ten times. Thus, after a holding time of 1 h the thickness of the intermetallic layer is 160 μm; with an increase in holding time up to 2 h it is 240 μm.

Fig. 16. Columnar orientation of structure of intermetallic phase. Heating to a temperature of 650°C for 4 h (×300).

In order to explain the nature of growth in the layer the dependences of layer thickness were plotted as a function of heating time for each of the studied temperatures (Fig. 17).[1] We are struck by the fact that at temperatures of 813 and 843°K the growth curves for intermetallic layers do not pass through the origin of the coordinates. Heating up to a temperature of 923°K causes intensive growth in the intermetallic layer, as already pointed out above. However, on the curve (Fig. 17) corresponding to a temperature of 923°K only the total thickness of the layer is noted. Moreover, heating up to a temperature of 923°K causes a change in shape and intensive growth in the forming intermetallide.

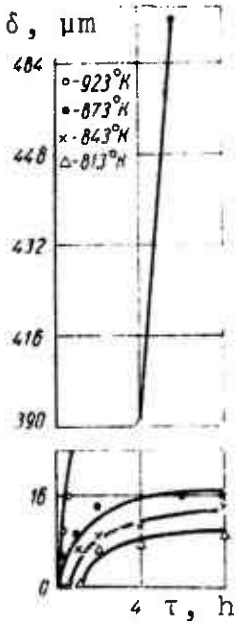

Fig. 17. Thickness of intermetallic layer in armco iron/aluminum bimetal as a function of holding time during heatings.

Detailed study of the structure of the layer forming in this case and measuring the thickness of the phases constituting the layer, diffusing in both aluminum and in iron, made it possible to plot a diagram (Fig. 18), from which we learn that as holding time increases at a temperature of 923°K the overall thickness of the

[1]In thermodynamic calculations the temperature is given in Kelvin degrees, in other cases - centigrade.

intermetallic layer increases, generally because of the thickness of phase Fe_2Al_5 (the growth of "tongues"). The growth of the layer, which consist of phase $FeAl_3$, toward the alumin[illegible] less intense than that consisting of phase Fe_2Al_5.

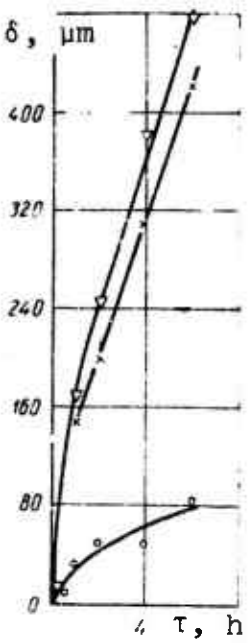

Fig. 18. Thickness of intermetallic layer in armco iron/aluminum bimetal as a function of holding time at a temperature of 650°C: ∇ - thickness of overall intermetallic layer, × - thickness of Fe_2Al_5 layer, O - thickness of $FeAl_3$ layer.

2. Intermetallic Layer and the Law of Its Growth

Studying the rate of growth of intermetallic phases in the presence of diffusion of the different metals has significant value. The intermediate layers, which are formed in the application of coatings and in the heating of the bimetallic compounds (in thermal processing, welding) usually consist of one or several phases. The properties of these compounds are determined by the structure and thickness of the individual phases. If during the diffusion process several intermetallic phases develop in the form of strictly delineated layers, then each of the layers will grow at a certain rate with the passage of time or with a change in temperature. The rate of growth of the intermetallic layer is usually measured by one of two methods: either the total amount of the diffusing element is determined through the interface or the thickness of the intermetallic layer is measured [36].

Most researchers who are studying the law of growth in the intermetallic layer measure its thickness and find the diffusion coefficient from equation $y^2 = 2pt$, assuming in advance that the law of growth is parabolic in nature [28, 81]. In addition, statistical processing of the results of a large number of measurings of the thickness of the intermetallic layer indicates that in not all cases by far can the law of growth be expressed uniquely in all stages of the process. Actually, in plotting a graph with respect to all experimental data for layer thickness in relation to holding time and in subsequent processing of these data by the method of least squares it is not possible to obtain a unique dependence for layer growth. Apparently this regularity is paralinear [77]. Similar data were obtained in studying the oxidation of a number of metals: the curve for the thickness of the oxide film versus time can include two or several dependences. The metal or the alloy begins to oxidize according to the parabolic law, and then there is a transition to linear oxidation.

We will attempt, based on the experimental data which we have obtained, to determine through calculation the law of growth in the layer [23, 92].

If we designate the thickness of the layer as x and the heating time as τ, then in the general case the relationship between them can be expressed as:

$$x^n = k\tau, \qquad (1)$$

where n is the exponent, k - the coefficient proportional to the diffusion coefficient.

If we take the logarithm of equation $n \ln x = \ln k + \ln \tau$, $\ln x = \frac{1}{n} \ln k + \frac{1}{n} \ln \tau$ and replace $\frac{1}{n} \ln k$ by quantity c and $\frac{1}{n}$ by quantity b, then we get an equation for the straight line which does not pass through the origin of the coordinates: $\ln x = c + b \ln \tau$, where b is the tangent of the slope of the line toward axis $\ln \tau$, and c is the segment which is intersected by the straight line on axis $\ln x$.

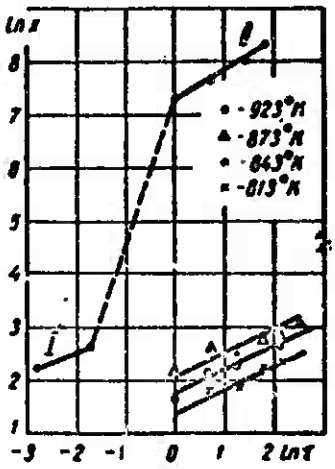

Fig. 19. The quantity ln x as a function of ln τ.

The dependence of ln x on ln τ is illustrated in Fig. 19.

If we determine the coefficient n with respect to the ratio of ln τ to ln x for the calculation lines obtained at temperatures of 540, 570, and 600°C, we will get a value which is close to two.

The dependence of ln x on ln τ for a temperature of 650°C is of considerable interest. As already mentioned, at this temperature we observe a rapid growth in the intermetallic layer. The dependence of ln x on ln τ for this temperature can be expressed as a straight line having a break, i.e., consisting of two parts (I and II).

The diagram in Fig. 19 reflects the growth of the overall layer, including the layer on the iron side and the layer on the aluminum side.

Segment I describes the growth of the layer on the aluminum side, which is caused by diffusion of the iron into the aluminum at holding times of 15 and 30 min while the aluminum is still in a solid state. Thus, this segment of the straight line is closer to the lines corresponding to temperatures of 813, 843, and 873°K.

Segment II describes the growth kinetics of the intermetallic layer toward the iron. The layer on the aluminum side has only a fraction of the thickness of that on the iron side. Segment II of the line describes the change in layer thickness which occurs in the solid state. Aluminum at 650°C and holding times of 15 and 30 min is already partially fused.

The intermetallic layer in segment I of the straight line resembles the layers which develop at temperatures of 813, 843, and 873°K, while the intermetallic layer corresponding to segment II is characterized by the "tongues."

If we determine exponent n in equation (1), we get a value close to two.

In order to explain the regularity of the growth in the intermetallic layer in the presence of interaction between the iron and the aluminum in a solid state, we will limit ourselves to segment I. In this case the growth law is parabolic in nature and can be expressed by the equation

$$x^2 = kt. \tag{2}$$

The established parabolic dependence of growth in the new phase on time lets us calculate activation energy Q of the diffusion process. According to the Arrhenius formula [25, 210]

$$K = K_0 \exp\left(-\frac{Q}{RT}\right). \tag{3}$$

where K_0 is a constant quantity, R - the gas constant, T - absolute temperature, °K.

Equation (3) shows that between K and $\frac{1}{T}$ there should be a linear relationship under the condition of a process activated one time. Quantities Q and K_0 are determined by the slope of the straight line and the point of its intersection with the axis of the ordinate, since

$$\ln k = \ln K_0 - \frac{Q}{RT}. \qquad (4)$$

The experimental values obtained by us for these quantities are shown in Fig. 20.

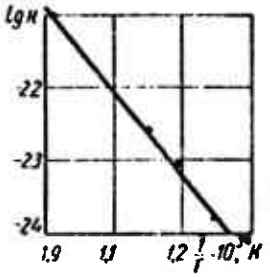

Fig. 20. Dependence of $\ln k = f(\frac{1}{T})$ for armco iron/aluminum bimetal.

Thus, the law of growth in the intermetallic layer when iron interacts with aluminum in the solid state at temperatures of 540-650°C can be written in the form of equation

$$x^2 = 3{,}3 \cdot 10^{-4} \exp\left(-\frac{25000}{RT}\right) t. \qquad (5)$$

The law of growth in the intermetallic layer in a temperature range of 605-655°C, obtained in [143], has the form of

$$x = 3.5 \cdot 10^3 t^{\frac{1}{2}} \exp\left(-\frac{27{,}000}{RT}\right).$$

Thus, the data obtained by us are extremely close to those of Sibata, Morodzumi, and Koda [143], despite the different method of processing the experimental data.

According to the data of [144] the law of growth in the intermetallic layer in the case of an interaction between liquid aluminum and solid iron, which forms primarily because of the diffusion of aluminum into iron, in the temperature range of 700-960°C has the form of

$$x^2 = 0{,}033 \exp\left(-\frac{13100}{RT}\right) \tau. \qquad (6)$$

As we learn from the equation, the activation energy when iron and aluminum interact in solid-liquid states is less by a factor of two than the activation energy calculated in our experiments and in [210]. For this reason it is obvious that in the solid state, where we observe primarily the diffusion of iron into aluminum, the growth of the intermetallic layer is slowed (Q = 25,000 cal/g·atom), whereas in the transition to the solid-liquid state, where diffusion of the aluminum into the iron predominates, there is an intensive growth in the layer (Q = 13,100 cal/g·atom).

The structure of the transition zone of bimetallic sheets of steel Kh18N10T and the alloy AMg6 (aluminum clad) immediately after rolling and after various heat treatment regimes was also studied. In studying the structure an electron microscope method was used along with metallographic, X-ray crystallographic, and X-ray spectral methods, and microhardness was also measured.

Results of microscopic and electron microscopic analyses showed that in bimetal specimens in the state after rolling intermetallic phases are not formed in the transition zone. The transition line in the bimetal is not uniform. Because of the different degrees of compression during rolling, the texture and structure of the steel are different in different sections.

In electrolytic polishing the basic components of the aluminum part of the section were very apparent. This part might consist of two to three regions, which could be distinguished from the basic mass of the metal by the nature of their etching (Fig. 21a).

The study of specimens under the optical microscope in the state following rolling showed that in the contact area between aluminum and steel there was a bright strip on the aluminum, which could be distinguished by its etchability from the basic aluminum; its microhardness was higher than that of the aluminum. In the annealing process, until the formation of the intermetallic compound takes place, there is a certain increase in the thickness of this strip

(Fig. 21b). After the advent of the intermetallic layer growth of the bright strip practically ceases, and it is gradually displaced by the intermetallic layer (Fig. 21c). We might assume that the increased microhardness of this strip, and its different reaction to the effect of the etching agents in comparison to the original metals could be explained by the formation of a solid solution zone of the diffusing element in the aluminum.

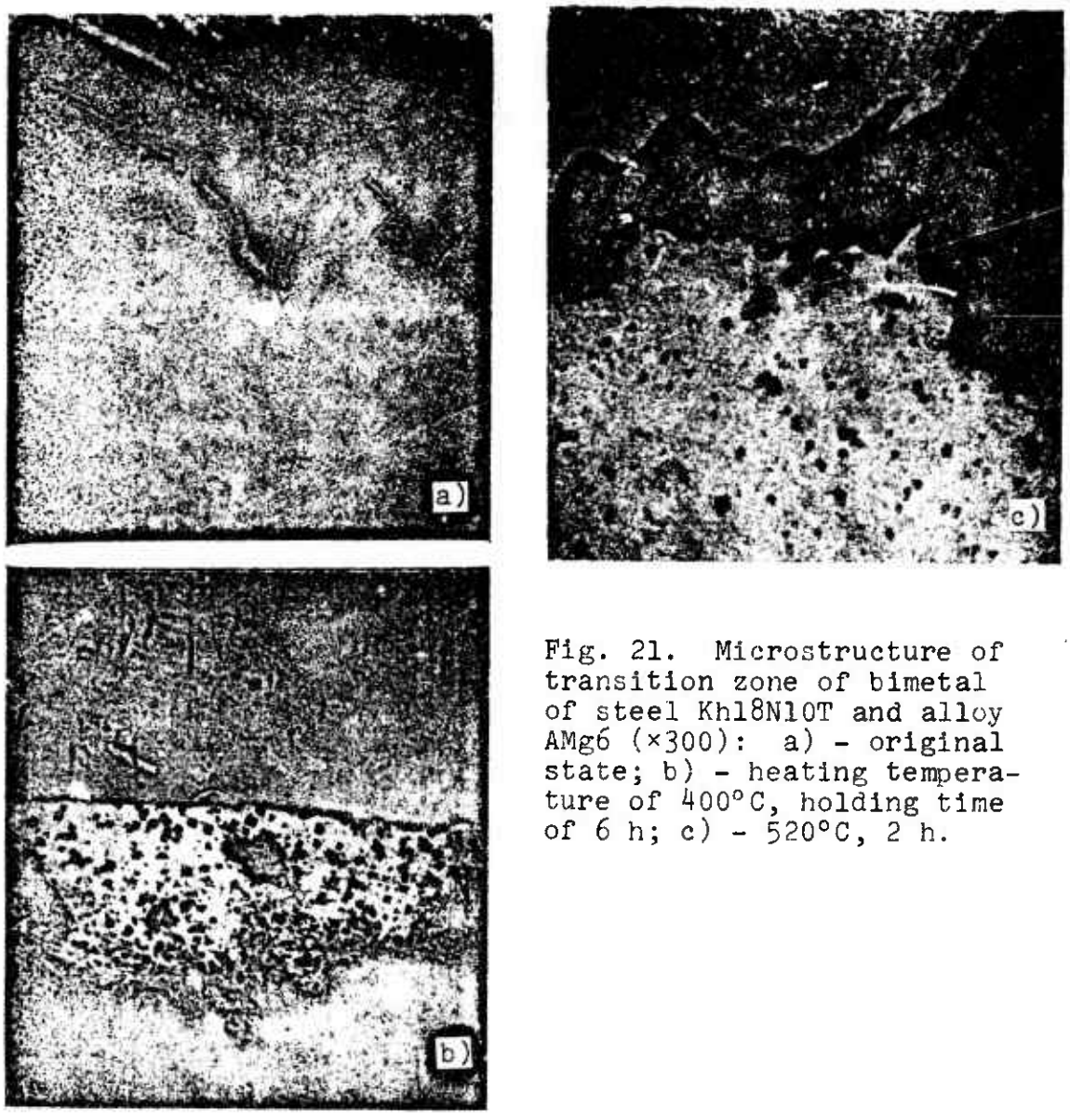

Fig. 21. Microstructure of transition zone of bimetal of steel Kh18N10T and alloy AMg6 (×300): a) - original state; b) - heating temperature of 400°C, holding time of 6 h; c) - 520°C, 2 h.

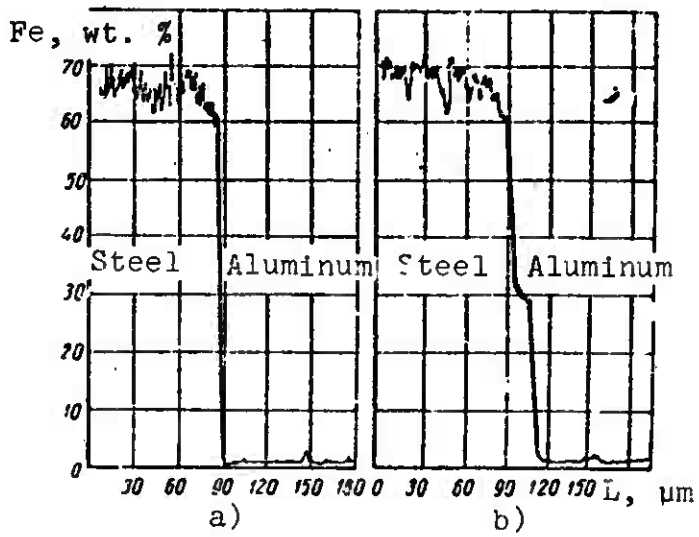

Fig. 22. Distribution of iron across zone of bimetal compound of steel Kh18N10T/aluminum AD1: a) - original state; b) - after heat treatment of bimetal (heating temperature of 550°C, holding time 4 h).

In microscopic X-ray spectral analysis of the bimetal in the original state intermetallic phases were not detected on the joint boundary (Fig. 22a). Furthermore, on the steel side a decrease in the concentration of iron in the border area is observed, which can apparently be explained by the influence of the previous heat treatment of steel Kh18N10T on the surface layers as well as by the diffusion of the iron into the aluminum under rolling conditions. The boundary of the contact metals is characterized by a bright strip on the aluminum and inclusions on the aluminum and steel sides.

The sections were subject to heating at temperatures of 300, 400, 450, 460, 500, 520, 550 and 600°C for various holding times. Figure 23 shows the microstructures of the transition line of the bimetal after heating. Heating up to temperatures of 450-460°C and holding for 12 h did not cause visible changes in structure. During heating for 10 min to a temperature of 520°C a thin interlayer of metallides 3-3.8 μm thick was detected. The formation of the intermetallic phase in the contact zones of the two specimens

did not occur simultaneously. An electron microscope study confirmed their uneven development. In one part we see pieces of the developed layer, in others this layer has significant dimensions, and in a few places it is absent all together. When holding time is increased up to 30 min the increase in width of the intermetallic layer up to 7.5 μm is already noticeable. The time of development of the intermetallide along the transition line is different at the same temperature in different batches of bimetal. This scatter in the data on the time of development for intermetallides on the weld boundary during heating to a temperature of 520°C is caused apparently by nonuniform cohesion in the different parts of the bimetal, which is caused by rolling, and by the nonuniformity of diffusion processes during heating. In heating up to a temperature of 550°C an intermetallic layer can be detected in all specimens approximately 2-2.5 μm wide as soon as 10 minutes. As heating time is increased up to 20-30 min the width of this layer constantly increases to 6-8 μm. It should be mentioned that a longer holding time does not result in as drastic an increase in the intermetallic layer as the first 30-40 min.

Figure 24 shows curves representing the relationship between layer thickness and holding time $\ln k - \frac{1}{T}$, plotted from experimental data. This dependence is expressed sufficiently well by a straight line, thus indicating satisfactory agreement with the basic law of diffusion reaction for a bimetal consisting of steel Kh18N10T and alloy AMg6. The activation energy of the diffusion process in the combination of metals selected is 26,300 cal/mole.

Through microscopic X-ray analysis in the bimetal consisting of steel Kh18N10T, aluminum AD1, and alloy AMg6 it was found that the transition layer consists of 30-33% iron (Fig. 22b). On the two sides of the boundary the naturc of diffusion was different: closer to the layer there was a decline in the iron concentration at a distance greater than 3-5 μm; no diffusion of iron was observed in the aluminum. It should be mentioned that the transition layer is distinguished by an uneven concentration of iron with respect to width.

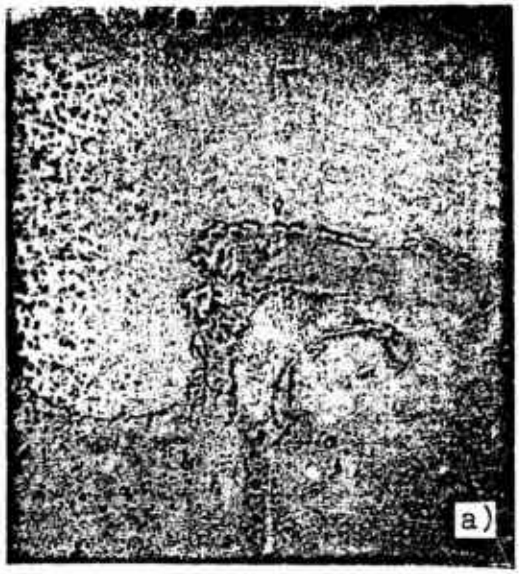

Fig. 23. Microstructure of transition zone of bimetal consisting of steel Kh18N10T and alloy AMg6 after heating (×300): a) - 450°C, 8 h; b) - 480°C, 4 h; c) - 600°C, 2 h.

3. Latent Period

The experiments performed on heating bimetal specimens of the aluminum-armco iron combination indicate that at each temperature there is a time interval in which intermetallides are not formed in the contact zone. This is the so-called latent period or the induction period. This period corresponds to the time during which the reaction does not develop noticeably.

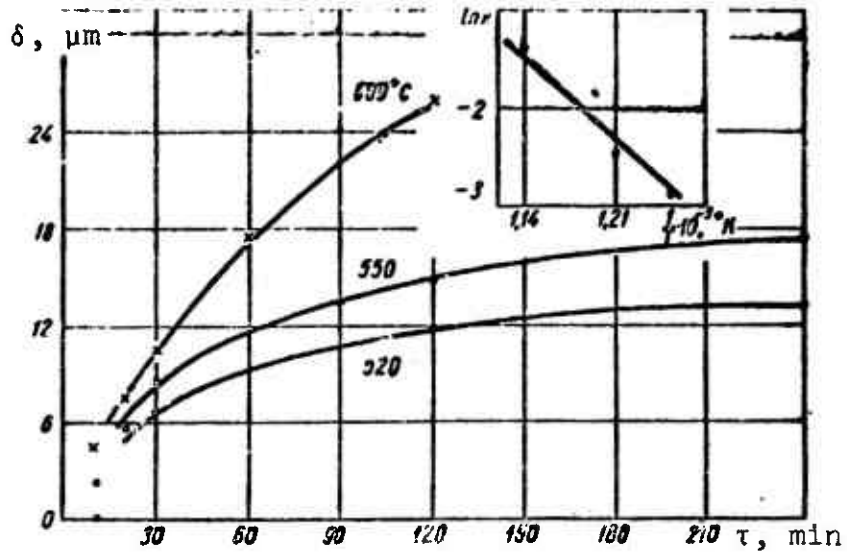

Fig. 24. Thickness of intermetallic layer as a function of holding time.

The slow development of intermetallides in the contact zone of bimetallic junctions has been pointed out in [174, 210]. For example, T. Heuman and S. Dittrich, studying the interaction between solid specimens of iron and aluminum, have shown that as a rule the reaction begins at a temperature above a certain critical temperature, between 590° and 600°C. The fact that new phases are not formed below this critical temperature cannot be explained by the proposal that the reaction interaction under these conditions has a slow rate. On the contrary, the reaction rate, despite sharp changes in the kinetic parameters observed over a longer period, is so high during this initial period that the intermetallic layer may even be formed at lower temperatures. The pattern which is actually observed can under the studied conditions be explained by the considerable slowing in the process of nucleus formation in the new phase, whose activation energy is apparently much greater in magnitude than the activation energy of the process of nucleus generation and growth, and results in noticeable nucleus generation only at a temperature of 873°K. If, however, part of this missing energy is supplied to the iron artificially, for example, by deformation, then this will cause a reduction in the critical temperature of nucleus formation. Thus, it was shown that

in forming iron/aluminum specimens of up to 50% it is possible to reduce the temperature at the beginning of the mutual reaction to 833°K.

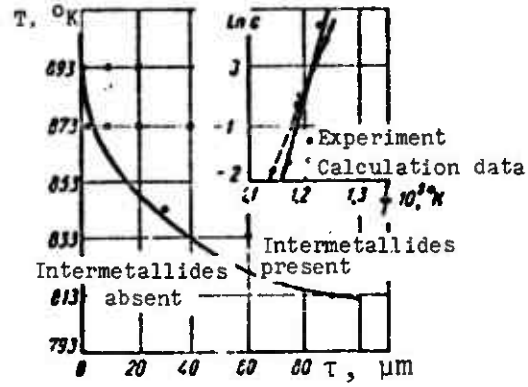

Fig. 25. Temperature and time conditions of intermetallide formation in armco iron/aluminum combination.

In our studies the latent period was determined experimentally for each of the studied temperatures. Figure 25 is a graph showing the dependence of intermetallide development time on temperature. As the heating temperature is increased the length of the latent period decreases. Thus, at a temperature of 813°K this period is 2 h, at 843°K - 0.5 h, and at a temperature of 873°K this period is less than 5 min. Let us attempt, based on experimental data obtained, to calculate the latent period for each temperature.

The growth of the layer of the new phase, with the latent period c considered, can be expressed by the equation

$$x^n = k(\tau - c), \tag{7}$$

where c is the latent period. The other symbols are the same as in formula (1).

Let us find the coefficients of equation (7).

If we solve the equation for τ, we get

$$\tau = \frac{1}{k} x^n + c. \tag{8}$$

Let us replace $\frac{1}{k}$ by quantity a:

$$\tau = ax^n + c.$$

If we take the logarithm of this expression, then we get $\ln (\tau - c) = \ln a + n \ln x$.

If we assume $\ln (\tau - c) = y$ and $\ln x = X$, then we get the linear dependence

$$y = bX + \ln a. \qquad (9)$$

In order to determine c let us compose the average geometric $x_s = \sqrt{x_1 x_m}$, where x_1 and x_m are the limiting values of variable x.

If we use the graph which represents layer thickness as a function of heating time for each temperature (see Fig. 17), we will find the appropriate values of y_s.

If we assume that points $M_1(x_1 y_1)$, $M_s(x_s y_s)$, $M_m(x_m y_m)$ lie on a curve, then we get three equalities: $y_1 = c + ax_1^n$; $y_s = c + ax_s^n$; $y_m = c + ax_m^n$.

If we raise $x_s = \sqrt{x_1 x_n}$ to the power of n and multiple by a, then we get

$$ax_s^n = \sqrt{ax_1^n \, ax_m^n} \quad \text{or} \quad y_s - c = \sqrt{(y_1 - c)(y_m - c)}.$$

After solving the last equality for c, we find

$$c = \frac{y_1 y_m - y_s^2}{y_1 + y_m - 2y_s}. \qquad (10)$$

The values of y in our experimental data correspond to holding time τ, whereas X corresponds to layer thickness x.

Now we can find the diffusion equations for each case, if we plot dependence ln x on ln (τ - c) and find exponents n and k graphically. These dependences were plotted in coordinates ln x - ln τ. In the case of the dependence ln x - ln (τ - c) the curves in coordinates x - (τ - c) pass through the origin of the coordinates. In general this does not influence the value of n and k.

For each temperature we determine values of c (Table 9). The calculated values of c were close to the experimental.

Table 9. Values of latent period for different temperatures.

Temperature, °C	Value of n	Coefficient proportional to diffusion coefficient, cm^2/s	Time during which intermetallides are absent (according to experimental data)	Time during which intermetallides are absent (calculation), h
540	2.1	$4.5 \cdot 10^{11}$	2.0	1.5
570	2.0	$9.1 \cdot 10^{-11}$	0.5	0.484
600	2.1	$1.5 \cdot 10^{-10}$	0.08	0.161
650	n_1 = 2.7 (Section I)	$7.5 \cdot 10^{-10}$	-	-
	n_2 = 2.0 (Section II)	$4 \cdot 10^{-9}$	1.0	1.5

The authors of [36] indicate that the activation energy of nucleus deposition in the intermetallide phases should be somewhat greater than the activation energy of the growth of the phases deposited. Let us attempt to calculate this value approximately. As we see from Fig. 25, the curve representing the development of intermetallides has an exponential nature. In this case the time lag can be determined very well by equation (3), which describes the transition time of the system from a nonequilibrium to an equilibrium state:

$$C=C_0\exp\left(\frac{Q}{RT}\right), \qquad (11)$$

where C_0 is the material constant and the remaining designations are the same as in formula (3).

After plotting the curves representing the dependence of ln c on $\frac{1}{T}$ from available experimental and calculation data for c (Fig. 25), we determine the activation energy of the intermetallide deposition process and the pre-exponential factor.

For the aluminum/armco iron pair, in direct contact with the studied bimetal, the temperature-time dependence for the development of intermetallides acquires the following form:

a) for the values obtained experimentally

$$C=0{,}18\cdot10^{-16}\exp\left(\frac{68000}{RT}\right); \qquad (12)$$

b) for values obtained through calculation,

$$C=0{,}6\cdot10^{-12}\exp\left(\frac{46000}{RT}\right). \qquad (13)$$

If we compare the activation energy values obtained for the latent period (the activation energy of intermetallic phase deposition in the contact zone) with the values of the activation energy which determines the growth of the intermetallic layer, we find that the former is almost two times greater than the latter ($Q_{deposition}$ = 192.6 kJ/mole; Q_{growth} = 104.6 kJ/mole, respectively). This confirms earlier proposals.

Metallographic analysis of the structure of the bimetal consisting of steel Kh18N10T and aluminum AD1/alloy AMg6 subjected to heating according to the indicated regimes, and processing of the experimental data made it possible to establish the following

temperature/time dependence, which resulted in the development of the intermetallides [232]:

$$C = 8.4 \cdot 10^{-10} \exp\left(\frac{25750}{T}\right). \qquad (14)$$

The data of the experimental studies and the calculation curve describing the temperature/time conditions for the development of the intermetallides are shown in Fig. 26.

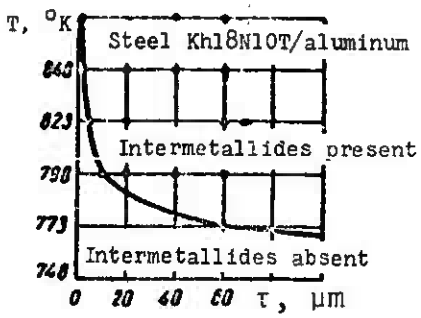

Fig. 26. Temperature and time conditions of formation of intermetallides in the combination of steel Kh18N10T and aluminum AD1.

4. Phase Composition of Transition Layers

We know from studies [195, 210] that when solid iron interacts with liquid aluminum alloy layers are formed, which are distinguished by their chemical and physical properties. Their formation and shape depend to a great extent on the temperature and length of the reaction. However, test results are different, and because of different conditions during testing it is not possible to compare them directly. Thus, this problem should receive additional study.

Figure 16 shows the microstructure of the bimetal consisting of armco iron and aluminum after heating. Aluminum rich layers stand out quite distinctly on the surface of the iron. These layers cut characteristically into the iron. The outer zone, which forms the predominant part of the alloy layer, consist of a brittle compound of iron and aluminum, which penetrates into the body of the iron specimen like tongues. Evidence of its brittleness are the cracks, which can be distinguished on the individual "tongues." The tongues are separated from the iron core by a narrow border of

the alloy of the other concentration. The proposal that the layers consist of several zones of different concentrations is also confirmed by the data of microscopic X-ray spectral analysis.

The study was made on a microanalyzer with an electron probe, produced by the "Samesa" firm. The probe diameter in all cases was 1-2 μm. The work regime: energy of electrons 29 kV, take-off angle 30°.

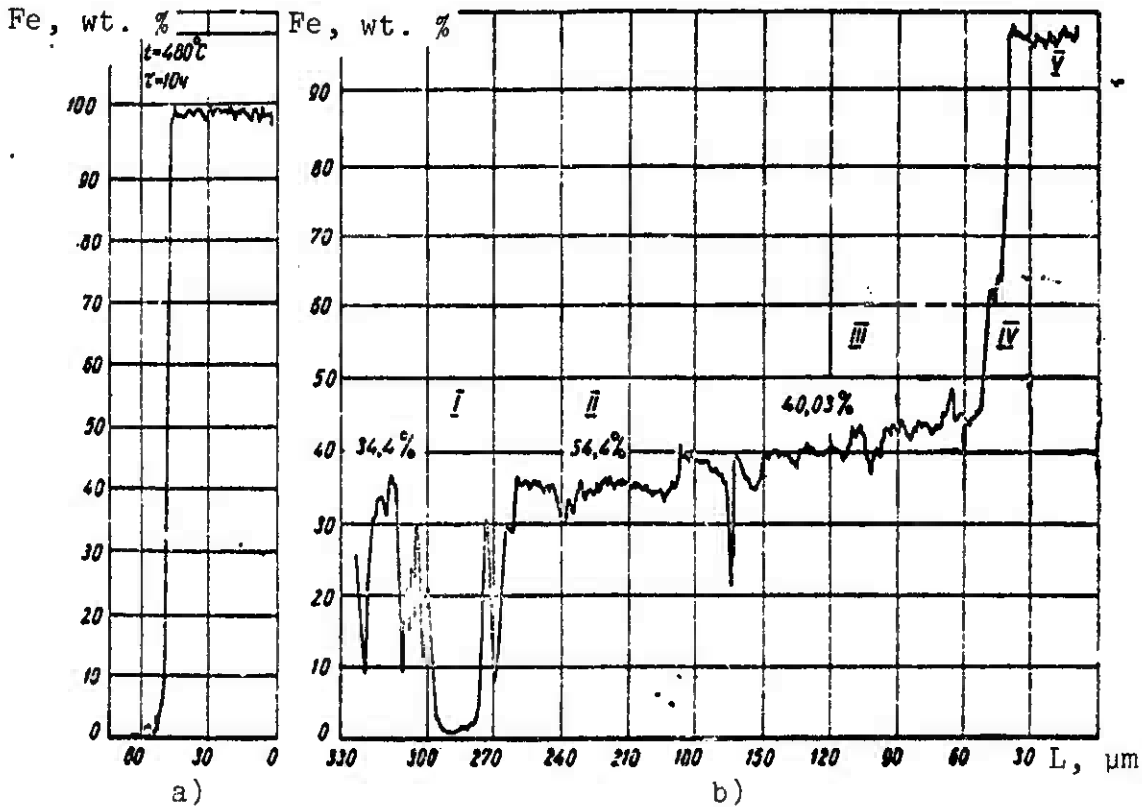

Fig. 27. Distribution of iron across weld joint of bimetal aluminum AD1/armco iron: a) - 480°C, 10 h; b) - 650°C, 6 h.

The distribution of the iron in the junction zone of the bimetal consisting of AD1 aluminum and armco iron after heating at a temperature of 650°C for 6 h is shown in Fig. 27. Section I shows inclusions of phase $FeAl_3$ in the aluminum. This is followed by section II, which borders the aluminum, where there is a zone

50-60 μm wide corresponding to phase $FeAl_3$. The basic section III, 100-140 μm wide, belongs to phase Fe_2Al_5. On the boundary of this phase we have the section IV - the zone of the solid solution of α-iron; V - iron.

Thus, the data of the microscopic X-ray spectral analysis confirmed the presence of a complex structure in the transition zone of the bimetal after prolonged heating.

From the data of microscopic X-ray spectral analysis we can also follow the kinetic growth of the intermetallic layers in the various bimetal combinations.

Figure 28 shows a diagram describing the distribution of iron across the weld zone in the bimetal consisting of steel Kh18N10T and alloy AMg6 during heating. In this state after rolling (curve 1), and also after heating to a temperature of 480°C for 10 h, we do not observe a formation of new phases along the transition line. In such heating the first nonuniform sections appear: in the specimen we observe both "pure" sections (curve 2) and sections with individual inclusions of the new phases (curve 3). A further increase in holding time at 480°C up to 30 h results in the appearance of a developed intermetallic layer consisting of 28-31% iron (curve 4). The same holding time increases the thickness of the intermetallic layer in several places up to 15-20 μm without noticeably changing its phase composition (curve 5). At the same time, there are areas along a transition line during holding of 60 h in which only new centers of intermetallic phases are generated (curve 6), and in several places these are absent (curve 7). At higher temperatures - 550°C - a holding time of 4 h results in the formation of a developed intermetallic layer (curve 8).

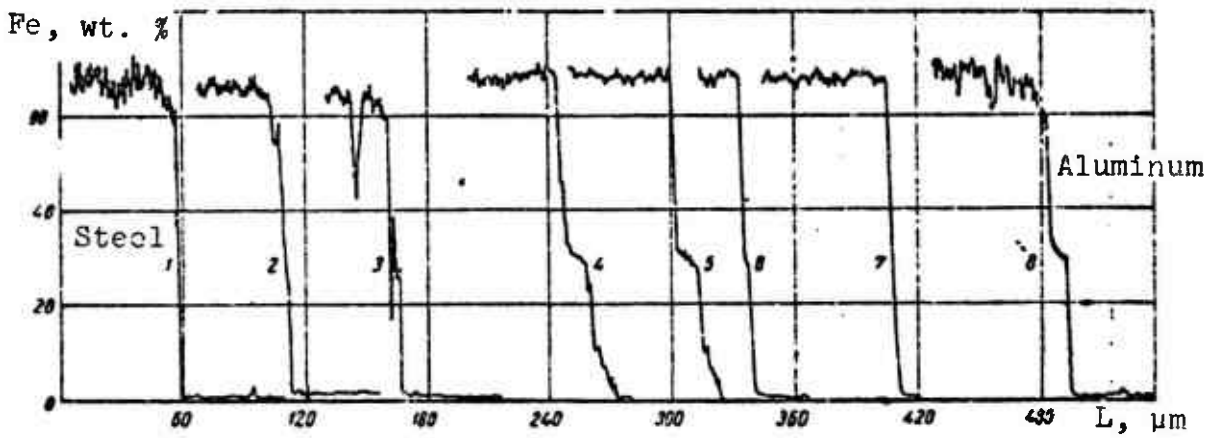

Fig. 28. Nature of distribution of iron across joint zone in bimetal of steel Kh18N10T/alloy AMg6 during heating: 1 - original state; 2 - 480°C, 10 h; 3 - 480°C, 10 h (intermetallide present); 4 - 480°C, 30 h; 5 - 480°C, 30 h; 6 - 480°C, 60 h; 7 - 480°C, 60 h; 8 - 550°C, 4 h.

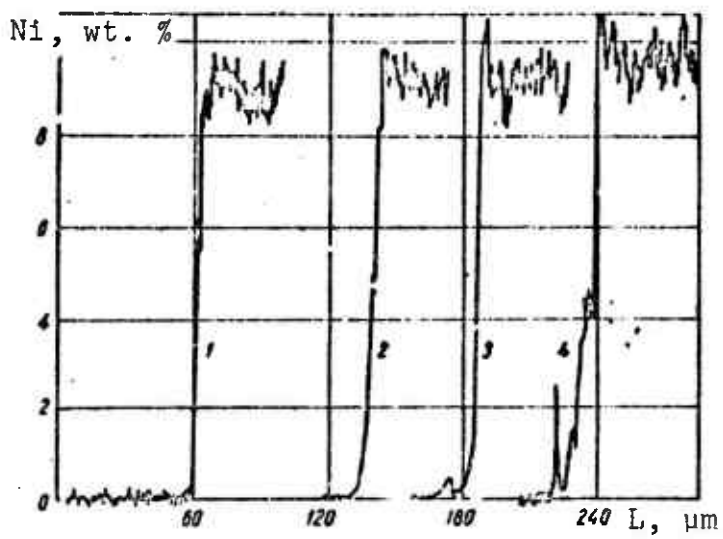

Fig. 29. Nature of distribution of nickel in bimetal of steel Kh18N10T/ alloy AMg6 during heating: 1 - 480°C, 10 h; 2 - 480°C, 30 h (intermetallides present); 3 - 480°C, 30 h; 4 - 480°C, 60 h.

The basic components of steel Kh18N10T - nickel and chromium - participate in forming the transition zone.

The nature of the distribution of nickel across the joint zone of the same specimens is illustrated in Fig. 29. The nickel participates in the formation of the intermetallic layer at practically the same temperatures as iron (curve 1). At a temperature of 480°C and a heating time of 30 h we observe segments with intermetallic phases being deposited (curve 2) and phases without them (curve 3). At a holding time of 60 h nickel has increased its participation in the formation of the intermetallic layer (curve 4).

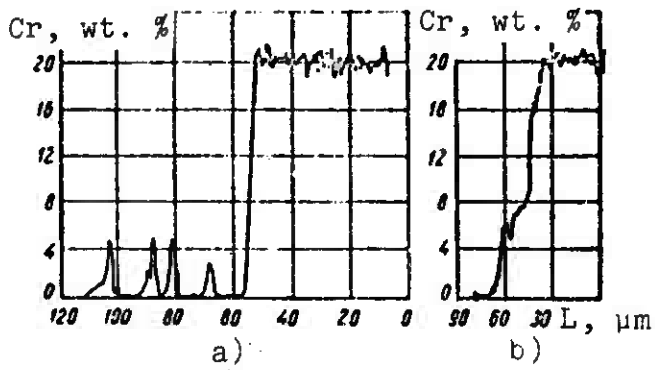

Fig. 30. Distribution of chromium across joint zone of bimetal consisting of steel Kh18N10T and alloy AMg6: a) - 480°C, 30 h; b) - 480°C, 60 h.

The distribution of chromium across the joint zone of the bimetal, as shown in Fig. 30, indicates that chromium at a temperature of 480°C and a holding time of 30 h is intensively diffused along the grain boundaries of the aluminum (Fig. 30a). Its magnitude reaches 4-4.5%. Only at considerable holding times (60 h) does the chromium begin to participate in the intermetallic interlayer, forming the compound $CrAl_6$ (Fig. 30b).

The data obtained are in agreement with the diffusion coefficients of the indicated elements in aluminum.

The diffusion coefficients for iron and nickel in aluminum were determined in a temperature range of 350-630°C by means of isotopic tracers [181, 209]:

$$D_{Fe/Al} = 4{,}1 \cdot 10^{-9} \exp\left(-\frac{13900}{RT}\right); \quad (15)$$

$$D_{Ni/Al} = 2{,}9 \cdot 10^{-8} \exp\left(-\frac{15700}{RT}\right). \quad (16)$$

The diffusion coefficient for chromium in aluminum was determined in a temperature range of 250-605°C and was [62, 196]

$$D_{Cr/Al} = 3{,}01 \cdot 10^{-7} \exp\left(-\frac{15400}{RT}\right). \quad (17)$$

Thus, the data obtained made it possible to establish the following:

1. The diffusion transition zone in bimetal specimens is formed in two stages. In the first stage a solid solution zone forms in the aluminum. Metallographically this appears as a bright strip. The formation of the zone begins in the process of preparing the bimetal sheets. In the second stage the layer of the intermetallic joint is formed.

2. The intermetallic joint contains, in addition to aluminum, the main alloy elements of the steel - Cr and Ni. The concentrations of these elements are uneven with respect to thickness - they decrease in the direction from the steel toward the aluminum.

5. Contact of Hard Steel with Aluminum Melt

When aluminum interacts with steel physicochemical processes occur which result in the formation of a transition diffusion zone along the transition line.

In [76, 126, 137, 174] an attempt has been made to explain the nature of the delay in diffusion processes and the chemical interaction in the light of modern concepts of the formation mechanism of a weld joint in a solid-liquid phase. The interaction between the liquid metal and the solid occurs in several stages [25, 170], mainly adsorption and heterodiffusion (chemical reactions).

When a molten metal interacts with a solid metal chemisorption processes (of the preliminary interaction stage) play a leading role in the formation of durable bonds. As a result of chemisorption the adsorbed particle (molecule, atom) and the lattice of the adsorbent form a single quantum-mechanical system. The formation of durable bonds occurs (according to Pauling) during the process of so-called weak chemisorption, described by the fact that the electron cloud of the adsorbed atom penetrates into the electron cloud of the metal, while the metal and the adsorbed atom each give up one electron with an unpaired spin to the "binding" orbit. Consequently, the process of heterodiffusion can occur only after the process of chemisorption, i.e., after the atoms of the interacting metals form a single quantum-mechanical system.

The time of chemisorption, or the time of delay in the diffusion processes, can be determined by the equation $\tau = \tau_0 e^{\frac{E_a}{RT}}$, where q is the heat of chemisorption; E_a is the activation energy of chemisorption.

The results of quantity τ for the interaction Fe + $Al_{ж}$ [126] are given below (where D_{Fe-Al} is the binding energy of the adsorbed atom on the surface of the metal):

Variant		1	2	3	4
D_{Fe-Al}, kcal/mole		49,5	49,5	49,5	49,5
q		49,5	32,9	37,0	20,4
E_a		12,4	12,4	12,4	12,4
$q+E_a$		61,9	45,3	49,4	32,8
τ, s:					
$T=973°$ K		$10^{-0,2}$	$10^{-3,0}$	$10^{-2,0}$	$10^{-5,6}$
$T=1123°$ K		$10^{-1,7}$	$10^{-4,4}$	$10^{-3,3}$	$10^{-6,7}$

According to the reduced data, the delay period in the diffusion processes can vary by several orders. When free bonds are present on the surface (variant 1) the heat of chemisorption q is close in magnitude to the activation energy of the diffusion of the adsorbed atom into the solid metal. If free bonds are absent on the surface (variant 4), then obviously the interaction is closer to the process of physical adsorption, as indicated by the small amount of adsorption heat.

The activation energy for the diffusion of atoms of a solid metal into a liquid is less than the activation energy in diffusing the liquid metal into the solid, and thus diffusion into the liquid metal may be more desirable. Assuming that the diffusion processes begin when, during energy exchange, the atoms of the solid body acquire an energy which is equal to the activation energy of the diffusion of the atoms of the solid metal into the liquid, then the delay period of the diffusion processes can be calculated according to the equation $\tau = \tau_0 e^{\frac{E_a}{RT}}$.

The calculation results indicate that when a molten metal interacts with a solid metal quantity τ is by several orders lower than the contact time of the solid metal with the liquid under braze-welding conditions. This means that it is difficult to suppress diffusion processes under actual welding conditions. However, the beginning of diffusion does not mean the beginning of the formation of intermetallic compounds. In practice the length of the delay in forming intermetallic compounds is many times greater than the length of the delay period in diffusion processes.

After chemisorption a further interaction between the atoms of the contact metals is possible. The delay period in the formation of intermetallic compounds is determined by the magnitude of activation energy in the reaction. Thus the delay period in diffusion processes coincides with the delay period in the formation

of the intermetallic compound only when $q + E_a \geq E_{ap}$, where E_{ap} is the activation energy of the chemical reaction. If, however, $q + E_a < E_{ap}$, then after chemisorption the heterodiffusion process occurs, which can lead to the formation of intermetallides, although under these conditions the chemical interaction is not very probable. In this case a certain time is required in order to obtain the limiting concentration above which the intermetallic compound is formed. We can assume that this time is also the period of delay in the formation of intermetallic compounds.

The authors of [115, 126] estimated through calculation the amount of activation energy in the reaction which forms the compound $FeAl_3$, and compared it with quantity $q + E_a$. For the case of the interaction of solid iron with liquid aluminum we have E_{ap} = 62 kcal/mole and $q + E_a$ = 49.4 kcal/mole. From the data which we have obtained we should not expect the delay periods of diffusion and the formation of the intermetallic compound to correspond.

Now let us estimate the length of the delay period in the formation of intermetallides for the reaction $Fe + 3Al = FeAl_3$: $-\Delta H_{298}$ = 26.8 kcal/mole, ΔS = -30.8 cal/mole-deg. The delay period in the formation of intermetallic compounds depends on temperature: at T = 973°K it is $1.98 \cdot 10^{-1}$ s; at T = 1073°K, $4.55 \cdot 10^{-2}$; at T = 1123°K, $2.86 \cdot 10^{-2}$ and at T = 1223°K, $3.60 \cdot 10^{-3}$ s.

Under braze-solder conditions the temperature of the interaction depends on the melting temperature of the low-melting metal, and thus its lower limit is limited. If at this temperature quantity τ is small, we should then seek another method (other than reducing the temperature of interaction) to slow down the reaction. One such method is that of introducing an additional element into the molten metal.

It has been established (considering the relatively high rate of cooling of the metal during welding) that temperatures below 520-505°C are safe in forming interlayers between steel and aluminum.

6. Intermetallic Compound Zone in Contact Between Liquid Aluminum and Solid Steel

From the preceding material it follows that if we increase the temperature of metals above 600°C the latent period quickly tends toward zero. If we extrapolate the straight line (see Fig. 25) to the melting point of aluminum (660°C), then we will be convinced that the latent period at this temperature will be almost equal to zero. This extrapolation from solid to liquid aluminum can be based on the data of V. Z. Bugakov [25], who demonstrated that the curve for the temperature dependence of the diffusion coefficient in the formation of reactive phases between zinc and copper, as well as between iron and zinc, shows no inflections whatsoever in the transition of zinc from the solid to the liquid state. This indicates that the activation energy of the process is practically independent of the state of matter of the low-melting metal. Nevertheless, the formation of a reactive phase during contact with the molten aluminum and the propagation of this phase can differ in some aspects, which are related to the intensive dissolution of the iron and the transfer of the reactive phase from the surface of the steel into the melt.

In order to test these proposals and their applicability for our case, steel specimens were immersed in an aluminum melt. They were calorized with a flux (Table 23) in graphite crucibles, which had an inner diameter of 80 mm in a high-frequency laboratory furnace. The temperature of the bath during the process was measured by a chromel-alumel thermocouple. The effect of the bath temperature of the aluminum and the holding time of the specimens at a given temperature on the depth of the diffusion zone was determined by measuring its thickness on the IMT-3 unit. Specimens measuring 20 × 20 × 3 mm were used. The thickness of the intermetallic compound zone was measured on a microscope with an accuracy

to within approximately 1 μm. In the case of a jagged layer, 3-5 series of measurements were taken from different parts of each section. First, the calorizing capacity was tested on steels of different compositions: Kh18N10T, 28Kh3SNMVFA, and St. 3. Clean steel specimens were heated for two minutes in a layer of molten flux before being submerged in an aluminum bath. The specimen was in motion in both the flux and the molten aluminum bath, which provided for better cleansing of its surface and more durable cohesion between the aluminum and the base metal.

The effect of heating on the depth of the diffusion layer was studied up to the following temperatures: 900, 850, 800 and 700°C and holding times of 15, 30, and 45 s and 1, 6, 10, 15, and 30 min. As follows from the diagram representing the dependence of the depth of the diffusion layer on the time that the specimen remained in the molten aluminum and on the temperature of the bath, the depth of the diffusion layer increases as temperature rises and as the time that the specimen remains in the bath increases. These data indicate that the thickness of the intermetallic layer increases parabolically in time.

It was discovered in studying microscopic sections of calorized specimens that the nature of the intermetallic layer on low-carbon steel is drastically different from this same strip on high-carbon steel 28Kh3SNMFVA and steel Kh18N10T (Fig. 31a, b).

As we see in a comparison of the characteristic microstructures of calorized layers of the three brands of steel, the thinnest layers with well defined even boundaries on the steel side were obtained from stainless steel Kh18N10T (Fig. 31d). The microstructure of calorized steel of brand St. 3 is characterized by tongue-like projections and by its unevenness, which, as we will show below, results in low-strength indicators in welded joints. On multialloy steel 28Kh3SNMVFA the layers occupy an intermediate position with respect to the thickness (Fig. 31c).

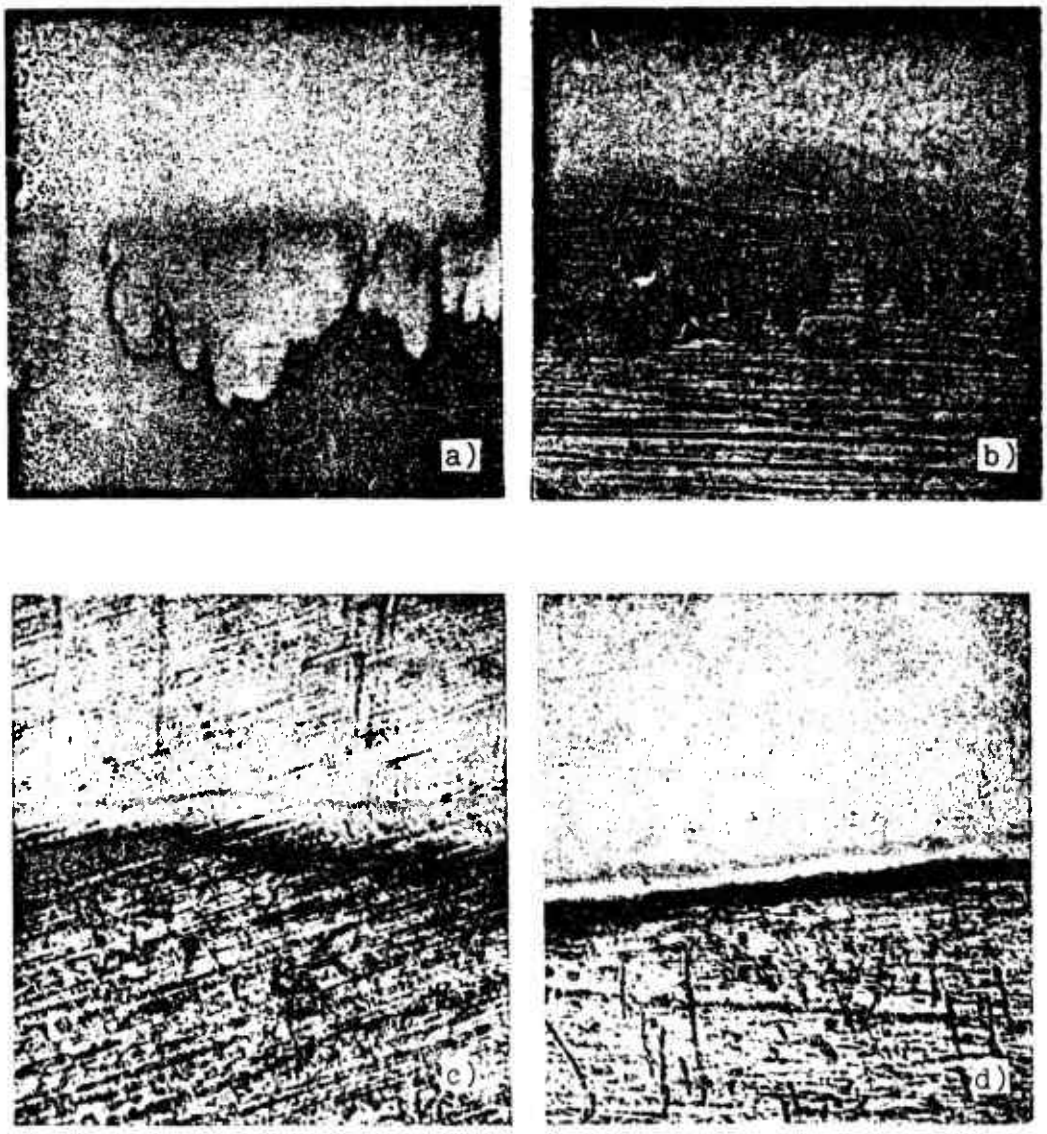

Fig. 31. Microstructure of calorized surface on low-carbon steel St. 3 (a, b), steels 28Kh3SI[illegible]VA (c) and Kh13N10T (d) (×300).

A detailed description of the formation mechanism of the structures in the diffusion layer has been given by S. Koda and others [67, 143]. Based on their studies they made the following proposal on the mechanism of formation and growth of the diffusion layers.

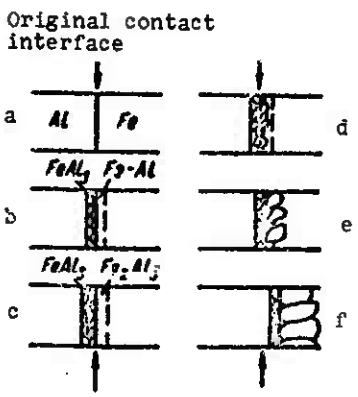

Fig. 32. Mutual reaction of molten aluminum and solid iron.

When the solid iron comes into contact with the molten aluminum (Fig. 32a) mutual diffusion occurs on the surface, and thus a diffusion layer is formed in each metal. When the concentration of iron is increased in the aluminum, $FeAl_3$ - the intermetallic compound with the least concentration of iron - is formed, which corresponds to the phase diagram (Fig. 32b). In this initial submersion period there is a local short-term decline in temperature near the specimen, and as a result the compound which is being formed ceases to grow into the melt and to some extent is delayed on the specimen surface. At the same time there is a significant formation of the solid aluminum solution in the iron.

As the reciprocal diffusion of the metals progresses the thickness of the layer reaches a certain magnitude and the compound Fe_2Al_5 is formed (Fig. 32c). Here the orientation of the crystals of $FeAl_3$ and Fe_2Al_5 are not necessarily ordered, but, as mentioned by Heuman and Dittrich [210], due to the specific nature of the structure the Fe_2Al_5 crystals begin to grow along axis C at a very fast rate, forming a zone of columnar crystals. Here the columnar crystals (Fe_2Al_5) grow toward the iron base, while the iron, which is diffused through the neighboring $FeAl_3$ layer, penetrates the aluminum. With further diffusion of the iron compound Fe_2Al_5 is transformed into the compound $FeAl_3$ (Fig. 32d). As a result of the growth of phase Fe_2Al_5 and the increased diffusion rate of iron into the aluminum the region of the solid solution of aluminum in iron disappears (Fig. 32e).

Thus, the process of the diffusion of aluminum into iron has been determined almost comprehensively by the behavior of the η-phase (Fe_2Al_5), which in the interaction of these two metals develops almost alone, and is not accompanied by any other phases

significant enough to be detected (Fig. 32f). Only after many attempts was it possible sometimes and with the aid of prints to detect over the tips of the individual "tongues" of the intermediate phase the extremely narrow disseminations of another phase, by all indications belonging to the α-solid solution of aluminum in iron

The reasons for the existence of the experimentally confirmed crystallographic anisotropy of the growth of the intermetallic phase have a unique interpretation in the crystallographic structure of the η-phase, which K. Schubert and his colleagues were able to decipher [210].

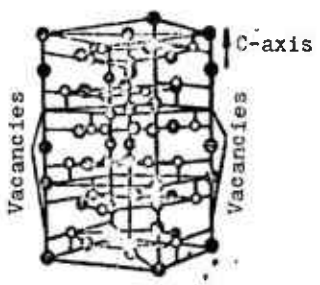

Fig. 33. Model of three elementary cells of the η-phase (Fe_2Al_5) in a stacked position (dark dots are aluminum atoms, light dots are iron atoms).

The Fe_2Al_5 phase, according to the data of these studies, has an elementary cell of the orthorhombic type and two C-axes directed vertically upward, one on top of the other (Fig. 33).

The nodes of the cascade along the C-axes are occupied exclusively by aluminum atoms. The other aluminum atoms and all of the iron atoms are found inside the elementary cell or on its lateral faces. At a distance of $\frac{c}{2}$ they form a ring around the individual structural chains of atoms along axis C. Consequently, in the crystals of the η-phase there should also be chain elements, relatively thickly populated by aluminum atoms, having the structure ($\frac{c}{2}$ = 2.10 kilo-X), within which, inside the limits of the surrounding quasi-circular formation of aluminum and iron atoms it is possible to assume an increased deformability and mobility of the atoms along axis C.

Most significant in this connection is the statement by K. Schubert, confirmed by calculating the intensity of X-ray reflections from corresponding structural elements, that the atom population density of the above-mentioned chain structural lattice elements in some cases reaches only 70%. This high concentration of "holes" in the individual parallel chain elements of the structure explains the increased selective mobility of the aluminum atoms in certain preferred crystallographic directions. The area of the basal plane of the crystal lattice coincides with the base area of the columnar crystals of the intermetallic η-phase, whereas axis C corresponds to the longitudinal axis of the columnar single crystals of this phase.

Thus, on the basis of these ideas we can find a simpler explanation for both the crystallographic anisotropy of the diffusion rate and for the relatively great integral rate of the mutual reaction between the two metals and the subsequent formation of the η-phase. At the same time it is possible to answer the question of why, besides the Fe_2Al_5 phase, we do not detect with sufficient accuracy the other intermetallic phases, which should, according to the aluminum-iron equilibrium diagram, be present in the studied range of concentrations and temperatures.

It should be mentioned that the data on the phase composition of the diffusion zones can refer to analogous zones in joints obtained by braze-welding, since the thermal cycle in this case does not introduce change in the width of the phase fields.

Thus, since at temperatures of 750-800°C intermetallides have the form of columnar formations which grow from the boundary into the steel, we can assume that the diffusion rate for aluminum in steel is higher than the rate of solution of the intermetallides in the aluminum. It is also possible that the aluminum melt is "sucked" into the steel by capillary forces through microscopic pores [195] and by the melting of the eutectic along the grain

boundaries [98]. The width of the interlayer in this case increases with an increase in the contact length. During crystallization in the aluminum melt it is also distinguished by a certain quantity of intermetallides.

Increase in the temperature up to 900-980°C apparently results in a more significant increase in the diffusion rate through an intermetallic layer of iron atoms than of aluminum atoms. The solution rate of the intermetallides also increases. In the general case layer thickness may not increase (and may even decrease) with an increase in the length of contact. This is due to its intensive dissolution in aluminum. The total amount of intermetallides increases, yet a significant part of them will be deposited from the volume of the aluminum melt as it crystallizes.

7. Kinetics of Iron Dissolution in Liquid Aluminum Under Mixing Conditions

The kinetics of dissolution of a solid metal in a liquid is one significant factor in the process of welding different types of metals, in particular, steels with aluminum melts [158]. The solution rate depends not only on the nature of the diffusing and base metals and the temperature of the processes, but also on the relationship of the area of the dissolving surface, the volume of the melt, and the mixing regime [106, 107]. Hence it is possible to regulate the relationship of the rates of growth and dissolution of the intermetallic layer, which is of interest from the technological standpoint.

The kinetics of the dissolution of iron in liquid aluminum in a temperature range of 720-820°C and specimen revolution rates of 20-35 r/min were studied by Darby and others [188]. They arrived at the conclusion that the dissolution of iron in liquid aluminum occurs under diffusion conditions. Kosaka and others [219, 220] studied the rate of dissolution of steel containing 1.8% chromium in liquid aluminum in a temperature range of 750-900°C under static

conditions, mixing the melt with an argon jet at a regulated rate. The dissolution of chromium steel in liquid aluminum is also a diffusion process, although the small values of the solution rate constants ($0.4\text{-}2\cdot10^{-5}$ cm/s) and the high activation energy (greater than 30 kcal/mole·deg) indicate the possibility of damping the solution process on the contact interface between the solid iron and the liquid aluminum.

In [55, 56] regularities were established for the rate of solution of armco iron in liquid aluminum. The specimen used - a revolving disk 11 mm in diameter - provided a uniformly excessible surface, and the formation of the intermetallic layer on the solution surface was considered. The materials used were aluminum of high purity (mark AV000), containing 99.99% Al, and armco iron in the form of bars with the following composition (in wt. %): 0.06 C, 0.15 Mn, 0.14 Si, 0.012 S, 0.05 Cr, 0.12 Ni, 0.07 Mo, 0.24 Cu, 0.04 P.

The solution kinetics of armco iron in liquid aluminum were studied at temperatures of 700, 750, 800, and 850°C and at four rates of rotation in a range of 63.1-351.6 r/min. The experiment was long enough to assure calculation of coefficient K (K is the solution rate constant) in the Nernst-Shchukarev equation with an error of less than 10% according to the formula

$$K=\frac{\lg c_н/(c_н-c)}{0{,}434St\rho/P}, \qquad (18)$$

where $c_н$ is equilibrium solubility; c - the concentration of the admixture in the melt; S - the surface area of the solid specimen; t - solution time; ρ - density of melt; P - weight of melt.

In the Nernst-Shchukarev equation [55]

$$\frac{dc}{dt}=\frac{S}{V}K(c_н-c) \qquad (19)$$

coefficient K does not depend on time in kinetic or diffusion solution. However, in certain cases a deviation from equation (19) was noted, apparently associated with the formation of an additional "barrier" in the solid phase in the region adjacent to the liquid.

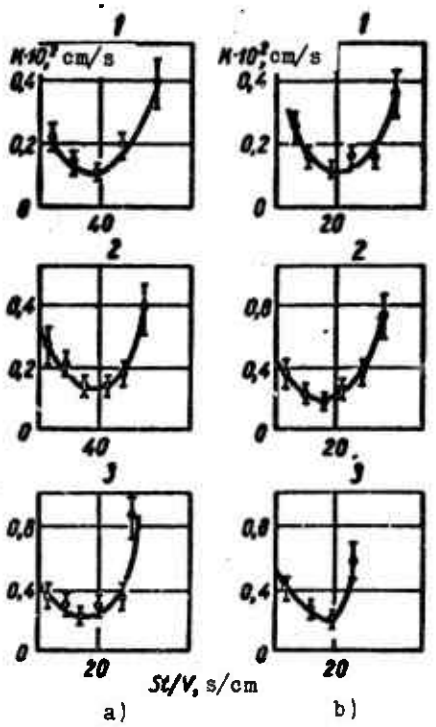

Fig. 34. Coefficient K as a function of reduced solution time at a temperature of 700°C (a) and 750°C (b): 1 - 63.1 r/min; 2 - 159.3 r/min; 3 - 239.0 r/min.

Since in system Al-Fe there are a number of intermetallic compounds which can serve as additional "barriers" during solution (besides the diffusion boundary layer), deviations from equation (19) would also be admissible in this case. In order to test the applicability of equation (19) dependences were plotted for K on t for temperatures of 700, 750, 800, and 850°C and rotation velocities of 63.1 r/min, 159.3 r/min, 239.0 r/min, and 351.6 r/min. At temperatures of 700 and 750°C all of the diagrams show a minimum in values of K, whose magnitude decreases as the rate of rotation of the disk increases (Fig. 34). At temperatures of 800 and 850°C there is a time increase in K values in all cases. We can assume that the nature of the change in K in the Nerst-Shchukarev equation is related to the sequence of development and to the growth characteristics of the intermetallic phases which are formed on the boundary between the solid and liquid metals.

In order to understand the results which we have obtained we can use the well established experimental fact that when the armco iron is submerged in the molten aluminum only two of the five intermetallic compounds which are formed in the Al-Fe system are observed on the boundary. Since the values for the heat of formation of intermetallides $FeAl_3$ and Fe_2Al_5 are extreme close, we can assume that of the two intermetallides the one richer in aluminum $FeAl_3$ should develop first. The growth of layer thickness in this intermetallide (θ-phase) should result in a decrease in coefficient K if the θ-phase has protective properties. The formation and the solution of the θ-phase occur simultaneously.

Thus, the concentration of iron in the melt corresponding to minimum K values on the diagrams is obtained as a result of the influence of two factors - the solution of the θ-phase and the diffusion of the iron through this phase layer. Since minimum values of K are obtained faster at a greater disk rotation rate, while diffusion of the iron in the θ-phase should not depend on the rotation rate, then the relationships which we can observe are the result of a change in the solution rate of $FeAl_3$ from the rotation rate of the specimen, i.e., the θ-phase layer dissolves according to a diffusion or combined mechanism. Upon reaching a certain critical thickness in the θ-phase layer the diffusion flux of iron is so diminished that the solution rate of the specimen becomes equal to the solution rate of phase $FeAl_3$. There is a simultaneous decrease in the amount of aluminum which is diffused in the opposite direction toward the boundary between Fe and $FeAl_3$, which causes intensive growth in the less aluminum rich phase Fe_2Al_5 (η-phase).

The Fe_2Al_5 phase layer which is formed during the solution process is characterized by very developed porosity. Thus, it is now possible for fragments of crystals of the η-phase to be transferred into the melt and subsequently dissolve in the liquid aluminum. As a result the actual rate of solution is greater than that obtained from the Nernst-Shchukarev equation. This treatment

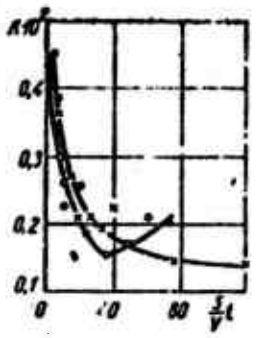

Fig. 35. Dependence of coefficient K on reduced dissolution time: O - solution in pure aluminum; × - solution in aluminum with 3 wt. % silicon added.

agrees with the results obtained from studying the composition of the intermetallic layer which develops when armco iron is submerged in liquid aluminum and aluminum with 3.3% silicon added. When armco iron dissolves in melts of aluminum and aluminum with 3% silicon added (700°C and 159.3 r/min) in the first stage the dependence of K on t is identical in both cases (Fig. 35). In the second stage of solution the rates of formation and dissolution of the $FeAl_3$ phase become almost equal for aluminum with silicon added. The solution rate constant of phase $FeAl_3$ is about 0.0015 cm/s, i.e., is about one third of that in the solution of iron.

Thus, in the first solution stage (descending branches on diagrams in Fig. 34) the process is slowed by the increased thickness of the intermetallic phase $FeAl_3$; in the second stage (ascending branches in Fig. 34) the process is accelerated by the breaking away of Fe_2Al_5 crystal fragments. The second stage of the solution process is not very suitable even for semiquantitative evaluation, despite the fact that the reason for the mechanical breakdown is in this case diffusion porosity, caused by the different diffusion concentrations of iron and aluminum in phase Fe_2Al_5 [88, 199]. The first stage of the process can obviously be estimated quantitatively by a combination solution of the main solution equation (19) and expression (2), which relates diffusion layer thickness and time.

In the first stage of the solution process $c \ll c_н$, and thus equation (19) can be written as:

$$\frac{dc}{dt} = \frac{S}{V} K c_н. \qquad (20)$$

After transformations Ya. V. Natanzon [55] proposed an equation which would describe the time change in the concentration of the dissolving material when solution was complicated by the growth of the intermetallic layer on the external boundary of the dissolving material, functioning in a protective role:

$$c = \frac{S}{V} At^{\frac{1}{3}}. \qquad (21)$$

The values for coefficients A calculated from the results of experiments on dissolving armco iron in a melt of pure aluminum and in aluminum with 3% silicon added are the same (0.057). This is one assurance that the described solution mechanism is correct.

Expression (21) is distinguished from the usual concentration/time dependence (without considering the effect of the intermetallic layer $c = \frac{R}{V}kt$) merely by the exponent for t.

Thus, in the case of the formation of an additional "barrier" during solution the transfer rate of the material from the rotating disk depends less on the rate of rotation than we might believe from the theory of V. G. Levich [90].

Let us use the expression $x^2 = k_1 t$ to estimate the size of k_1 in the case where the rate of formation (growth of thickness) of the intermetallic layer and its rate of solution in the melt are the same.

The rate of growth of the thickness of the layer

$$\frac{dx}{dt} = \frac{k_1}{2x}. \qquad (22)$$

From equation (20) we get

$$c = \frac{S}{V} Kc_n t. \qquad (23)$$

Since $c = \frac{m}{V}$ (m is the weight of the dissolving intermetallide) and $m = Sd_{инт}$ ($d_{инт}$ is the density of the studied intermetallic compound), then

$$x = \frac{Kc_n t}{d_{инт}} \text{ and } \frac{dx}{dt} = \frac{Kc_n}{d_{инт}}. \quad (24)$$

If we use (22) and (24), then we get

$$k_t = \frac{2Kc_n z}{d_{инт}}. \quad (25)$$

The last expression enables us to calculate the constant for the rate of growth in the thickness of the intermetallic layer when the formation rate of the layer is equal to its solution rate, i.e., when the thickness of the intermetallic layer remains constant during the solution process.

The rate of growth in the thickness of the layer in phase Fe_2Al_5 was obtained at a temperature of 800°C and rotation rates of 159.3 and 615.4 r/min and under nominally static conditions. In experiments with specimens in the form of rotating disks the surface solution area was 1 cm^2, and the volume of the melt was 5 cm^3, i.e., ratio $\frac{S}{V}$ was 0.2 cm. The thickness of the η-phase layer was determined by the average distance of the displacement front of the η-phase of the Al/Fe_2Al_5 boundary. This type of error in measuring was determined primarily by error in estimating the position of the Al/Fe_2Al_5 boundary, which was usually unclear as a result of the section being "buried."

Figure 36 shows the change in layer thickness of the η-phase as a function of time as the armco iron specimens are dissolved under nominally static and dynamic conditions at rotation rates of 159.3 and 615.4 r/min and a temperature of 800°C. Characteristic of the curves in Fig. 36 is the fact that the thickness of the intermetallic layer is independent of solution time at the initial moment in time. This time interval in experiments conducted under nominally static conditions corresponds to 30 s, whereas for

experiments under dynamic conditions it rises to 10 min (159.3 r/min). This feature in curves representing the thickness of the η-phase layer in relation to time had not previously been observed in experiments with solid specimens submerged in a melt for the purpose of obtaining intermetallic iron/aluminum layers.

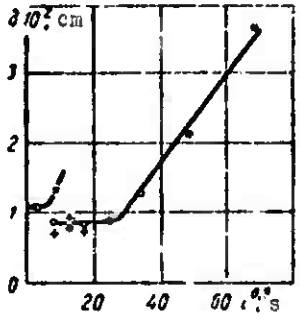

Fig. 36. Thickness of intermetallic layer of Fe_2Al_5 (δ, cm) as a function of solution time at 800°C: + - static conditions; O - dynamic conditions (160 and 615 r/min).

Thus, the indicated deviations from the parabolic law of the growth in thickness of the intermetallic layer are apparently related to the accelerated dissolution of the intermetallic layer at the initial moment. It is characteristic that a layer thickness of approximately 0.1 mm is observed after a minimal solution time, equal in the experiments to 1 s. We can assume that a layer of minimal thickness develops when specimens are cooled in a vacuum from the experimental temperature (800°C) to 400-600°C for 1-3 min.

Expression (25) lets us calculate the constant of the rate of growth in the θ-phase in the following case:

$$k_1 = \frac{2Kc_{ш}x}{d_{ш\text{-}т}} = \frac{2 \cdot 0{,}0015 \cdot 0{,}0625 \cdot 0{,}002}{3{,}45} = 1{,}05 \cdot 10^{-7} \text{ cm}^2/\text{s}.$$

If we compare this value with that obtained in [219] for the growth rate constant of the Fe_2Al_5 phase at a temperature of 715°C $K_1 = 2.2 \cdot 10^{-6}$ cm^2/s, we find that the θ-phase layer increases 20 times as fast as the η-phase layer. Numerically this confirms the fact, observed by various authors [220] that the η-phase has a rapid growth rate in comparison to the other intermetallic phases in the aluminum-iron system.

If the bond between the iron and the aluminum is to have sufficient strength, then the intermetallic layer which forms on the boundary (of the η-phase primarily) should not have cracks or large pores. In order to estimate the effect of the solution rate on the porosity of the intermetallic layer a series of experiments was performed at a temperature of 850°C and rotation rates of 63.1, 159.3, 239, and 527 r/min. From the data of these experiments it follows that the rate of rotation of a specimen considerably influences the porosity of the intermetallic layer.

The experiments indicated that the thickness of the intermetallic layer can be regulated as follows: 1) by selecting an optimal temperature for the welding process, which will provide an optimal ratio between the formation rate of the intermetallic layer and its solution rate; 2) selecting an optimal ratio of $\frac{S}{V}$ (the area of the solid surface and the volume of the liquid bath); 3) by selecting alloys (for example, containing silicon) which have a substantial effect on the composition and growth rate of the intermetallic layer.

If this is considered, then, as we will show below, we will first obtain steel-aluminum compounds which do not have an intermetallic layer (or a significant intermetallic layer) along their transition lines.

The nature of the behavior of the processes on the aluminum/steel boundary is caused by a drastic temperature change in the welding process, and thus as a rule we do not observe either an intensive development in the diffusion zone or a significant dissolution of the base metal in the metal of the joint (aluminum).

The thermal welding regime from the standpoint of the formation of intermetallic phases was estimated according to a method proposed by L. A. Fridlyand [165], who considered the characteristic features of heat propagation in the combination steel-aluminum weld. The

heating and cooling curve for a point on the contact surface between the metals during welding (Fig. 37) is divided into a certain number of equal and rather small temperature intervals t_1, t_2, ..., t_n, within the limits of each of which the latent period (of induction) is considered constant. The ratio of the length of time that t remains at a given temperature interval to c expresses the unused part of the period of induction. The condition of the absence of intermetallic phases in the combination is in this case expressed as:

$$\sum_{1}^{n} \frac{t_n}{c} < 1. \qquad (26)$$

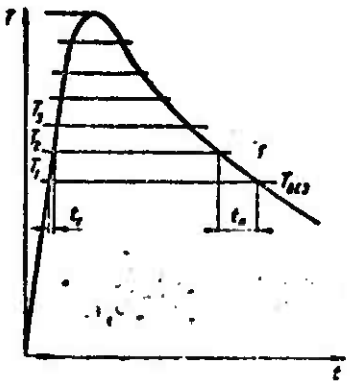

Fig. 37. Diagram illustrating the method of using the data on isothermic holding for constant heating and cooling conditions.

On the basis of the above it can be assumed that preventing the formation of brittle intermetallic phases is related to control over the rate of formation of this layer. However, to obtain specific data for calculating according to formula (26) we must first of all study the actual thermal cycle of the points on the transition line of the aluminum/steel joint.

CHAPTER III

INVESTIGATING THE HEAT PROPAGATION PROCESS IN AN ALUMINUM/STEEL JOINT

The interface between the aluminum and the steel in a composite welded joint is a very important zone, in which processes (reactions) arise, which determine technological and operational strength, seam tightness, and also its corrosion resistance. The intensity of the occurrence of these processes and the degree of their completeness depend primarily on the thermal effect during welding.

The number of intermetallic iron-aluminum phases, formed on an interface, is determined by the highest temperature of the thermal cycle and by the length of time the interface remains at high temperatures. To accurately designate the technological regime, which excludes or inhibits the appearance of intermetallic phases, it is necessary to study the laws governing the formation and the development of these phases. The first stage in the study of the indicated regularities is the investigation of the processes of heat propagation in steel/aluminum welded products. Such composite joints, as a consequence of the considerable difference in the thermophysical properties of the components, have characteristic pecularities in their heat propagation. There is a dearth of data in literature [6, 30, 238] on the unique nature of heat propagation in steel/aluminum joints. Thus, the problem of the author in this section was to determine and to calculate the maximum temperatures at the interface between the aluminum and the steel

in bimetallic models. In order to do this, it was necessary to experimentally obtain basic initial data for the calculation. Calculation was carried out on the basis of the theory of heat propagation during welding, developed by Rykalin, an academician of the AS USSR.

During the course of the investigations it was necessary to resolve the following problems: a) to select a calculational scheme for determining the maximum temperatures and the temperature bound for the application of the accepted calculational system; b) the heat input values during the welding of a composite joint; c) to select the constant coefficients, characterizing the thermophysical properties of the aluminum alloys being welded and of the steels, which are components of the bimetal, which would satisfy the calculational equation; d) to determine for various combinations of components of bimetals the time that the interface between the aluminum and the steel is higher than the specific "critical" temperatures.

1. The Efficiency of the Process of Heating a Steel/Aluminum Joint with an Arc

In connection with the absence of data on the effectiveness of heating a steel/aluminum joint with an arc, burning in an argon medium, it was expedient to carry out experiments to clarify the effect of the parameters of the argon-arc welding regime on the degree of heating of this type of joint both in the case of the welding of the aluminum cladding, as well as of the steel base.

In this case, 08kp steel-AMg3 aluminum alloy bimetallic patterns with dimensions of 75 × 200 mm were employed for the experiments; the total thickness of the bimetal was 3.5, 4.2, 5.8, and 10 mm. The patterns simulated lap welded joints.

First, a bead was deposited on a clad layer of aluminum alloy on a ADSV-2 automatic machine by argon-arc welding (the ac was from a IPK-350 power supply). The welding regimes were: welding rate - 12.5-16.8 m/h, the wire feed rate - 2.2 m/min, the argon flow rate - up to 16 *l*/min. To avoid significant heat transfer into the backing before depositing the bead the sample was placed on the two v-shaped guides of the jig. The beaded sample immediately after depositing of the bead was placed in a calorimetric vessel (a water calorimeter with a capacity of 12 *l*). The temperature was measured with a standard thermometer with a scale graduation of 0.2°C. The arcing time and the time that the sample remained in the calorimeter was measured by a stopwatch, and the electrical parameters - voltage and current magnitude - visually on panel measuring instruments. Each experiment was repeated not less than three times under identical conditions. Efficiency was determined for three values of welding current - 120, 150, and 170 A; the voltage in this case was very stable - 12-13.5 V. After the calorimetric measurement the samples were weighed to within an accuracy of up to 0.1 g.

The efficiency of the heating of the bimetallic model by the arc $\eta_{бим}$ was computed as a ratio of the heat input by the arc, including the heat, going to the heating of the base metal and the welding (filler) rod, to the total heat input, considered to be equal to the thermal equivalent of the electrical energy:

$$\eta_{бим} = \frac{q}{0{,}24IU} \qquad (27)$$

(q was determined from the data of the calorimetric experiments).

The total quantity of heat, introduced into the sample, was determined from equality

$$Q_{эф} = q = [m_в c_в (T_м - T_0) + m_к c_к (T_м - T_0) + m_{обр} c_{обр} (T_м - T_к)] \cdot 1{,}02, \qquad (28)$$

where $m_в$ - the mass of the water in the calorimeter, in our experiments $m_в$ = 12 ℓ; $c_в$ - the specific heat of water - equal to 4.1868×10^3 J/(kg·deg); T_m - the maximum established water temperature in the calorimeter (final water temperature); T_0 - the initial water temperature; $m_к$ - the mass of the calorimeter with the agitator, in our experiments $m_к$ = 3950 g; $c_к$ - the specific heat of the calorimeter of mild steel, $c_к$ = 669.8 J(kg·deg); $T_в$ - the temperature of the ambient air; $c_{обр}$ - the specific heat of the sample.

The specific heat of the bimetallic sample was

$$c_{бим.\,обр} = \frac{x}{100} c_{ал} + \frac{(1-x)}{100} c_{ст}, \qquad (29)$$

where x - the weight percents of the aluminum content in the bimetallic sample.

The coefficient 1.02 (2%) considered the losses from water evaporation, heat losses during welding and during the transfer of the sample, and also the heat losses due to the difference in enthalpies.

The calculated heat input was determined from expression

$$Q_{расч} = 0{,}24 I v t_{св},$$

whence the efficiency of the process of the heating of the bimetal by the arc was

$$\eta_{бим} = \frac{Q_{эф}}{Q_{расч}}.$$

The results of the measurements of the parameters for determination of $\eta_{бим}$ during bead forming with respect to the aluminum cladding and the steel base and the nature of the variation in the heating efficiency of the bimetallic joint by the arc are illustrated in Fig. 38. An analysis of the graph makes it possible to draw the following conclusions.

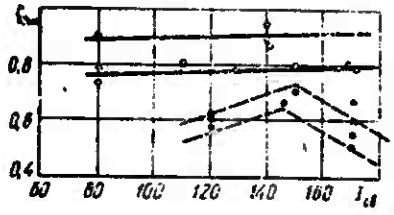

Fig. 38. Average value of the efficiency $\eta_{бим}$ of the heating of a manufactured article by an arc: ○ - bead forming on the aluminum cladding; ● - bead forming on the steel base.

1. With identical electrical arc power its heat input, received by the bimetal, is greater in the case of bead forming on the steel base ($\eta_{ср.ст}$ = 0.82), than for the aluminum cladding ($\eta_{ср.ал}$ = 0.62).

2. The increased value of the efficiency $\eta_{ср.ст}$ as compared with the efficiency $\eta_{ср.ал}$ can be explained, apparently, by the distinctive supplemental heating by the thermal wave, passing through the aluminum cladding, situated under the steel base.

3. The presence in the bimetal of the steel base, "ideally" adjoining the aluminum cladding, intensifies the heat transfer from the latter as compared with a plate, cooled in air. This corresponds to the data obtained by A. A. Kazimirov and A. Ya. Nedoseka [63, 64] for the case of the welding of aluminum on steel backing. Actually, a comparison of the values $I_{св}$ and Q for the aluminum and the bimetal shows, that if for welding of AMg6 alloy with a thickness of 1.5 mm $I_{св}$ = 105-115 A, then in the forming of a bead on a bimetal, having a clad layer of 1.5 mm 150-160 A are required, i.e., 1.3-1.4 times greater current magnitudes.

For checking the convergence of the results obtained during calorimetric measurement, calorimetric measurement of samples of the following experimental bimetals was carried out: St. 3 steel-AMg5V alloy, 1Kh18N9T steel-AMg6 alloy and 28Kh3SNMFVA steel-AMg6 alloy. The obtained values fell within the range, indicated on the graph (Fig. 38).

2. Calculating the Thermal Cycle of Argon-Arc Welding of an Aluminum-Steel Bimetal

A bimetallic sheet is a composition of two metals, "ideally" adjoining each other, which is brought about by the technological process of rolling, in which an 80% reduction of area of the aluminum alloy occurs. The considerable increase in the contact surface during reduction of area contributes to the disintegration of the oxide film. In this case, there is no impairment of contact, no gaps, etc., thus, from the point of view of the study of heat transfer there is no necessity to take the low thermal conductivity of the oxide film (3.34 W/(m·deg)) on the aluminum alloy [63] into account. However, in the heating of the interface between the aluminum and the steel above 520-535°C an intermetallic layer can be formed, the presence of which changes the nature of heat propagation in the bimetallic model, since the thermophysical properties of the intermetallic phases, of steels and aluminum, are different.

The data on the effect of an interlayer of intermetallic phases on heat propagation are contradictory. Work [182] indicates, that in producing bimetallic castings by the al-fin process there is a continuous metallic transition between the aluminum and its alloys, on the one hand, and the steel, on the other hand, which ensures a strong joint and good thermal conductivity of the transition layer.

Throttling of the heat flow is not observed at the site where the two metals come into contact due to the presence of the metallic transition layer [198].

As will be shown below, during optimum welding regimes the thickness of the intermetallic layer does not exceed 1-2 μm, which practically does not introduce any variations into the nature of heat propagation. Thus, we did not take the discontinuity in the thermal conductivity curve into account in the subsequent calculations.

The generally accepted arrangements of the theory of concentrated sources can be employed for calculating the thermal processes of argon-arc welding of a steel/aluminum joint [128, 129]. However, in this case it is necessary to take into account the pecularities of the removal of heat from the welding site by the steel base of the bimetal [69, 173].

We took the equation of the limiting state as the basic calculational formula in welding with a concentrated linear heat source, travelling at a constant rate in an unlimited plate with heat transfer:

$$T(x,r)=\frac{q}{2\pi\lambda\delta}\exp\left(-\frac{vx}{2a}\right)k_0\left(r\sqrt{\frac{v^2}{4a^2}+\frac{b}{a}}\right). \qquad (30)$$

In analyzing this equation, it is necessary to conclude, that to employ it, it is necessary to know the magnitude of heat input by the arc, determining the quantity of heat, introduced into the bimetallic plate during welding:

$$q=0{,}24\,Iu,$$

where I - current, A; u - voltage, V.

The remaining designations in the formula (30): δ - the thickness of the sheets being welded, cm; λ - the coefficient of thermal conductivity of the aluminum alloy, which is the clad layer in the bimetal, W/(m·deg). Satisfactory convergence in the calculations was obtained by substituting in the formula not the total values of λ, i.e., the values for the bimetal, but only the values for the aluminum alloy; v - the mean velocity of motion of the arc, cm/s; $r=\sqrt{x^2+y^2}$, cm (x, y - the moving coordinates of the point in question, the center of which we will consider an arc with radius r); a - the coefficient of thermal diffusivity, cm^2/s for the aluminum alloy, which is the clad layer in the bimetal,

$$a=\frac{\lambda}{c\gamma},$$

where c - the specific heat of the aluminum alloy, J/(kg·deg). The values of the thermophysical properties of the metals λ and c, which we applied in the calculations, are cited on the graphs of Figs. 3 and 4 for the temperature range 300-400°C; $b = \frac{2\gamma}{c\gamma\delta}$ - the coefficient of heat transfer for a homogeneous plate, 1/s (α - the coefficient of total surface heat transfer: for aluminum $\alpha_{ал} = 0.000715$; for steel $\alpha_{ст} = 0.00709$).

As A. A. Kazimirov and A. Ya. Nedoseka [64] demonstrated, on the basis of the processing of experimental data, the value of the coefficient of heat transfer of aluminum with a thickness of 2 mm on a steel plate trasferring heat is 0.0280 1/s.

Figure 39 presents the thermal cycles of three points of the St. 3 steel-AMg3 alloy bimetal, obtained by calculation.

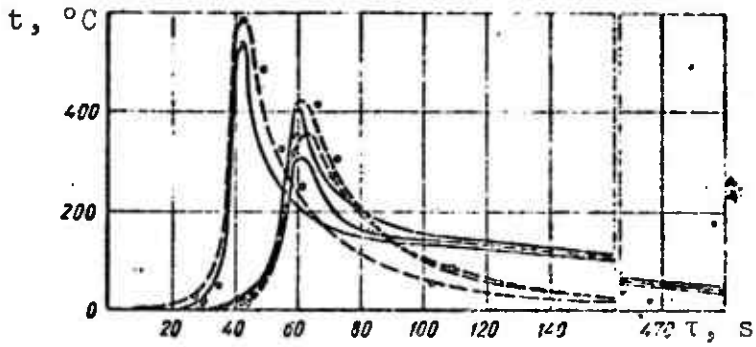

Fig. 39. Experimental (solid curves) and calculational (broken curves) thermal cycles of a steel/aluminum joint.

3. Experimental Determination of Heat Propagation in Bimetallic Metals During Welding

To obtain the initial calculational data, and also to compare the experimental thermal cycles with the calculational cycle composite samples (bimetallic models) were manufactured; St. 3-AMg3; St. 3-AMg6; 1Kh18N9T steel-AMg6; 28Kh3SNMVFA steel-AMg3 alloy; 28Kh3SNMVFA steel-AMg6 alloy. The effect of various parameters of the welding regime was studied on these models.

The thermal cycles were recorded on a N-700 loop oscillograph with the paper moving at a rate of approximately 0.25 cm/s, and measured with copper-constantan thermocouples with a diameter of 0.4 + 0.4 mm. These cycles were determined for points, lying on the transition line from the steel to the aluminum clad layer, and for points, situated on the surface of the para-seam zone. During the time the oscillograms were being made the sample was situated on angle brackets.

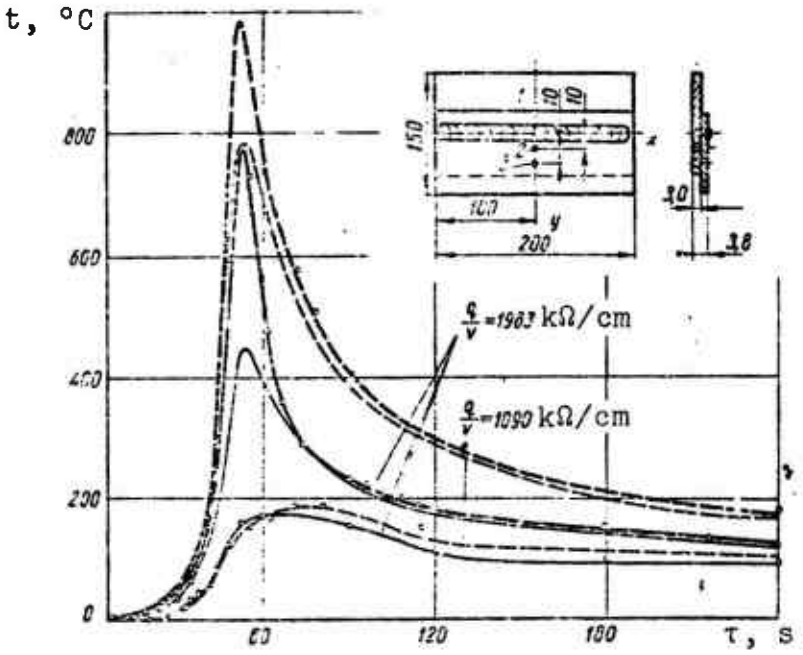

Fig. 40. Thermal cycles of three points of a bimetal with a thickness of 3.8 mm.

Figure 40 presents the thermal cycles of three points of a bimetal with a thickness of 3.8 mm with a clad layer of aluminum alloy with a thickness of 0.8 mm and with a base of armco iron. The welding regimes are $I_{св}$ = 105-110 A; $u_д$ = 12 V; $v_{св}$ = 6.5 m/h. As follows from the figure point 1 situated on the line of transition of the bimetallic model (t_{max_1} = 775°C). The points situated at a distance of 10 and 20 mm from the axis are subjected to a lesser thermal effect (respectively t_{max_2} = 450°C and t_{max_3} = 175°C).

With an almost twofold increase in heat input (from 1090 cal/cm to 1983 cal/cm) due to an increase in current the aluminum clad layer is completely fused.

A comparison of the thermal cycles of the transition zone of armco iron-AMg3 alloy bimetal during the welding at various heat inputs shows, that the most significant variation in temperatures is observed at points 1 and 2.

The degree of similarity of the curves on the cooling branch increases in proportion to the distance from the seam axis. Here in the case of welding at low values of heat input the cooling of point 1 takes place more intensely: the effect of the armco iron backing is expressed. In the case of complete fusion penetration (the broken lines) the bimetallic sample cools more slowly. The noted pecularity has significance in determining the parameters of the welding regime of a bimetallic joint: experiments have shown the possibility of narrowing the zone of high heating temperatures and consequently, of the possibility of decreasing the time that the interface between the steel and the aluminum remains in the region, where the temperature is higher than the formation temperature of the intermetallic layer.

In view of the fact, that in measuring thermal cycles of bimetallic models with a thin clad layer thickness no sharp difference was observed in the thermal cycles; models were manufactured with a thickness of 10-12 mm, in which the thickness of the cladding was half the thickness of the bimetal. In this case it was established, that:

1) an increase in the thickness of the steel base increases heat transfer, as a consequence of which the maximum temperatures at all points are reduced; 2) the drop in maximum temperatures is proportional to the increase in the thickness of the steel base; 3) for all points the curves of a thermal cycle are similar; 4) with an increase in the thickness of the steel base the time for the

attainment of the maximum temperatures is increased, i.e., the maxima on the thermal cycle curves are displaced in the direction of lower temperatures, which is attained as a result of a decrease in the time that the interface between the steel and the aluminum remains in the region of dangerous temperatures, for example, by supplemental cooling of the aluminum clad layer of the bimetallic metal.

For comparing the nature of the variation in welding thermal cycles employing a bimetal, experiments were carried out on samples with dimensions of 150 × 200 mm with a total thickness of 6-10 mm. Seams were imposed with a ADSV-2 automatic welding machine; a welding rod was not employed. The thermocouples were tentatively positioned at an angle of 45° to the seam being imposed to avoid distortion of the thermal field.

The maximum temperature values are attained during the welding of the aluminum clad layer; the steel base seemingly plays the role of a heat-insulating backing. In the welding of the steel base of the bimetal the degree of cooling is greater (the values of maximum temperatures at the same points are lower), but the rate of heat propagation in this case is also greater: the maximum values of temperatures at the same points are obtained 2-4 s earlier. This can possibly be explained by the facts, that during the welding of the steel base of the bimetallic model the aluminum clad layer, playing the role of the backing, due to its high thermal conductivity and limited cross section promotes more rapid heat propagation along the backing. Thus, the temperature gradient between the steel and the aluminum and the intensity of heat transfer to the backing are reduced (at slow welding rates).

Figure 39, besides the curves of the calculated thermal cycles, also presents the curves of experimental thermal cycles. The calculated temperatures are higher than the temperatures of the experimental thermal cycles for like points of the curves of a welded joint and for the same time of reading. Certain characteristic

regularities are observed in the variation in the differences between the calculated and the experimental values of temperatures. On the section of the curve, corresponding to heating, the calculated and experimental curves, as a rule, coincide, in the temperature range above 200-250°C the nature of the calculated thermal cycles is similar to the nature of the experimental cycles and only in the cooling stage below 200°C is a significant divergence observed in the nature of the curves.

A correction coefficient, which takes into account the effect of the steel base of the bimetal on the heat propagation process in a bimetallic plate, was determined by dividing the values of the temperatures of the thermal cycle curves, obtained by calculation, by the values of the temperatures of like points of the curves, obtained experimentally. The results of a comparison of the calculated and experimental values of the temperatures of points lying on the transition line of the bimetal, showed, that the magnitude of the correction coefficient on the average was equal to 0.8.

The necessity for employing correction coefficients complicates the procedure of obtaining values of the necessary temperatures by calculation. In this case, it is difficult to obtain coefficients, which are suitable for various combinations of welded thicknesses and types of metal joints.

4. Employing the Modeling Method for Investigating the Thermal Fields of a Steel/Aluminum Joint

As was indicated in the preceding sections, determination of the nature of heat propagation at various points of a steel/aluminum joint is complicated, theoretically, as well as experimentally. In practice, the determination of the time that a point remains, lying on a transition line above the temperature of the formation of the intermetallic phase, for numerous existing

bimetallic compositions of steel with aluminum, is impracticable, since it depends on the composition of the metals going into the bimetal, the relationship of the thicknesses of the thermophysical properties of the components [sic] and other factors. In connection with this, it was necessary to attempt to find general dependences, which would establish a connection between the cited parameters. For this purpose, to investigate an unsteady thermal field the method of mathematical modeling or the method of analogies, developed at the Laboratory of Electrical Modeling of the Institute of Mathematics of the AS UkSSR [166, 167], was employed.

To determine optimum welding conditions it is necessary, first of all, to determine the unsteady temperature field within the two-layer plate, having a certain initial temperature t_0 and the temperature at the boundary of the weld pool $t_{пл}$. The solution of this problem makes it necessary to solve a boundary value problem for the equation of thermal conductivity

$$\frac{\partial}{\partial x}\left[\lambda(x, y)\frac{\partial t}{\partial x}\right] + \frac{\partial}{\partial y}\left[\lambda(x, y)\frac{\partial t}{\partial y}\right] = c_p\gamma(x, y)\frac{\partial t}{\partial \tau}, \qquad (31)$$

where $t(x, y, \tau)$ - temperature, °C; $\lambda(x, y)$ - thermal conductivity, W/(m·deg); $c_p(x, y)$ - specific volumetric heat, J/(m^3·deg); x, y - current coordinates, cm.

It has not as yet been possible to develop sufficiently effective analytical methods for solving equation (31), with the exception of the simplest particular cases. For solving this equation, as was indicated, the analogy method was employed. The essence of electrothermal analogy consists in replacing the temperature field, which is subject to study, by an electrical potential field. The equations, defining both fields in dimensionless representation, are identical, the dimensionless boundary conditions are also identical, if the field of the unknown magnitude at the boundaries of the system is directly defined by them, i.e., if the thermal problem is posed under boundary conditions of the first or second type [49].

In the course of the work we employed the method of modeling of equation (31) on electrical conducting paper with distributed capacitance [166].

The potential distribution equation in the electrical model, made from the paper, has the following form

$$\frac{\partial}{\partial x}\left[\rho(x, y)\frac{\partial \varphi}{\partial x}\right] + \frac{\partial}{\partial y}\left[\rho(x, y)\frac{\partial \varphi}{\partial y}\right] = c(x, y)\frac{\partial \varphi}{\partial \tau}, \qquad (32)$$

where $\varphi(x, y, \tau)$ - potential, rel. units; $\rho(x, y)$ - average specific conductivity, $1/\Omega$; $c(x, y)$ - average specific capacitance, F/cm^2.

From the joint solution of the full-scale equation (31) and the model equation (32) we obtain the similarity number for the corresponding zones:

$$\frac{c_M l_M^2}{\rho_M \tau_M} = \frac{c_H l_H^2}{\lambda_H \tau_H}, \qquad (33)$$

where c_M - the specific capacity of the model; l_M - unit length of the models; $\rho_M = \frac{1}{R_M}$ - the conductivity of the electrical conducting paper (R_M - resistance of the square of the electrical conducting paper); τ_M - unit time during modeling; λ_H - coefficient of thermal conductivity of the corresponding full-scale zone; $c_H = c_\gamma$ - volumetric specific heat of the corresponding full-scale zone; l_H - unit length of the modeling object (full-scale); τ_H - real unit time of the modeling process.

Parameters λ_H, c_H, l_H are given. Parameters R_M, c_M, l_M are defined by the model. The ratio of the corresponding time in expression (33) is characterized by dimensionless values: by the length scale α_l, by the time scale α_t, by the capacity scale α_c and by the resistance scale α_R:

$$\alpha_l = \frac{l_H}{l_M}; \qquad (34)$$

$$\alpha_t = \frac{t_н}{t_м} = \frac{c_н l_н^2}{\lambda_н c_н R_н l_н^2}; \quad (35)$$

$$\alpha_c = \frac{c_н}{c_м}. \quad (36)$$

$$\alpha_R = \frac{1}{\lambda_н R_н}. \quad (37)$$

The selection of these similarity factors is restricted only by the following condition

$$\frac{\alpha_R \alpha_c \alpha_l^2}{\alpha_t} = 1 \quad (38)$$

and, consequently, it is possible within broad limits to select convenient parameters of the model.

Proceeding from the formulated problem the model length scale α_l and the scale of the type of electrical conducting paper are selected for its manufacture so that the ratios of the average specific resistances of the model zones are equal to the given ratios of the corresponding full-scale coefficients.

A square of necessary dimensions is cut from electrical conducting paper to determine $R_м$. Then the resistance of the square with respect to the two mutually perpendicular directions is measured. The arithmetical mean of these measurements is found, which is also taken as the specific resistance of the corresponding zone of the model. As a dielectric for the manufacture of the models polyethylene or other nonpolar films with a thickness of 0.005-0.2 mm are employed. In the manufacture of a model the ratio between the average specific capacities should be equal to the given ratios of the corresponding coefficients of full-scale capacities.

For modeling two-dimensional unsteady fields, described by the equation of thermal conductivity, a special integrator has been developed based on the electrical conducting paper with distributed capacitance [167]. It consists of a rack of power supply and measuring devices and a stand for the electrical model (Fig. 41).

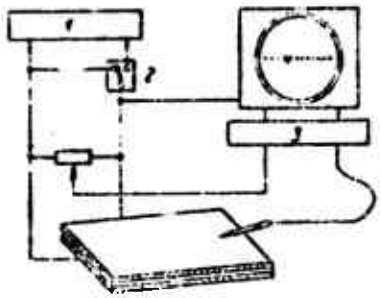

Fig. 41. Schematic diagram of an integrator in the measuring regime: 1 - rectifier; 2 - voltage divider; 3 - comparison element.

For realizing boundary conditions of the first type φ = const a wire with a diameter of 0.1-0.2 mm is attached to the model with a given contour of the weld pool with an electrical conducting glue and the required potential is supplied to it.

In modeling based on an integrator dimensionless, or, as they are frequently called, reduced magnitudes are employed. The reduced unit of potential is considered to be the difference of the potentials at the output of the integrator power supply (the minimum value of voltage is taken to be equal to zero, and the maximum - to unity). All measurements are carried out in fractions or in percents of the maximum operating voltage.

Between electrical potential φ and temperature t which corresponds to it the following dependence exists:

$$\varphi = \frac{t - t_{min}}{t_{max} - t_{min}}, \qquad (39)$$

where t_{min} and t_{max} - respectively, the minimum and maximum values of the temperature of the process being modeled, °C.

The temperature of the bimetallic plate at an initial moment of time was 20°C. The following boundary conditions were accepted: on the boundary of the weld pool the temperature is instantaneously increased to 660°C, if the aluminum is fused, or to 1539°C, if the steel is fused (boundary conditions of the first type). The contour of the weld pool was predetermined on real bimetals, especially manufactured for this purpose.

In accordance with formula (39), employing the given boundary values t at full-scale, all of the necessary boundary values of the reduced potentials are computed, and then the electrical model is structured in accordance with these values. Taking into account, that the ratio of the specific resistances of the model zones should be equal to the ratio of the specific resistances of the full-scale zones, it was assumed, for example, for the zone simulating the AMg6 alloy, the resistance of the paper was 80 $k\Omega/cm^2$, and for the zone simulating St. 3, the resistance of the paper was 150 $k\Omega/cm^2$. They were cut from corresponding sheets of paper at a scale (for our problem the scale is equal to 1/15) of the zone and they were attached by electrical conducting glue. On the boundary of the weld pool a conducting bus was attached, to which a potential of $\varphi = 1$ was supplied.

Since the ratio of specific capacities of the model zones should be equal to the ratio of the specific capacities of the full-scale zones, for the zone, simulating the AMg6 alloy a specific capacity of $c = 6.5 \cdot 10^{-12}$ F/cm^2 (two layers of polyethylene film of appropriate thickness), and for the zone, simulating the St. 3, - $c = 13 \cdot 10^{-12}$ F/cm^2 (one layer of the same film).

Potential $\varphi = 0$ was supplied to the conducting plate. After measuring the values of potential φ on the model at the points which were of interest to us, the unknown value of temperature t was computed by formula (39) at these same full-scale points at moments of time which were of interest to us (the time scale was $\alpha_t = 12.9 \cdot 10^3$).

An unsteady temperature field for various bimetallic plates was set up in 50 variants, in which both the ratio of the thicknesses of the plates of bimetal were taken into account, as well as for thermophysical properties.

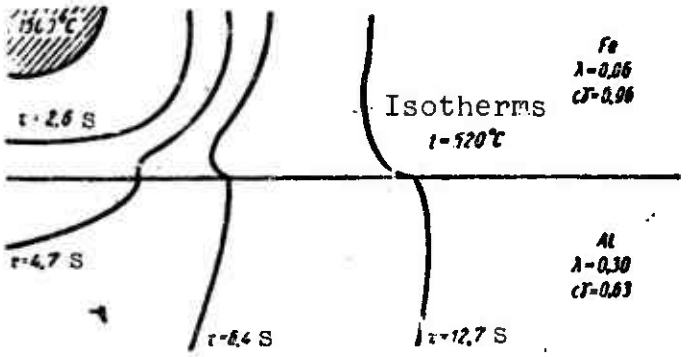

Fig. 42. The nature of isotherm motion when t = 520°C with time.

Figure 42 shows one of the variants of the motion of critical isotherm 520°C for the 1Kh18N9T steel-AMg6 alloy bimetal at a layer ratio of 1:1.

Calculation of the time of attainment of critical temperature $\tau_{сеч}$ for a large number of different bimetals (AD1-1Kh18N9T, AMg6-1Kh18N9T, AD1-St. 3, AMg6-St. 3, etc.) made it possible to construct the nomograms, presented in Fig. 43. The time of attainment of critical temperature at a point, located under the weld pool at the line of transition from one metal to another, was determined depending on the ratio of thermal conductivities (λ_1/λ_2) of the component metals, the ratio of the thicknesses (δ_1/δ_2), which were varied sequentially from 3/1 to 1/3, and the ratio of the specific heat of a unit volume $(c_1\gamma_1/c_2\gamma_2)$ (the metal, on which the heating was carried out, is indicated in the numerator).

The estimation of the stay time of the transition line of a steel/aluminum joint in the region above critical temperature with respect to the data of the draft for various actual combinations of aluminum alloys with steels and a comparison of this time with the magnitude of the latent period, obtained experimentally by the method described in the preceding chapter (formula (26)) is illustrated by the data presented in Table 10.

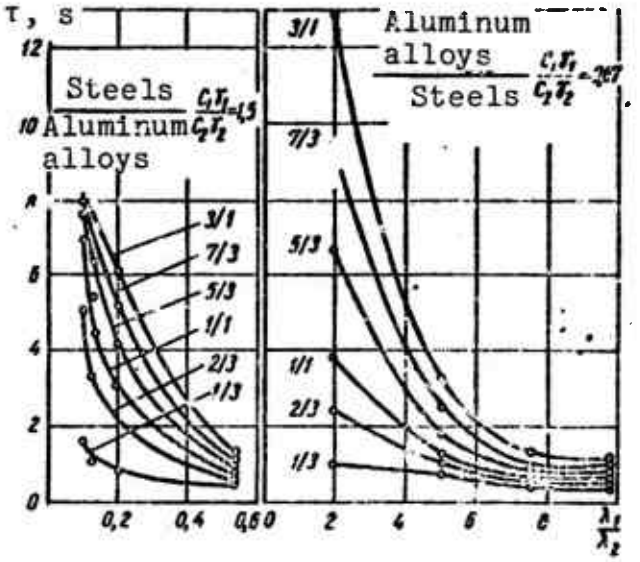

Fig. 43. Nomograms for calculating the stay time of the joint transition line above the critical temperature.

Table 10. Data, obtained in determining τ_n.

λ_1	λ_2	$\frac{\lambda_1}{\lambda_2}$	τ_n at a thickness ratio of 3/1	1/1	1/3	c	$\frac{\tau_n}{c}$	Average values $\frac{\tau_n}{c}$ for a combination of metals
0.57	0,12	4,75	3,2	2,0	0,8	3–4	0,5—0,7	For a combination with St. 3 0.7-0.9
0,38	0,12	3,16	6,5	2,6	0,85	3—4	0,6—0,84	
0,32	0,12	2,66	9,0	3	0,9	3—4	0,78—1,0	For a combination with 1Kh18N9T 0.6-0.7
0,57	0,06	9,5	1,3	0,7	0,4	1,5—2	0,35—0,46	
0,38	0,06	6,3	2,0	0,8	0,6	1,5—2	0,4—0,53	
0,32	0,06	5,3	2,9	1,5	0,65	1,5—2	0,7—0,75	

Thus, the temperature-time factor is important for estimating the possibility of obtaining a combined [composite] joint. However, based only on this factor, it is not possible to completely eliminate the formation of brittle phases. As will be shown below, the alloying of the weld pool has a significant effect.

5. Investigating the Direct Welding of Aluminum with Steel

The data obtained in the preceding sections made it possible to establish, that the ratio of stay duration in a region of higher temperatures 520-535°C to the latent period for a steel/aluminum St. 3-AD1 aluminum joint is 0.7-0.9, and for a 1Kh18N9T steel-AD1 aluminum joint - 0.6-0.7. At such a ratio, in a narrow range of welding regimes it is possible to accomplish direct welding of aluminum with steel and to obtain a joint with limited strength (on the level of the strength of pure aluminum). Actually, from the practice of the welding of aluminum and its alloys, it is known, that when carbon or stainless steel are employed as removable backings, cases of the strong welding of aluminum edges to steel backing occur. The checking of this phenomenon during the argon-arc welding of aluminum/steel lap joints showed, that an extremely narrow range of values of the magnitude of welding current exist, during the employment of which the obtaining of a joint with the strength, equal to the strength of pure aluminum (Fig. 44) is possible. In this case, the plasticity of the welded joints is low as a consequence of the great fusion of the metals being joined, as a result of which the content of the elements in the seam exceeds their mutual soluability and brittle intermetallic joints of iron with aluminum form in the seam metal.

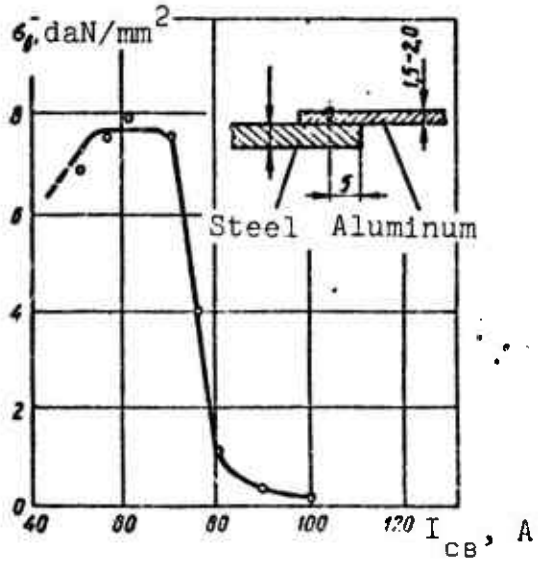

Fig. 44. The dependence of the strength of a lap joint on the magnitude of welding current.

The results of the determinations are very unstable, and welding under the indicated conditions cannot be recommended as one of the technological procedures for obtaining a steel/aluminum joint.

Argon-arc welding of aluminum with steel on a ADSP-2 automatic welding machine was carried out employing a AD1 welding rod and a sv. 10GS steel wire. The welding regimes of AD1 brand aluminum with St. 3 steel with aluminum wire are the following: u_{xx} = 28 V; arc voltage $u_д$ = 25-28 V; $I_{св}$ = 290-310 A; electrode diameter is 2 mm; electrode wire feed rate is $v_{н.э}$ = 400 m/h; the welding rate is $v_{св}$ = 30 m/h. The regimes for welding aluminum with steel employing a steel wire are: u_{xx} = 28 V; $u_д$ = 26-28 V; $I_{св}$ = 120-180 A; $d_{эл}$ = 1 mm; $v_{н.э}$ = 230 m/h; $v_{св}$ = 24 m/h.

To reduce the quantity of fused iron going into a seam, bevelling of the steel samples was carried out at an angle of 30°, and the bluntness was 2 mm (Fig. 45a), or with respect to the pool profile (Fig. 45b), aluminum samples were employed without bevelling.

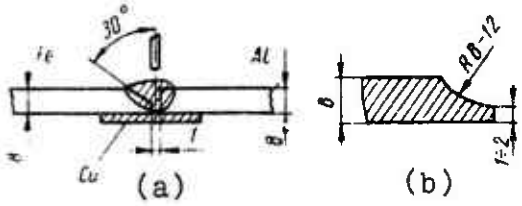

Fig. 45. Diagram (a) and type of bevelling (b) in the direct welding of aluminum with steel.

Automatic welding with flux was carried out on a A = 862 device especially designed for this purpose. The welding regimes were: $I_{св}$ = 400 A, $v_{св}$ = 21.5 m/h; $v_{п.э}$ = 290 m/h, $u_д$ = 40 V. Wire of brands AD1 and AK, and flux AN-A1 were employed. In beading AD1 wire based on St. 3 steel with AN-A1 flux it is possible to obtain a seam of good form, but with transverse cracks. On an

unpickled microsection the fusion zone has a characteristic brownish-yellowish hue. The hardness of the beaded metal exceeds the hardness of the base metal by 2-3 times.

To obtain a relative plastic layer in the seam elements are introduced (for example, zinc), which give a low-melting eutectic at least with one of the metals being joined. The zinc was introduced into the seam by several methods: via the flux by adding $ZnCl_2$ and ZnF_2, by adding a specific quantity of zinc to the composition of the rod metal, by pulling in the fuse metal or by obtaining fusion of a zinc plate during welding. Seams were obtained by the indicated methods either with the presence of a small transition layer from the steel to the aluminum, or joints - without a transition layer (Fig. 46).

Fig. 46. The nature of the transition layer in beading on St. 3 steel under a layer of zinc and AN-A1 flux with a AD1 wire.

From the hardness graph (Fig. 47, the broken line) it is evident, that the hardness of the beaded metal in this case is lower than the hardness of the base metal - steel. The beaded metal possesses satisfactory plasticity, permitting bending without failure up to 90°, which makes it possible to accomplish subsequent welding of elements of aluminum alloys employing, for example, argon-arc welding.

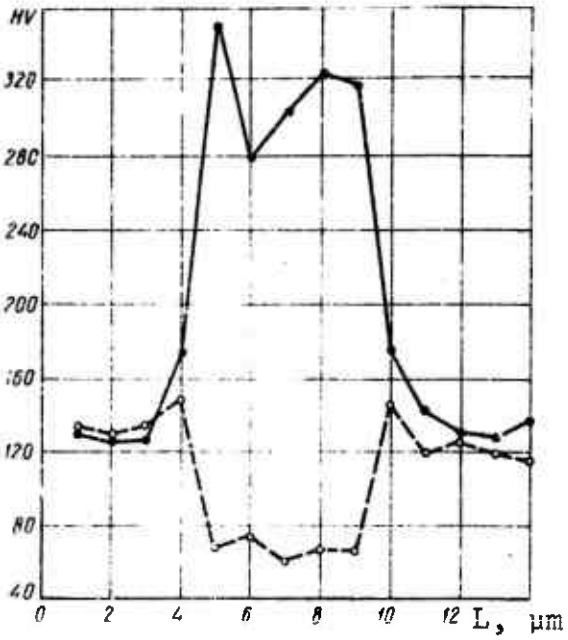

Fig. 47. Hardness distribution over the cross section of a seam during beading based on St. 3 steel (solid curve) with AD1 wire and AN-A1 flux and with a AD1 wire under binary flux-zinc shielding (broken curve).

Besides the works on beading, experiments were also carried out on the direct welding of aluminum with St. 3 steel and AD1 aluminum (the thickness of the metals being joined was 10 mm). The character of seam forming was satisfactory; during tensile testing the ultimate strength was the same, as the ultimate strength of pure aluminum (up to 10 daN/mm^2). Failure of the joint occurred along the transition zone or in the base metal-aluminum.

Thus, by the given welding method the obtaining of the ultimate strength of a steel/aluminum joint not lower than the ultimate strength of pure aluminum is possible, which is attained as a result of welding technology and complex alloying of the seam metal (zinc, aluminum wire, flux). However, this welding method is extremely complex, applicable only for a metal of specific thickness and a limited number of joint types. The possibility of obtaining joints without intermetallic layers requires accurate observance of the

positioning of the electrode and the introduction of a sufficient quantity of zinc, which is extremely difficult in practice.

CHAPTER IV

THE FORMATION OF INTERMETALLIC PHASES DURING WELDING AND THEIR EFFECT ON THE PROPERTIES OF STEEL/ALUMINUM WELDED JOINTS

1. Kinetics of the Wetting of Iron with Aluminum

Let us examine the first stage of the contact interaction of aluminum with steel - the wetting process. Consideration of this, and also of the data on dissolving makes it possible to a certain degree to regulate the formation of intermetallic joints for the purpose of finding the optimum conditions for fusion welding.

Since the published data on the flow of liquid metals over the surface of solid metals are limited, and are completely absent for the iron-aluminum system, special experiments were conducted [54].

Contact angles on the interface of phases (θ) were taken as the basic criterion of wetting and flow. Contact angle was determined by the quiescent drop method. The vacuum in the chamber at the maximum temperature of the experiment was $1\text{-}3 \cdot 10^{-5}$ mm Hg.

In the method which was developed for investigating the kinetic dependences of θ on various factors the active interaction of aluminum and iron was taken into account at elevated temperatures and the dissociation pressure of the aluminum oxides was low.

As follows from the kinetic dependences of the contact angle (Fig. 48), the iron-aluminum system is characterized by satisfactory wetting and by a high rate of flow. An increase in temperature leads to a decrease in wetting angle.

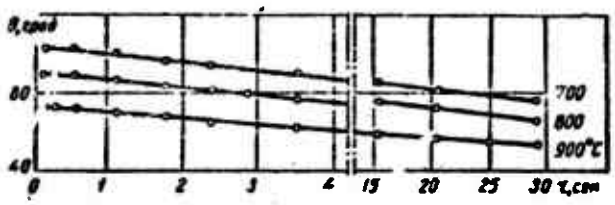

Fig. 48. Time dependence of the contact angle of aluminum on iron (data of N. D. Lesnik, and others).

The computed energy of adhesion even for the first moments of contact is rather great and constitutes 0.65-0.7-1.03 MJ/m^2 at temperatures of 700-800-900°C. The molar energy of adhesion in the temperature range 700-900°C is 28.47-44.8 kJ/mole.

When there are low-melting galvanized coatings on a steel surface the wetting of the iron by the aluminum is noticeably improved. In the case of argon-arc deposition of aluminum on iron, of all the tested galvanized coatings (zinc, silver, tin, nickel, copper-zinc, nickel-zinc, and others) the zinc and the combined (zinc-copper, zinc-nickel) coatings ensure the best technological properties. Alloying additives in an aluminum alloy considerably affect wetting. This is connected with the variation in the surface tension of aluminum and with the nonuniform distribution of additives in the melt due to their diverse nature (surface-active, inactive). The effect of alloying additives on the surface tension of the melt depends on the relationship of the atomic volumes of the dissolved element and the solvent: the greater is the atomic volume of the introduced element, the greater is the reduction in the surface tension of the metal-solvent. It was established [28], that the surface tension of a melt is sharply reduced upon the introduction of small additions of surface-active elements. Improvement of aluminum flow over the steel is attained upon the addition to the melt of strong reducing agents (Mg, Na, K, and others), since they reduce the oxide film.

To determine the flowability Japanese investigators [169] investigated alloy samples with the following additives: Ag, Be, Bi, Ca, Cd, Co, Cr, Cu, In, K, Li, Mg, Mn, Mo, Na, Ni, Pb, Sb, Se, Si, Sn, Te, Ti, Tl, and Zr. The specimens had the following dimensions: a diameter of 3 mm, a height of 5 mm; they were mounted on iron backings and were placed in an electric furnace at a temperature of 680°C, where they were held for 2 min. In all cases KF-54 flux was employed. It was established, that bismuth most effectively increases the flowability of aluminum alloys.

The investigations show that the effect of alloying components on the flow of liquid aluminum i intimately connected with their effect on surface tension. In this case, the additives, which raise the surface tension or do not affect it, worsen the wetting of steel by the aluminum. Those additives, which reduce the surface tension of a melt improve its flowability. For example, the addition to aluminum of silicon, manganese, copper, zinc practically do not have any effect on the flowability of aluminum over steel, since these additives have little effect on its surface tension. Whereas, the introduction of magnesium, lead, bismuth, cadmium to aluminum to a significant extent decrease $\sigma_{расп}$ (Fig. 49a) and improves flowability (Fig. 49b) [28].

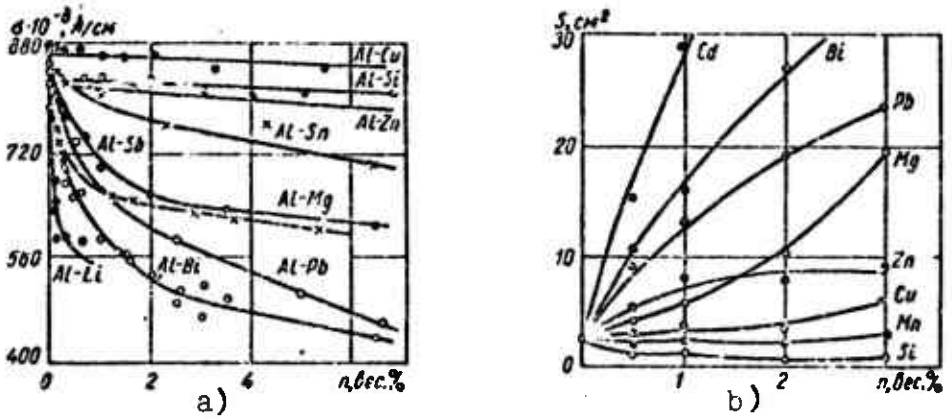

Fig. 49. The effect of various additives on the surface tension of aluminum a) and its flow over steel b). S - flow area; n - additive content.

The flowability of a melt depends not only on the wetting and the surface tension at the liquid-gas interface, but also on other factors - the viscosity and the fluidity of the melt, the presence on the melt surface of oxide films, oil spots, oxides, roughness, and others.

2. The Effect of the Chemical Composition of an Additive Material on the Properties of a Layer

As was noted, the interaction of aluminum with steel leads under specific conditions (temperature and time) to the formation of intermetallic phases along the contact line.

At the present time several practical methods of calculating the entropy of intermetallic joints are known: simple addition of the entropy of the solid components, calculation by the methods of M. Karapet'yants and Viner and by the formula of Eastman and Hertz [2, 32, 65, 66]. The most accurate is the method of calculating by Eastman's; the remaining methods are either inaccurate (the sum of the entropies of the components, calculation by Hertz' formula) or require knowledge of the values of certain coefficients, the determination of which for iron/aluminum compounds is not possible (calculation by the methods of Karapet'yants and Viner).

Eastman's formula, which defines the variation in the entropy of a reaction, has the form

$$S^{\circ}_{298} = \frac{3}{2} R \ln A_{cp} + R \ln v_{cp} - \frac{3}{2} R \ln T_{пл} + a [\text{джоуль} \cdot \text{град} \cdot \text{г-ат}]. \qquad (40)$$

where A_{cp} - the average atomic weight, i.e., molecular weight, relative to the number of atoms in a molecule of the compound; V_{cp} - average atomic volume, i.e., average atomic weight of a compound, relative to its density; a - constant, equal to 12.5 $\pm$ 2

(for related substances the fluctuation range of value a is less); $T_{пл}$ - absolute melting point of the compound.

The data, necessary for calculating entropy by Eastman's formula (Table 11), were obtained from works [147, 168].

Table 11. Certain data on the compounds of the Al-Fe system.

Compound	Molecular weight of compound, g-mole	No. of atoms in the molecule	A_{cp}, g-atom	V_{cp}, cm^3/g-atom	Melting point	
					Centigrade	Kelvin
$FeAl_3$	136.76	4	34.19	8.65	1160	1433
Fe_2Al_5	246.55	7	34.22	8.6	1173	1446
$FeAl_2$	109.79	3	36.6	8.4	1158	1431
FeAl	82.82	2	41.41	7.77	1103	1376

The calculated values of the intermetallic compounds obtained on the basis of the data of Table 5 are presented in Table 12 [136].

Table 12. Calculated values of entropy S^0_{298} and of the heat of formation ΔH^0_{298}.

Compound	S^0_{298}, J/g-mole	$-\Delta H^0_{298}$, J/mole [32, 77]
$FeAl_3$	22.76	26,800
Fe_2Al_5	39.69	46,200
$FeAl_2$	17.46	1,950
FeAl	12.12	12,200

The variation in the Gibbs free energy of the reactions was computed up to a temperature of 933°K (the melting point of aluminum) by formula

$$\Delta Z^0_1 = \Delta H_{298} - T\Delta S^0_{298}, \qquad (41)$$

where ΔS^0_{298} - the variation in the entropy of the reaction.

At a temperature higher than 933°K computation was carried out in accordance with the following dependence

$$\Delta Z^0_2 = \Delta Z^0_1 + \Delta Z^0_{2-1}. \qquad (42)$$

where $\Delta Z^0_{пл}$ - the variation in the Gibbs free energy of the reaction, taking into account the increase in chemical activity of aluminum in the liquid state.

In calculating the values of ΔS^0_{298} and $\Delta Z^0_{пл}$ the values of the entropy of iron and aluminum were taken to be equal to, respectively 27.16 and 28.33 J/g-mole, and the heat of fusion of aluminum - 10.46 J/mole [77] (Table 13 and Fig. 50). As follows from Fig. 50, at the initial moment of the interaction of aluminum with the iron the formation of phases, rich in the low-melting component, is most probable; with an increase in temperature the difference of the magnitudes of Gibbs free energy of the formed phases is reduced.

Table 13. Results of the thermodynamic calculations for the intermetallic phases of an iron-aluminum system in calculating for one atom of iron.

Compound	Magnitude of Gibbs free energy, J/mole at temperature, °K	
	up to 933	above 933
$FeAl_3$	-26,800 + 4.04 T	-34,300 + 12.08 T
Fe_2Al_5	-23,100 + 3.56 T	-29,350 + 10.27 T
$FeAl_2$	-19,500 + 2.57 T	-24,500 + 7.93 T
FeAl	-12,200 + 1.14 T	-14,700 + 3.82 T

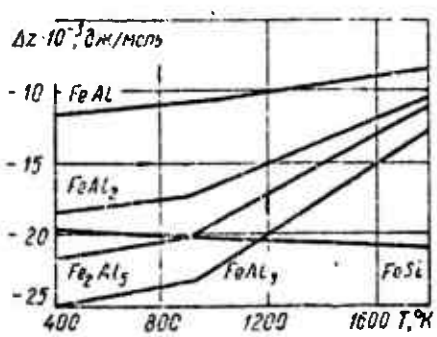

Fig. 50. The temperature dependence of Gibbs free energy ΔZ of intermetallic phases in FeAl and FeSi systems.

It is known, that in alloys based on transition metals alloying electropositive elements, for example, aluminum, zinc, give up part of their valence electrons to transition element atoms, which can fill its incomplete 3d-subshell [36, 101].

In this case, the atoms of the alloying element become more electropositive with respect to the atoms (or ions) of the transition element, which leads to the appearance in the alloy of an ionic (along with a metallic) component of forces of the interatomic bond. In proportion to the increase in the content of alloying element in the alloy the completeness of the 3d-subshell of the transition element is increased, and the fraction of the ionic component of forces of the bond simultaneously increases, i.e., the strength of the chemical bond of heterogeneous atoms in the alloy lattice and, consequently, its stability. Thus, on the basis of the data on the completeness of the 3d-subshell of transition element atoms it is possible to get an idea of the strength of the forces of the bond in the lattice of the intermetallic compound, i.e., about its thermodynamic stability.

One of the basic indications of the completeness of the 3d-subshell of transition element atoms is the displacement of the K absorption edge of the element in the shortwave direction - the decrease in the index of asymmetry of certain spectral K lines of this element, determined by employing X-ray spectral analysis [101]. S. A. Nemnonov and K. M. Kolobova [102] established, that for iron-aluminum and iron-zinc alloys with an aluminum and zinc concentration of up to 75 at.% the dependence of the decrease in the index of asymmetry of the K line on the content and the valence of these elements in the alloy is expressed by the following formula:

$$a_{спл} = a_{Fe} - k_{nc}, \qquad (43)$$

where $a_{спл}$ - the index of asymmetry of the K_{a_1} line of the iron in the alloy; a_{Fe} - the index of asymmetry of the K_{a_1} line in pure iron, equal to 1.52 ± 0.02; n - the valence of the alloying element, equal for aluminum to 3; c - the concentration of alloying element; k - the proportionality factor, equal to $1.51 \cdot 10^{-3}$.

In accordance with formula (43) with an increase in the content of aluminum in an alloy the index of asymmetry of the K_{a_1} line of the iron decreases continuously; an alloy of the $FeAl_3$ type has its least magnitude. The latter attests to the fact, that the stability of intermetallic iron/aluminum compounds actually increases in proportion to the increase of the aluminum content in them and it is greatest for the compound $FeAl_3$. The correctness of the thermodynamic calculations which have been carried out is confirmed by this.

It is evident from Fig. 50, that with an increase in temperature only the degree of chemical affinity of the iron and aluminum atoms varies (decreases); the relative stability of the intermetallic compounds remains the same. This means, that with an increase in temperature the phase state of the diffusion layer does not vary.

The thermodynamic calculations also make it possible to conclude, that the alloying of aluminum, for example with silicon, can inhibit and even suppress the formation in the intermetallic layer of phases of the Fe_nAl_m type and lead to the appearance of iron-silicon or ternary iron-aluminum-silicon phases (Fig. 50, the straight line is FeSi). Thus, one of the radical methods for affecting the structure and the properties of intermetallic phases, and consequently, also the strength of steel/aluminum welded joints is the alloying of the bath with various additives.

In selecting the additives, it was taken into account, that the more complex is the composition and the structure of the evolved phases and the more they differ from the composition and the structure of the initial solution, the slower, as a rule, the diffusion processes occur [24]. The experiments to explain the effect of additives of various elements on the form of the evolution of the Fe_nAl_m phase during argon-arc deposition of aluminum on zinc-galvanized steel, preceded the selection of the

additives. In the course of these investigations the possibility of varying the quantity, the form and the nature of the arrangement of the intermetallic phases was established.

The effect of additives of various metals introduced into the weld pool on their interaction mechanism with solid steel and the structure of the joint zone formed in this case has been little studied. The available published data pertain to the production of bimetallic aluminum cast alloys - steels or pig-iron castings.

It was established by the works of P. Stroup and G. Pardi [68], D. Gittings, I. Mack and D. Rowland [196], K. I. Vashchenko and others [30, 31, 228], that silicon, beryllium and other elements have an effect on the thickness of the transition layer. Cast aluminum alloys were subjected to an investigation, and in this case various data were obtained on the effect of certain elements, for example zinc.

In a study of the effect of the composition of welding wires on the properties and the dimensions of the intermediate intermetallic layer both standard welding wires of brands AK, AMg5, AMg6 as well as experimental welding wires were tested. Argon-arc welding with a nonconsumable electrode on an ADSV-2 automatic welder was employed to obtain stable and comparable results. The regimes of the automatic argon-arc welding and the data on the testing of steel/aluminum joints, carried out in two ways, employing standard welding wires (also including ADi wire) are presented in Table 14. As is evident from the table, the employment of standard welding wires, with the exception of brand AK, does not ensure the obtainment of welded joints with sufficient strength. For the purpose of increasing the strength characteristics of steel/aluminum joints the effect of the following alloying elements, introduced into the seam via the welding wire, was investigated: silicon (to 8%), copper (to 5%), zinc (to 15%), nickel (to 3%) and beryllium (1.6%). The selection of the alloying elements within the indicated limits is due to the possibility of

obtaining composite welding wire, making it possible to carry out welding on automatic welders.

Table 14. Regimes of argon-arc welding of composite joints.

Combination of metals being welded	Thickness, mm	Welding regimes: Weldir. wire	Current force, A	Welding rate, m/h	Wire feed rate, m/h	σ_B^*, daN/mm^2	Nature of failure
AMg6-St. 3	6 + 6	AMg6	220	5.4	30	-	The seam resulted in a crack along the transition line to steel during the welding process
AMg6-St. 3	6 + 6	AMg5V, Ø2.5	220	5.4	28		The same
AMg6-St. 3	6 + 6	AK, Ø2.5	220	5.6	28	11.2-22.3 / 22.0	In certain seams there are micro-cracks
AMg5V-St. 3	5 + 5	AK, Ø2.5	220	6.2	28	12.0-21.3 / 21.0	-
AMg5V-St. 3	5 + 5	AD1, Ø3	200	6.2	28	9.3-10.7 / 9.8	-

*Average value of five tests.

The wires were manufactured on a laboratory device by the method of drawing from a melt of brand AV00 aluminum [60]. After extraction the wires were first tested by manual argon-arc welding, and were then drawn on a wire drawing machine to obtain the required diameter. A total of 18 experimental wires were manufactured. The data on the chemical and spectral analyses of the experimental wires (AV00 base) are presented in Table 15 (the

wire, containing 1.6-1.9 Be is not included in the table). Plane specimens were cut from welded plates for tensile testing; sections were manufactured for micro- and macrotesting, corrosion testing, etc. Metallographic investigations showed, that the introduction of the indicated additives into the weld pool can cause a sharp variation in the form of the layer of formed intermetallic compounds.

Table 15. Data of the chemical analysis of the investigated wires.

Experimental wire number	Content of elements, %				
	Si	Cu	Ni	Zn	Fe
1	Traces	Traces	-	2.0	0.2
2	"	"	-	7.0	0.2
3	"	"	-	10.2	0.2
4	"	"	-	13.2-15.0	0.25
5	1.1-1.22	"	-	Traces	0.12
6	2.11-2.33	"	-	"	0.18
7	2.8-3.5	"	-	"	0.10
8	3.7-4.5	"	-	"	0.20
9	5.0	"	-	"	0.20
10	6.2	"	-	"	0.10
11	7.0	"	-	"	0.10
12	7.8-8.0	"	-	"	0.19
13	Traces	1.2-1.45	-	"	0.10
14	"	2.5-2.8	-	"	0.10
15	"	5.1	-	"	0.10
16	"	Traces	1.0	"	0.10
17	"	"	2.9-3.2	"	0.10
18	"	"	2.9-3.2	"	0.10

Note. All wires contain hundredths of a percent of magnesium.

Silicon. The results of the investigation of the effect of silicon are illustrated by Fig. 51 and Fig. 52, a-d, from which it

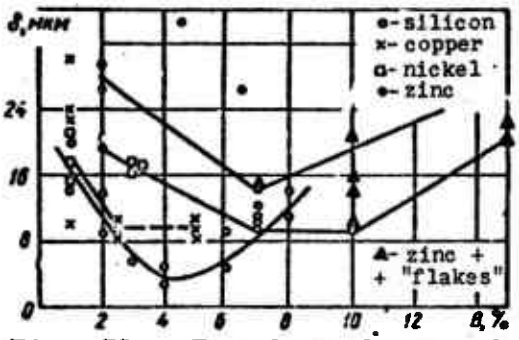

Fig. 51. The dependence of the thickness of the intermetallic layer δ of a steel/aluminum welded joint on the content of B alloying elements in the wire.

is evident, that silicon in amounts of 1-8% has a considerable effect on the thickness of the intermetallic layer. The width of the layer varies from 18-20 μm upon the introduction of 1% silicon up to 3-5 μm when its content is 4-4.5%. A subsequent increase in silicon content (up to 8%) increases the width of the layer up to 10-15 μm, which subsequently remains practically constant. This type of effect of silicon, which leads to a decrease in the thickness of the layer by three-four times is confirmed by published data, pertaining to the production of bimetallic castings [86, 87, 189].

The silicon, contained in a weld pool, very intensely retards the diffusion of aluminum, as a result of which the layer either does not form, or its formation is inhibited. Apparently, such a considerable reduction in the magnitude and the rate of formation of the transition layer can be explained by the reduction in the coefficient of aluminum diffusion as a consequence of the formation of the solid solution and the chemical compounds of silicon with iron.

Copper. The effect of the addition of copper was studied when it was introduced in amounts of up to 5%. The results of the investigation of the effect of copper on the thickness of the intermetallic layer are presented in Figs. 51 and 52. Copper, introduced into welding wire in small quantities (up to 2.5%), reduces the thickness of this layer from 23-30 μm to 10-12 μm, i.e., almost by 2.5 times. The further addition of copper does not lead to a significant change in the dimensions of the intermetallic layer: at 5% the thickness of the layer is 12-15 μm.

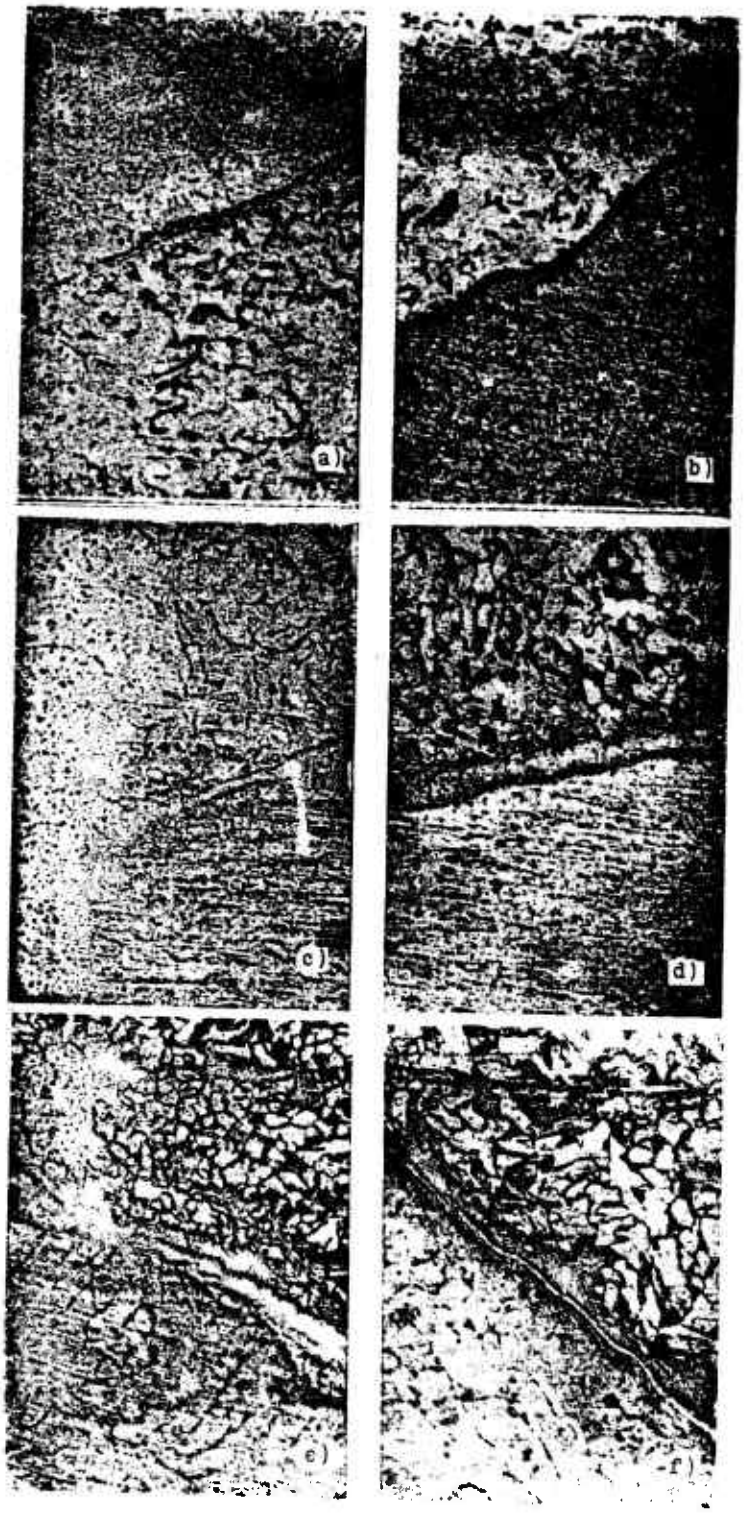

Fig. 52. Microstructure of the transition layer (×150), obtained in the welding of St. 3 steel with AMg5V alloy employing additives containing a) 2% Si; b) 5% Si; c) 8% Si; d) 1% Cu; e) 5% Cu; f) 1.6% Be.

In view of the fact, that with the introduction of the indicated amounts of copper the thickness of the layer is greater, than with the introduction of silicon, the strength of the compounds in this case can be as high as 18-25 daN/mm^2.

The introduction of copper does not reduce the microhardness of the transition layer.

Nickel. The introduction of nickel in an amount of up to 1% did not cause a variation in the thickness of the intermetallic layer (Fig. 53, d and f [sic]) within the limits of 16-22 μm and also practically did not vary the microhardness of the layer (Fig. 54).

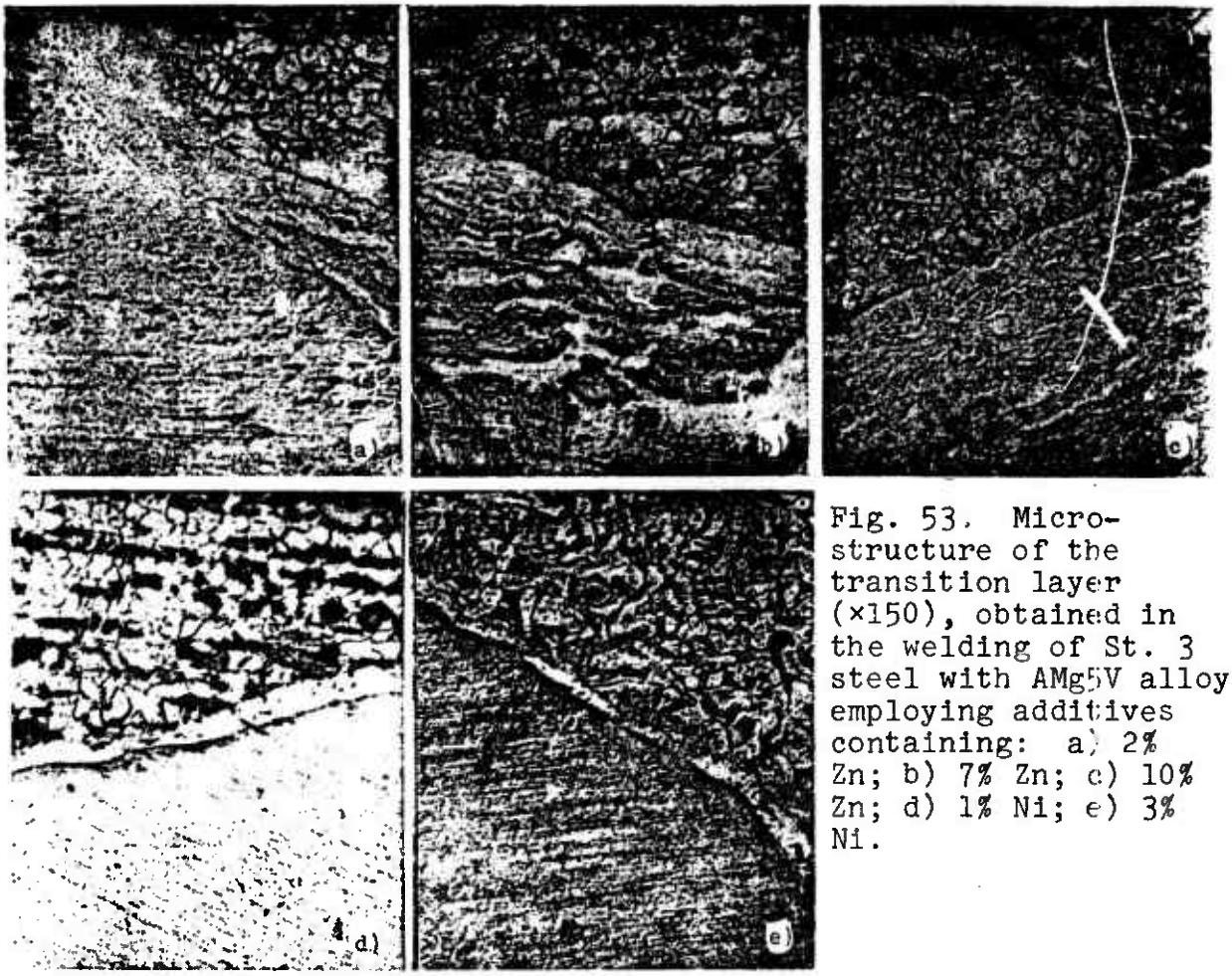

Fig. 53. Microstructure of the transition layer (×150), obtained in the welding of St. 3 steel with AMg5V alloy employing additives containing: a) 2% Zn; b) 7% Zn; c) 10% Zn; d) 1% Ni; e) 3% Ni.

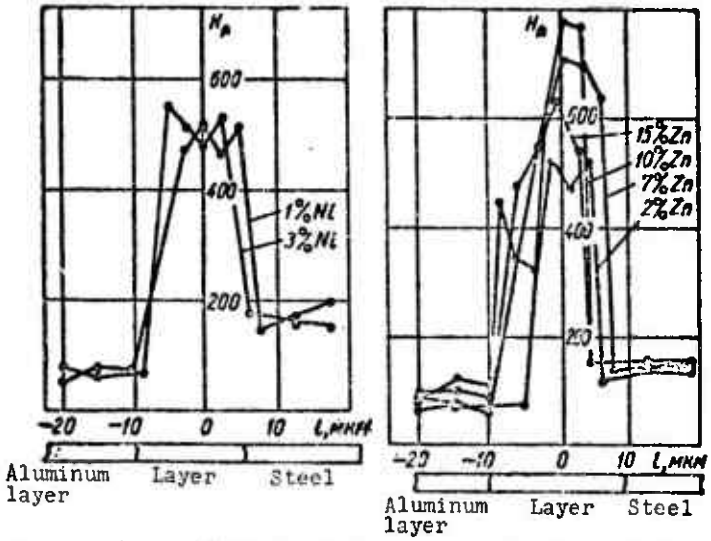

Fig. 54. Microhardnesses of the transition layers of a steel/aluminum joint during alloying with various elements.

Beryllium. The introduction of beryllium in an amount of up to 1% [68] also did not change the thickness and the microhardness of the intermetallic layer.

Zinc. The effect of the addition of zinc was investigated when its content in the welding wire was as high as 15%, since with a large content of zinc it was not possible after drawing to obtain a sufficient quantity of wire for automatic welding due to its brittleness.

The dependence of transition layer thickness on zinc content is illustrated by Figs. 51 and 53a, b, and c, from which it is evident, that zinc has a distinctive effect on the intermetallide layer. For example, upon increasing the zinc content up to approximately 7% the thickness of the layer is reduced from 28-30 μm to 10-12 μm, and then increases with the appearance in the joint zone of a large quantity of inclusions, having the form of "flakes" (Fig. 53b). The absence of a clearly defined intermetallic layer (a zinc content of 10 and 15%), is characteristic here, which is accompanied by a sharp drop in joint strength.

The indicated regularities of the variation in the transition layer under the effect of zinc can be explained by the fact, that aluminum-zinc alloys are distinguished by increased reactivity with respect to iron [30, 68, 228]. As a result of this the intermetallic layer which is formed dissolves intensely in the weld pool. Under specific temperature-time conditions the rate of dissolving of intermetallides is equal to their formation rate. In this case the layer is clearly expressed and its thickness can be measured rather accurately. A further increase in zinc content creates those types of conditions, when the rate of dissolving begins to predominate over the rate of formation of the intermetallic diffusion layer. Its density is considerably reduced; a large quantity of intermetallides, which are completely or partially dissolved, is observed on the microsections (Fig. 53b, c), which also leads to a sharp drop in joint

strength [53]. The effect of zinc and the microhardness of the transition layer of a St. 3 steel-AMg5V alloy joint is interesting.

If the average magnitude of microhardness (see Fig. 54) is reduced comparatively slightly (645-775 daN/mm^2), then the strength during tensile testing is at first sharply increased, attaining a maximum value of 27-34 daN/mm^2 with a zinc content of about 7%, and then decreases and with a zinc content of 12-15% can be as low as 5-8 daN/mm^2, which agrees with the data of zinc-galvanizing [157].

The effect of rare-earth elements was studied by introducing mischmetal into wire. The rare-earth elements have a favorable effect, when their content is less than 0.2%.

On the basis of the data obtained in a study of the effect of the chemical composition of additive material on the properties of the layer and the strength of a steel/aluminum joint an optimum composition of the welding layer was proposed for welding St. 3 brand galvanized steel with aluminum alloys: 5-8% Zn; 3-5% Si; 2-2.5% Cu; Al - the remainder.

The data, obtained by metallographic methods, and also by measuring microhardness illustrate the significant change in the width of the layer and indicate the variation in its composition. This is insufficient to explain the structure of the intermetallic layer and its composition.

We made an attempt to study the structure of the layer, by employing very high magnifications on an UZM-100 electron microscope. There are no published recommendations on a method for obtaining replicas from any pairs of bimetals. For the investigation of microstructure replicas were prepared by the methods described in works [52, 89, 3] with respect to homogeneous metals.

Figure 55a presents the boundary of the transition from steel to the intermetallic layer during alloying of the pool with silicon, and Fig. 55b - with alloying with copper. As is evident, the intermetallic layer does not differ in external appearance in both cases.

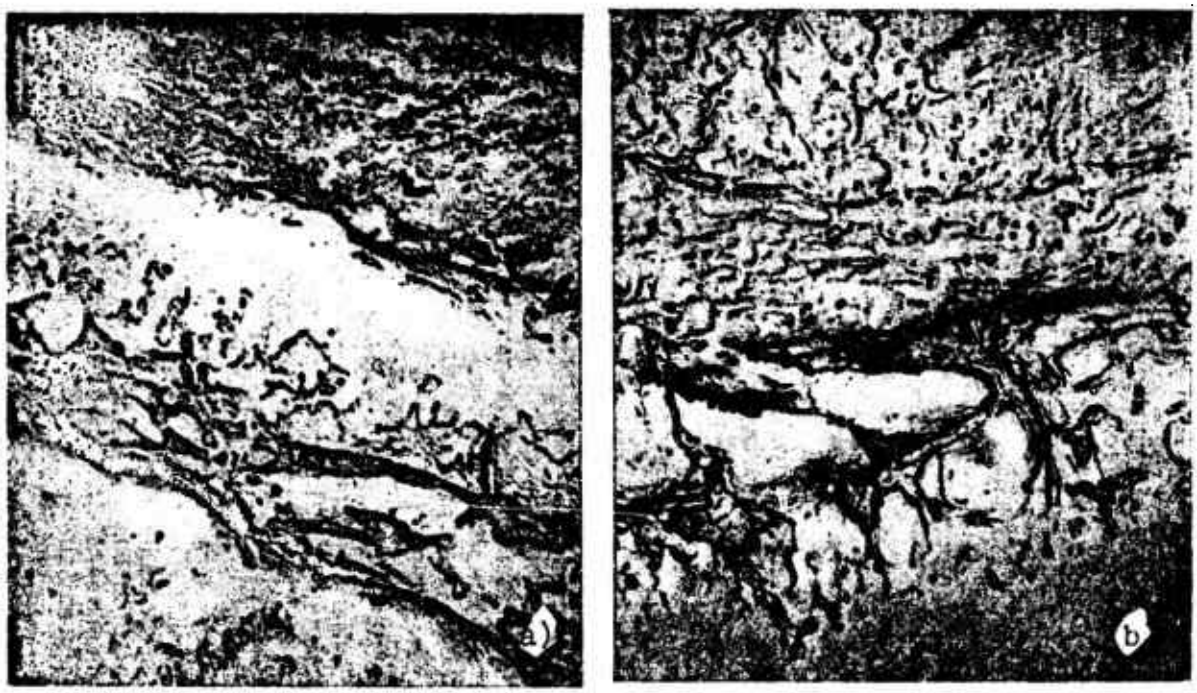

Fig. 55. Transition boundary from the steel to the intermetallic layer in the alloying of a pool: a) additive of 4% silicon (×6500); b) additive of 1% copper (×15,000).

Thus, methods of metallographic analysis and electron microscope analysis do not make it possible to detect any difference in the structure of the transition layer, which has the appearance of a single layer, frequently interrupted, in the form of a number of inclusions, the relief of which is different from the relief of the base metal and the seam metal.

The attempt to employ the microhardness method for identifying phases in a seam layer did not lead to positive results, since, first, in measuring the microhardness of phase standards of a Fe-Al system a large spread of values was observed and, secondly the microhardness of the phases, constituting the seam layer, could not

always be measured with the required accuracy due to the small thickness of the layer (1-2 μm). Thus, for studying the composition of layers in iron/aluminum seams, and also in these same seams with their alloying with other metals (Zn, Mg, Cu, Si, Be) and for determining ways to increase joint strength X-ray phase analysis and micro-X-ray spectroanalysis were employed.

3. Phase Composition of Steel/ Aluminum Seams

X-ray Investigation Method

The method of X-ray phase analysis was employed as the main method for investigating the phase composition of iron/aluminum seams. For the X-ray structural analysis of a metal, isolated from an intermetallic layer, the powder method was also employed. The powder for the making of X-ray photographs was obtained either by the mechanical method, or by the chemical method - the method of electrochemical dissolving of a metal. In this case, electrolytes were employed, the compositions of which are cited in literature [83, 117].

For isolating intermetallides of the Fe_nAl_m type a method (the author was G. P. Manzheley) was developed, based on the chemical dissolving of seam metal in a 10% alcohol solution of iodine in methanol. Uniform dissolving of the given section of the specimen metal surface takes place in this medium; the metal obtained from the section was washed free of the solvent by methyl alcohol in a centrifuge; it was dried in a carbon dioxide medium and then subjected to X-ray structural analysis.

Results of Investigations

Many opinions have been expressed relative to the phase makeup of an intermetallic layer. Thus, for example, G. A. Bel'chuk [15]

assumes, that the $FeAl_3$ phase is formed in a layer, however these data are not confirmed by direct experiments.

The most developed fusion layers are obtained during prolonged interaction of aluminum with steel. The authors of works [144, 210, 236] showed, that the layer consists of two zones: a thin layer, adjacent to the aluminum, and a thick layer, growing within the iron. It was established by these investigations, that both zones of the layer have an identical composition - the intermetallic compound $FeAl_3$ and Fe_2Al_5. At the same time, other investigators [198] by means of metallographic investigations and measurement of microhardness detected Fe_2Al_5 and Al_4C_3 phases in the layer [21].

The contradictory results obtained by investigators concerning the phase composition of the diffusion layer are explained by the difficulty in studying fine diffusion layers, by the absence of complete and reliable data on the crystalline structure and properties of the intermetallic phases of the iron-aluminum system, by the low symmetry of the crystal lattices of these phases, especially with a high content of aluminum.

To study the phase composition of iron/aluminum seam layers, obtained by argon-arc welding, specimens of aluminum-steel compounds were prepared with a different type of preparation for welding, and also by the introduction of alloying additives. These seams were arbitrarily broken down into four groups.

Seams, made by the argon-arc deposition on a plate of St. 3 steel (or 1Kh18N9T steel) with a welding wire of AD1 pure aluminum (Fig. 56a), were included in the first group. The deposition formed in this case is readily separated from the base metal; in this case failure occurs along the brittle intermetallic layer. The phase composition of this group of seams was studied on 15 specimens. The powders, obtained by the successive removal of the deposition layers (samples) with a fine file, beginning with the

surface, from which it was spontaneously separated from the steel plate, into the depth of the deposition, were subjected to X-ray analysis.

The second group consists of seams, obtained by the welding of galvanized steel (without edge preparation) plate with pure aluminum (Fig. 56b). These seams (investigation was carried out on 18 specimens) had insufficient strength, equal to the strength of pure aluminum, and it was possible to separate them into iron and aluminum parts. For the X-ray analysis metal layers were removed from the seam surface (intermediate layer) both from the aluminum, as well as from the iron with a file.

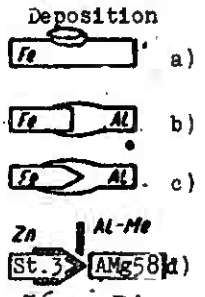

Fig. 56. Diagrams of the alloying of welded seams.

The third group (22 specimens were investigated) consists of the strongest and the most perfect joints, obtained by the welding of aluminized 1Kh18N9T steel with AMg6 alloy. A diagram of this type of seam is represented in Fig. 56c. With regard to the strength of the seams of this group it was not possible to separate the aluminum and iron parts; the layers of metal, removed with a file successively from the aluminum to the iron, for the purpose of recovering the intermetallic iron-aluminum phases in the transition through the seam, were subjected to X-ray analysis.

Iron/aluminum seams alloyed with other metals (Zn, Mg, Si, Cu, and Be) were included in the fourth group.

The alloying of the seams was carried out in three different ways (Fig. 56d): a) the iron (St. 3 steel) was galvanized with a layer of zinc with a thickness of 35-45 μm; b) for the welding aluminum, alloyed with magnesium - AMg5V alloy (Al + 5% Mg) was employed; c) the aluminum welding wire was alloyed with zinc (15; 10; 7 and 2%), with silicon (8; 5; 3 and 1%), with copper (2.5 and 1% and with beryllium (1%).

As follows from the alloying diagram, in the preparation of the fourth group of seams only the composition of the welding wire was varied (subsequently, for seams of this group only the alloying of the aluminum welding wire is indicated).

Investigation of the phase composition was carried out on two specimens for each composition of welding wire. The seams were separated along the intermetallic layer and, as in the investigation of the phase composition of seams of the second group, layers of metal were removed from the surface of the intermetallic layer of the iron and the aluminum and these were subjected to X-ray analysis.

Precision measurements of the lattice constants of phases in the seams were carried out along line 211 α (for iron), 311 α and 222 α (for aluminum) and along lines 103 α, 110 α and 004 α (for (zinc).

For a microstructural investigation of iron/aluminum seams sections of the seams were prepared perpendicular to the plane of the intermetallic layer and they were processed in a corresponding manner.

X-ray analysis [172] of the phase composition of seams of the first, second, and third groups indicates that in all specimens of each group of seams the sequence of the variation in the phase composition of the removed layers of metal was identical. The investigational data of the phase composition of typical seams of the first, second, and third groups are presented in Table 16. (The ordinal number of the sample reflects the sequence of the removal of the metal layers.) The phase composition of the seams of the fourth group are more diverse and depends on the qualitative (and quantitative) composition of the welding wire. Thus, on the X-ray photographs of samples of seams, alloyed with zinc (which contain zinc in the aluminum welding wire as an alloy additive),

besides the lines of α-iron and aluminum, zinc and $FeAl_3$ lines are observed (Table 17). In other seams (Table 18) of this group, besides Fe, Al, and Zn, $FeZn_7$ (in seams, alloyed with silicon) $FeZn_7$ and traces of $FeAl_3$, in the alloying of seams with copper) and traces of $FeAl_3$ (in seams, alloyed with beryllium) were also detected.

Table 16. Phase composition of samples of three groups of seams.

Sample number	Seam of first group (to aluminum deposition)	Seam of second group		Seam of third group (from Al to Fe)
		to Al	to Fe	
1	Fe_2Al_5	Al + Fe_2Al_5	Fe + Al + Fe_2Al_5	Al
2	Fe_2Al_5	Al + Fe_2Al_5 (traces)	Fe + Fe_2Al_5 + Al	Al
3	Fe_2Al_5 + $FeAl_3$	Al + Fe_2Al_5 (traces)	Fe + Fe_2Al_5	Al
4	Fe_2Al_5 + $FeAl_3$	Al	Fe + Fe_2Al_5 (traces)	Al + Fe_2Al_5 (traces)
5	$FeAl_3$ + Fe_2Al_5	Al	Fe	Fe + Al + Fe_2Al_5 (traces)
6	$FeAl_3$ + Al + + Fe_2Al_5 (traces)	Al	Fe	Fe + Fe_2Al_5 (traces)
7	$FeAl_3$ + Al	Al	Fe	Fe
8	$FeAl_3$ + Al	Al	Fe	Fe
9	Al + $FeAl_3$	Al	Fe	Fe
10	Al + $FeAl_3$	Al	Fe	-

The lattice constant of the α-phase in welded seams increases with an increase in the aluminum content percent in them, which agrees well with the dimensions of the atoms (the atomic radius of iron is equal to 1.26 Å, aluminum - 1.43 Å [22, 168]). It is interesting to note, that the lattice constant of FeAl is less than the lattice constant of the α-phase, which contains the maximum

Table 17. Phase composition of seams alloyed with zinc.

Sample No.	Seams, alloyed with Zn (to Fe)	Seams, alloyed with Zn (to Al)		
		15% Zn	10% Zn	2% Zn
1	Fe + Zn + Al (traces)	Al + Zn	Al + Zn + $FeAl_3$	Al + Zn + $FeAl_3$
2	Fe + Zn	Al + Zn	Al + Zn + $FeAl_3$ (traces)	Al + Zn + $FeAl_3$ (traces)
3	Fe + Zn (traces)	Al + Zn	Al + Zn + $FeAl_3$ (traces)	Al + Zn + $FeAl_3$ (traces)
4	Fe	Al + Zn	Al + Zn	Al + Zn + $FeAl_3$ (traces)
5	Fe	Al + Zn (traces)	Al + Zn	Al + Zn + $FeAl_3$
6	Fe	Al + Zn (traces)	Al + Zn (traces)	Al + Zn (traces)
7	Fe	Al + Zn	Al + Zn (traces)	Al + Zn (traces)
8	Fe	Al + Zn	-	Al + Zn

Table 18. Phase composition of seams, alloyed with Si, Cu, Be.

Sample No.	Seams alloyed with Si, Cu, Be (to Fe)	Seams alloyed with Si, Cu, Be (to Al)		
		Si	Cu	Be
1	Fe + Zu + Al	Al + Zn + $FeZn_7$	Al + Zn + + $FeZn_7$ + $FeAl_3$ (traces)	Al + Zn + $FeAl_3$ (traces)
2	Fe + Zn (traces) + Al (traces)	Al + Zn + $FeZn_7$ (traces)	Al + Zn + $FeZn_7$ (traces)	Al + Zn
3	Fe + Zn (traces)	Al + Zn + $FeZn_7$ (traces)	Al + Zn	Al + Zn
4	Fe	Al + Zn	Al + Zn	Al + Zn (traces)
5	Fe	Al + Zn (traces)	Al + Zn (traces)	Al + Zn (traces)
6	-	Al + Zn (traces)	Al	Al
7	-	Al	Al	Al
8	-	Al	-	-

amount of aluminum, in spite of the fact, that the amount of the latter in FeAl is greater, than in the α-phase. The anomalous variation in lattice constant is due, apparently, to the supplemental interaction between the heterogeneous atoms, arising after their ordering.

Thus, the phase composition of the layer between the iron and aluminum in welded seams can be most clearly traced in studying seams of the first group. In metal samples, removed from the deposition surface, on which it was separated from the steel plate, X-ray analysis records a pure Fe_2Al_5 phase. In deposition layers more remote from the failed surface a mixture of phases is already contained - first Fe_2Al_5 + $FeAl_3$ and then $FeAl_3$ + Al.

Thus, the sequence of phases in the deposition in moving away from the surface, on which the failure of seams of this group occurred, into the depth of the deposition, can be represented as α-Fe → Fe_2Al_5 → ($FeAl_3$) → Al.

The investigation of the phase composition of seams of the second group was carried out from their failure surface both for aluminum, as well as for iron. The sequence of phases in the transition from steel to aluminum is as follows: α-Fe → Fe_2Al_5 → Al, and in the metal layers, removed from the failed surface of the seam both for the iron, as well as for the aluminum, always contained the Fe_2Al_5 phase.

Only traces of Fe_2Al_5 were detected in the high-quality seams of the third group. On the basis of these data it is possible to conclude, that the low strength of the iron/aluminum welded seams is due to the appearance in them of the more brittle Fe_2Al_5 phase in the Fe-Al system; with a reduction in the amount of Fe_2Al_5 in the seams their strength is increased.

The negative effect of the Fe_2Al_5 phase on the strength of iron/aluminum seams is further confirmed by the fact, that the Fe_2Al_5 phase was not detected in sufficiently strong seams of the fourth group. The phase composition of seams of this group is more diverse. In seams, alloyed with zinc (15%), Fe, Al and Zn are found and no intermetallic phases were detected. With a lesser zinc content in the welding wire, besides Fe, Zn and Al, the $FeAl_3$ phase appears. In seams, alloyed with other metals (Si, Cu, Be), besides Al, Zn and Fe, intermetallic phases are also detected: in alloying with silicon - the $FeZn_7$ phase, in alloying with copper - small quantities of the $FeZn_7$ phase and traces of $FeAl_3$, and in seams, alloyed with beryllium, - traces of $FeAl_3$ and moreover $FeZn_7$ and $FeAl_3$ were found in the samples, removed from the surface with a file, on which joint failure occurred. Consequently, the formation of these phases in seams also negatively affects the strength of the seams, but to a lesser extent, than with the appearance of the Fe_2Al_5 phase. The seams, alloyed with Zn (15%) in which no intermetallic phases were detected, were the strongest.

Since in a high-quality welded joint the thickness of the intermetallic layer does not exceed a few microns, then the determination of its chemical composition is made difficult. In connection with this, to study the distribution of elements and to determine the phase composition of the fusion zone of aluminum with steel the method of micro-X-ray spectral analysis [micro-radiography] was employed.

4. Distribution of Elements in the Fusion Zone in the Welding of Aluminum with Steel

An investigation of the distribution of elements in the fusion zone and a determination of the chemical composition were carried out on an electron microanalyzer manufactured by the French firm "Cameca," and developed by R. Castaign [192]. The

design and technical characteristics of this instrument are described in works [20, 97].

The microradiographic method [micro-X-ray spectral analysis] consists in the fact, that a beam of electrons is directed on the section of the specimen being investigated - the electron probe, the diameter of which can be varied within broad limits (the minimum dimension of the probe is equal to 1 μm). At the site where the electrons hit the sample characteristic radiation of the elements, making up the composition of the sample, is excited. By decomposing the radiation into a spectrum with the aid of a crystal analyzer, it is possible to qualitatively and quantitatively determine the chemical composition of the micro-volume being irradiated [192, 214]. An additional attachment, a "Scanner" is hooked up to the microanalyzer to obtain a photographic image of the qualitative distribution of the elements on the specimen surface with a resolving power of approximately 1 μm.

The image is obtained in the following manner. The specimen surface section being analyzed is moved in two mutually perpendicular directions so that the electron beam line after line passes over the section being analyzed. Potentiometers of the continuously rotating type supply a periodic sawtooth voltage, employed to move the specimen and the spot on the oscilloscope screen. These two motions are very accurately synchronized and the oscilloscope spot is modulated by a pulse signal coming from the radiation counter. It is possible to set the sweep field employing mechanical attachments at 100 × 100 μm; 200 × 200 μm; 300 × 300 μm. Photographing is carried out with "Polaroid" camera with instantaneous development.

Variation in the quantitative composition can be ascertained in accordance with the variation in the intensity of the spectral line of a given element. However, the presence of the atoms of other elements in the specimen and other factors has an effect on this intensity, and the taking into account of these

factors is frequently rather difficult.

Various methods for introducing corrections have been proposed to obtain more accurate quantitative data [210, 214]. The simplest of these is the standardizing method [96, 97]. For this it is necessary to select standard alloys, the basic requirement imposed on which - is a good degree of homogenization checked on the micro-probe.

Having measured the intensity of the characteristic line of element A in standard J_A and the intensity of the same line in the pure element $J_{|A|}$, graphs of $C_A\% - J_A/J_{|A|}$ 100 are plotted, where - C_A should be determined by the chemical method or by another method.

In this work the graphs of such dependences were plotted to determine the concentration of aluminum and silicon in the iron with an accelerating voltage of 16.5 kV and a probe current of 0.045-0.05 μA (Fig. 57). For this a number of alloys were prepared by fusing a compressed mixture of powders of especially pure iron carbonyl (99.98% Fe, the remainder is C, Ni) and AV000 brand aluminum (99.99% Al, the remainder is Fe, Si, Cu) in an electric arc furnace in a helium atmosphere. These alloys were subsequently employed as standards for X-ray analyses, for measuring microhardness, etc. The obtained ingots were subjected to homogenizing annealing at a temperature of 900°C over a period of 36 h and then were quenched in water. Graphs of dependences, similar to the graphs in Fig. 57, for higher contents of aluminum in iron, were not plotted. In this case the concentration of iron was determined, and the aluminum was determined from the difference after having taken into account the percent content of other alloying elements. In all of the measurements the diameter of the probe was 1-3 μm [123].

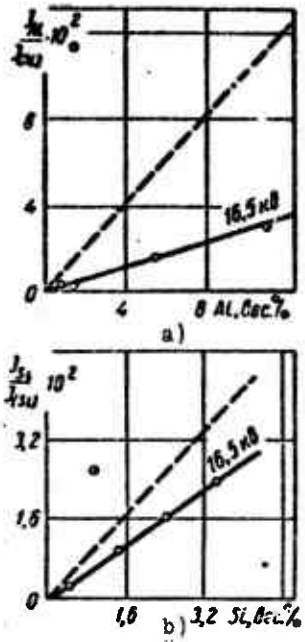

Fig. 57. Graduated curves for determining the content in iron of: a) aluminum; b) silicon.

Three characteristic types of steel/aluminum welded specimens, cut from the aluminum-to-steel transition zone were investigated:

1) a St. 3 galvanized steel (the thickness of the galvanized coating was about 40 μm) and AD1 brand aluminum joint. The seam was made by automatic welding employing a double-electrode arc;

2) a joint of the same St. 3 steel with AMg5V alloy. The seam was made by argon-arc welding on an ADSV-2 automatic welder employing welding wires, containing pure AV000 brand aluminum with additives of 2 and 5% silicon;

3) a joint of aluminized 1Kh18N9T steel with AMg6 alloy. The aluminizing was carried out in pure AV000 aluminum under the following conditions: temperature of 780-820°C, and aluminizing time of 90-120 s. The seam was made by automatic argon-arc welding employing standard AMg6 welding wire. In all cases the values of heat input during welding were maintained constant.

The detection of the structure on the section was accomplished by the method described above [104]. To eliminate the effect of relief in investigating the indicated sections on the micro-probe, they were subjected to slight pickling for a period of 2-3 s, and in certain cases (with a clearly observable zone), they were not pickled. The sites being analyzed were first checked on a PMT-3 instrument, as an example, Fig. 58 shows the microstructure of the intermetallic layer on a section, in which measurements of the concentration of aluminum and iron were carried out. The layer with traces of burning by the electron beam is clearly evident.

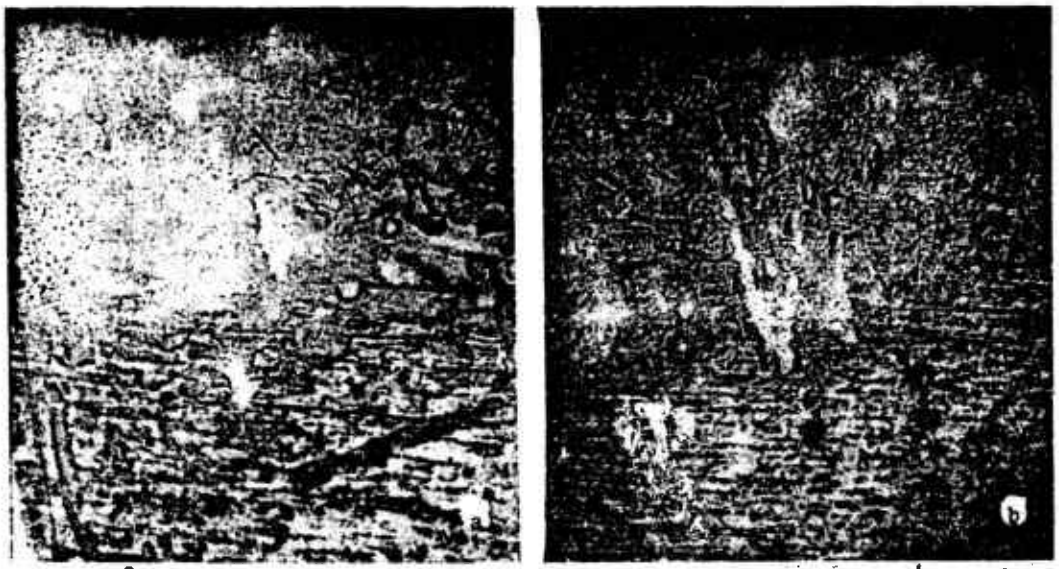

Fig. 58. Microstructure of the transition layer (×500): a) galvanized St. 3 steel with AMg5V alloy; b) aluminized 1Kh18N9T steel with AMg6 alloy.

The curves of the distribution of aluminum, iron and zinc in the transition layer in a steel-pure aluminum joint are presented in Fig. 59. The curves illustrate the sharp drop in concentration in the transition from aluminum to the intermetallic layer and from the intermetallic layer to the steel. The width of the intermetallic band is variable and fluctuates within the limits of 5-20 μm. As is evident from the graph, the content of iron in the intermetallic layer is approximately 42-43%. It is necessary to note, that on the microstructure (Fig. 58) a dark narrow intermediate layer of insignificant width is observed with respect to the steel.

In studying the zinc distribution it turned out, that the amount of zinc in the phase is uneven - closer to the steel (in the cited band) it is greater and constitutes about 0.6-0.7%, whereas in the transition layer - 0.3-0.4%. The higher content of zinc in the region, adjacent to the steel, should be assumed tentative, since the diameter of the probe was somewhat greater than the width of the dark band. It is also characteristic, that the diffusion of aluminum into steel is almost absent.

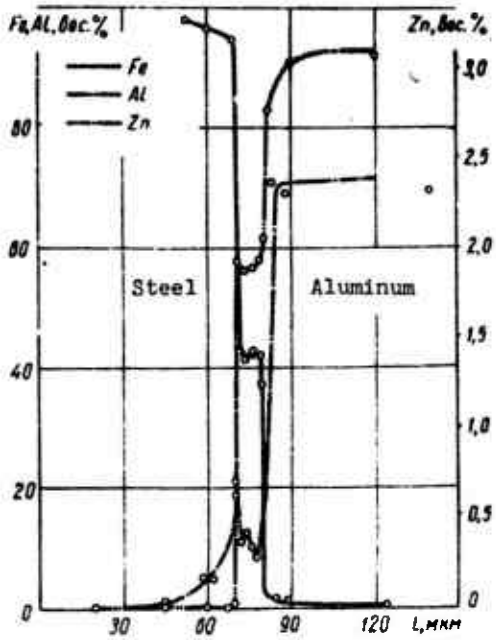

Fig. 59. The distribution of iron, aluminum and zinc across the fusion zone in the welding of St. 3 steel with pure AD1 aluminum.

The study of the effect of silicon additives in the weld pool on the composition and the dimensions of the intermetallic layer is of special interest. The fact itself of the sharp decrease in the thickness of the intermetallic layer is known [85, 189], however, various hypothesis exist concerning the nature of the effect of silicon. Thus, D. I. Layner and A. G. Yemel'yanov [87] made a hypothesis concerning the formation in this case of the complex ternary compound $Fe_xAl_ySi_z$; as a consequence the process of the formation of iron-aluminum phases ($FeAl_3$) is made difficult. K. Siguyasi, S. Mcrozuki, and K. Akira [144] deny the formation of new compounds with silicon, by explaining the decrease in the layer by the intense dissolving of iron.

Figure 60 shows the distribution curves of iron, aluminim and silicon in welding with aluminum wire with 5% silicon. As is evident from the graph, the distribution of iron and aluminum approximately corresponds to the graph in Fig. 59. Worthy of note are the considerably reduced dimensions of the transition layer, the width of which in this case is almost over the whole extent of the joint 4-6 μm; only at individual sites does it attain 10 μm and more.

The silicon content in the steel fluctuates within the limits of 0.15-0.2%; in the intermetallic layer - 2.5-3%. The silicon content in the aluminum - 0.4-0.5%. Moreover, a nonuniform distribution of silicon was established in the seam metal: on the

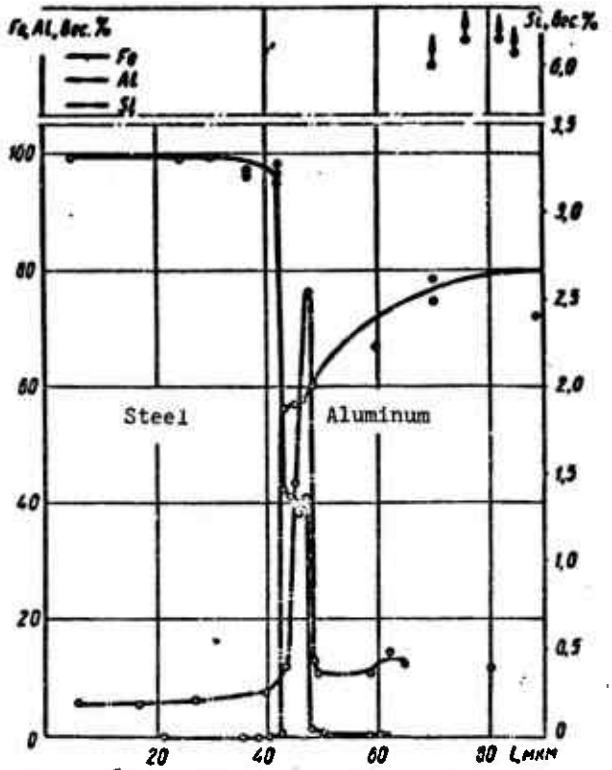

Fig. 60. The distribution of iron, aluminum and silicon across the fusion zone in the welding of St. 3 steel with AMg5V alloy.

grain boundaries - increased silicon content from 6 to 15% as compared with the grain body (0.4-0.5%). The sharper segregation of silicon is connected with the presence of magnesium in the aluminum solid solution. It was not possible to detect any characteristic dependence of zinc distribution in the transition layer, since the dimensions of the regions, enriched with zinc, are small and have an "insular" nature.

The distribution curves of iron, nickel, chromium and aluminum in the transition layer of an aluminized 1Kh18N9T steel and AMg6 alloy joint are presented in Fig. 61. The width of the layer in this case is 15-18 μm. In the upper corner of the diagram it is shown, how these elements are distributed in the aluminum at a distance from the layer of up to 60 μm. The maximum content close to this layer does not exceed 0.3-0.4%; at a distance of 50-60 μm from the layer it reduces to hundredths of a percent. Numerous measurements of the iron distribution in the layer showed the nonuniformity of its distribution. Thus, for example, it was established, that near the transition from the layer to the aluminum the iron content is somewhat increased.

A photographic image (scanogram) of the element distribution was obtained for clear representation of the established regularity in the iron distribution. A representation of the photographed section is presented in Fig. 62. On the left - the steel section (the lighter background), then comes the intermetallic

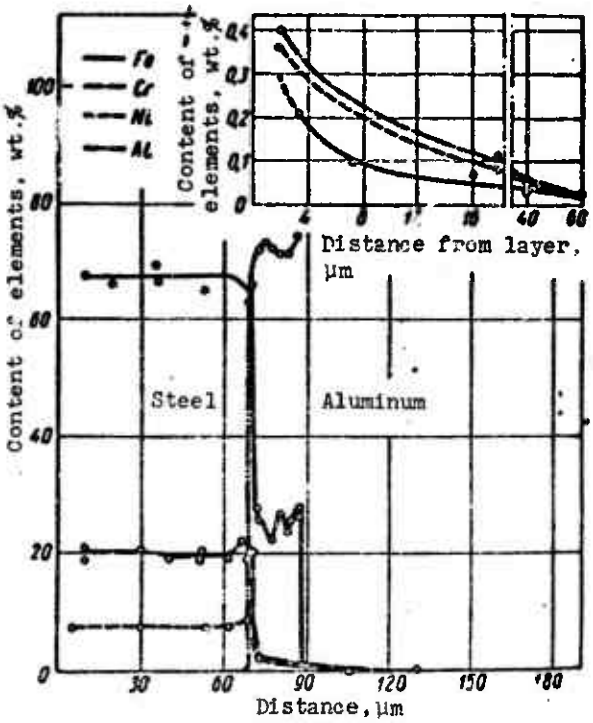

Fig. 61. Distribution of iron, chromium, nickel and aluminum across the fusion zone of aluminized 1Kh18n9T steel with AMg6 alloy.

band (the gray background), and then - the seam metal. Lighter coloring is observed on the seam in the band, which with respect to the steel, indicates an increased content of iron in this region. At the same time sections of reduced iron content (the darkish "islets") are evident in the layer. The contrast of the transition from the steel to the layer and from the layer to the seam with sharply expressed transition boundaries is clearly observed, which indicates an uneven variation in the concentration of iron content in the layer. The observed gray spots in the seam metal are sections with an increased iron content as compared with the total iron content in the seam, which is connected with the results of the subsequent (after aluminizing) argon-arc welding.

Fig. 62. Scanogram of the transition layer in a 1Kh18N9T steel and AMg6 alloy joint.

It follows from Fig. 61, that 38-43% iron is contained in the intermetallic layer - on the phase diagram respectively of the $FeAl_3$ and the Fe_2Al_5 phase [33, 168].

To explain the effect of magnesium on the nature of the formation of the transition zone from aluminum to steel spectral analyses were conducted on the "Cameca" device. In this case 1Kh18N9T stainless steel was welded with special fused aluminum alloys, containing

8% Mg (the sum of the remaining additives was not more than 0.1-0.2%). An analysis of the chemical composition of the intermetallic layer (its thickness was 20-25 mm) showed, that the iron content in the layer fluctuates within the limits of 21-24% (Fig. 63). It is characteristic, that magnesium (1-2%) takes part in the formation of the intermetallic layer. Apparently, the presence of magnesium atoms instead of aluminum atoms in the crystal lattice of one of the phases causes the appearance of weak bonds, since magnesium is practically insoluble in iron. Thus, wire of AMg6 alloys should not be employed as a filler.

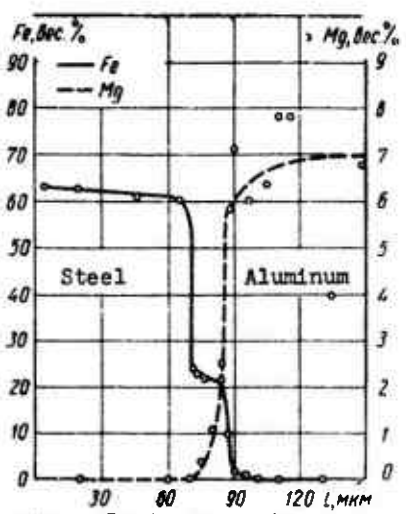

Fig. 63. The distribution of iron and magnesium across the fusion zone.

5. The Effect of an Intermetallic Layer on the Strength Properties of Steel/Aluminum Joints

An intermetallic layer formed as the result of the reactive diffusion of aluminum and iron has increased hardness and brittleness, which negatively affects the strength of the layer. However, the strength of the layer to a considerable extent also depends on its thickness.

The processing of data of numerous strength tests and a comparison of these data with the microstructure of the transition layer made it possible to establish, that the strength of a welded aluminum joint and of its alloys with steel is higher, the smaller is the thickness of the layer of intermetallic compounds (Fig.64). This is explained by the fact, that in a layer with great thickness pores form and considerable internal stresses arise, sometimes leading to the appearance of cracks. The appearance of internal stresses is due to the fact, that the formation of intermetallic compounds of an aluminum-iron system occurs with a considerable increase in volume [210], thus, new layers of intermetallides,

forming, for example, during aluminizing, exert pressure on the formed layers, which are in the solid state, which leads to the appearance of stresses and cracks in the layer.

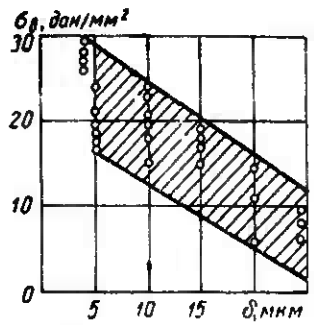

Fig. 64. The dependence of the strength of a steel/aluminum joint on the thickness of the intermetallic intermediate layer δ.

To determine the actual site of the failure of a steel/aluminum joint (St. 3-AMg6 and St. 1Kh18N9T-AMg6) experiments were conducted, in which the specimen was not subjected to failure during tensile testing, and the load was reduced after the appearance of the first crack. A section was prepared from the specimen. An investigation of it showed, that the failure of the joint with a developed width of intermetallic layer always occurs not in the aluminum, but in the layer of the intermetallic compound (Fig. 65). Its thickness can be as much as 20 μm. An analogous phenomenon is also observed in producing joints by brazing, for example, in welding 1Kh18N9T steel with AMg6 alloy (in this case the thickness of the thin intermetallic layers is as much as 2-3 μm). The nature of the failure was studied on a MKU-1 cinemicrographic device on specimens of special design. It was established, that in this case the crack forms initially in the layer of the intermetallic phase, and then, developing, frequently extends to the adjacent boundary where the layer comes into contact with the steel and the aluminum (Fig. 66).

In conducting investigations on an IMASh-5 device it was ascertained, that isothermic exposure at 500°C for a period of 5 h causes layer separation in the contact zone of bimetallic samples, for example, of an AMg6-St. 3 combination. With a subsequent increase in exposure the process of layer separation progresses. Apparently, this is connected with the sharper difference in the

Fig. 65. A crack along an intermetallic layer (the thickness of the layer is 20 μm; thermal pickling - is at 300°, for 5 s).

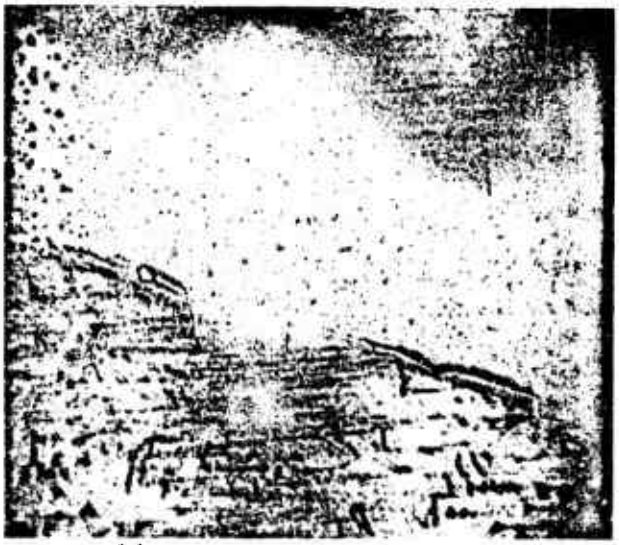

Fig. 66. Failed specimen of aluminum-steel bimetal.

coefficient of linear expansion of the component parts of the bimetal, than in the St. 1Kh18N9T-AMg6 alloy joint. The difference in the coefficients of linear expansion of metals being welded plays a large role in the premature failures of joints involving heterogeneous metals. Assumptions have been made [48], that the difference in the coefficients of linear expansion of metals being welded should facilitate the development in the fusion zone of the crystallizing phase and the accumulation of submicroscopic defects of the vacancy and dislocation type.

Thus, the experiments confirmed, that the most dangerous site in a welded steel/aluminum joint is the layer of the intermetallic phase. Thus, a decrease in the thickness of the intermetallic layer or its total removal, and also a reduction in its hardness

and brittleness should increase the strength properties of a welded joint.

As was indicated at the beginning of this chapter, the alloying of welding wire causes a variation in the thickness of the intermetallic layer and its microhardness. The strength properties of steel/aluminum joints also change simultaneously with this.

Graphs have been plotted (Fig. 67) on the basis of the data of mechanical tests. The strength of a steel/aluminum joint (St. 3-AMg5V alloy) with the employment of wire containing silicon, can be as high as 22-29 daN/mm^2. Butt specimens of the indicated combination, as a rule, fail along the seam [138]. The strength of a joint, made with wire containing copper, can be as high as 18-25 daN/mm^2. The strength of a welded joint, made with welding wire containing zinc, at first sharply increases, attaining a maximum value of 27-34 daN/mm^2 with a zinc content of about 7%, and then decreases and with a zinc content of 12-15% can be as high as 5-7 daN/mm^2, which agrees with the data on zinc-galvanizing [157]. The introduction of nickel in an amount of up to 2%, as was noted, did not affect the variation in the thickness of the intermetallic layer and practically did not change the strength of the steel/aluminum joint. Beryllium only insignificantly increased the strength of a joint with its addition to the wire in an amount of up to 1% (Fig. 68a). The addition of rare-earth elements (mischmetal) to welding wire in amounts of more than 0.4% caused a drop in strength.

and brittleness should increase the strength properties of a welded joint.

As was indicated at the beginning of this chapter, the alloying of welding wire causes a variation in the thickness of the intermetallic layer and its microhardness. The strength properties of steel/aluminum joints also change simultaneously with this.

Graphs have been plotted (Fig. 67) on the basis of the data of mechanical tests. The strength of a steel/aluminum joint (St. 3-AMg5V alloy) with the employment of wire containing silicon, can be as high as 22-29 daN/mm^2. Butt specimens of the indicated combination, as a rule, fail along the seam [138]. The strength of a joint, made with wire containing copper, can be as high as 18-25 daN/mm^2. The strength of a welded joint, made with welding wire containing zinc, at first sharply increases, attaining a maximum value of 27-34 daN/mm^2 with a zinc content of about 7%, and then decreases and with a zinc content of 12-15% can be as high as 5-7 daN/mm^2, which agrees with the data on zinc-galvanizing [157]. The introduction of nickel in an amount of up to 2%, as was noted, did not affect the variation in the thickness of the intermetallic layer and practically did not change the strength of the steel/aluminum joint. Beryllium only insignificantly increased the strength of a joint with its addition to the wire in an amount of up to 1% (Fig. 68a). The addition of rare-earth elements (mischmetal) to welding wire in amounts of more than 0.4% caused a drop in strength.

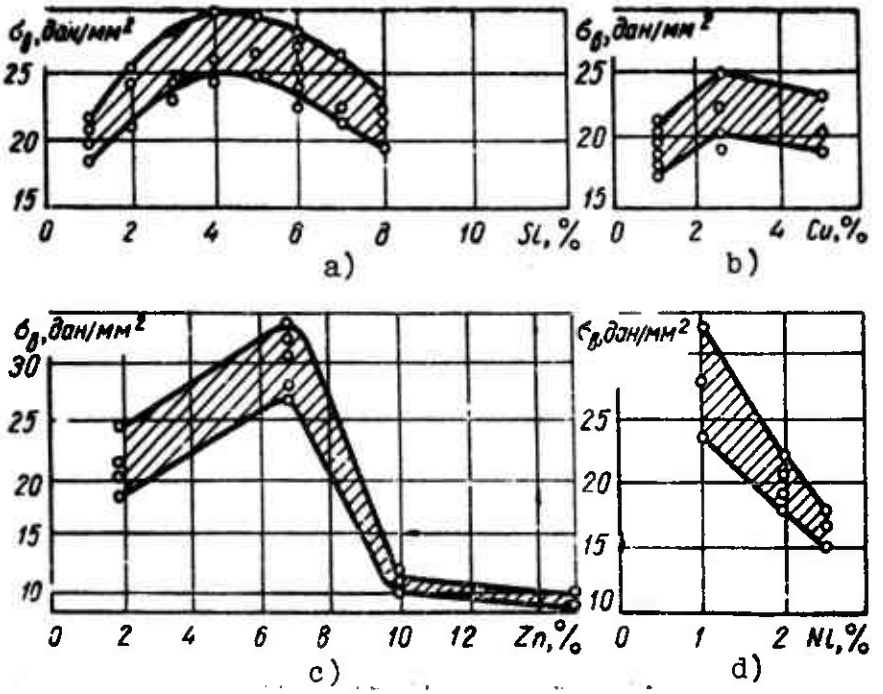

Fig. 67. The dependence of the strength of a welded joint on the content of alloying additives: a) silicon, b) copper, c) zinc, d) nickel.

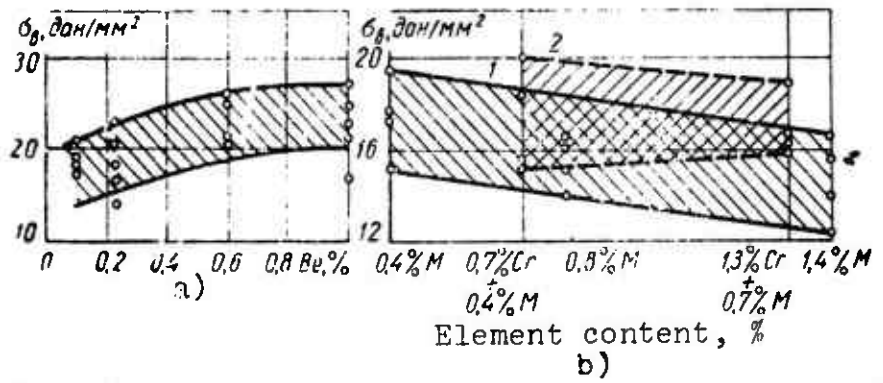

Fig. 68. Dependence of the strength of a welded joint on the content of alloying additives in welding wires: a) beryllium, b) mischmetal (1) and chromium with mischmetal (2).

CHAPTER V

DEVELOPMENT OF THE TECHNOLOGY FOR WELDING ALUMINUM AND ITS ALLOYS TO STEELS

The technology for joining the two steels St. 3 and Kh18N9T to aluminum alloys differs in principle: preliminary galvanizing of the steel surface is applied when joining steel St. 3 with the indicated alloys, and argon-arc welding is carried out either with an aluminum-wire filler or with filling by special wires containing alloying additives. To joint stainless steel with the alloys the steel is first calorized with aluminum AV000 with subsequent welding with standard welding wires. In both cases it is necessary to solve these problems: selection of the rational technology for applying the coating on the steel surface and proper selection of filler materials, and the problem of determining the effect of grooving, the sequence and conditions for manual and automatic welding, and the strength properties of the joint.

1. Welding Low-Carbon St. 3 Steel to Aluminum Alloys

Welding of low-carbon steel St. 3 to the alloys AMts, AMg3, AMg5V, and AMg6 can be done in three ways: a) welding zinc-coated steel St. 3 to aluminum alloys with type AD1 aluminum used as the filler metal; b) welding aluminum alloys to steel St. 3 which has a galvanic coating, also using aluminum AD1 as the filler metal; c) welding zinc-coated steel St. 3 to aluminum alloys with alloyed welding wires used as the filler metal.

We will examine each procedure.

Welding of Zinc-Coated Steel

G. A. Bel'chuk [16], D. R. Andrews [183, 184], and other investigators [9, 122, 212] have carried out major work on using a zinc coating on steel and its subsequent welding to aluminum.

Investigation of the process of argon-arc welding of A0 and A1 aluminum and the alloys AMts, AMg3, AMg5V, and AMg6 to steel St. 3 was carried out with a metal thickness of 2-4 mm. It was established experimentally that a zinc layer up to 30-40 μm thick is adequate for both types of zinc plating (Fig. 69).

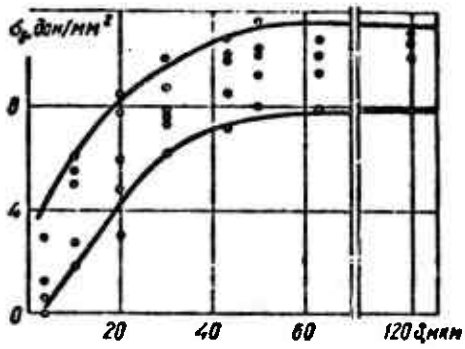

Fig. 69. Strength of a joint between St. 3 and aluminum A1 as a function of the thickness of the zinc coating.

During study of the microstructure of the transition layer it was established that there is a transition layer 15-20 μm thick between the surfaces of the steel and the aluminum; in certain points there is local thickening up to 40-60 μm. The hardness of the layer comprises 1040, 960 daN/mm^2. A sharp transition is observed from the steel to the layer - a hardness jump; the transition from the layer to the aluminum is smoother. A characteristic of such a joint is the fact that the aluminum contains no needles of intermetallic phases, such as are observed during buildup of aluminum on steel. The transition layer is porous - has porous areas - which confirms the data obtained by E. Gebhardt and W. Obrowski, as well as others [195-197], with analogous interaction. There is a layer which is nonuniform in thickness and which is

discontinuous. The thickness of the layer varies within the limits 20-50 μm. Layer microhardness comprises 775, 850, 960 daN/mm^2; the hardness of the steel is 184-194 daN/mm^2 and that of aluminum, 88-96 daN/mm^2.

For the most part the evaluation of mechanical properties has been carried out with respect to tensile strength, relative elongation, and results from static bend tests. A standard bending test for such joints is somewhat tentative, since bending occurs along the aluminum portion of the specimens. During tensile testing of specimens the load at destruction corresponding to a certain weld cross section was determined. A weld between aluminum and steel, together with bilateral reinforcement, comprised an effective zone of joining. Relative elongation was measured with respect to the aluminum portion of the specimen.

Since scattering of values is observed during the tests, no less than six measurements were carried out to construct a single point on the curve.

Table 19 presents characteristic results of mechanical testing of butt-joined specimens without removal of reinforcement of steel St. 3 welded to the alloys AMg3M and AMg5V. Analyzing the results presented in Table 19, we can note that welding of low-carbon steel St. 3 with a galvanized zinc coating gives satisfactory strength indices when AD1 wire is used as the filler material. However, the stability of the results is low; besides this, the joint is destroyed (in this case along the weld). Application of standard wires containing magnesium (AMg5V, AMg6) does not ensure high joint quality: destruction occurs, as a rule, along the coating.

Table 19. Results of mechanical tests of butt-welded specimens.

Combination of welded materials	Load at destruction, N	Ultimate strength, daN/mm^2	Bend angle, deg	Nature of joint destruction
Alloy AMg3M-St. 3 with a galvanized zinc coating 30-40 μm thick. Filler AD1.	830-1170 / 1005	11.1-15.0 / 12.2	15-15 / 12	Failure along the weld; in one case along the coating
Alloy AMg3M-St. 3 with a galvanized zinc coating 30-40 μm thick Filler AMts	300-1315 / 688	3.6-16.2 / 10.0	10-12 / 10.6	Failure along coating and weld
Alloy AMg3M-St. 3 with a 30-40 μm galvanized zinc coating. Experimental filler wire.	175-550 / 370	2.3-5.9 / 4.4	0-5 / 2.4	Failure predominantly along the coating
Alloy AMg3M-St. 3 with 4 μm galvanized coating and 30 μm zinc coating. Filler wire AD1.	740-1015 / 830	14.0-20.7 / 19.2	20-38 / 25	Failure along the base metal AMg3M and along the near-weld zone
Alloy AMg3M-St. 3 with a 12 μm galvanized nickel coating and 30 μm zinc coating. Filler AD1	660-880 / 752	16.7-17.7 / 17.3	20-32 / 26	Failure along the aluminum-alloy base metal and over the coatings
Alloy AMg6-St. 3 with a 6 μm galvanic copper coating and a 30 μm zinc coating. Filler - AMg6	390-580 / 480	4.5-6.3 / 5.3	0-5 / 2.6	Failure along the coating
Alloy AMg3M-St. 3 with a 30 μm galvanized zinc coating. Experimental filler wire.	845-1550 / 1140	9.0-15.3 / 12.2	-	Failure along the coating. In two cases failure along the weld and the coating.

Experiments carried out in welding of steel St. 3 covered with a layer of zinc up to 30 μm thick to A0 and A1 aluminum (using fillers AD1, AMcs, AMg5V) showed that pure aluminum welds well to steel covered with zinc - with both galvanic and hot-immersion coatings. The obtained data coincide with the conclusions in works [15, 221]. During bend tests of both double and single welds of such joints a bend angle up to 180° is obtained. Bend testing of such joints is somewhat tentative, since bending occurs along the aluminum portion of the specimens. During bend testing of specimens with longitudinal arrangement of the welds the magnitude of bend angle does not exceed 10-25°.

Tensile tests showed good adhesion of filler metal to the steel base and substantial magnitudes of destructive forces. A brittle layer is also formed in this case.

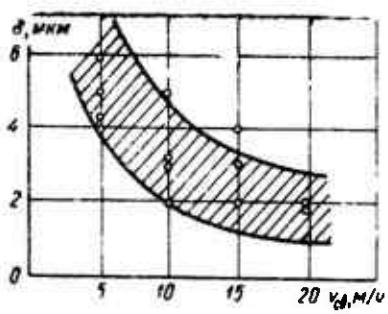

Fig. 70. Thickness of the intermetallic layer as a function of welding speed.

Experiments established that in order to obtain a layer of minimum thickness it is necessary to increase the welding speed. Figure 70 shows curves of layer thickness as a function of the speed of manual argon-arc welding. The application of very high welding speeds is hampered due to incomplete fusion and other defects. Tests of welded joints made at the optimum speed (about 12 m/h) showed satisfactory adhesion of filler metal to the steel base. The strength of such joints is comparatively small - around 9-10 daN/mm^2; the bend angle is substantial (along the aluminum portion of the specimen).

In the majority of tensile test cases the specimens failed brittlely over the zinc coating; pores are frequently observed in the fracture (Fig. 71). It follows from the figure that the strength of a joint in this case is determined by the strength and

quality of the joining zinc interlayer: on the majority of specimens a characteristic "parting line" is visible over the point of joining. The given data indicate that the application of only a single zinc coating is inadequate to increase the strength of the welded joint.

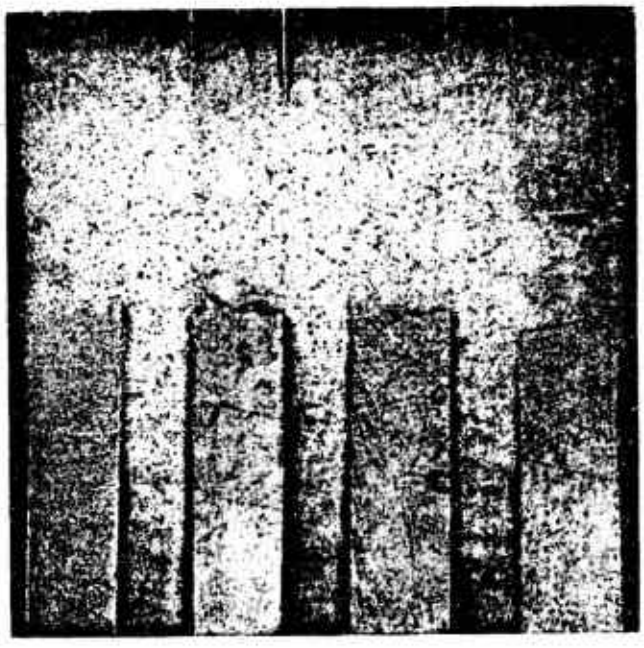

Fig. 71. Fracture specimens of hot-zinc-coated steel St. 3 welded to alloy AMts.

Welding to Steel with Complex Coatings

Studies were also made of joints between the aluminum alloys AMts, AMg3, AMg5V, and AMg6 with steel St. 3 with various combined coatings. The joints were made by argon-arc welding. The thickness of the tested material was 2-4 mm. Tests were made of welding the indicated alloys to steel with galvanized coatings of copper, nickel, lead, tin, brass, and also magnesium and aluminum; these coatings were obtained by hot immersion [121, 122, 139]. Also tested were specimens with combined nickel-copper-zinc, copper-zinc, nickel-zinc, silver-zinc, and brass-zinc galvanized coatings. Aluminum

coated with chromium and nickel was also tested; such specimens were then welded to steel. The preliminary experiments did not give positive results.

When combined coatings are used (combination of stable and unstable [coating]) the following is assumed: owing to the fact that the melting temperature of the aluminum welding rod is higher than the melting temperature of the zinc coating, during welding the layers of zinc are substantially overheated and float upward, protecting the molten metal from oxidation. Aluminum interacts with the layer of silver underneath the zinc, or with copper or some other sublayer, partially dissolving it. Thanks to this good contact of the aluminum or its alloy and the sublayer is achieved.

Coating thickness was varied within the limits 3-50 μm for galvanized coatings and up to 100-120 μm for coatings obtained by hot dipping. Results of preliminary experiments indicated that the formation of a joint on the indicated types of coatings is possible at certain thicknesses of them; however, except for zinc, tin, and silver the strength properties of the joints are extremely low, since a brittle layer containing intermetallic compounds is also formed in this case.

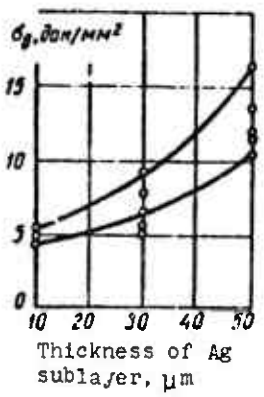

Fig. 72. Strength of a joint between alloy AMg3M and steel St. 3 with a combined silver-zinc coating as a function of the layer of silver.

Application of a combined silver-zinc coating facilitated an increase in the strength of a joint between aluminum and steel; however, the high strength indices (15-18 daN/mm^2) will obtain only

with a thickness δ of the silver sublayer equal to 50 μm (Fig. 72); this makes the application of a coating of this type in the production of large parts or units economically unfeasible.

The application of a combined copper-zinc coating yielded satisfactory strength indices (Table 20).

Table 20. Results of mechanical tests of butt-welded specimens (the steel has a galvanized coating).

Type of coating	Coating thickness, μm	$\sigma_в$, daN/mm^2	Bend angle, deg	Type of failure
Silver	30-50	$\frac{18.4\text{-}6.7}{11.2}$	15-45	Failure along the coating
Zinc	30-40	$\frac{15.0\text{-}11.1}{12.5}$	12-18	Failure along the weld and the coating
Combined: first layer copper and second, zinc	2-6 30-40	$\frac{20.7\text{-}14.6}{18.7}$	12-22	Failure over the base metal, weld, and coating
Zinc*	40-60	$\frac{15.6\text{-}10.2}{13.2}$	20-25	Failure along the weld
Brass	To 20	$\frac{15.3\text{-}9.0}{12.7}$	10-25	Failure along the base metal, weld, and coating
Combined: first layer nickel and second, zinc	2-6 30-40	$\frac{19.7\text{-}21.3}{19.2}$	15-38	

*Coating applied by hot dipping.

As has been indicated, it was established experimentally that with subsequent zinc coating a layer of zinc up to 30-40 μm in thickness is sufficient.

Pyrophosphate baths, whose composition is indicated in work [122], were used for direct application of a copper coating to steel St. 3.

Before welding them to steel, specimens of alloys of the type AMg, AMts, and others must be extremely well etched. Specimens were etched in 15-20% solution of NaOH or KOH, washed off, passivated with 20% HNO_3, and then washed and dried.

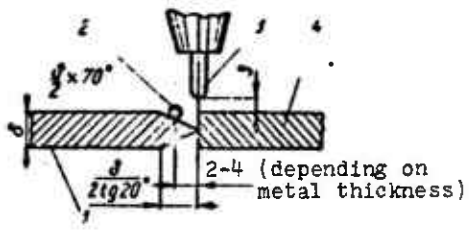

Fig. 73. Mutual arrangement of the electrode and the filler metal when making a steel/aluminum joint:
1 - steel specimen; 2 - filler wire; 3 - tungsten electrode; 4 - specimen of aluminum alloy.

The specimens were welded on a standard UDAR-300-1 installation at a current of 80-120 A and an argon flow rate of 6-8 l/min. The diameter of the tungsten electrode was 3 mm and the tentative speed for manual welding was 12 m/h. As a rule, a welding rod 3 mm in diameter was used. During the production of steel/aluminum butt and lap joints it is necessary to guide the arc exactly during the entire welding process along the edge of the aluminum sheet, approximately 1-2 mm from the line of the joint, to avoid letting the arc hit the coating and burn it (Fig. 73). During slow accomplishment of double welding the coating on the opposite side can also be burned and the ability of metal to spread over it can be sharply impaired; as a result of this such joints have low strength indices. Filler wire is supplied either along the joining line or shifted a little toward the pool. Thanks to the presence of a coating on the steel the molten filler metal is easily spread over this steel.

Comparative results from testing specimens with different thicknesses of the copper sublayer showed that the optimum thickness for the copper sublayer is 4-6 μm (Fig. 74).

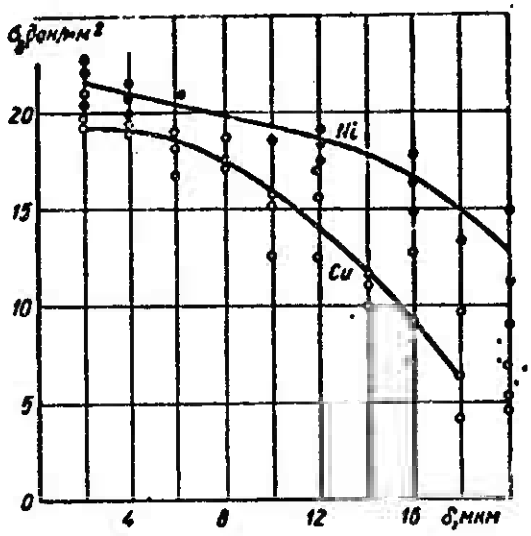

Fig. 74. Strength of a butt weld between alloy AMg3M and steel St. 3 as a function of magnitude δ of a layer of copper and of nickel.

The layer, which plays the role of a brazing metal, does not have sharply marked boundaries; diffusion of this layer into the aluminum portion of the spectrum is observed, and in certain sections the continuity of the layer is disturbed. The presence of "naked" segments can lead to the appearance of random crushed zones of intermetallic phases; however, in this form the latter have no influence on the strength of the joint.

Preliminary experiments in applying a thin sublayer of brass (about 3 μm) on steel with subsequent zinc coating also gave positive results.

Results of mechanical tests of butt-welded specimens of steel St. 3 (without removal of the reinforcement) on alloy AMg3M are given in Table 20.

Application of a combined nickel-zinc coating with a nickel sublayer thickness of 2-6 μm gave stable high strength indices. First this was checked on thick layers (up to 50 μm), but the smaller thickness of the sublayer turned out to be adequate. Before electrolytic nickel-plating the steel specimens were subjected to standard treatment. With welding of steel St. 3 with such a coating to the alloy AMg3M the specimens were destroyed during tensile testing, as a rule, along the base metal of the aluminum alloy (Fig. 75).

Fig. 75. Fracture specimens of steel St. 3 with combined galvanized coating of nickel (6 μm) and zinc (30 μm), welded to the alloy AMg3M.

Results of tensile testing of specimens of alloy AMg3 welded to steel St. 3 with a nickel-zinc coating are given in Table 20.

Analysis of the microstructure of the transition layer in specimens fractured along the base metal showed that in this case a layer averaging 2-3 μm wide of very uniform thickness is located between the joined metals.

Data from mechanical tests show that the application of a galvanized coating on steel St. 3 can ensure high destructuve forces.

On combined welded joints of steel St. 3 with copper-zinc coatings and alloys AMg3M and AMg61 an increase in strength is observed as compared with the same specimens with a simple zinc coating. The maximum value of ultimate strength of combined welded joints was obtained when a nickel-zinc coating was applied to the steel (strength 20-22 daN/mm^2).

During bend tests of selected specimens bend-angle values within the limits 15-38° were obtained (thickness of aluminum alloy layer 4 mm, bending along the transition zone of the aluminum-alloy base metal with a base-metal thickness of 2 mm).

Welding of Zinc-Coated Steel by Means of Alloyed Welding Wire

To obtain stable and comparable results, we carried out argon-arc welding with a nonconsumable tungsten electrode on an ADSV-2 automatic welder.

The surface of steel specimens (edge 30 mm in width) was coated galvanically with a 35-40 μm layer of zinc. Both standard wires and experimental types were used as fillers. Initially experiments were carried out on specimens without grooving of the edges. Welding of steel St. 3 to alloy AMts using wires of types

ADl, AMts, and AK yielded ultimate strength equal to that of the aluminum-maganese alloy AMts, i.e., σ = 12-14 daN/mm^2. However, the results of mechanical tests were unstable.

Study of the nature of destruction of numerous specimens during tensile testing, along with study of macro- and microstructures of the welds showed that failure (the appearance of tears and cracks) began as a rule on the face side of the steel plate. Pores, oxide scales and incomplete fusion of the aluminum edge were observed on the fracture surfaces.

Since the strength of steel/aluminum joints made over coatings depends on the value of surfaces in contact, tests were made of various types of edge dressing: complete absence of a face segment on the steel, U-shaped dressing, and dressing with 1-2 mm shoulders. Results of mechanical tests carried out on specimens made by automatic argon-arc welding from both sides indicated that use of edges of type a (Fig. 76) ensures an increase in strength in the joint by approximately 25%. Optimum value of the edge dressing angle on the steel plate is 70-75°.

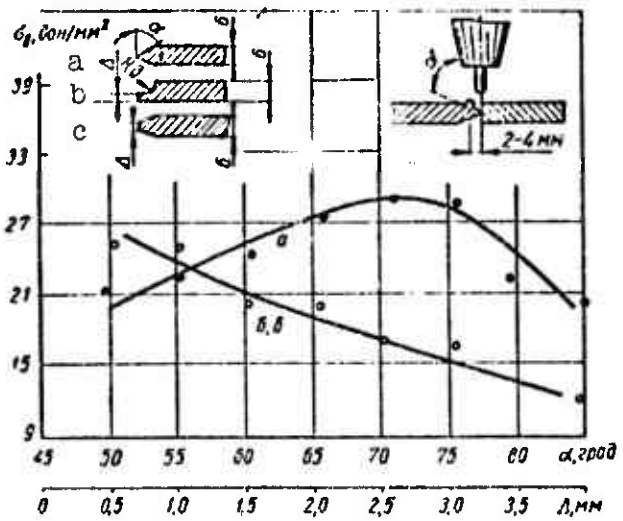

Fig. 76. Strength of a welded steel/aluminum joint as a function of the type of edge dressing on the steel plate (of edge bevel angle α and shouldering of the edge, Δ).

Table 21. Conditions of automatic argon-arc welding of combined joints.

Welded metals	Thickness, mm		Rod diameter, mm	$I_{св}$, A	$v_{св}$, m/h	$v_{п.э}$, m/h	
	steel	aluminum alloy				1st bead	2nd bead
AMts-St.3	5	5	2	160-180	6	72	48
AMg5V-St.3	4	4	2.5	160-180	7.2	61	41
AMg5V-St.3	4	4	2	150-170	7.2	68	50
AMg5V-St.3	3	3	2.5	160-180	8.2	72	61
AMg5V-St.3	6	6	2.5	180-200	7.2	72	61
AMg6-St.3	6	6	2.5	200-220	5.4	30	30

Table 22. Results of mechanical tests of combined specimens.

Welded metals	Thickness, mm	Type and diameter of wire, mm	$\sigma_в$, daN/mm^2
AMts-St. 3	4	AMts; Ø 2	11.1-11.5 / 11.3
AMg5V-St. 3	4	Wire No. 1; Ø 2	20.1-23.3 / 23.7
AMg5V-St. 3	4	Wire No. 2; Ø 2	25-29.5 / 25.9
AMg5V-St. 3	4	Wire No. 3; Ø 2	22.3-30.9 / 29.3
AMg5V-St. 3	4	Wire No. 4; Ø 2	19.4-23.3 / 21.0
AMg5V-St. 3	4	Wire No. 5; Ø 2	20.7-32 / 22.9
AMg5V-steel 28Kh3SNVFA	6	Wire AK; Ø 2.5	21.3-27.1 / 24.4
AMg6-St. 3	6	Wire AK; Ø 2.5	19.8-25.3 / 22.56
AMg5V-St. 3	4	Wire AK; Ø 2	25-30.8 / 28.2

The optimum automatic argon-arc welding conditions which we found for various combinations of steel St. 3 with aluminum alloys are shown in Table 21.

During welding of double welds the second one should be made after the first has frozen completely (the first being located on the opposite side).

The results from mechanical tests of steel/aluminum specimens made by automatic argon-arc welding (Table 22) show that the strength of the welded joint in this case reaches 25-29 daN/mm^2. Table 15 gives the composition of the wires.

2. Welding of Stainless Steel 1Kh18N9T to Aluminum Alloys

Direct joining (welding) of aluminum to stainless steel, just as in the case of welding aluminum to low-carbon steel, does not lead to positive results, although the nature of interaction in the first case is different and depends on the allotropic form of the steel [26, 35, 38, 39, 43].

On the first stage of the work a study was made of joining steel 1Kh18N9T to aluminum and aluminum alloys with galvanized coatings of nickel, and also with a number of combined coatings - nickel-copper-silver, nickel-copper-tin, and nickel-zinc. These types of coatings did not give positive results owing to poor wettability (nickel), burning of the coating and the formation of cracks in the build-up metal (nickel-copper-silver), the formation of cracks, and the complexity of correcting defects in the welded joint (nickel-copper-tin). Significantly better results were obtained by using a nickel-zinc coating [19]. Here the combination of a stable (nickel) and unstable (zinc) coating ensures obtaining a reliable bond. The quality of such a joint depends significantly on care in applying the nickel plating.

The following procedure was used to prepare the stainless steel for welding to aluminum alloys: degreasing, washing in water, etching in hydrochloric acid, nickel-coating, copper-coating, zinc-coating, drying, calorization, and checking the quality of the coating.

Conditions for applying the galvanized coatings and also particular features of these processes are outlined in work [37].

Accumulated experience in applying coatings on stainless steels allows us to assert that the most laborious and critical operation is calorization. The quality of an applied aluminum layer is the major factor determining the quality of the welded joint.

To obtain a high-quality coating by a layer of aluminum (or the alloy AMts) on the surface of stainless steel it was necessary to select the material of the crucible, to choose the protective atmosphere during calorization, and to ensure proper cleaning of the surface of the specimens, to create the necessary apparatus for calorization, and to develop the technology and optimum conditions of calorization. From a number of materials tested (stainless steel 1Kh18N9T, grey cast iron, graphite-carbon electrodes) it was found that crucibles manufactured from grey cast iron gave satisfactory stability. However, cast-iron crucibles are rapidly oxidized at a temperature of 800-840°C and become coated with a thick layer of scale, which disrupts calorization.

We succeeded in improving the quality of the calorized surface by carrying out the process in vacuum. For calorization in vacuum we manufactured a vacuum furnace (Fig. 77). The temperature in the furnace was measured and controlled by a type ERM-47 electronic bridge. Calorization of specimens in the furnace was carried out according to the following cycle: oil and dirt were removed from the aluminum before loading it into the furnace by etching in an alkaline solution and in nitric acid.

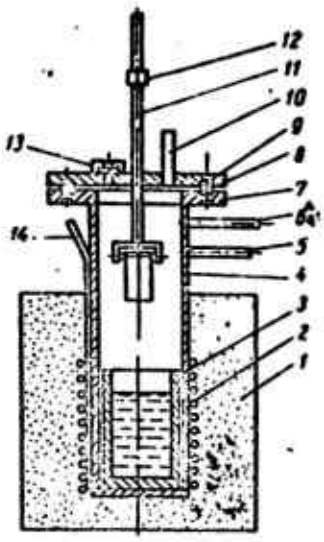

Fig. 77. Vertical cross section of a vacuum furnace for calorization of stainless steel: 1 - thermal jacket; 2 - electrical coils; 3 - crucible; 4 - vacuum cavity of furnace; 5 - connecting fitting for monovacuum gauge; 6 - fitting for releasing the vacuum; 7 - cavity for cooling the sealing ring; 8 - cover with flange; 9 - sealing ring; 10 - fitting for attachment to vacuum pump; 11 - attachment for loading specimens into the furnace; 12 - seal; 13 - inspection attachment; 14 - attachment for thermocouple.

After loading the AD1 aluminum, the vacuum pump, the furnace heater, and the automatic temperature regulator were switched on. The working temperature in the furnace was maintained within the limits 780-820°C. Evacuation was monitored with a VIT-2 vacuum gauge. Upon achievement of maximum vacuum (0.5-1 mm Hg) the specimen was dipped into molten aluminum by means of a special attachment.

To obtain a high-quality coating with aluminum, a small rotary motion should be imparted to the specimen; the specimen should be held in molten aluminum until it is completely heated and then should be pulled from the crucible. The duration of this operation is 15-30 seconds.

The calorized layer is checked by inspection, where the coating must completely cover a segment no less than 40 mm in width and it should not have any bulging or contaminated segments.

Work on testing standard fluxes for arc and gas welding of aluminum (fluxes of types AF-4A, AN-A1, etc.), experimental fluxes based on them, and also a special flux for gas welding of calorized steel to stainless steel [78] preceded the selection of the optimum

composition of fluxes for cleaning the surfaces of the metals. None of these fluxes ensured proper cleaning, flowability, and wettability of molten aluminum over the surface of steel.

Tests were made of a series of fluxes consisting of mechanical mixtures of chlorine and fluorine salts of lithium, sodium, and potassium. The fluxes were dissolved in water and applied as a thin layer on the specimens and tubes of stainless steel. Table 23 gives the compositions of certain experimental fluxes for calorization. Best results were obtained when using fluxes containing sodium chloride and sodium fluoride, lithium choride (variant 1), and also a flux containing 65% AF-4A flux (variant 3).

Table 23. Composition of experimental fluxes for calorization.

Component	GOST or TU	Composition of fluxes in variants			
		1	2	3	4
Lithium chloride	TUMKhP No. ORU 104.58	47	20	-	-
Sodium chloride	GOST 153-54 "Ekstra"	14	-	-	10
Potassium chloride	GOST 4568-49	29	20	28	20
Sodium fluoride	GOST 4463-48	10	10	7	10
Flux AF-4A	AMTU 219-60	-	50	65	-
Flux 34A	-	-	-	-	60

In the course of the experiments it was established that preliminary coating of the steel surface with zinc before calorization has a substantial influence on the strength of the welded joint. During studies of the effect of the sublayer of zinc, applied electrolytically, on the quality of calorization and subsequent weldability of the steels 1Kh18N9T and St. 3 to aluminum alloys, the surface of the plates (or articles) was treated according to the technology described in work [37]. A study was made of the affect of a 25 μm zinc coating on the quality of calorization and

the subsequent weldability, using specimens 3 × 150 × 200 in size made from steels St. 3 and 1Kh18N9T. The temperature during calorization was 780-820°C and the hold time was 1.5-2 minutes. Calorized steel plates were subjected to the same treatment as plates of aluminum alloy before welding.

Calorized steel plates were butt-welded to plates of the same dimensions made of aluminum alloy AMg6. Welding was carried out on the ADSV-2 automatic welder, using as filler material AMts6 wire 2 mm in diameter, per STU-5-54 and with a tungsten electrode 3 mm in diameter, per TUVM2-529-57. Welding conditions: $I_{св}$ = 130-150 A; $v_{св}$ = 4.6-6.2 m/h; $v_{пр}$ = 40-62 m/h. Specimens for mechanical and vibration testing and cross sections for metallographic research were made from the welded plates. Figure 78 illustrates the results of the mechanical tests of the specimens.

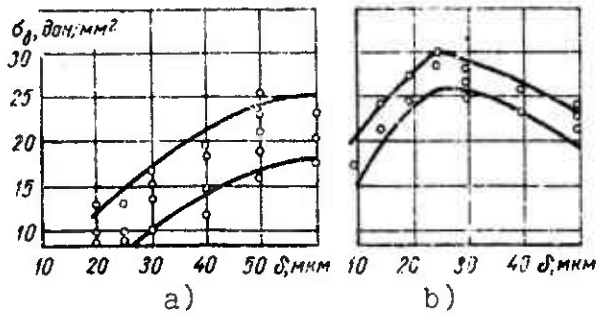

Fig. 78. Strength of the welded joint between steel 1Kh18N9T and alloy AMg6 as a function of the thickness δ of the coating applied on the steel: a) - steel surface coated only with a layer of galvanic zinc; b) - steel surface calorized over a layer of galvanized zinc.

When the steel was galvanically coated with a 40-μm layer of zinc with subsequent calorization the ultimate strength comprised 31.5 daN/mm^2 (average from five tests) and the bend angle was about 32°. If the steel was degreased and etched according to manufacturing technology prior to galvanizing with zinc and then calorized according to the procedure described above, ultimate strength comprised 25.4 daN/mm^2 and the bend angle was 24°.

Thus, results of mechanical tests showed that the developed technology ensures obtaining stable strength in a steel/aluminum joint between steel 1Kh18N9T and alloy AMg6, on a par with the strength of a weld between two pieces of AMg6 - i.e., 30-32 daN/mm^2 (Fig. 79). The conducted investigations made it possible to select the technology for preparing the surface and for welding experimental structures from steel 1Kh18N9T and aluminum alloys [124].

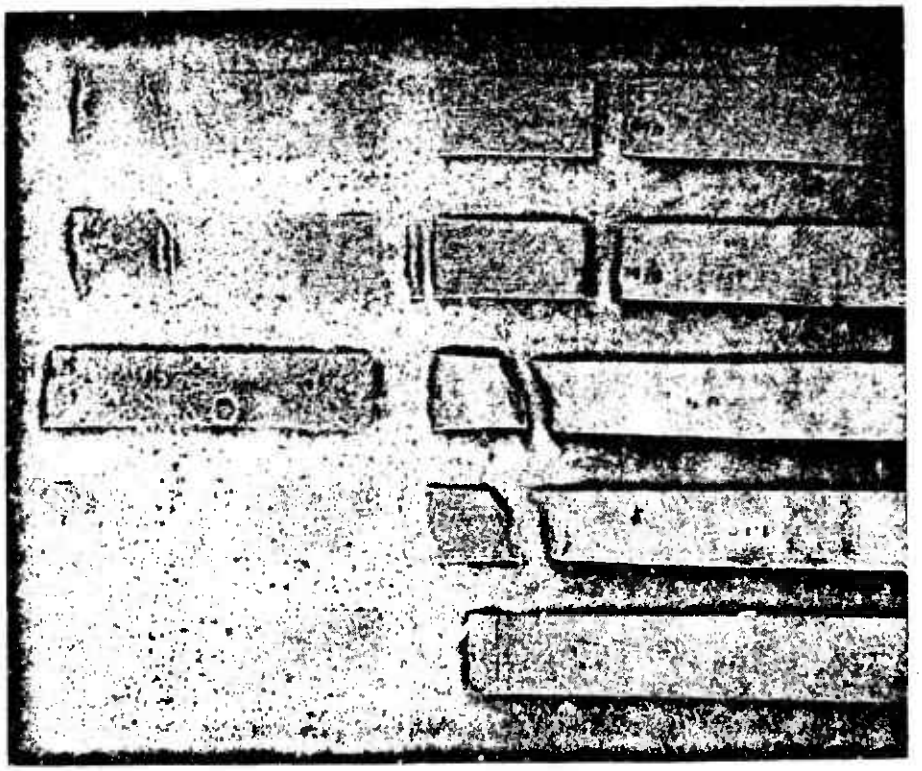

Fig. 79. Fracture specimens of a joint between steel 1Kh18N9T and alloy AMg6 (on the right) (width of diffusion zone 5 μm).

3. Argon-Arc Welding of Tubes of Steel 1Kh18N9T with Tubes Made from Alloys AMts and AMg6

In connection with production of tanks for storing liquefied gases, the need arose to obtain strong and tight joints between aluminum and aluminum alloys and other metals. These vessels have double walls, with the space between them being evacuated. The use

of vessels with vacuum insulation permits a sharp reduction in volatility of the gases and, consequently, a sharp reduction in losses both during storage and during transportation. In certain types the inner vessel is made up of chrome-nickel steel 1Kh18N9T, and the aluminum alloys AMg5V and AMg6 from which the outer shell is made represent a structural material. Joining the vessels requires joining unlike tubes. As a rule telescopic joints are used to connect unlike tubes 60-70 mm in diameter with a wall thickness up to 5 mm; the inner tube is the steel one.

When nickel-zinc and nickel-copper-zinc coatings were used with subsequent argon-arc welding of telescopic tube joints good mechanical properties were obtained for such connections (destructive force 2000-4200 daN); however, vacuum testing (down to 10^{-3} mm Hg) in conditions of deep cold (to -196°C) led to failure of some of the specimens. It was found that fulfillment of all the conditions of the assigned tasks - ensuring vacuum tightness at low temperatures, elevation of mechanical properties of the joint, convenience in carrying out repair operations, etc. - is possible by using the technology of preliminary application of a layer of galvanized combined nickel-copper-zinc coatings on the surface of the stainless steel Kh18N10T with subsequent calorization of the tube (specimen) in a melt of AD1 aluminum. Argon-arc welding to an aluminum tube was carried out without any complex technological procedures over the calorized surface of the stainless steel tube. In this case three aluminum alloys are joined - the calorization alloy, the filler metal, and the molten base metal AMts.

Assembly of Telescopic Tube Joints

Prior to application of a coating the tubes should freely enter into one another; it has been established experimentally that the gap between the tubes should not exceed 0.3 mm.

It is advisable not to produce the telescopic connections during assembly (i.e., during manufacture of the basic tank), but to make them separately as composite tubular joints (fittings) 350-400 mm in length which are subsequently welded to the tank. Naturally, the length of segments of steel and aluminum tubes should be calculated so that during subsequent welding of the obtained fitting to the appropriate tubes strength properties and vacuum tightness will not be lost at the point where the alloy AMts is joined to steel 1Kh18N9T. Maximum permissible heating is no more than 300°C. To ensure this the weld between steel 1Kh18N9T and the alloy AMts should be cooled with a water jacket during welding of the fitting to the base metal. As measurements have indicated, the temperature in the joint does not exceed 250°C.

Argon-arc welding of steel Kh18N10T tubes to tubes made from alloy AMts up to 100 m [sic] in diameter and with a wall thickness up to 5 mm was carried out with a nonconsumable tungsten electrode 2-3 mm in diameter, using pure mark A argon and AD1 filler wire 2-3 mm in diameter.

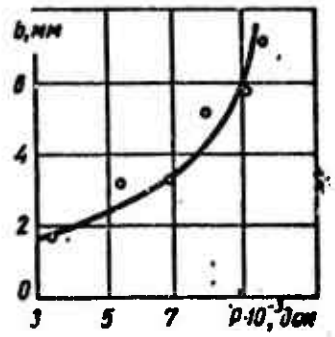

Fig. 80. Strength of a telescoping joint between tubes 70 mm in diameter (load at destruction P) as a function of the width of the bead b.

The production of annular welds should be continuous and should be done on a rotating attachment. In all cases when the arc is broken it is mandatory that welding be begun on the aluminum section of the tube. Craters should be carefully welded in. It has been established that the strength of a telescoping joint between tubes depends essentially on the width of the connecting bead (Fig. 80). Therefore, as a rule, welding should be carried out in one-three

layers, where it is recommended that the first layer be made by melting the edge of the aluminum tube without the use of filler material. Here the arc is carefully drawn along at a distance of 2-3 mm from the face. Filler wire is used in the following layers.

Table 24. Conditions for calorization of tubes of steel Kh18N10T.

Tube diameter, mm	Temperature of melt, °C	Hold time, s
35/31	720-760	8-10
50/46	750-770	10-12
63/59	760-770	12-15
108/98	780-800	16-20

Mastery of welding unlike tubes 110 mm in diameter became possible only after the development and refinement of procedures for calorizing tubes of steel 1Kh18N9T. Investigations indicated that in order to obtain quality welds of unlike tubes a fairly short hold time of 8-20 seconds during calorizing is sufficient; in this case the temperature of the bath should be determined by the mass (diameter) of the steel tube to be calorized. Table 24 gives the procedures developed for calorization. Calorization of tubes 159 mm in diameter showed that after the application of a two-layer galvanized Ni-Cu coating it is necessary to increase the hold time to 40-60 seconds.

During calorization of the large mass of a cold tube in a small bath, the aluminum is cooled and the obtained coating tends to be nonuniform; therefore it is desirable that the diameter of the bath be no less than 200 mm for tubes 110 mm in diameter. Besides this, for large-diameter tubes it was found to be advisable to fit the aluminum tube tightly onto the steel tube, since the presence of a gap within limits of 1 mm sometimes caused annular cracks along the welds.

As subsequent tests indicated, for greater structural rigidity and better operation of the unit under conditions of bending forces and vibration it is desirable that a lap-welded joint be made with welds on both sides. A special head [37] (height of operating portion 35-38 mm) was used to accomplish this; this head made it possible to weld internal seams in tubes 50 mm in diameter.

Quality of the welded joint was checked by external inspection, selected mechanical tests, low-temperature testing down to -196°C, and testing for air-tightness (vacuum seal). Vacuum tightness of the welded unit was checked after testing with a PTI-6 helium leak detector at a rarefaction of 0.02-0.001 mm Hg.

In the course of the work we established the possibility of correcting macroleaks and vacuum leaks by rewelding the defective point on the seam with the use of filler wire. In this case the additional welding or overlapping of the seam with two-three beads using filler material and welding conditions similar to those used for the basic welds did not reduce the mechanical properties and vacuum tightness of the joint. Characteristic test data and also welding conditions are given in Table 25.

Figure 81a shows welded joints between steel and aluminum tubes, while Fig. 81b shows a tube after tensile testing. It is clear that destruction occurred along the AMts base metal far from the weld. Specimens for tensile testing and for study of microstructure of the obtained joints were cut from tubes which withstood vacuum testing after deep cooling. The thickness of the intermetallic layer comprises 5-25 μm.

The strength of flat specimens of steel Kh18N10T and the alloy AMts 2 mm thick made by a double weld is also close to the strength of the AMts base metal.

Table 25. Characteristic results from tests of steel/aluminum tubes (alloy AMts and calorized steel 1Kh18N9T).

Calorization time, seconds	Type and diameter of filler, mm	Welding conditions: current, A	Welding conditions: argon flow rate, l/min	Results of air-tightness tests	Destructive force, daN	Nature of failure	Remarks on surface preparation
5	Wire SvAl (AD1) per GOST 7871-63, diameter 3 mm	100-110	14-16	No leaks were detected at the determined density with the PTI-6 leak detector prior to and after cooling down to -196°C with a hold of 15 min	7100	Failure over the base metal of the tube made of AMts; internal weld was delaminated over the entire cross section	Calorization with flux No. 1. Aluminum tube subjected to scraping prior to welding
10		110-115	14-15	No leaks detected during check of air-tightness with the PTI-6 leak detector prior to and after cooling to -196°C, hold 30 min	9200	Failure over the AMts base metal and destruction of the inner weld with delamination of the coating on 50% of the length	Coating layer thickness 0.007 mm
20		105-115	12-15	No leaks detected during determination of vacuum tightness with the PTI-6 leak detector prior to and after cooling to -196°C	9550	Failure over the AMts base metal. Internal weld delaminated over 40% of the length	Coating layer thickness 0.02 mm

Table 25. (Cont'd.)

5-10	Filler AMts, diameter 2-2.5 mm	90-100	10-12	No leaks according to check with PTI-6 leak detector prior to and after cooling to -196°C	25000	Failure along the cannelure of the base metal of the AMts tube; tear through the coating along 1/3 of the tube perimeter	A second tube of alloy AMts is welded on at a distance of 35-40 mm from the joint. Calorization with flux No. 1
5-10		110-115	12-14	—	18500	Failure over the cannelure of the aluminum tube; individual tears on the inner weld and failure over the calorized layer at a distance of 1-3 mm from the inner weld	Coating layer thickness to 0.12 mm

Remark. Diameter of tungsten electrode 3 mm.

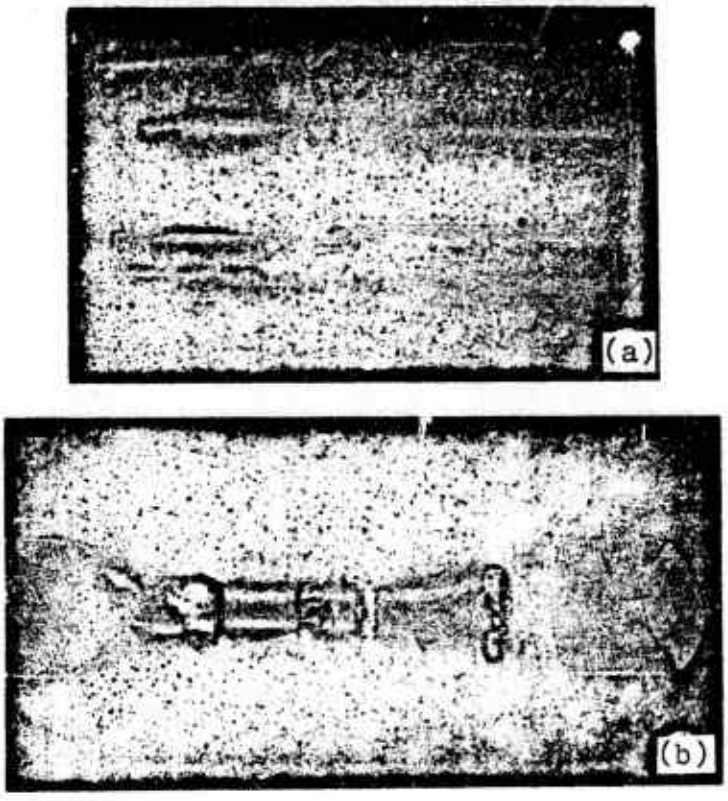

Fig. 81. External appearance of a welded joint between steel and aluminum tubes (steel Kh18N10T and alloy AMts) made by argon-arc welding over a calorized layer (a); (b) shows the nature of destruction of this joint.

A check was made of the possibility of using argon-arc welding to join AMg6 to 1Kh18N9T. The investigations showed that in a given case the welded seam delaminates from the stainless tube. Application of Sv. AMg6 wire for this purpose is undesirable. Improved results were obtained with the following welding sequence: preliminary buildup of two or three beads of filler material AD1 or the wire whose composition is shown in Table 15, neither containing magnesium, followed by connection of the AMg6 tube with the built-up bead using AMg6 wire or some other filler wire. Argon-arc welding conditions: for 70/63 mm tubes welding current 90-110 A, welding in three layers with the first without filler; for 90/108 mm tubes current 120-130 A and welding in four layers;

for 159/170 mm tubes current 150-190 A and welding in four layers. In all cases the argon flow rate is 8-12 l/min and the diameter of the tungsten electrode is 3 mm.

Table 26. Results of checking the strength of reducers.

Tube diameter, mm	Rupture force at a temperature of °C	
	+20	-196
50/60	–	15300
63/70	16900	20100
90/108	24500	45300
159/170	31400	–

The strength of joining steel/aluminum reducers combining steel 1Kh18N9T and alloy AMg6 was checked at room temperature and at the temperature of liquid nitrogen for tubes of different diameters. Strength values are given in Table 26.

Tubes 90/108 mm in diameter showed the highest strength indices at low temperature, with the strength of the joints being 1.6-2 times higher at this temperature than at room temperature.

Automatic argon-arc welding of steel Kh18N9T to the aluminum alloys AMg6 and AMts was carried out on the A-973 installation, manufactured at the Ye. O. Paton Institute of Electric Welding (Fig. 82). The head of the A-973 installation operates on the principle of heads for automatic argon-arc welding of aluminum. Welding was carried out on currents of 140-160 A; the diameter of the tungsten electrode is 3 mm, and the filler wire has the same composition as the aluminum portion of the reducer - i.e., AMts or AMg6 - and is 2 mm in diameter.

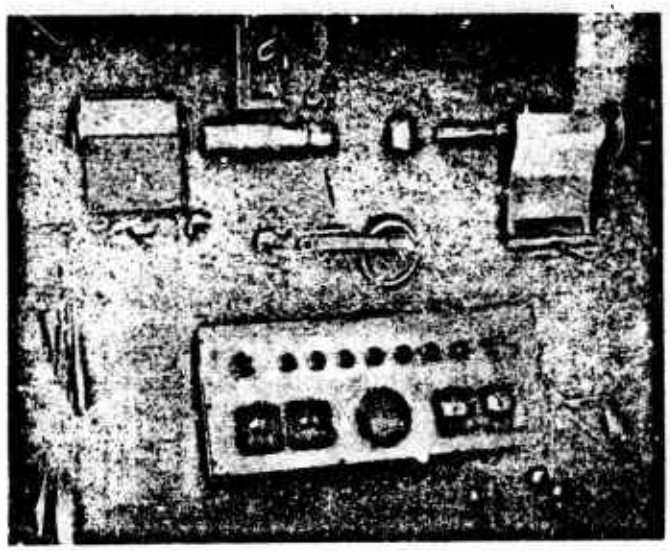

Fig. 82. Overall view of the A-973 installation for argon-arc welding of unlike tubes.

Before welding to tubes of aluminum alloys, tubes of steel Kh18N9T were subjected to treatment under standard conditions. The tubes were joined telescopically, with the tube of aluminum alloy covering the steel tube. Welding was carried out in one pass and from the outside only. A number of steel/aluminum reducers welded according to the described technology were tested to destruction at internal pressure up to 200 at.

As is evident from the photograph of a failed reducer (Fig. 83), destruction occurred over the weakest cross section - i.e., along the weld.

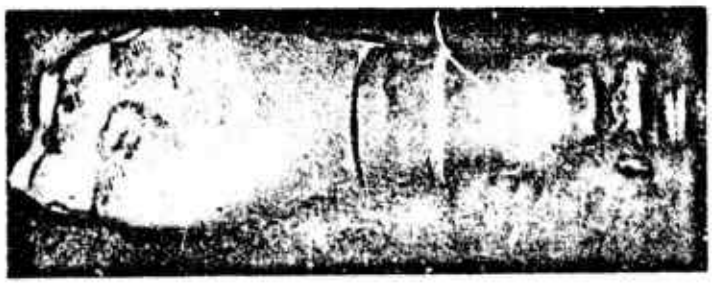

Fig. 83. Failed tubular joint between steel Kh18N10T and the alloy AMts, produced by argon-arc welding over the calorized layer.

Reducers with joints between AMts and 1Kh18N9T and between AMg6 and 1Kh18N9T, welded by the described technology, were tested according to the following program: check of vacuum tightness with a helium leak detector; testing for triple thermal shock (cooling in liquid nitrogen -196°C, heating at room temperature); a check of vacuum tightness with a helium leak detector; tensile testing (under tension at temperatures of +20°C and -196°C).

The tests results indicated that the joints were airtight. Destructive loads at +20°C fell within the limits 7250-7400 N; at -196°C the values were 6660-11,850 kg.

Thus the work gave the possibility of mastering and introducing the technology of argon-arc welding of steel/aluminum reducers 20-110 mm in diameter.

Subsequently the manufacture of reducers of steel 1Kh18N9T 159 mm in diameter with wall thickness of 6 mm and alloy AMts 170 mm in diameter with wall thickness of 8 mm was mastered.

Optimum argon-arc welding conditions: welding current strength 160-200 A, filler diameter 4 mm, tungsten electrode diameter 3-4 mm; first layer made without filler and the subsequent 3-5 layers with a filler wire.

After triple cooling in liquid nitrogen and a check of airtightness with the PTI-6 leak detector under tension [rarefaction] of $2 \cdot 10^{-2}$ mm Hg no leaks were detected. Destructive force at standard temperature comprised approximately 38,000-44,500 kg.

4. Production Tests of Steel/Aluminum Welded Units

Testing Welded Steel/Aluminum Tubes

This section presents results of investigations of combined tubes made from alloy AMts and steel 1Kh18N9T under specific conditions of article operation [109, 161].

There has been very little study of the properties of welded joints between unlike metals at low temperatures. At the same time the effectiveness of such joints depends on many factors: type of crystal lattice of the joined metals, physical properties of the two metals and the nature of the change in them with a reduction in temperature, the properties of the intermediate diffusion layers, the type of loading during operation, size, type of joint, etc. [142].

Studies were made with welded units - pipelines. They underwent hydraulic, pneumatic, and vacuum tests prior to and after fifteen cycles of freezing and heating. The tests were carried out by a procedure which is standard at VNIIKIMASh [All-Union Scientific Research Institute of Oxygen Machinery], working from the basis of specific operating conditions of the manufactured articles. The lines were also subjected to thermal shock tests with subsequent checking of the strength and tightness of the welded joint. Hydraulic tests were carried out without destruction during checking of strength and tightness of the welded joints. During the tests a pressure of 90 at was maintained. During the pneumatic tests welded units which had already been subjected to hydraulic testing were first immersed in a water bath and then filled with compressed air under a pressure of 32 at. The most widely applied methods of vacuum testing in industry are methods utilizing halide and helium leak detectors. The second method is especially sensitive. The PTI-6 helium leak detector was used to carry out the check. Leak-detector data make it possible to detect leaks in evacuated tested tanks down to $3\text{-}5\cdot10^{-3}$ lμm/s.

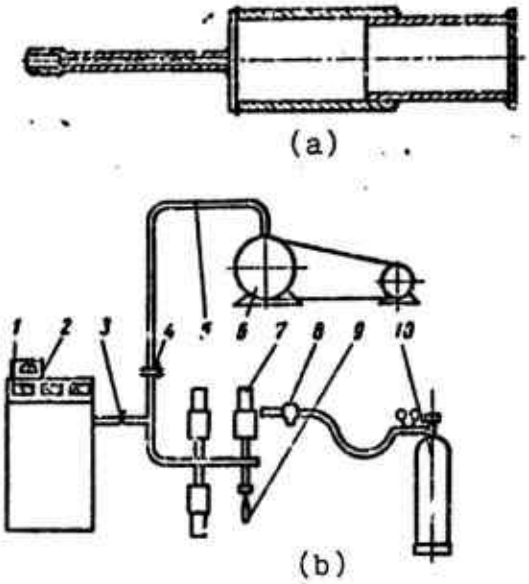

Fig. 84. Welded line (alloy AMts-steel 1Kh18N9T) manufactured for testing (a), and the setup of the stand for testing the lines (b): 1 - leak detector; 2 - remote control panel; 3 - DU25 choke valve; 4 - clamp; 5 - connecting line; 6 - VN-461 high-pressure vacuum pump; 7 - tested article; 8 - blower; 9 - vacuum-indicater lamp; 10 - helium bottle.

Figure 84b shows a diagram of the vacuum stand for testing pipelines.

Mechanical properties of steel/aluminum welded joints at standard temperature. To make it possible to carry out test to failure, the ends of the prepared tube were closed by lap-welding rods manufactured to fit the inner diameter of the steel and AMts tubes. In certain cases steel/aluminum tubes 300-400 mm long were manufactured and their ends were pinched together in a press so that they could be clamped in a tensile testing machine.

Table 26 gives results from tests of steel/aluminum tubes of various diameters at room temperature. As is evident from the table, within the limits of the selected parameters of the calorization of steel tubes (t = 5-10 s and 20 s and T = 750-780°C) the change in the thickness of the coating layer does not influence the strength indices of the tubes at room temperature to any sharp degree. For tubes with a diameter 70/63 mm the destructive force comprises 7100-9550 daN; for 115-108 mm tubes the values are 18,500-25,000 daN. A typical nature of failure of one of the tested tubes is illustrated on Fig. 81b.

The significant transfer of heat into a large-diameter tube makes it necessary to increase the heating time during welding; this is apparently reflected on the nature of destruction of the welded joints. During the tests unlike welded tubes 25-75 mm in diameter were, as a rule, destroyed along the base metal, while tubes 105-110 mm in diameter were destroyed with total or partial delamination of the coating.

Metallographic investigation of steel/aluminum welded tubes showed that the transition zone is adequately dense; this is also indicated by results from testing the vacuum tightness of the tubes, as presented in Table 25.

Results from checking mechanical properties of steel/aluminum tubes at low temperatures. To determine static strength of steel/aluminum welded tubes at the temperature of liquid nitrogen (-196°C), a special device was developed (Fig. 85). Steel and aluminum plugs with threaded openings were welded to the respective ends of the specimen, 3. The tube was set in cup 4 (developed for thermal isolation from the stainless steel with low heat conductivity) 150 mm in diameter and 400 mm high; drawbolt 1 was screwed into it and the cup was fastened to the latter. Before the tests the specimen was filled with liquid nitrogen 2, drawbolt 5 was screwed in, and cup 4 together with a specimen was fastened into the clamps of the tensile testing machine. The specimen was maintained at

this temperature for 10-15 minutes, up to vigorous boiling of the liquid nitrogen. Then the specimen was loaded as in ordinary tests and tested to destruction.

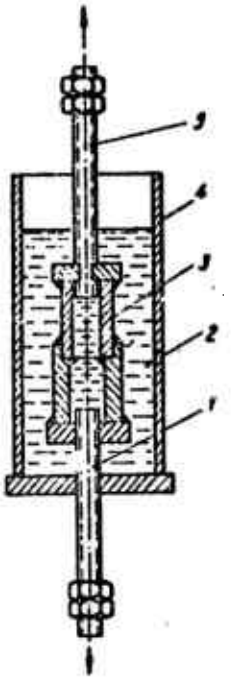

Fig. 85. Device for low-temperature testing of steel/aluminum welded tubes:
1 - lower drawbolt;
2 - liquid nitrogen;
3 - tube; 4 - cup;
5 - upper drawbolt.

The results of the low-temperature tests are shown in Table 27. As is clear from the table, the strength properties of steel/aluminum welded tubes at low temperatures are, as a rule, 1.5-2 times higher than those at room temperature (except for tubes 115 mm in diameter). This may be explained on the one hand by the increase in strength properties and the retention of the plastic properties of the alloy AMts at low temperatures; on the other hand, apparently, there is a substantial change in the state of stress of the transition layer (work under compression), caused by the "fastening" effect of the outer tube of alloy AMts. Actually, if we trace the change in the magnitude of the coefficient of linear expansion in the test-temperature region (from 0 to -196°C), we can note a greater "contraction" in alloy AMts than in steel 1Kh18N9T in the low-temperature area. Therefore, after welding or in the course of operation when these joints are cooled compressive stresses are created which not only have no negative effect on the mechanical properties of the weld, but actually represent a favorable factor.

Table 27. Results of checking mechanical properties of steel/aluminum tubes at -196°C.

Diameter of tubes multiplied by wall thickness, mm		Number of layers		Type and diameter of filler, mm	Welding conditions		De-struc-tive load, kg	Nature of destruction
aluminum tubes	steel tubes	ex-ter-nal	in-ter-nal		welding current, A	argon flow rate, l/min		
42 × 5	35 × 2	3	—	AD1.3	90-110	10-12	9600	Failure along the weld attaching the steel plug; neck on the aluminum tube
70 × 5	63 × 2	4	1	AD1.3	90-110	10-12	18400	Failure of welds with partial delamination (50%)
115 × 5	105 × 2.5	4	1	AD1.3	100-110	11-12	24000	Failure of welds with delamination (60%)
115 × 5	105 × 2.5	4	1		100-110	10-12	27200	Failure of welds with delamination of coating
70 × 5	63 × 2	3	—	AD1.3	90-110	11-13	14100	Failure on the AMts tube along the cannelure
70 × 5	63 × 2	1	1	AD1.2	100-120	11	10500	Failure on the weld with delamination of the coating
70 × 5	63 × 2	4	1	AMts2.85	110	10-14	14100	Failure on the aluminum tube and the internal weld
115 × 5	105 × 2.5	5	1	AMts2.85	110	10-14	22300	Delamination of the coating

Remark. Test temperature -196°C. Diameter of tungsten electrode 3 mm.

Testing tubes under conditions of low temperatures and hard vacuum. In order to determine the maximum vacuum which steel/aluminum welded tubes made according to the developed technology can withstand, several fittings were sent to the Physicotechnical Institute of Low Temperatures, Ukrainian Academy of Sciences. Tests were carried out in a vacuum chamber (Fig. 86) at a vacuum of $1.5 \cdot 10^{-7}$ mm Hg. The vacuum chamber is a cylinder which is covered on the inside by a shield with a temperature of -196°C. Gases which do not condense at the temperature of liquid nitrogen are evacuated by a diffusion pump. The pumping rate comprises 125 l/s. The tested specimen, a welded tube with bottoms and a capacity of about 0.5 l, was soldered into the vacuum chamber on a tube through which the cavity of the test specimen was filled with liquid nitrogen. The weld was in the middle of the tube. Each specimen, at room temperature, was successively filled with liquid nitrogen. The specimens were held at the liquid nitrogen temperature for 5 minutes. Then the liquid nitrogen was evaporated from the specimen and the latter was heated by an electric heater located on the specimen, being brought up to room temperature in 3 minutes. Specimen temperature was monitored by a copper-constantan thermocouple. The above cycle was repeated 10 times for each specimen. Pressure was measured continuously during the tests with a VIT-1 vacuum gauge.

During the last evaporation of liquid nitrogen the cavity formed by the test specimen was filled with helium and the gas pumped out of the vacuum chamber was sent into a helium leak detector, tuned to maximum sensitivity.

At the level of the pressure drop between the cavity of the test specimen at the liquid nitrogen temperature and the vacuum chamber the leak detector did not reveal penetration of helium from the test specimen through the weld into the vacuum chamber when the pressure in the latter was on the order of $1.5 \cdot 10^{-7}$ mm Hg.

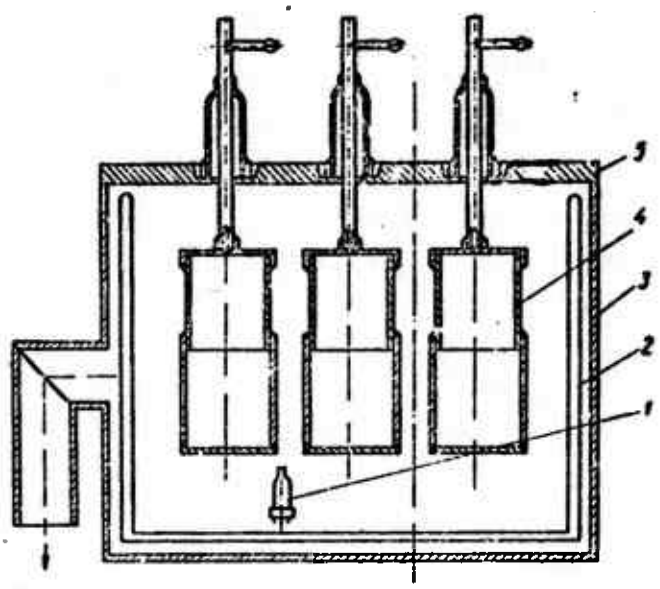

Fig. 86. Diagram of the vacuum chamber for testing tubes under conditions of low temperatures and a vacuum of 1.5×10^{-7} mm Hg. 1 - vacuum gauge sensor; 2 - nitrogen screen; 3 - chamber housing; 4 - test specimens; 5 - cover.

Testing of full-scale units. Full-scale units for tanks with capacities of 60, 32, 6, and 2 m^3 were manufactured according to the developed procedures for lot production. To check weld quality one full-scale unit from each set was subjected to tensile testing. In addition, all welded reducers were tested for resistance to cold by cooling them to -196°C for 15-30 minutes; they were tested for air-tightness with a PTI-6 helium leak detector at a rarefaction of $2 \cdot 10^{-2}$ to $1 \cdot 10^{-3}$ mm Hg.

Out of all the full-scale units tested, only one reducer, diameters 63/70, revealed a leak in the region of a crater in a first weld on the AMts tube. The defect was eliminated by additional argon-arc welding with AD1 filler. A repeated triple check by cold and with a leak detector showed the absence of the defect.

The lines on a vessel made of aluminum alloy AMts and stainless steel Kh18N10T were connected by argon-arc welding with the help of the obtained steel/aluminum fittings.

During subsequent assembly each welded line was checked for strength by hydrostatic testing at a pressure of 5-5.25 daN/mm^2. The lines were also checked for gas-tightness by pneumatic testing at a pressure of 3.25-3.5 daN/mm^2 and for vacuum tightness with a PTI-6 helium leak detector at a rarefaction of $2 \cdot 10^{-2}$ to 10^{-3} mm Hg.

Tubular steel/aluminum reducers installed on the article are shown in Fig. 87.

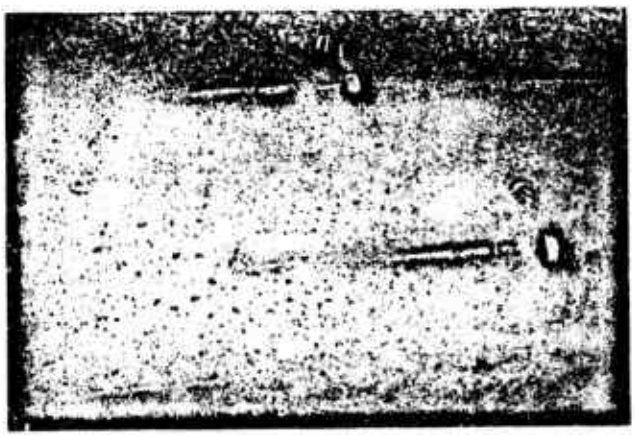

Fig. 87. Steel/aluminum tubular reducers installed on the finished article.

The basic index of weld quality during the manufacture of tanks is the magnitude of the flow of uncondensed gases during evacuation of the insulating space, which is a condition for prolonged operation of the vessel between repairs. The quality of the entire tank is characterized by the magnitude of average daily losses of the stored product due to spontaneous evaporation.

The tests showed that replacement of the aluminum lines by the steel/aluminum type was sufficient, other conditions being equal, to reduce the average daily losses of stored products due to spontaneous evaporation by approximately 25%.

Vibration tests of steel/aluminum reducers. To check the vibration resistance of steel/aluminum reducers (steel 1Kh18N9T and alloy AMts), special test specimens were manufactured (Fig. 88). The sample has a connecting pipe to permit checking the gas-tightness without removing the unit from the installation. Tests were carried out on a stand. The tested specimen was rigidly attached to the stand by a steel flange, while an aluminum flange was used to connect it through a bearing with a cam rotated by a motor.

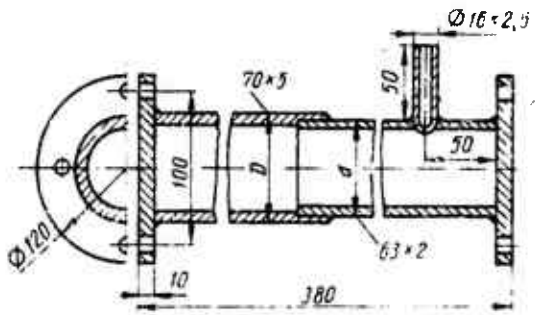

Fig. 88. Tubular steel/aluminum specimen manufactured for vibration testing.

The tubes were tested at a vibration amplitude of 1.3 mm and at 4500 r/min. Gas-tightness was checked prior to the testing and after each $5 \cdot 10^6$ cycles of oscillations. No leaks were observed in the welded lines after $10 \cdot 10^6$ tests cycles.

Testing of Experimental Structures

Welded steel/aluminum joints in structures must frequently operate under complex states of stress in conditions of static and variable loads in a medium of aggressive products. High requirements

are imposed on such joints with respect to commercial form, structural strength, retention of gas-tightness, and corrosion resistance over a prolonged period of time.

Together with O. S. Kuz'menok, the author carried out work on fusion-welding connection of thin-walled tanks of tubes made from steel Kh18N10T and alloy AMg6. The inner diameter of the tanks was 170 mm, their length was 380 mm, the wall thickness of the steel tube was 3 mm, and that of the AMg6 tube was 5 mm.

The dimensions of the optimum grooving of the welded edges in preparation for welding are given on Fig. 76. Preliminary experiments did not indicate any positive results with the use of lap joints. Zinc-coated (layer thickness 25-30 μm) steel tubes were calorized by immersion in a melt of pure AV000 aluminum in an open crucible of an induction furnace with a flux before welding. The calorizing temperature was 750-780°C and the hold time was 1-2 minutes. The thickness of the calorized layer was 0.2-0.3 mm.

The tubes were welded by the argon-arc method by two programs: first by manual welding of the interior and then by automatic welding of the exterior.

The automatic welding was carried out on the USA-500 automatic welder with a UDAR-300 power source, a tungsten electrode 3 mm in diameter, and Sv. AD1 filler wire 2.5 mm in diameter.

Welding conditions are given in Table 28.

After welding the calorized layer was removed from the surface of the steel tube by chemical milling and the blind flanges were cleaned and etched for the strength tests.

The weld of a steel/aluminum joint connecting shells is shown on Fig. 89.

Table 28. Conditions for welding the experimental tanks.

Type of welding	Current strength, A	Welding speed, m/h	Wire feed rate, m/h	Argon flow rate, l/min
Internal, manual	100	7.5	–	8-10
External, automatic	140-[illegible]	8.5	32.5	10-12

Remark. The limits of current strength regulation are shown from the beginning to the end of the weld.

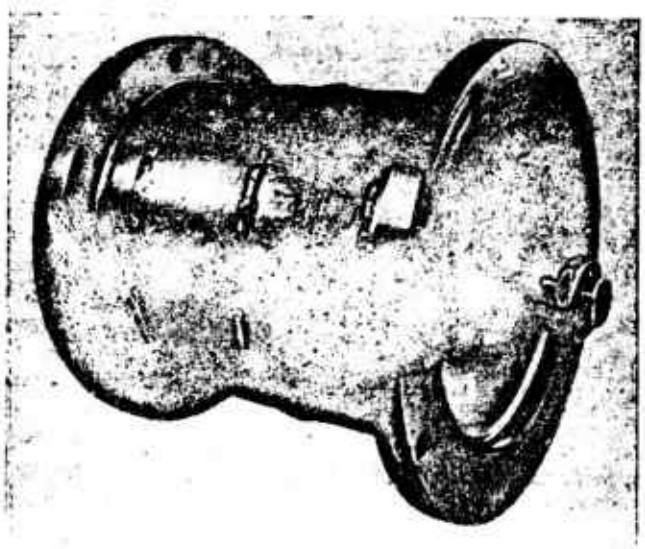

Fig. 89. Welded steel/aluminum tank.

Tests of specimens 15 mm wide cut from tubes welded with filler wire AD1 show that the strength of the steel/aluminum joints is sufficiently stable and with automatic welding amounts to 28-30 daN/mm^2. It was established that a second supplemental welding of defective spots reduces the strength of the joint by 10-30%. Destruction occurs viscously over the built-up metal. As a rule a portion of the deposited aluminum remains on the steel part of the specimen. Destruction of specimens welded with filler wire Sv. AMg6 is brittle and occurs by separation of the deposited filler metal from the surface of the steel. The deformability of such

steel/aluminum joints is comparatively low. Operating conditions of welded bimetallic joints in a plane state of stress are variable. The calculation diagram for a metallic thin-wall shell is shown in general form on Fig. 90.

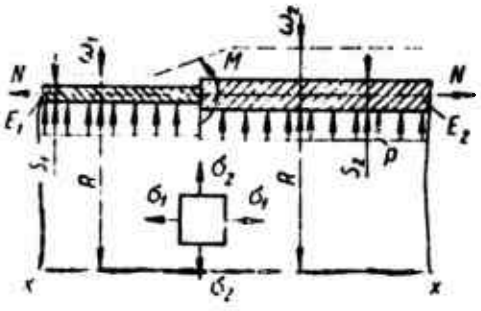

Fig. 90. Calculation diagram for a bimetallic thin-wall shell in general form: S_1, ω_1, E_1 and S_2, ω_2, E_2 - thickness, radial displacement, and Young's modulus of steel and the alloy AMg6.

In the general case during calculation of bimetallic shells it is necessary to consider bending stresses at the point of connection of shells of different thickness and having different Young's moduli:

$$\sigma_1 = \frac{pR}{2S} \pm \frac{N}{2\pi RS} \pm \frac{M}{S^2}; \quad \sigma_2 = \frac{pR}{S}, \tag{44}$$

where σ_1 and σ_2 are the meridian and annular stresses, respectively; p is pressure; N is the axial force; and M is moment.

As was indicated above, the wall of the tube made from AMg6 was thicker than the steel wall and so destruction occurred along the weld. Such a procedure makes it possible to obtain the true mechanical characteristics of the weld. In this case the cylindrical rigidities Es were levelled, making it possible to carry out calculations according to the zero-moment theory of shells.

Under the condition of equality of radial displacements of points on the contour of both shells ($E_1 s_1 = E_2 s_2$) the calculation of a bimetallic shell can be carried out according to the zero-moment theory of strength:

$$\sigma_1 = \frac{pR}{2S} \pm \frac{N}{2\pi RS}; \quad \sigma_2 = \frac{pR}{S}. \tag{45}$$

When the tubes were welded with Sv. AMg6 filler wire brittle destruction occurred along the boundary of the joint. In this case structural strength of annular welds, calculated by the zero-moment theory, comprises 10-15 daN/mm^2.

Application of the filler wire Sv. AD1, which has no magnesium in its composition, ensures better interaction of the weld metal with the steel and the increased ductility improves the operating conditions of the welded joint in the structure. In this case structural strength comprises 15-21 daN/mm^2. The effect of the filler wire on structural strength is illustrated by Fig. 91.

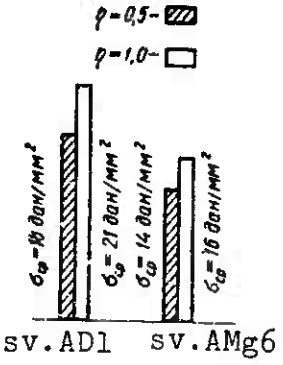

Fig. 91. Effect of filler wire on structural strength of steel/aluminum joints.

In order to study the structural strength of welded bimetallic tanks in a two-axial state of stress, they were tested under different ratios of annular and meridian stresses (Table 29).

Analysis of the results of strength tests shows that conditions of loading by internal pressure with $\eta = 0.5$ should be considered to be the most severe operating conditions. But even during these tests the tentative strength coefficient of the weld in a steel/aluminum joint comprises 0.5-0.6 (Fig. 92). This coefficient can be introduced into the calculation of strength of similar structures made of unlike metals.

Table 29. Data obtained during tests of steel/aluminum tanks welded with filler wire Sv. AD1 and calculation of stresses by the zero-moment theory.

Tube No.	Load at destruction		Calculated destructive stress, daN/mm²		Ratio of stresses	Tentative strength coefficient
	P, daN/cm²	N, kg	σ_1	σ_2	$\tau = \frac{\sigma_1}{\sigma_2}$	$K_1 = \frac{\sigma_1}{\sigma_{B\ AMg6}}$
16	140	—	19,8	39,6		0,62
23	110	—	15,6	31,2		0,49
26	152	—	21,6	43,1	~0,5	0,67
29	147	—	20,8	41,7		0,65
35	150	—	21,3	42,5		0,67
2	75	14000	19,2	21,2		0,60
7	76	14000	19,3	21,5		0,60
11	86	16800	22,5	24,5	~1	0,70
15	92	18000	24,0	26,0		0,75
22	76	14000	19,4	21,6		0,61
4	44,8	28100	23,4	12,7		0,73
19	48,0	32700	26,6	13,6		0,83
27	51,2	33800	27,7	14,5	~2	0,87
32	44,8	26700	22,96	12,7		0,71
43	44,8	28900	23,9	12,7		0,75

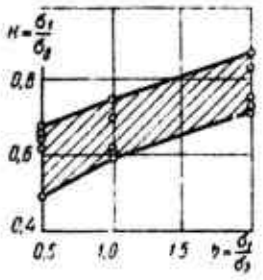

Fig. 92. Tentative coefficient of strength as a function of internal pressure (ratio of stresses). Filler wire Sv. AD1.

The corrosion resistance of steel/aluminum joints and the effect of prolonged holding in a medium on strength and gas-tightness were also investigated. After holding in a corrosive medium the tubes were subjected to hydraulic tests at a pressure of 30 atm, pneumatic tests at a pressure of 15 atm, and then to checking for gas-tightness with a helium leak detector with a sensitivity of $1 \cdot 10^{-2}$ $l\mu m/s$. The tubes withstood these tests. Besides this, they were also subjected to static testing to destruction under a biaxial state of stress with the ratio σ_1/σ_2 equal to 0.5 and to 1.

The program for strength tests included conducting hydraulic tests (30 atm) and gas-tightness tests with compressed air (15 atm). Then six tubes were subjected to vibration testing on a shaking program (200 hours).

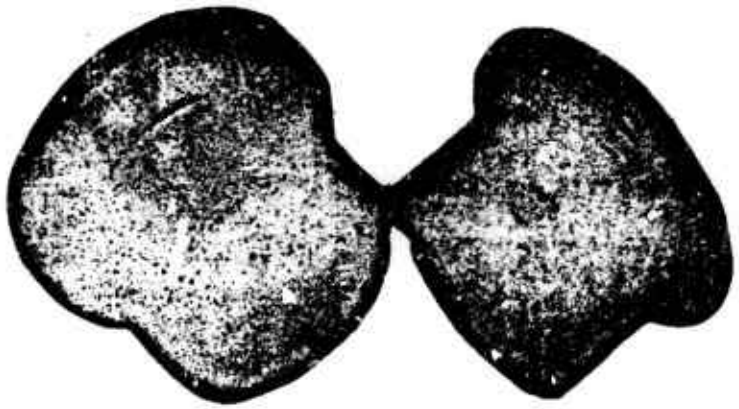

Fig. 93. Steel/aluminum joint destroyed by internal pressure of 41 atm with tension after buffeting and vibration (force of tension $9.1 \cdot 10^4$ N).

Most characteristic destruction of the units was observed after static and dynamic tests (Fig. 93).

Data from the static tests indicate that the structural strength of welded steel/aluminum joints in tanks corresponds to a stress of σ = 10-12 daN/mm^2, which amounts to 0.45 of the lower limit of the strength of alloy AMg6.

Results of these works indicated that steel/aluminum articles obtained by argon-arc welding have sufficient structural strength, the necessary gas-tightness and corrosion resistance, and good resistance to vibration. They can be applied successfully in a variety of article constructions. Their application is especially effective in large structures and during welding of fittings under assembly conditions.

Results of Strength Tests of Models

The models were manufactured by argon-arc welding over a calorized layer. The steel portion of the model was cut from a steel tube (steel Kh18N10T) 108 × 5 mm in diameter. The edges were dressed before welding with aluminum AD1 - double beveling of the edges at an angle of 70°.

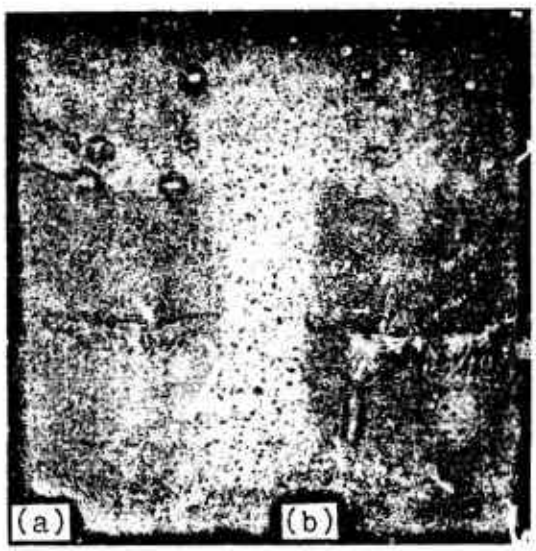

Fig. 94. Steel/aluminum models prior to (a) and after (b) hydraulic tests.

The aluminum part of the model was manufactured from 7-mm sheet by rolling and welding. Two fittings were made to supply pressure to the stainless [steel] portion of the model. All models were tested at +20°C with a hydraulic pressure of 32 daN/cm^2 (hold 10 minutes) and then with a pneumatic pressure of 25 daN/cm^2 (hold 10 minutes). All models withstood the tests. During testing in a cold chamber and with cooling to -50°C models filled with kerosene were destroyed. The destroying load amounted to 137-162 daN/cm^2. Figure 94 shows a model prior to and after hydraulic testing to 120 daN/cm^2. As is evident from the figure, the aluminum portion of the model was not destroyed, although it was strongly deformed.

Ten models were cooled in the chamber to -50°C, held at this temperature for 1 hour, heated to room temperature (+20°C), and then heated in hot water to +60°C. This cycle was repeated twenty times for all models. After this the models were destroyed by hydraulic pressure. The destructive load was found to lie within the limits 125-155 daN/cm^2.

Welding of Dewar Vessels

The Sverdlovsk Oxygen Plant produces 12 standard sizes of Dewar vessels with capacities ranging from 5 to 100 liters for various branches of the national economy. The inner and outer vessels are made from the aluminum alloy AMts, 2-4 mm thick. In order to reduce heat losses during storage of liquid gases the inner and outer vessels are joined by a neck of steel Kh18N10T. The wall thickness of a seamless tube of steel Kh18N10T comprises 0.3 mm and the tube diameters are 14, 25, 95, 150, and 282 mm. In the process of manufacturing the vessel the stainless-steel tube must be welded to the inner and outer vessels.

The steel tube is calorized in a graphite or cast iron crucible under a layer of flux AN-A1. Aluminum of type A99 per GOST 11070-64 is used; calorizing temperature is 700-740°C. The amount of flux over the aluminum is 30-40 mm; the steel tube is joined to a tube of alloy AMts and welded to both vessels. Finished vessels are checked for evaporation and tested for cold resistance at temperatures from +20°C to -196°C.

Welding Ship Units

A number of structures have been manufactured at the Zhdanov and Admiralteyskiy Leningrad Shipbuilding Plants.

In 1961-1962 a number of experimental structures were manufactured at the Zhdanov Plant [18]: struts 2000 × 220 × 3 in size from alloy AMg6 with a steel coaming; a unit for connecting a zinc-plated steel coaming with a panel of AMg5V 900 × 1000 × 3 in size; a bulkhead of alloy AMg5V 1500 × 1500 × 8 in size with four steel coamings; a unit for connecting a zinc-coated steel tube 70 mm in diameter with a sheet of AMg5V 250 × 250 in size. The experimental structures were manufactured from standard elements available at the plant.

Steel elements intended for zinc coating were carefully cleaned on a sand-blasting installation. Zinc-plating was carried out in galvanic baths; the thickness of the zinc coating comprised 40 μm. 20-mm flanges were provided for lap welding of edges of elements of alloy AMg5V; flanging was produced on a forge. Immediately before welding the edges of elements made of AMg5V were trimmed.

The unit for joining the zinc-coated tube with a sheet of AMg5V was welded in a pass. Welding of struts and a panel of AMg5V with steel coamings was carried out with preliminary arrangement of tack welds on the side opposite to the first weld (pass). Welding panels of alloy AMg5V to steel coamings was accomplished by the back-step method. All structures were welded in one pass. Current strength in all cases was I_{CB} = 120-130 A; the diameter of the tungsten electrode was 3 mm, and AD1 filler wire 2 mm in diameter was used. The welding speed was 8-12 m/h.

The experience in manufacturing the structures showed that it is advisable to weld comparatively short butt joints (up to 0.5 m) directly end-to-end. In the case of long butt edges (1 m and more) the joints should be made with flanging of the element of light alloy; this simplifies fitting of long edges and in addition with thin metal (less than 3 mm) this eliminates premature burning off of the zinc on the steel coamings on the side opposite to the first weld. During the welding of combined structures one should apply the same technological methods to

combat deformations as during the welding of structures made from light alloys - i.e., mainly rigid fastening.

The need for rigid fastening is especially important when welding such elements as narrow steel coamings. Welded joints also tolerate cutting on press-shears; cutting should be begun on the steel side.

Struts manufactured at the shipbuilding plant were tested to failure for longitudinal compression. The compression test was selected on the basis of the fact that such a strut is an elemental portion of a cross member (or bulkhead), articles which take up basic loads in the ship's hull. During the tests the struts lost stability at forces of 3500-4500 daN. Detailed inspection of the strut as a whole and of the welds joining alloy AMg5V to the steel coamings did not show any destruction along the welds.

Considering the satisfactory results obtained during tests of the strength of welded joints between aluminum alloys and steel, the Admiralteyskiy Plant designed and manufactured two experimental production ship fairings of alloy AMg6 of different thickness and of high-alloy steel [18]. A particular feature of the fairing was the fact that the rig was a structure of rod steel. This required not only the development of technology but also additional strength tests.

Considering the small dimensions of the rods the cleaned girders of the steel frame were first subjected to hot zinc plating. The coating thickness comprised 60-90 μm. After this deposition of a continuous seam 50 mm in length with a pitch of 100 mm on the rod adjacent to the outer skin was carried out in the shop.

Deformation of the girders was prevented by fastening them rigidly to a plate during the deposition. The facing was carried out by the argon-arc method on a current I_{CB} = 65 A at a welding speed v = 12-15 m/h; the filler was AD1 2 mm in diameter and the tungsten electrode had a diameter of 2 mm.

The assembly skeleton consisted of longerons and a keel; it was attached to a supporting flange by welding and to the stern cross member by rivets. Sheathing was installed from the supporting flange and the keel to the stern section. With increasing reduction the sheets were welded to the assembly, and then sheathing of alloy AMg6 was welded to the stern section.

The following are the conditions for welding the plates to the assembly: welding with a tungsten electrode 3 mm in diameter with I_{CB} = 130-140 A, v = 12-15 m/h; AD1 filler 3 mm in diameter was used. After welding of this sheet to the assembly of the stern section and to the supporting flange bottom sheets were installed, beginning from the keel toward the stern, being reduced along the framing, clamped to it, and also to the remaining portion of the outer sheathing; this was followed by welding of the sheathing sheets on a current of I_{CB} = 150-160 A, with an electrode 3 mm in diameter and AMg6 filler rod 3 mm in diameter. After this the outer plates were welded to the steel framing. Welded fairings were subjected to hydraulic testing by filling, and after drilling out of openings in the supporting flange by filling with the creation of an excess pressure up to 0.8 daN/cm^2. Testing showed that the structure used was gas-tight and strong.

CHAPTER VI

CORROSION RESISTANCE OF WELDED STEEL/ALUMINUM JOINTS

Broad-scale introduction of steel/aluminum structures is hindered by a lack of standard data on their corrosion resistance. Published data are extremely contradictory.

In using aluminum and aluminum alloys in combination with other metals we must take special measures to prevent the development of contact corrosion. We know that in the contact area between aluminum and steel parts (bolts, rivets) in the presence of an electrolyte an electrochemical couple can develop, in which the wet medium plays the role of the electrolyte, conducting the electrical current and thus promoting the development of contact corrosion. Conducting liquids, for example, sea and fresh water and salt, acid, and alkali solutions, can act as the electrolyte.

The degree of development of corrosion between different metals depends on a number of factors: the composition of the electrolyte, the ratio of the steel and aluminum contact surfaces, the brand of steel and aluminum, etc.

The behavior of the galvanic aluminum/steel pair has been studied by a number of researchers. Rogers and Hume have published their data [222] on the behavior of aluminum plating of ships on a wooden hull in combination with a great many parts made of

special steels. According to these studies the combination of aluminum and steel at an outer surface ratio of 1:5 for both materials is resistant to corrosion.

According to S. E. Bird and W. R. Evans [171] in the elements of aluminum and steel which have been short-circuited in a liquid (sea water), the aluminum is always the anode; the outside film does not hinder corrosion of the aluminum, since the ratio of the outer cathode surface to the inner surface of the anode must be sufficiently great in order to provide cathode protection of the steel. In conducting water aluminum becomes the cathode and the protective action ceases. Although adding dissolved ferrous salts to the liquid also decreases propagation of the aluminum corrosion, this addition nevertheless localizes and intensifies corrosion, so that the steel can cause under certain conditions an intense local corrosion in the sections of the neighboring light metal with or without electrical contact. It is also noted that aluminum in combination with steel in building materials (asbestos cement, insulating materials, etc.) is only oxidized on the surface, and after a certain time the corrosion process ceases. Here even the smallest trace of water - in the cement, for example - is sufficient to develop a current of 100 mA.

W. L. Horst, after a great many experiments with light metals, established the fact that combinations of soft steel and aluminum in moist air are more subject to corrosion than contact combinations of special steels and aluminum.

Ye. D. Vernika and F. B. Murphy believe that a galvanic current develops between aluminum and carbon steel only when the chloride concentration is above 50 mm. This current has a weaker effect on aluminum electrodes than on steel.

Finally, according to the studies of F. F. Seppins, joints of steel and aluminum are subject to corrosion even if their outer surface is protected.

To prevent a sudden contact between the two metals or contact of surfaces through the electrolyte in the case of bolt and rivet joints, special insulating liners, paste, protective coatings, oxide coatings, etc., are used. An example of total insulation of bolt joints is shown in Fig. 95. In most cases painting is sufficient to protect contact surfaces in combination structures. In this case the use of red lead or other paint containing lead should be avoided [246].

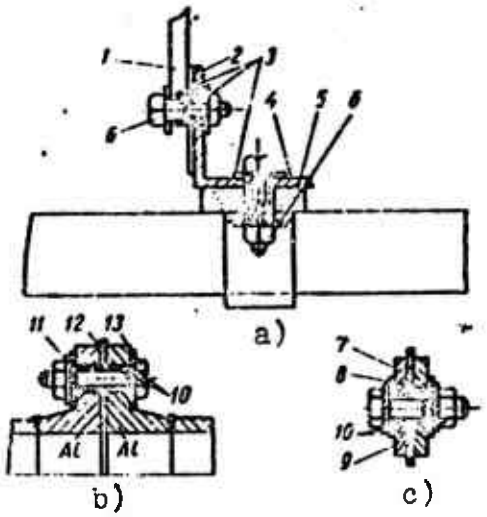

Fig. 95. Standard clamp on horizontal pipelines which eliminates corrosion: 1 - aluminum bar; 2 - galvanized steel bolts; 3 - steel clamp; 4 - thick asbestos liner; 5 - galvanized steel angle bar; 6 - plastic washer; 7 - fabric liner; 8 - insulation paste; 9 - steel galvanized washer; 10 - steel bolt; 11 - plastic liner; 12 - aluminum; 13 - steel.

There is little information concerning the corrosion resistance of welded steel/aluminum joints [208, 226]. Furthermore, welded joints of aluminum and steel, particularly if an intermetallic compound is present in the joint, are extremely subject to corrosion, since the electrode potential of the indicated chemical compound is more electropositive (-0.200 V) than aluminum [33].

There are as yet no published figures for the currents which develop between the contact of steels and aluminum in an electrolyte [242]. A number of authors, who have obtained values for normal electrode potential in the indicated metals, suggest that such compounds are characterized by low corrosion resistance. However, as Evans [171] so correctly points out, for practical purposes the values of electrode potentials obtained by submerging pure metals in normally active solutions of their own ions have limited significance.

The values of stationary potentials in sea water are also used only roughly, since the values of the potentials depend to a great extent on the composition of the sea water, the degree of its aeration, and the state of the surface of the metals. Thus, we must formulate direct experiments to establish corrosion resistance.

We studied the corrosion resistance of welded aluminum/steel joints at a marine corrosion station. The test lasted one year. Welded joints consisting of alloys AMts and AMg6 and steels St. 3 and 1Kh18N9T, produced by argon-arc welding, were studied. The dimensions of the test specimens were 300 × 200 (5-7) mm. A number of joints were obtained by means of extra wires, providing the joint with additional alloys of silicon, zinc, and beryllium. Prior to the test some specimens were covered in lacquer-paint coatings. The total number of test specimens was 150.

The corrosion tests were conducted under conditions of total and variable submersion in sea water and under a spray of sea water in the atmosphere. Specimens tested under constant submersion were secured in a specially designed holder (Fig. 96), where they were placed in a parallel formation 20 mm apart. In the case of variable submersion the specimens were also placed in holders. The test conditions: the specimens were placed at a distance of 1 m above sea level for one day, for two days they were submerged to a distance of 1 m from the surface. The test in the sea atmosphere was conducted in holders placed at an angle of 45° toward the horizon and at a height of 1 m above sea level. In all types of tests the specimens were electrically insulated from the holding elements.

The dependence of the electrode potential on time was determined on specimens of the studied materials under total submersion in sea water on a special stand. The crevices in the contact areas between the specimens and the organic glass holders were insulated by epoxy putty to avoid the development of crevice

corrosion. The electrode potential was measured by the cavitation method with the aid of the LP-58 potentiometer. A silver chloride electrode was used as the comparison standard. The potential was measured at the following time intervals: 1, 10, 15, 25, 35, and 55 min from the moment of submersion, then every hour for the course of one day, followed by once every 24 hours for 8 months.

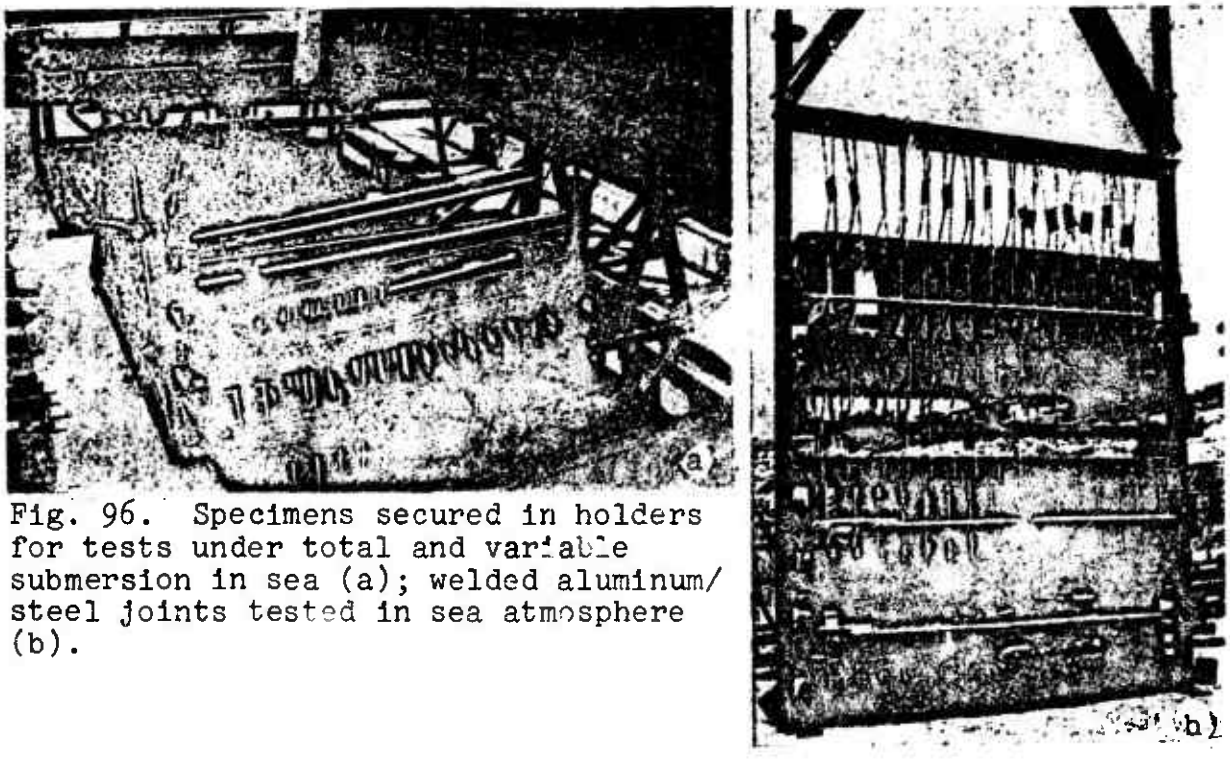

Fig. 96. Specimens secured in holders for tests under total and variable submersion in sea (a); welded aluminum/steel joints tested in sea atmosphere (b).

The degree of corrosive effect of sea water on the studied specimens was estimated from the results of mechanical tests made before and after the test experiments. These consisted of visual observation and by establishing the depth of existing corrosion damage (clock-type indicator) with an accuracy to within 0.01 mm. Microscopic sections were prepared from all of the tested specimens, which, after electropolishing, were studied under magnification of 300×.

The specimens were observed without being removed from their holders at 10, 30, and 60 days from the beginning of the experiment.

Observations in which one specimen was removed were made at 3, 6, and 12 months. The temperature of the sea water, the air, and the moisture in the air varied daily. Data on the composition of the sea water and its oxygen content are given in Table 30.

Table 30. Concentration of ions and salts in sea water.

Ions	Concentration of ions		Salts	Concentration of ions	
	in g/l	in percentage of total amount of salts		in g/l	in percentage of total amount of salts
Na^+	5.430	30.2	NaCl	13.81	76.74
K^+	0.190	1.05	$MgCl_2$	2.095	11.63
Mg^+	0.680	3.78	$MgSO_4$	0.715	3.87
Ca^{++}	0.240	2.22	$MgBr_2$	0.03	0.017
$Fe_{взв}$*	$1.4 \cdot 10^{-4}$	-	K_2SO_4	0.420	2.33
Cu^{++}	$1.2 \cdot 10^{-6}$				
	$+1.6 \cdot 10^{-5}$		$CaSO_4$	0.802	4.45
Cl^-	10	55.5	$CaCO_3$	0.008	-
Br^-	0.026	0.14			
SO_4^{--}	0.380	7.8			
Si	$5.4 \cdot 10^{-4}$	-			
S^-	$1.5 \cdot 10^{-5}$	-			
HCO_3^-	0.016	0.092			
CO_3^{--}	0.005	0.025			
Salinity	1.8%				

Under total submersion in sea water all of the specimens were covered by acorn barnacles measuring 1-12 mm in diameter, pearl weed, etc.

After the test the specimens were freed of these growths and washed. The corrosion products were removed from the specimens by pickling the aluminum alloys and the stainless steel in a 5%

*[Translator's note. Russian взв may in this case be abbreviated in the form of ВЗВЭШЕННЫЙ (Suspended)].

solution of HNO_3; steel St. 3 was pickled in a 5% solution of H_2SO_4 with inhibitor PB5. Zinc-coated steel St. 3 was rinsed in hot water without pickling.

For specimens of the base metal the corrosion rate was calculated based on weight losses, although for welded joints of different metals weight monitoring does not give a true picture of corrosion.

Welded Joints of Alloy AMts and Steel St. 3

Following the constant submersion test in the sea welded joints of AMts and St. 3 showed good corrosion resistance. The surface of alloy AMts was slightly darkened, and traces of barnacles and corrosion damage were visible; the surface of galvanized steel St. 3 was covered with corrosion products in some places, and the unglavanized steel with rust.

Metallographic studies indicated that intercrystallite corrosion could be observed in certain places only on alloy AMts after year-long studies; corrosion damage was not revealed along the fusion line of St. 3 steel.

In the variable submersion test the surface of the base metals remained the same as under continuous submersion. The joints were subject to total corrosion. One specimen developed transverse cracks. Intercrystallite corrosion was observed as early as 6 months after the beginning of the test along the fusion line and along the weld. The base metal in alloy AMts was subject to general corrosion damage.

After the weld compound was tested in the sea atmosphere the joints were found to be in good condition; the surface of the specimens retained their metallic shine. Individual spots of corrosion products were observed on the aluminum alloy, on the

steel, and on the galvanized covering. Microscopic sections from tests conducted in the sea atmosphere did not show corrosion damage.

Tests on painted (base paint VL02 - first layer, paint PF64 - second layer) of welded specimens of the combination AMts/St. 3 under conditions of constant and variable submersion in sea water indicated that lacquer paint has poor protective properties. The active zone was galvanized steel St. 3, the fusion zone, and the joint. The coating was destroyed right down to the metal, where intensified corrosion was observed. There was pitting (constant submersion) on the joints and joint damage (variable submersion).

The lacquer coating demonstrated good anticorrosion resistance in atmosphere testing.

Welded Joints of Aluminum Alloy AMg6 and Steel St. 3 (AD1 as Additional Material)

These combinations revealed insufficient corrosion resistance under total submersion in the sea. The alloy AMg6 darkened, and traces of barnacles could be seen over a great part of the surface. The pitting depth varied between 0.20 and 0.76 mm on the surface and went up to 0.90 mm under the rubber at the point where it was attached to the holder. After 6 months of testing pitting damage to a depth of 1 mm could be observed along the fusion line. After year-long tests the joints were subject to intense corrosion damage, and cracks could be observed along the fusion line.

Under variable submersion tests sparce, point-like corrosion products were noted, under which the surface was shiny. Alloy AMg6 revealed point damage (6-8 × 1 cm^2). There were individual point-like areas of corrosion products on the welded joints.

Metallographic studies on welded joints of AMg6 and St. 3 after both types of tests did not reveal intercrystallite corrosion. General corrosion damage was observed only on alloy AMg6.

Welded Joints of Aluminum Alloy AMg6 and Steel St. 3 (Additional Alloy Wires)

AMg6/St. 3 combinations with additions of 5% Si to the joint were tested after total submersion in the sea. The tests showed that the base metals - the aluminum alloy AMg6 and Steel St. 3 - have the same corrosion resistance as in the preceding case. Intensive deposition of white corrosion products was observed along the joint. After these were removed corrosion damage to the joints was visible (Fig. 97). After testing under variable submersion the specimens had an external appearance corresponding to that of the combinations tested under total submersion. On the joint alloyed with 5% Si uniform corrosion damage was detected.

Fig. 97. Intercrystallite corrosion of alloy AMg6 in welded joint of alloy AMg6 and Steel St. 3 alloyed with 5% Si after variable submersion tests in the sea (×300).

The introduction of 5% zinc does not increase the corrosion resistance of joints in welded combinations of AMg6 and St. 3. After tests lasting one year the welded joint was completely covered with white corrosion products, and when these were removed corrosion damage could be detected in the form of fine, solid pits.

Welded joints with 1% beryllium added showed poor corrosion resistance. When tested under constant

submersion the specimen was corroded along the joint and disintegrated after 9 months. After variable submersion 80% of the surface was destroyed.

Welded Joints of Alloy AMg6 and Steel 1Kh18N9T (Additional Material AD1)

When tested in sea water these combinations have poor corrosion resistance. After just 6 months of testing the weld was completely corroded.

After 12 months of testing cracks formed along the fusion line and the specimens fell apart. However, on the specimen joint, where the potential had been measured for 8 months, only a deposition of corrosion products covering an area of about 5% could be detected. Of these specimens 15-20 showed pit damage on the side of alloy AMg6 to a depth of 1 mm.

When alloy AMg6 was subjected to constant submersion in the sea, the pits were located under the barnacles, the rubber, and the paint in places where the specimens were attached to the holder, which indicates the crevice corrosion tendency of this alloy. The described phenomenon is not observed under variable submersion; first, point-like areas of corrosion products are noted, under which the surface is shiny.

On the unpolarized surface of steel 1Kh18N9T a thin layer of cathode deposit was observed; the aluminum covering was preserved as a thin layer. Microsections of this combination for both test methods showed corrosion damage on the aluminum side along the edges and along the weld; on the steel side there were individual areas with general corrosion damage.

The base metal of the alloy AMts had virtually no corrosion damage. The rate of corrosion, calculated by weight losses under

constant submersion, were 0.0035-0.0037 $g/m^2 \cdot h$; under variable submersion, 0.001-0.007 $g/m^2 \cdot h$.

No weight losses were detected for specimens tested in the sea atmosphere.

Pit damage was found on alloy AMg6. The depth of the pit after 8 months of tests under conditions of constant submersion was 0.6-1.7 mm. The average corrosion rate during the time of the tests was 0.003-0.009 $g/m^2 \cdot h$ for constant submersion and 0.0005-0.0037 $g/m^2 \cdot h$ for variable submersion.

Steel 1Kh18N9T when tested under conditions of constant submersion was subject to pit damage in areas covered by barnacles and where the specimens were attached to the holder. Under conditions of variable submersion no corrosion damage was observed. Steel St. 3 was subject to solid uniform corrosion at a damage rate under constant submersion of 0.1 $g/m^2 \cdot h$, under variable submersion - 0.2 $g/m^2 \cdot h$.

As noted above, the electrode potential was determined as a function of time. Measurements were taken from the steel and aluminum alloy specimens and from their weld joints under conditions of total submersion in sea water. The data obtained from these measurements and from measurements taken in a 3% solution of NaCl under laboratory conditions are shown in Fig. 98 and in Table 31. As follows from the table, after 8 months of tests the combination of AMg6-1Kh18N9T, along with AMg6-St. 3, had the most positive potential. When alloy elements were introduced into the weld the corrosion resistance of AMg6-St. 3 deteriorated, and there was a sharp negative increase in its potential. The weld combination of AMts-St. 3 was characterized by a more negative potential than compounds of steel St. 3 and alloy AMg6.

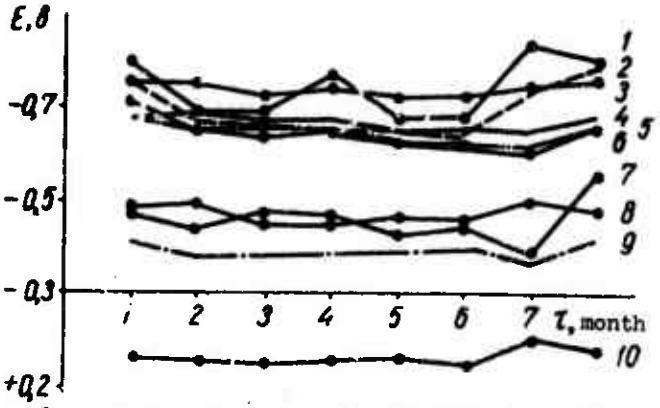

Fig. 98. Dependence of electrode potential on time for total submersion of specimens in sea water: 1 - joint of AMg6 and St. 3 alloyed with 7% Zn; 2 - AMg6; 3 - AMg6 and St. 3, 5% Si; 4 - AMts; 5 - AMts and St. 3; 6 - AMg6 and St. 3, 1% Be; 7 - AMg6 and Kh18N10T; 8 - AMg6 and St. 3; 9 - St. 3; 10 - Kh18N10T.

Table 31. Values of potentials E_{H_0} in aluminum/steel joint.

Metals and combinations of metals	Laboratory tests in 3% solution of NaCl		Natural tests in Black Sea		
	3 h	22 h	3 h	24 h	8 months
AMts	-	-	0.740	-	-0.680
AMg6	-0.644	-0.604	-0.740	-0.675	-0.775
St. 3	-0.419	-	-0.300	-	-0.410
1Kh18N9T	-	+0.131	-	+0.070	+0.140
AMts-St. 3	-	-	-0.715	-	-0.650
AMg6-St. 3	-0.534	-	-0.480	-	-0.575
AMg6-St. 3 (5% Si)	-	-	-0.770	-	-0.740
AMg6-St. 3 (7% Zn)	-	-	-0.880	-	-0.780
AMg6-St. 3 (1% Be)	-	-	-0.735	-	-0.650
AMg6-1Kh18N9T	-	-0.554	-	-0.450	-0.550

Table 32 gives averaged data for mechanical tests on the studied specimens, performed before and after experiments in sea. As we see from the reduced data, weld joints of AMts and St. 3 did well under atmospheric conditions. Weld joints of AMg6 and

Table 32. Results of mechanical tests on steel/aluminum joints.

Combination of weld materials	In original state	Total submersion in sea			Variable submersion in sea			Atmospheric corrosion		
		3 months	6 months	12 months	3 months	6 months	12 months	3 months	6 months	12 months
AMts-St. 3	12-14	10.5	9.3	10.4	10.3	9.3	9.5	10.8	10.2	10.1
AMts-St. 3; specimens completely painted	12-14	9.0	-	10.6	8.9	9.3	5.8	10.6	10.6	8.8
AMg6-1Kh18N9T	25-30	13.4	-	11.2	16.7	18.1	17.8	-	-	-
AMg6-St. 3; Additional material:										
silicon 5%	25-29	18.2	7.7	10.2	19.9	15.6	4.0[1]	-	-	-
zinc 7%	27-32	10.2	13.1	10.4	7	6.5	-	-	-	-
beryllium 1%	22-24	6.6	13.2	7.5	8.2	16.5	7.0	-	-	-

[1]Most of specimens destroyed.

1Kh18N9T showed the greatest resistance under conditions of variable submersion in the sea.

Additional alloying of the weld metal in welded joints of AMg6 and St. 3 under all test conditions showed deterioration in the mechanical properties of the welded joints. Thus the use of steel/aluminum structures is only possible if coatings are used. Lacquer and paint coatings on welded steel/aluminum joints offer good protection from the destructive effect of the sea atmosphere.

Bibliography

1. Агеев Н. В. Природа химической связи в металлических сплавах. Изд-во АН СССР, М., 1947.
2. Агеенков В. Г., Михин Я. Я. Металлургические расчеты. Металлургиздат, М., 1962.
3. Астров Е. И. Плакированные многослойные металлы, «Металлургия», М., 1965.
4. Алов А. А. Основы теории процессов сварки и пайки. «Машиностроение», М., 1964.
5. Алексеевский Е. В., Гольц Р. К., Мусакин А. Л. Количественный анализ. Госхимиздат, Л., 1957.
6. Английский патент № 713333 от 11. VIII, 1954 г.
7. Английский патент № 705749 от 17. III, 1954 г.
8. Американский патент № 2914641 от 24. II, 1959 г.
9. Американский патент № 227242 от 31. VIII, 1958 г.
10. Американский патент № 253247 от 23. I, 1950 г.
11. Американский патент № 2687565 от 31. VIII, 1954 г.
12. Аппен А. А. — В кн.: Жаростойкие покрытия. «Наука», М., 1965.
13. Бахметьев Е. Ф. — В кн.: Труды ВИАМ, 8, 1935.
14. Бельчук Г. А., Глускин Д. Я., Федоров И. А. — В кн.: Труды ЛКИ, XXIX, 1959.
15. Бельчук Г. А. — Сварочное производство, 1961, 5.
16. Бельчук Г. А. Технология аргоно-дуговой сварки алюминия и его сплавов со сталью. ЛДНТП, Л., 1961.
17. Бельчук Г. А., Глускин Д. Я., Федоров Н. А. — В кн.: Труды ЛКИ, XXXIV, 1961.
18. Бельчук Г. А., Рябов В. Р., Юматова В. И. Современное состояние технологии аргоно-дуговой сварки алюминия и его сплавов со сталью. ЛДНТП, Л., 1967.
19. Белозерцев И. Н. и др. Авторское свидетельство № 157744 от 18. VIII 1962 г., «Бюллетень изобретений и товарных знаков», 17, 1963.
20. Биркс Л. С. Рентгеновский микроанализ с помощью электронного зонда. «Металлургия», М., 1966.
21. Бобро Ю. Г. Алюминиевые чугуны. Изд-во ХГУ, Харьков, 1964.
22. Бокий Г. Б. Кристаллохимия. Изд-во МГУ, М., 1960.
23. Борисов В. Г., Голиков В. М., Дубинин Г. Н. — В кн.: Диффузионные покрытия на металлах. «Наукова думка», Киев, 1965.
24. Бочвар А. А. Металловедение. Машгиз, М., 1956.
25. Бугаков В. З. Диффузия в металлах и сплавах. Гостехиздат, Л., 1949.
26. Бугаков В. З., Глускин Д. Я. — ЖТФ, 1936, VI, 2.
27. Буше М. Е., Семенов А. — Литейное производство, 1962, 2.

28. Ващенко К. И., Жижченко В. В., Фирсов А. И. Биметаллические отливки железо—алюминий. Машиностроение, М., 1966.
29. Ващенко К. И., Жижченко В. В., Фирсов А. И. Биметаллические отливки алюминий—железо с диффузионной связью. ЛДНТП, Л., 1962.
30. Ващенко К. И., Жижченко В. В. — В кн.: Машиностроение, НТП ГНТК СМ УССР, Киев, 1961, 3.
31. Ващенко К. И. и др. — Известия вузов. Черная металлургия, 1966, 4.
32. Вагнер К. Термодинамика сплавов. Металлургиздат, М., 1957.
33. Вол А. Е. Строение и свойства двойных металлических систем, I. Физматгиз, М., 1959.
34. Воронов С. М. — В кн.: Избранные труды по легким сплавам. Оборонгиз, М., 1957.
35. Вульф Б. Е., Ромадин К. П. Авиационное металловедение. Оборонгиз, М., 1962.
36. Герцрикен С. Д., Дехтяр И. А. Диффузия и металлах и сплавах в твердой фазе. Физматгиз, М., 1960.
37. Гейнрихсдорф Н. Г. и др. — В кн.: Производственно-технический бюллетень. МДТ, 7, 1963.
38. Глуекин Д. Я. — ЖТФ, X, 18, 1940.
39. Глуекин Д. Я. — ЖТФ, XXIII, 5, 1953.
40. Грабин В. Ф. — Автоматическая сварка, 1959, 5.
41. Грабин В. Ф., Рабинкин Д. М. — Автоматическая сварка, 1958, 8.
42. Горбунов Н. С. Методы нанесения диффузионных покрытий на железо и сталь. Изд-во ВИНИТИ, М., 1957.
43. Городнов Л. Т. Повышение жаростойкости стальных изделий методом алитирования. Машгиз, М., 1962.
44. Патент США № 2769231 от 6. X, 1956 г.
45. Патент США № 2769318 от 6. X, 1956 г.
46. Гуляев А. П. Металловедение. Оборонгиз, М., 1951.
47. Гуляев Б. Б. — ДАН СССР, 1965, 164, 1.
48. Готальский Ю. Н. — Автоматическая сварка, 1964, 12.
49. Гухман А. А. Введение в теорию подобия. «Высшая школа», М., 1963.
50. Горелик С. С., Расторгуев Л. Н., Скаков Ю. А. Рентгенографический и электронографический анализ металлов. Металлургиздат, М., 1963.
51. Гуревич С. М., Замков В. Н. — Автоматическая сварка, 1962, 3.
52. Даровский Г. Ф., Малевский Ю. Б. — Автоматическая сварка, 1959, 3.
53. Данченко В. Г., Залоторевский Ю. С. — В кн.: Металловедение. Судпромгиз, Л., 6, 1962.
54. Еременко В. Н. и др. Исследование кинетики растекания алюминия на железе. Доклад на IV Всесоюзной конференции по поверхностным явлениям в расплавах и возникающих на них твердых фазах. Кишиневский госуниверситет. Кишинев, 1968.
55. Еременко В. Н., Натанзон Я. В., Рябов В. Р. — Физико-химическая механика материалов, 4, 3, 1968.
56. Еременко В. Н., Натанзон Я. В., Рябов В. Р. — Физико-химическая механика материалов, 4, 6, 1968.
57. Засуха П. Ф. и др. Бюллетень ЦНИИ черной металлургии № 23/20, 2, 1965.
58. Зубова Г. Е., Петров Г. А., Рохлин Э. А. — В кн.: Сварка. Судпромгиз, Л., 1967.
59. Иванов-Сибиряков Н. Н., Даровский В. М., Голубев Б. Н. — В кн.: Труды ВАМИ. Металлургиздат, М., 19, 1939.
60. Ищенко А. Я. — Автоматическая сварка, 1963, 8.
61. Ильин Н. Н. — Известия АН СССР, сер. физ., XXV, 8, 1961.
62. Исследования при высоких температурах, перевод с англ. под ред. В. А. Кириллина, ИЛ, 1962.
63. Калимиров А. А., Недосека А. Я. — Автоматическая сварка, 1962, 8.
64. Калимиров А. А., Недосека А. Я. — Автоматическая сварка, 1963, 7.
65. Карапетьянц М. Х. — ЖФХ, XXVII, 5, 1953.
66. Карапетьянц М. Х. — Химическая термодинамика, Металлургиздат, М., 1949.
67. Като М., Минова С. Реф. ж. «Металлургия», 1966, 8.

68. Кейз С. А., Ван Горн К. Р. Алюминий в чугуне и стали. Металлургиздат, М., 1959.
69. Кодолов И. Д. — Сварочное производство, 1963, 4.
70. Кренинг И. О. — Цветные металлы, 1931, 7.
71. Корнилов И. И. Железные сплавы, 1 и 2. Изд-во АН СССР, М., 1945, 1951.
72. Корнилов И. И. и др. Металлохимические свойства элементов периодической системы. «Наука», М., 1966.
73. Костецкий Б. И., Шевченко И. П. — Автоматическая сварка, 1961, 5.
74. Красулин Ю. Л., Шорыгоров М. Х. — Сварочное производство, 1963, 8.
75. Красулин Ю. Л. — Сварочное производство, 1960, 11
76. Красулин Ю. Л., Шорыгоров М. Х. — В кн.: Сварка разнородных металлов. 1. ЛДНТП, Л., 1966.
77. Кубашевский О., Эванс Э. Термохимия в металлургии. ИЛ, М., 1954.
78. Кулакова Г. И. — В кн.: Научные труды, 1. Изд-во Харьковского горного института, 1952.
79. Лашко Н. Ф., Лашко-Авакян С. В. Металловедение сварки (некоторые вопросы). Машгиз, М., 1954.
80. Лашко Н. Ф., Лашко-Авакян С. В. — Автоматическая сварка, 1963, 4.
81. Лакедемонский А. В. Биметаллические отливки. «Машиностроение», М., 1964.
82. Лакедемонский А. В., Хряпин В. Е. Паяние и припои. Металлургиздат, М., 1961.
83. Лакедемонский А. В. — Технология автомобилестроения, 1959, 4.
84. Лайнер Д. И. и др. — Цветные металлы, 1966, 7.
85. Лайнер Д. И., Куракин А. К. — В кн.: Труды института «Гипроцветметобработка», 1965, 24.
86. Лайнер Д. И., Куракин А. К. — Физика металлов и металловедение, 11, 1, 1961.
87. Лайнер Д. И., Емельянов Л. Г. — В кн.: Труды института «Гипроцветметобработка». Металлургиздат, М., 1957.
88. Ларионов Л. Н. и др. — Автоматическая сварка, 1968, 5.
89. Лебедев А. А. — Электронная микроскопия. Машгиз, М., 1954.
90. Левич В. Г. — Физико-химическая гидродинамика. Физматгиз, М., 1959.
91. Лобанов Ю. Н. — Сварочное производство, 1967, 2.
92. Ларяков Л. И. и др. — В кн.: Металлофизика, 28, «Наукова думка», К., 1969, 5—49.
93. Лукьянович М. М. Электронная микроскопия в физико-механических исследованиях. Изд-во АН СССР, М., 1960.
94. Липшин Б. Г. — Физические свойства металлов и сплавов. Машгиз, М., 1959.
95. Маиаров Е. С. Строение твердых фаз с переменным числом атомов в элементарной ячейке. Изд-во АН СССР, М., 1947.
96. Масленков С. Б. — В кн.: Новые методы испытаний металлов, 32, 1963.
97. Масленков С. Б., Егоршина Т. В. — Заводская лаборатория, 1962, 12.
98. Мовчан Б. А. Микроскопическая неоднородность в литых сплавах. Гостехиздат УССР, К., 1962.
99. Мориага Т. и др. — Реф. ж. «Металлургия», 1964, 10.
100. Медведев А. С. — В кн.: Пайка металлов в производстве и перспективы ее развития. МДНТП им. Ф. Э. Дзержинского, III, 1962.
101. Немонов С. А., Колобова К. М. — ФММ, 1958, VI, 1, 183—185.
102. Немонов С. А., Колобова К. М. — ФММ, 1958, VI, 3, 466—474.
103. Никитин В. П. Русское изобретение — электрическая дуговая сварка. Изд-во АН СССР, М., 1952.
104. Никитина А. В., Рябов В. Р., Рабинк Д. М. — Автоматическая сварка, 1963, 4.
105. Никифоров Г. Д. и др. — Сварочное производство, 1967, 12.
106. Оников М. Г. — Металлург, 1935, 2.
107. Оников М. Г., Глускин Д. Я. — Металлург, 1938, 12.
108. Погодин-Алексеев Г. И. Теория сварочных процессов. Машгиз, М., 1950.

109. Погодин-Алексеев Г. И., Назарова С. Г., Ганченко М. Н. Методы испытаний сварных соединений и конструкций. Машгиз, М., 1952.

110. Петров Г. Л. Неоднородность металла сварных соединений. Судпромгиз, Л., 1963.

111. Пинес Б. Я. — Физика твердого тела, 1959, 1, 3.

112. Поволоцкий А. М. — Вестник электропромышленности, 1961, 11.

113. Поплавко М. В., Лоцманова С. Н. и Гостенина В. Н. Авторское свидетельство № 92834.

114. Попов А. А. Теоретические основы химико-термической обработки стали. Металлургиздат, Свердловск, 1962.

115. Постников В. С. — В кн.: Релаксационные явления в металлах и сплавах. Металлургиздат, М., 15, 1963.

116. Преснов В. А. Основы техники и физики спая. Изд-во Томского ун-та, Томск, 1961.

117. Парфесса Г. И., Сидляренко В. Н. — Автоматическая сварка, 1959, 7.

118. Рабкин Д. М. — Автоматическая сварка, 1954, 3.

119. Рабкин Д. М. Диссертация. Институт электросварки им. Е. О. Патона, АН УССР, Киев, 1962.

120. Рабкин Д. М., Лозовская А. В., Рябов В. Р. Информационное письмо Института электросварки им. Е. О. Патона, 18 (517), 1968, № 7.

121. Рабкин Д. М., Рябов В. Р. — Автоматическая сварка, 1962, 7.

122. Рабкин Д. М., Рябов В. Р. Сварка алюминия и его сплавов со сталью и медью. Машиностроение, М., 1965.

123. Рабкин Д. М. и др. — Автоматическая сварка, 1966, 1.

124. Рабкин Д. М. и др. — Авторское свидетельство № 172931 от 24 апреля 1964 г. Бюллетень изобретений и товарных знаков, 14, 1965.

125. Раздуй Ф. И., Засуха П. Ф., Рябов В. Р. — Сварочное производство, 1965, 1.

126. Рохлин Э. А. — В кн.: Сварка. Судостроение, Л., 1968.

127. Розери Ю. М. Введение в физическое металловедение. «Металлургия», М., 1965.

128. Рыкалин Н. Н. Тепловые основы сварки, 1. Изд-во АН СССР, М., 1947.

129. Рыкалин Н. Н. Расчеты тепловых процессов при сварке, Машгиз, М., 1951.

130. Рыкалин Н. Н., Шорников М. Х., Красулин Ю. Л. — Неорганические материалы, 1965, 1, 1.

131. Рябов В. Р. — В кн.: Машиностроение, ИТИ, ГНТК СМ УССР, 6, 1962.

132. Рябов В. Р., Лозовская А. В., Васильев В. Г., ФММ, 1969, 27, 4, 668—673.

133. Рябов В. Р. — В кн.: Машиностроение, ИТИ, ГНТК СМ УССР, 1, 1963.

134. Рябов В. Р. — В кн.: Машиностроение, ИТИ, ГНТК СМ УССР, 1, 1964.

135. Рябов В. Р., Дунляк В. Д. — В кн.: Физико-химическая механика материалов, 3, 3, 1967.

136. Рябов В. Р., Дунляк В. Д. — Сварочное производство, 1965, 2.

137. Рябов В. Р., Дунляк В. Д. — Сварочное производство, 1968, 2.

138. Рябов В. Р., Юматова В. И. — Сварочное производство, 1966, 1.

139. Рябов В. Р., Рабкин Д. М., Ягупольская Л. Н. Авторское свидетельство № 146167 от 7 августа 1961 г. Бюллетень изобретений и товарных знаков, 7, 1962.

140. Рябов В. Р. Авторское свидетельство № 157201 от 30 июля 1962 г. Бюллетень изобретений и товарных знаков, 17, 1963.

141. Савицкий Е. М., Терехова В. Ф., Буров И. В. — Металловедение и термическая обработка металлов, 1959, 3.

142. Савицкий Е. М. Влияние температуры на механические свойства металлов и сплавов. Изд-во АН СССР, М., 1959.

143. Сибата К., Мородзуми С., Кодв С. — Реф. ж. «Металлургия», 1967, 2.
144. Сигуяси К., Морозуки С., Акира К. — Реф. ж. «Металлургия», 1963, 8.
145. Связцов Н. П. и др. — Автомат.ическая сварка, 1969, 8
146. Сугиямв С. — Реф. ж. «Металлургия», 1966, 2.
147. Синельникова В. С., Подергин В. А., Речкин В. И. Алюминиды. «Наукова думка», К., 1965.
148. Смирнов А. А. Авторское свидетельство № 125115 от 29. XII, 1959.
149. Справочник по металлам и сплавам, ч. 1 и 2, Дом техники, М., 1957.
150. Справочник по авиационным материалам. Оборонгиз, М., 1958.
151. Под ред. М. В. Приданцева. Стали с пониженным содержанием никеля. Металлургиздат, М., 1961.
152. Самарин А. П., Савицкий Е. М. Железоалюминиевые сплавы с добавками редких и редкоземельных металлов. Изд-во АН СССР, М., 1961.
153. Стрижевская Л. Г. — Производственно-технический бюллетень МДТ, 1, 1962.
154. Семенов А. П. Схватывание металлов. Машгиз, М., 1958.
155. Семенова Н. М., Сизова Р. М. — В кн.: Труды ВИЛС, 3, М., 1964.
156. Славинский М. П. Физико-химические свойства элементов. Металлургиздат, М., 1962.
157. Смирнов А. С. Горячее цинкование. Машгиз, М., 1959.
158. Технология электрической сварки плавлением, под редакцией Б. Е. Патона. Машгиз, М., 1962.
159. Тихомиров М. В. Авторское свидетельство № 77569.
160. Уманский Я. С. и др. Физическое металловедение. Металлургиздат, М., 1955.
161. Ужик Г. В. — Известия АН СССР, 1955, 1.
162. Утевский А. М. — Заводская лаборатория, 1952, 6.
163. Френкель Я. И. Введение в теорию металлов. Гостехиздат, М., 1950.
164. Френкель Я. И., Сергеев М. И. — ЖЭТФ, 1939, 2.
165. Фридлянд Л. А., Зиновьева Т. П., Конов Ю. К. — Сварочное производство, 1963, 11.
166. Фильчаков П. Ф., Панчишин В. И. — В кн.: Моделирование краевых задач на электропроводной бумаге. Изд-во АН УССР, К., 1961.
167. Фильчаков П. Ф. и др. — Автоматическая сварка, 1966, 7.
168. Хансен М., Андерко К. Структуры двойных сплавов. Металлургиздат, М., 1962.
169. Харигути С., Оно А. Влияние легирующих элементов на растекаемость алюминиевых сплавов по железу. Реф. ж. «Металлургия», 9, 1960.
170. Хауффе К. Реакции в твердых телах и на их поверхности. М., ИИЛ, 1962.
171. Эванс Ю. Р. Коррозия и окисление металлов. Машгиз, М., 1962.
172. Черкашин Е. Е. — В кн.: Сварка разнородных металлов. II. ЛДНТП, Л., 1966.
173. Шоршоров М. Х. — В кн.: Общественный университет при ЦПНТО Машпром. Профиздат, М., 1960.
174. Шоршоров М. Х., Красулин Ю. Л. — Сварочное производство, 1967, 12.
175. Штеринн Л. А., Прокофьев С. Н. — Сварочное производство, 1961, 11.
176. Японский патент № 5062 от 23. VII, 55 г.
177. Японский патент № 2355 от 11. IV, 55 г.
178. Японский патент № 20756 от 27. X, 61 г.
179. Японский патент № 14471 от 27. 11, 59 г.
180. Японский патент № 17968 от 26. I, 60 г.
181. Agarwala R. P., Murarka S. P., Anand M. S. — В кн.: Acta metallurgica, 12. 1964.
182. Aluminium Clad Strip — manufacture of «Feran» steel in Germany. — Iron and Steel, 1948, 2.

183. Andrews D. R. — Welding and Metal Fabrication, 1961, 11.
184. Andrews D. R. — British Welding Journal, 1962, 9, 12.
185. Black P. I. — В кн.: Acta Crystallogr., 8, 1, 1955, 43—58, 175—182.
186. Brenner P. — Metall, 1958, 12.
187. Bural F., Holmann W. — Abhandl, Braunschweig. Wiss. Ges., 8, 1956, 85—98.
188. Darby I. B., Iugli D. B., Kleppa O. I. — Transection met. Soclaly, AIME.
189. Dovey D. M., Waluski A. — Metallurgia, 1963, 67, 403.
190. Galsek L. — Welding Design and Fabrication, 1965, IX, 38, 9.
191. Garcia I. — Reviu aluminium, 1952, 36, 296.
192. Caslaing R. — Thesis, Univ. Paris, ONERA Publ., 1951, 55.
193. Cabane G., Monturat P. Contribution à l'etude de la fra gilitè de la solution solide fer—aluminium. — Academie des sciences, 1963, 8.
194. Gelb A. — Aircraft and Missiles Manufact, 1959, 2, 1.
195. Gebhardt E., Obrowski W. Z. Metallkunde, 44, 4. 1953.
196. Gittings D. O., Rowland D. H., Mack I. O. — Trans. American Societi Metals, 1951, 43.
197. Gürtler G. — Automobil Technische Zeilung, 1951, 53, 4a.
198. Gürtler G., Sagel K. — Z. Metallkunde, 1956, 46, 10,
199. Gröbner P. Koeficient difuse Hliniku v zelezе pro oblast Tuhеno Roztoku. Hutnicke listy, Roc. X., 1955.
200. Cooke, A Levy. — Journal of Metals, 1948, II
201. A Handbook of lattice spacings and structures of metals and alloys. Ed. W. B. Pearson, London, 1961.
202. Hughes I. E. — Metallurgia, 1951, 49, 291.
203. Holmann, W., Groove K. — Z. Metallkunde, 1954, 45, 8.
204. Hofmann W., Schüller H. — Z. Metallkunde, 1958, 48, 6.
205. Holmann W., Kornberger G. — Z. Metallkunde, 1956, 47, 2.
206. Hnlmann W., Wilde G. — Aluminium (BRD), 1961, 37, 3.
207. Hess W., Nippes E. — Welding Journal, 1946, 3, 25.
208. Holler H., Maier A. — Aulogene Metallbearbeilung, 1935, 28, 12.
209. Hirano K., Agarwala R. P., Cohen M. — В кн.: Diffusion of iron, nickel and coball in aluminium, Acta metallurgica, 10, 1962.
210. Heumann T., Dittrich S. — Z. Metallkunde, 50, 1959, 10.
211. Joining aluminium to steel Light metal Age, 1968, 26, 6.
212. Joining aluminium to other metals, Aluminium Courier, 1957, 14, 40.
213. Morgan E. K., Lackay V. F. — Metall Progress, 1955, 68, 4.
214. Lamb H. L., Wheeler M. I. — J. Instit. Metals, 1964, 92, 5.
215. Lehrheuer W. Kerntechnik, 1968 10, 4.
216. Lukaes I. — Kahasz Lapok, 11, 10, 1956.
217. Lutz K. — Ind. and Welding, 30, 5, 1957.
218. Keel C. F. — Zeitschrift für Schweisstechnik, 1938, 28, 9.
219. Kosaka M., Minowa S. — Iron and Steel, 1965, 51, 2.
220. Kosaka M., Minowa S., Kalo M., Mizuto M. — Repts. Iont. Industr. Res. Institute, 1964, 13, 4.
221. Kupe E. I. — Welding Engineer, 1958, 1.
222. Macau W., Köhler W. — Werkstaffe und Korrosion, 1962, 10, 13.
223. Mille M. A. — Ingeneria e Industria, 1954, 22, 249.
224. Miller M. A., Mason E. — Welding Journal, 1956, 35, 7.

225. Miller M. A. — Welding Journal, 1953, 8.
226. Nilsson A. — Metallen, 1962, 2.
227. Orrok E. — Metall Progress, 1966, 89, 2.
228. Phillips H. W. — J. Instit. Metals, 1953/54, 82, 5.
229. Pelly E. R. — J. Instit. Metals, 1960/61, 89.
230. Röhrig H. — Zeitschrift für Metallkunde, 1934, B. 26, H. 4, S. 87.
231. Rolh A. — Z. Metallkunde, 1939, 31, 9.
232. Rjabow W. R., Losowskaja A. W. — Schweisstechnik, (DDR), 1968, 9.
233. Salcher H. — Aluminium, 1962, 2.
234. Schneider K., Kessler H. — Metall, 1953, 7, 15.
235. Scott M. M., Squires I. F. — British Welding Journal, 1966, 13, 8.
236. Seil W., Ochsenfarth C. — Z. Metallkunde, 1943, 35, 12.
237. Sugiyama Y. — J. of the Japan Welding Socialy, 1965, 34, 4.
238. Sommeren E. H. — Welder, 1955, 24, 121.
239. Stru R. — Schweisstechnik (Oster) 1966, 20, 2.
240. Storchelm. — Iron Age, 1957, 180, 23.
241. Sugiyama Y. Some experiments on joining aluminium to mild steel by TIG Welding «Посяну rakkau», 1965, 34, 4.
242. Tajima S., Mori T., Komiya M. — Corrosion Engeneering, 1965, 14, 3.
243. Tamman G., Rocha H. — Zs. an Chem., 1931, 199.
244. Welmarth G., Dudovicz W. — Iron Age, 1961, 188, 18.
245. Westbrook I. H. (ed.). Mechanical Properties of Intermetallic Compounds. I. Wiley, V. I, 1959.
246. Whitlerlord I. M. — The Shipping World, 1953, 2.
247. Young I. G., Smith A. A. — Welding and Metal Fabrication, 1959, 8—9.
248. Zimmer F. — Metall Progress, 1963, 1.
249. Zurbrügg E. — Aluminium suisse, 1956, 6, 5.